NASA CONTRACTOR REPORT

NASA CR-132675

INSTRUMENTATION REQUIREMENTS FOR AIRCRAFT PARAMETER IDENTIFICATION WITH APPLICATION TO THE HELICOPTER

by J.A. Sorensen, R.L. Mohr, and T.B. Cline

Prepared by
SYSTEMS CONTROL, INC. (Vt)
Palo Alto, California 94304
for Langley Research Center

NATIONAL AERONAUTICS AND SPACE ADMINISTRATION • WASHINGTON, D.C. • JUNE 1975

FOREWORD

This report was prepared under Contract No. NAS1-12876 by Systems Control, Inc., Palo Alto, California, for Langley Research Center, National Aeronautics and Space Administration, Hampton, Virginia. NASA project monitors were W.F. Hodge and W.H. Bryant. At SCI, the project manager was J.A. Sorensen. Project engineers were T.B. Cline and R.L. Mohr. Project programmer was N. Taniguchi. Report preparation was done by D. Buenz.

TABLE OF CONTENTS

TABLE OF CONTENTS (CONCLUDED)

SYMBOLS

a_x, a_y, a_z	longitudinal, lateral, and vertical aircraft accelerations
A	state weighting matrix in cost function for quadratic synthesis of feedback gains
B	vector of biases affecting measurement of y
B_c	vector of biases affecting measurement of u
B_Q	control weighting matrix in cost function for quadratic synthesis of feedback gains
b_θ, b_q, b_α, b_u, b_{ax}, b_{az}, $b_{\dot{q}}$	biases in the longitudinal output measurements
b_β, b_p, b_r, b_φ, b_{ay}, $b_{\dot{p}}$, $b_{\dot{r}}$	biases in the lateral output measurements
C	matrix of feedback gains
C_ζ	correlation of wind disturbance ζ
c.g.	center-of-gravity
d_ζ	correlation distance of wind disturbance ζ
D, D(p)	control measurement matrix relating u to y
$D(\hat{p})$	model of D containing parameter estimates $\hat{p}$
E_{noise}	covariance of parameter estimate errors due to the output noise n_i
e	measurement errors
e_{ij}	elements of the T matrix
e_M	mean measurement errors
e_R	random constant measurement errors
e_θ, e_q, e_α, e_u, e_{ax}, e_{az}, $e_{\dot{q}}$	scale factor errors in the longitudinal output measurements

L_v, L_β, L_p, L_r, $L_{\delta a}$, $L_{\delta r}$	roll moments due to lateral velocity, sideslip, roll rate, yaw rate, aileron (or roll cyclic) deflection, and rudder (or yaw cyclic) deflection perturbations
M	Mach number
M	covariance matrix of control (fourth chapter)
M_q, M_w, M_u, $M_{\delta e}$, $M_{\delta c}$	pitching moment due to pitch angle, vertical speed, longitudinal speed, elevator (or differential collective) deflection, and collective pitch deflection perturbations
N_v, N_β, N_p, N_r, $N_{\delta a}$, $N_{\delta r}$	yaw moments due to lateral velocity, sideslip, roll rate, yaw rate, aileron (or roll cyclic) deflection, and rudder (or yaw cyclic) deflection perturbations
n	number of points collected in the measurement sequence
n(k)	quantity representing error due to signal quantization
n_{ci}	control measurement noise vector
n_i	contaminating output measurement noise vector
p	vector of parameters to be estimated
$\hat{p}$	estimated value of the vector p
p, q, r	roll, pitch and yaw attitude rates
p_b	unknown biases to be estimated
p_p	unknown stability and control derivatives to be estimated
p_{IC}	unknown state initial conditions to be estimated
P	covariance matrix of state when influenced by wind gusts
Q	quantization level (second chapter)
Q	power spectral density of wind disturbance (fourth chapter)
R	weighting matrix in parameter identification performance index (cost function)

SYMBOLS (CONTINUED)

R_c	covariance matrix of control measurement noise n_{ci}
s	Laplace transform independent variable
S	covariance matrix of output measurement noise n_i
t	time
T	matrix representing scale factor errors and cross-coupling errors in the measurement of y
T_c	diagonal matrix representing scale factor errors in the measurement of u
T_ζ	effective correlation time of wind disturbance
$\mathscr{L}$, $\mathscr{L}(s)$	Laplace transfer function matrix
u	control input vector
u, v, w	forward, lateral, and vertical velocity perturbations
u_I	indicated value of control input vector due to scaling and bias errors
U_o	nominal longitudinal velocity
u_L	value of u_I due to measurement system lags
u_m	measurement value of u_L corrupted by noise
w_θ, w_q, w_{ax}, w_{az}	standard deviation of noise in the longitudinal output measurements
W_o	nominal vertical velocity
x_{Vcg}	angle-of-attack vane distance from the aircraft center of gravity
X_w, X_u, X_q, $X_{\delta e}$, $X_{\delta c}$	longitudinal force due to vertical and longitudinal speed perturbations, pitch rate, and differential collective and collective pitch perturbations
x, x_o	aircraft state vector and its initial value

x_{cg}, y_{cg}, z_{cg}	components of the accelerometer position from the aircraft c.g.
Y_v, Y_β, Y_p, Y_r, $Y_{\delta a}$, $Y_{\delta r}$	side force on aircraft due to lateral velocity, sideslip, roll rate, yaw rate, aileron (or roll cyclic) deflection, and rudder (or yaw cyclic) deflection perturbations
y	measurement vector of aircraft state and its derivatives
y_I	indicated value of y_T due to scaling, cross-coupling, and bias errors
y_L	value of y_I due to measurement system lags
y_T	true value of y
Z_q, Z_w, Z_u, $Z_{\delta e}$, $Z_{\delta c}$	vertical force due to pitch rate, vertical speed, longitudinal speed, and elevator (or differential collective) and collective deflection perturbations
$z(k)$	sampled signal
α_o, α	nominal angle-of-attack
$\Delta\alpha_e$	angle-of-attack error
α_i, β_i	roots of characteristic equation
β	sideslip angle
γ_{ax}, γ_{ay}, γ_{az}	misalignments of the longitudinal, lateral, and vertical accelerometers about the aircraft axes
γ_p, γ_q, γ_r	misalignments of the roll, pitch, and yaw gyros about the aircraft axes
$\gamma_p^\bullet$, $\gamma_q^\bullet$, $\gamma_r^\bullet$	misalignments of the roll, pitch, and yaw angular accelerometers about the aircraft axes
Γ	process noise distribution matrix in state dynamics equation
Δp	error in p obtained from an individual set of measurement data
$\overline{\Delta p}$	mean value of Δp over several sets of measurement data
Δt	time step of the numerical integration method

SYMBOLS (CONCLUDED)

Δt_s	sample time step
δ_e, δ_c, δ_a, δ_r	elevator (or differential collective), collective, aileron (or roll cyclic), and rudder (or yaw cyclic) deflections
δ_{ij}	Kroneker delta function (=0 if $i \neq j$, and =1 if $i = j$)
δp	the difference between p and $\hat{p}$
$\varepsilon_{a\ell x}$, $\varepsilon_{a\ell z}$	errors in the accelerometer location
ε_{cgx}, ε_{cgz}	error in c.g. location
ε_{vx}	error in α-vane location
ζ	wind disturbance
θ_o	nominal pitch angle
ψ	nominal yaw angle
ρ	correlation of consecutive sampled terms
σ	standard deviation
σ_n	standard deviation of n(k)
τ	time delay in sampling control input
φ	nominal roll angle

NOTATIONS

$\dot{(\,)}$	time derivative of variable
$(\,)_i$	sample of variable at i^{th} instant
$\hat{(\,)}$	estimated value of a parameter
$E\{\ \}$	expected value of a variable
$(\,)^T$	matrix transpose
$(\,)^{-1}$	matrix inverse
$\frac{\partial(\,)}{\partial p}$	gradient of a constant with respect to the vector p. For a constant, this is taken to be a row vector. For a vector, this is taken to be a matrix with the number of columns equal to the order of p and the number of rows equal to the order of the vector.
$\sum_{i=1}^{n}(\,)$	summation of points from 1 through n
$\Delta(\,)$	perturbation of a quantity about the nominal value or trim position
$(\,)_m$	measured value of aircraft states and their derivatives
$(\,)^*$	when applied to an aircraft parameter, it denotes modification due to the cross-product of inertia; when applied to a matrix, it denotes the matrix has been augmented.

CONVERSION TABLE

(Conversion from English Units to the International System of Units (SI))

TO CONVERT FROM	TO	MULTIPLY BY
foot	meter	3.048×10^{-1}*
foot^{-1}	meter^{-1}	3.2808399
inch	meter	2.54×10^{-2}*
inch^{-1}	meter^{-1}	3.9370079×10^{-1}
knot	meter second^{-1}	5.1444444×10^{-1}
degree (angle)	radian	1.7453293×10^{-2}
degree^{-1} (angle)	radian^{-1}	5.7295780×10^{1}
inch foot^{-1}	meter meter^{-1}	8.3333333×10^{-2}
foot inch^{-1}	meter meter^{-1}	1.2×10^{1}*
foot degree^{-1}	meter radian^{-1}	1.7463754×10^{1}
slug foot^{2}	kilogram meter^{2}	1.3558179
g (gravity)	meter second^{-2}	9.80665 *
g^{-1}	second^{2} meter^{-1}	1.0197162×10^{-1}
degree second^{-1} g^{-1}	radian second meter^{-1}	1.7797405×10^{-3}
degree hour^{-1} g^{-1}	radian second meter^{-1}	6.4070659
degree hour^{-1} g^{-2}	radian second^{3} meter^{-2}	6.5333890×10^{-1}

*denotes an exact number

INTRODUCTION

The process of determining stability and control derivatives of an aircraft from flight test data is called aircraft parameter identification. There are several reasons why this process has developed into a very important field of endeavor. These include:

1. Many instances where the prototype aircraft do not have the same characteristics as predicted by their wind tunnel models. The cost to the United States government due to out-of-control aircraft losses has been substantial [1]. Major cost and safety considerations motivate determining ways of obtaining better knowledge of the aircraft parameters.

2. Requirements for better understanding and calibration of wind tunnel testing and its relationship to actual flight vehicle performance.

3. The potential of allowing the fuller understanding of aerodynamic phenomena and the relationship to vehicle stability.

4. Requirements for ground-based simulators which are more accurate representations of the aircraft in all flight regimes.

5. Requirements for superior stability augmentation and adaptive flight control systems.

There are three essential elements in the development of more adequate methods for identifying aircraft parameters from flight data:

1. Improved algorithms and computer programs to identify the derivatives, their confidence levels (variances), and related parameters such as sensor errors and wind gusts.

2. The determination of proper sequences of flight control inputs (surface deflections) which will excite all the aircraft response modes from which parameters are to be extracted, and methods of displaying this information to the test pilot so that he is aware of when a suitable maneuver has been executed.

3. Adequate instrumentation (the right kind of sensors with necessary accuracy) and recording equipment with which to collect the flight data.

This study is concerned with this last point, namely, the establishment of what constitutes necessary instrumentation accuracy to enable the collection of flight data which is of adequate quality for identifying the aircraft parameters to the accuracy desired.

Flight instrumentation is usually not specified for the direct intention of identifying stability and control derivatives. Rather, its intended purpose is for checking aircraft handling qualities and general measures of performance. If instrumentation specification is made, it is typically based on what is known to be available. Part of the reason for this status is that estimating stability derivatives from flight test data has only been a secondary activity of companies building aircraft. If a problem arises in the handling qualities, the manufacturer may attempt to determine the derivatives responsible for the undesirable characteristic as an aid to the best design fix; however, generally, no full identification program is undertaken. Flight simulators are built using wind tunnel estimates of stability derivatives, and only corrections for gross discrepancies are made.

The effects of instrumentation errors on the accuracy of stability and control derivatives determined from flight test data have been analyzed before to some extent. The most detailed study conducted to date on instrumentation requirements was the work of Hill, et al. [2] for the XC-142A V/STOL airplane. This study developed design and accuracy requirements for four levels of measurement equipment. Particular errors studied include random noise, high frequency sinusoids (elastic modes and faulty demodulation), scale factor error, bias, time delay (high order filter or instrumentation stiction), time lag (filter or servo), and aliasing. The state-of-the-art in available equipment is discussed in detail in Ref. 2 prior to specifying the instrumentation system design. Focus was placed on the need for further sensor development for low airspeed, direct thrust, angle-of-attack and angle-of-sideslip, and pressure altitude. However, an important conclusion of this study was that it is as important to understand the nature of an instrument as it is to attempt to develop the more nearly perfect instrument. If an instrument's errors are well known, they can be taken into account.

In another study, Burns [3] noted that a 3° phase lag in the gyros produced a 5% error in $c_{\ell\beta}$. He recommended that instrument alignment be kept within 0.1°, and that mounting locations be selected so that less than 0.1° error resulted from structural flexibility. He concluded that many more test flights have been made than needed because of poor data, and better instrumentation is a more effective use of money. Thus, it has been recognized for some time that there are strong economic reasons to understand the effects of instrumentation errors and to provide the means by which an organization that is conducting flight tests can be assured that their instrumentation is adequate.

Gerlach [4] and others at the Technological University of Delft, the Netherlands, have developed instrumentation systems with digital data acqusition, precision temperature controlled electronics for uniform instrument dynamics, and inertial instruments in a temperature controlled housing. However, data of individual instrument contributions to identification errors were not collected, nor were the individual error effects on particular stability derivatives determined.

References 5-7, which are the predecessors of this study, report the development of two specific methods for analyzing the effect of instrumentation errors on the accuracy of the identified stability and control derivatives. These methods are referred to as ensemble analysis and Monte Carlo analysis. The computer programs which mechanize these methods are extended in the current study.

The ensemble analysis method was first applied to study the effect of static output measurement errors for typical flight tests of the F-4 and DC-8 aircraft [5,6]. This was extended to also include the effects of control measurement errors and lags in Ref. 7 using the Monte Carlo analysis method.

The results of this present study were as follows:

1. The computer programs developed for previous work [5] were expanded to include more extensive capabilities (such as modeling the identification of helicopter dynamics with a stability augmentation system operating). Details of these programs appear later.

2. A survey was made of instrumentation and data processing techniques used at various flight test centers. From this survey, the error sources affecting identification accuracy were identified and quantified. The error models developed in the previous work were validated and extended as necessary.

3. The error analysis programs and instrumentation error models were used to study error effects on identification of stability and control derivatives of a simulated CH-46 helicopter. The statistical accuracy of these coefficients was determined for various points on a typical landing approach trajectory. Recommendations are offered concerning further analysis required.

This report, which contains the details and results of the study, is organized as follows:

1. The second chapter entitled, "ERRORS IN MEASUREMENT AND DATA PROCESSING SYSTEMS USED FOR PARAMETER IDENTIFICATION," presents the instrumentation survey, the resultant instrument error models, and the range of error magnitudes for typical flight test instrumentation.

2. The third chapter entitled, "ERROR ANALYSIS TECHNIQUES," presents the analytical techniques used in the error analysis programs.

3. The fourth chapter entitled, "STUDY OF THE EFFECTS OF INSTRUMENTATION ERRORS ON THE ACCURACY OF PARAMETER ESTIMATES," presents the effects of instrumentation errors on the statistical uncertainty of identified parameters. These results are obtained using the instrument error models presented in the second chapter and the error analysis techniques discussed in the third chapter.

4. The last chapter summarizes the information gained from the study regarding instrumentation accuracy requirements and further analysis and experimentation efforts needed to ensure adequate flight test results.

Page Intentionally Left Blank

ERRORS IN MEASUREMENT AND DATA PROCESSING SYSTEMS USED FOR PARAMETER IDENTIFICATION

This chapter describes and quantifies the errors which affect the nature of the data used for parameter identification. Error sources include those of the airborne sensors, the airborne data conditioning and recording, possible telemetry, and ground-based data processing. First, a general instrumentation error model is presented which is used to incorporate the primary error sources which affect the accuracy of the flight test data. Each of the main sensors and data processing steps is then discussed with respect to this model. A general discussion is given of some of the procedures followed at various flight test centers to limit these error sources and magnitudes. Finally, ranges of values of the parameters which are contained in the various instrument error models are given, based on a survey of flight test center personnel, instrument manufacturers, and flight test reports.

The material used to compile this chapter is by no means exhaustive. Every flight test is different as are the aircraft being tested and the objectives of the engineers conducting the tests. The practices used to ensure accuracy of flight data vary substantially between each flight test center. To obtain descriptions of all the procedures followed in the tests and to quantify the errors would require several months of investigation. Instead, this chapter presents more of an overview of known error sources and summarizes limited data which reflects overall instrumentation accuracies and sources of error. The resulting error models are subsequently used to determine the effects of instrument errors on identified parameter accuracy. Thus, the data and models of this chapter provide the means to determine: (1) which instrument error sources are more important, and (2) what is the sensitivity of parameter accuracy to specific error magnitudes.

To obtain this material, visits were made to NASA Ames, Flight, and Langley Research Centers. In addition, conversations were held with personnel associated with the Naval Air Development Center, the Naval Air Test Center, Boeing, Douglas, and Lockheed aircraft companies, and several instrument manufacturers. Additional material was obtained by review of some of the existing literature on flight testing and instrumentation.

General Measurement System Error Model

As is seen in the following sections, the data actually used for parameter identification are modified by several types of errors. These errors change each measured variable's magnitude from its true time history. Nonlinear, stochastic, and time-varying effects are all present. This section reduces these effects to parameters contained in simple linear error equations suitable for analysis. In the subsequent analysis, the errors are simulated by these equations, and the error effects are evaluated.

The data used for parameter identification consist of recorded measurements of the aircraft states and their derivatives and the control inputs used to perturb the aircraft from steady flight conditions. The instrumentation system measures, processes, and records the data variables essentially simultaneously. This instrumentation system is mathematically represented by a set of equations describing the different data channels. The data in each channel are the measurements of one of

the time-varying control inputs, states of the aircraft, or state derivatives. The parallel data channels each have the same basic sources of error, which are now discussed.

Figure 1 is a block diagram which illustrates major sources of error which affect the data. The purpose of this illustration is to introduce the types of errors which are considered here. The exact form of the submodels contained within each block of the figure may change somewhat from channel to channel, as is explained shortly. Figure 1 shows the typical sequence of error effects which modify a variable y_1 starting from its assumed true value y_{1i} and ending with the recorded value y_{1o} used for parameter identification.

The assumed true value of the variable (y_{1i}) is first subjected to the dynamic response of the sensor which is indicated in Figure 1 by the second-order term. Such a model approximately characterizes the response of a rate gyro, for example. For some instruments, such as the airspeed measurements and rate integrating gyros, this term is more appropriately modeled as a first-order term.

The measurement is next subjected to a scale factor error indicated by ε_{11}. This term is assumed to be constant; however, it encompasses the effects of nonlinear scaling and time-varying scaling such as scale factor errors caused by temperature and power supply variations. The effect of boom bending and upwash effects on the wind vanes are other examples included by this term.

Another error term is the cross-coupling between the measurements. This is indicated by the term ε_{12} which multiplies the variable y_2 before it is added to

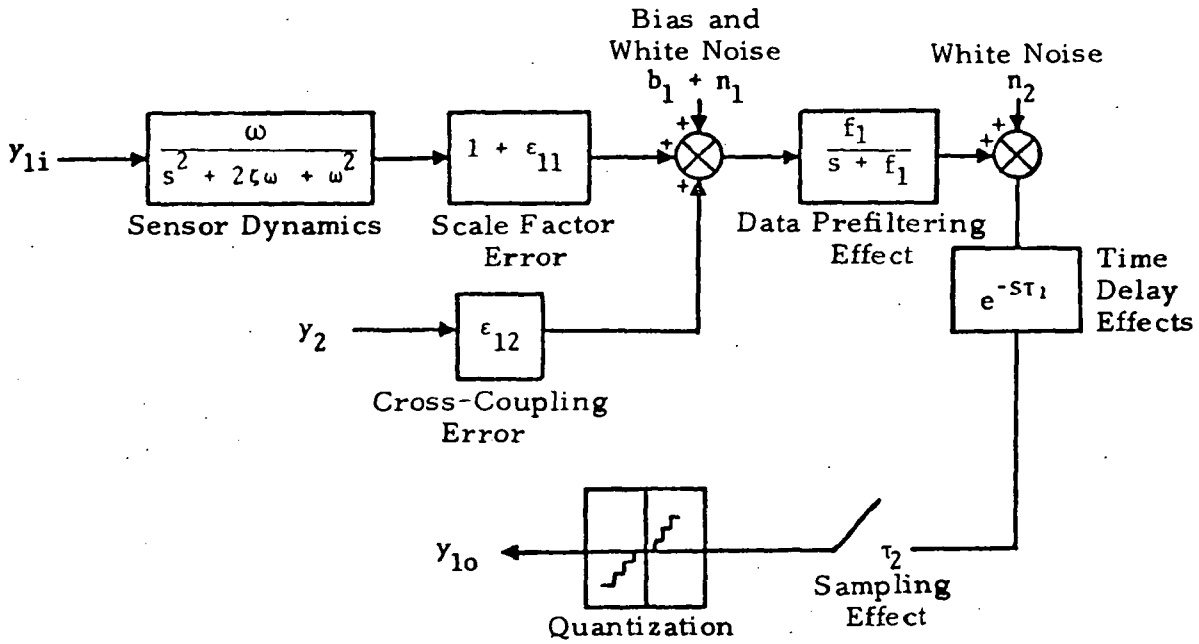

FIGURE 1.- BLOCK DIAGRAM OF BASIC MEASUREMENT ERROR MODEL

y_1. Such terms exist when the measurements of one variable are affected by changes in magnitude of other variables. Sources of cross-coupling error are instrument misalignment, center of gravity (c.g.) and instrument location uncertainty, linear acceleration dependent terms of the gyro and angular accelerometer readings, and angular rate dependent terms of the wind vane measurements.

Other error terms which affect data accuracy are instrument bias b_1 and noise n_1. The noise is due to vibration, electrical sources, unsteady aerodynamics and various other sources which are discussed subsequently. The noise can be modeled as white noise passed through a shaping filter, and as sinusoidal terms. However, this noise can be encompassed into the bias term; also, prefilters are commonly used to remove the noise and sinusoidal terms adequately so that n_1 can be neglected.

Next, the measurement is subjected to another dynamic term shown in Fig. 1 as a first-order lag. This represents the prefilter. A second lag would be required to model the response of recording equipment. The phase error from these filter effects has usually higher than first-order characteristics. But the model constant f_1 can be adjusted so that phase lag is approximately correct for frequencies in the region of the prefilter break frequency. This first-order model limits the computational load of the subsequent analysis because only one integration is then required per channel. The errors that result from the filtering effects are due to the inequality of the time constants in parallel data channels. In another sense, the error can be considered to be due to incorrect compensation for known phase lags.

The filter terms in each data channel usually produce lower cutoff frequencies than the basic sensor response dynamics, so the effect of the instrument dynamics can usually be ignored. This isn't true for pressure-dependent measurements, as is discussed later. However, it is assumed in this study that pressure-dependent lags are adequately compensated for in the software before data processing. Thus, in the subsequent analysis, the effects of lags due to sensor responses are ignored, and concentration is placed on studying the effects of differences in the time constants of the total dynamics in each channel.

After passing through the prefiltering, other white noise due to various electrical sources affects the data. This is modeled by the addition of the term n_2.

Up to this point, the data which exist in each channel are considered to be in continuous analog form. However, for data transmission and parameter identification purposes, the data are usually sampled and digitized. The data are sampled at regular intervals and converted to a digital number at each sample point. The data from several channels are typically sequentially sampled so that the data points taken from each channel are not taken simultaneously. This effect can be modeled as a variable time delay in each channel represented by $e^{-s\tau_1}$, where τ_1 is the delay time. The error here is due to the difference in the delay times τ_1. If sampling is done rapidly enough (e.g., ten times highest system frequency which is to be measured), this error is insignificant. For high performance aircraft, or where accurate vibrational data is desired the error can be significant, and the delay effect must be removed during data processing.

The data is sampled once every τ_2 seconds and passed through a quantizer. For the flight instrumentation systems reviewed, the standard deviation (σ) of the signal noise is much larger than the quantization level Q. Thus, as is seen shortly, it can be assumed that the distribution of the noise error on the final digitized output y_{1o} is the same as that for the noise n_2.

To summarize, for the example of the variable y_1 just discussed, the following random error sources are assumed to be predominant:

ε_{11}: scale factor error

ε_{12}: cross coupling error

b_1: bias

f_1: inverse of data channel's dynamic time constant (break frequency, or bandwidth)

n_2: white noise

All these random terms can be assumed to have Gaussian distribution. The cross-coupling errors and time constants have nonzero mean values; the rest are zero mean. Installation errors, such as ground loops, are ignored because they are assumed to be removed during calibration.

There are several sources of phase lag due to dynamic effects (sensor response, high order prefilters, tape recorders) in each channel. However, these effects are assumed to be all lumped into one first-order lag represented by the inverse time constant f_1. This represents the overall dynamics of the specific channel.

The noise n_1 is assumed to be removed by filtering. Also, it is assumed that the time delay $e^{-s\tau_1}$ due to sequential sampling is removed in data processing, and quantization effects (Q) are negligible. The scale factor errors and biases are set large enough to encompass the effect of nonlinear type errors (e.g., threshold, hysteresis) and time-varying errors (e.g., power supply fluctuation). These assumptions and models are justified in the next section.

In this study, the aircraft state variables and their derivatives (such as y_1 in Fig. 1) that are measured are represented by the vector y. The effect of the dynamic lags in each of the parallel data channels is represented by the matrix F_m. It consists of a diagonal matrix with the inverse time constants (such as f_1) along the diagonal. If y_T is the true value of the vector y being measured, and if y_L is the lagged value, then these terms are related by the differential equation

$$\dot{y}_L = - F_m y_L + F_m y_T \quad ; \quad y_L(0) = y_T(0) \tag{1}$$

The scale factor errors and cross-coupling terms (such as ε_{11} and ε_{12}) are included in another matrix T. In T, the diagonal terms represent scale factor errors, and off-diagonal terms represent cross-coupling errors. Also, the bias terms and the noise (such as b_1 and n_2) are represented by vectors B and n, respectively. Then, the final indicated output vector y_I is described by the vector equation

$$y_I = Ty_L + B + n \qquad (2)$$

In the representation of the errors modeled by Eqs. (1) and (2), the dynamic error sources (F_m) are seen to precede the static error sources (T, B, n) in the order that they affect the data accuracy. This placement was done because it lowered the computation requirements of the ensemble analysis, as explained in the next chapter. For small errors which are assumed in using the ensemble analysis, it can be easily shown that the order is of no consequence on the results.

Now assume that the true control input is represented by the vector u. Also define

u_L = lagged control measurement due to dynamic effects of the measurement channel,

F_c = diagonal matrix whose elements are the inverse control measurement time constants,

T_c = diagonal matrix whose elements are control measurement scale factor errors,

B_c = control measurement bias vector, and

n_c = control measurement noise vector

Then, the measured control vector is related to the actual value by

$$\dot{u}_L = - F_c u_L + F_c u \; ; \quad u_L(0) = u \qquad (3)$$

$$u_I = T_c u_L + B_c + n_c \qquad (4)$$

Here, u_I is the indicated control input vector.

Equations (1)-(4) are the linear instrumentation error models used in this study. Details of the elements in these matrix error equations are presented in the next chapter. The range of values of the error sources (parameters in Eqs. (1)-(4)) are presented at the end of this chapter.

These simple models of the error sources are used in the subsequent analysis of error effects on parameter accuracy. They contain most of the elements required to determine the effect of different kinds of errors. The Monte Carlo analysis computer programs developed for this study (presented in the next chapter) are flexible such that if increased complexity of the models is desired, the programs can readily be changed.

Each of the various instruments, data processing elements, and the error sources which affect the recorded digital data are now discussed. The intent of this discussion is to justify the simple instrumentation error models represented by Eqs. (1)-(4) and to present the range of magnitudes of specific error sources. At the end of the chapter, these error magnitudes are summarized in tabular form. The exact form of the T matrix (Eq. (2)) for specific instruments studied is presented in the next chapter.

Sensor Errors

The largest contributions to the data errors are from the sensors used on the aircraft. These include the gyros, accelerometers, air data measurements, wind angle measurement, and control input measurement.

Gyroscope errors.- The basic transfer function of the gyroscope [8] is:

$$\frac{\theta_o(s)}{\omega_i(s)} = \frac{H}{Is^2 + Bs + K} \tag{5}$$

where $\theta_o(s)$ is the angular deflection of the output axis due to the angular rate $\omega_i(s)$ of the input axis. In Eq. (5), H is the gyro's angular momentum and I, B, and K are the inertia, damping coefficient, and spring constant which produce torque about the gyro input axis. If K is dominant compared to I and B, the instrument is a rate gyro and suitable to measure the roll, pitch and yaw rates (p, q, r) of the aircraft. For a typical rate gyro, the undamped natural frequency is 25 Hz and the damping ratio is 0.5. If K is negligible, the instrument is a rate integrating gyro which can be used to measure the aircraft roll, pitch, and yaw angles (φ, θ, ψ). A typical transfer gain (H/B) would be 0.05 with a time constant I/B of 0.001 sec.

Commonly known and modeled errors of a single degree-of-freedom gyro include:

1. Misalignment of the instrument with respect to the reference coordinate system of the aircraft (cross-coupling term between gyro measurements in three axes).

2. Mass unbalance (cross-coupling term between gyro and linear acceleration).

3. Anisoelasticity (nonlinear term; included in scale factor and bias).

4. Unequal spin and input axes float inertias (bias).

5. Kinematic rectification (noise term).

In addition, there are random output errors and errors in the output pickoff characterized as contributions due to resolution, null (bias), scale factor, and linearity inaccuracies. The scale factor can be directly proportional to the current frequency and voltage so it is susceptible to variations in the power supply.

Temperature change can affect the null point. Threshold and hysteresis effects are also present.

A good portion of the gyro error can be removed by careful calibration and subtracting the effects of known nonlinear terms. However, gyro models are not unique. Reference 9 presents ten different ways of modeling six different kinds of gyros to account for the presence of bias and nonlinear scale factor errors. It also demonstrates with recorded laboratory data the amount of variation that exists in gyro performance during day-to-day operation. Thus, the error magnitudes used in analysis must be set large enough to account for these uncertainties.

Table 1 presents the results of a survey of some typical rate gyros which are commercially available and which could be used for flight testing. The error sources are specified in either absolute sense ($\pm$ value given by manufacturer) or by standard deviation (1σ) based on laboratory testing. For absolute values, the actual error distributions are unknown; the $\pm$ absolute numbers given in Table 1 are assumed to be equal to twice the normal standard deviation (2σ). A great deal more manufacturers' data exists on specific gyro models. However, Table 1 is representative. In Table 1, the nonlinearity of the scale factor is assumed to be included in the linear scale factor error. The resolution error is included in the white noise, and the mass unbalance is modeled as cross-coupling between the rate and the linear acceleration along the gyro input axis.

From Eq. (5), it can be seen that the response of the gyros is modeled as a second-order system. Damping ratios for rate gyros typically range from 0.5 to 1; however, this number changes [10] with temperature and the viscosity of the gyro fluid, and it can be adjusted for individual requirements. The natural frequencies range from 20-100 Hz. For the gyro having a damping ratio of 0.7 and a natural frequency of 20 Hz, the output of the gyro for a 2 Hz input will have a phase lag of about 7°. This is reduced to 4°, if the natural frequency is 50 Hz.

The response of the rate integrating gyro is found by setting K to zero in Eq. (1). Thus, this system responds as an integrator with a first-order lag. A typical time constant (B/I) is 0.001 sec.

Table 2 presents the characteristics of representative rate integrating gyros. The predominant error is drift from the null position. Over the time span of a typical flight test data set, this would appear as an error which would grow with time. For drift of 15°/hr, this would be about a 0.13° change of the null point over a 30 sec time span. This is included in the bias term in the error model of Figure 1.

For the Systron Donner Model 5610 miniature attitude reference units, the quoted alignment of each sensing element in its case is $\pm$ 0.5°. The total sensor case alignment is highly dependent upon the procedures used when constructing the reference unit and mounting the package in the aircraft. Again, this misalignment is included as cross-coupling between rates about the input axes of each gyro.

Accelerometer errors.- For flight test purposes, linear accelerometers are used to measure the inertial acceleration along the longitudinal (Δa_x),

TABLE 1.- ACCURACY CHARACTERISTICS OF TYPICAL COMMERCIAL RATE GYROS
(Values Given are Manufacturers' ± Quotes Unless Noted)

TYPE	RANGE	BIAS	NOISE	NONLINEARITY OR SCALE FACTOR	RESOLUTION	MASS UNBALANCE	COMMENT
	deg/sec	deg/sec	deg/sec	% Full Scale	deg/sec	deg/sec g	
Timex SD-060	60	±.03-.12	±.18	± 2	±.01	±.05	a.
Sperry DG 312		.0011-.036		.04-.23			From Ref. [9] Numbers are 1σ
Northrup GI-G6		.015-.094		.07-.32			
Kearfott Alpha 2		.001-.003		.02-.09			
Kearfott T2010	40			±.5-1	±.04	±.01	
Systron Donner 8160	40	±.4		±1.0	$\pm.4 \times 10^{-3}$		b.
Lear Siegler	80	±.03	±.1				
Sperry	40	± .1	±.04	±2.5-5	±.04	±.05	

a. Scale factor proportional to voltage and power supply frequency
b. Scale factor and bias vary with temperature

TABLE 2.- ACCURACY CHARACTERISTICS OF TYPICAL COMMERCIAL RATE INTEGRATING GYROS

TYPE	LINEARITY %	DRIFT DEPENDENCE			
		DETERMINISTIC	g	g^2	RANDOM
		deg/hr	deg/hr/g	deg/hr/g^2	deg/hr
Timex IG 140	3	15	15	.5	3
Timex IG 140H	3	5	5	.5	1
Lear Siegler 1903HJ	.1	10	10	.5	.2
Kearfott Alpha	.01-.25	.1-.5	.3-.7	.01-.02	.02
Kearfott King	.02	.003	.2	.01	

lateral (Δa_y), and vertical (Δa_z) body axes. Angular accelerometers can be used to measure the time rate of change of roll, pitch, and yaw rates ($\dot{p}$, $\dot{q}$, $\dot{r}$). Two parallel linear accelerometers placed at opposite extremities of the aircraft can also be used to measure angular accelerations.

There are several types of linear accelerometers available including non-integrating, single-integrating and double-integrating types. For flight testing, the nonintegrating accelerometer is more appropriate. A typical steady-state error model [11] for an accelerometer expresses the output Δa as

$$\Delta a = D + H + k_o + k_1 a_1 + k_2 a_1^2 + k_3 a_1^3 + k_{12} a_2 + k_{13} a_3 + k_{41} T \qquad (6)$$

where

a_1 = acceleration along the input axis

a_2, a_3 = cross-axis acceleration components

T = difference between operating and calibration temperature

D = threshold in sensitivity to a_1

H = hysteresis in output for variation in a_1

k_0 = bias (different each time instrument is used)

k_1 = linear scale factor

k_2, k_3 = nonlinear terms

k_{12}, k_{13} = cross-axis sensitivity terms

k_{41} = temperature coefficient

The effects of k_2 and k_3 are included in the scale factor error of Figure 1. The terms k_{12} and k_{13} are cross coupling terms. The terms D, H, k_o and $k_{41}T$ are included in the bias and noise terms. Dynamic rectification effects also exist which are included in the white noise term. The natural frequency is typically greater than 50 Hz.

Table 3 presents values of the error magnitudes for typical linear accelerometers. Again, a great deal more manufacturers' data exists. Note in Table 3 that cross-coupling error is due to both misalignment of the instrument case and sensitivity of the instrument output to the perpendicular component of acceleration.

Another source of accelerometer error is due to the instruments not being mounted at the vehicle's center-of-gravity. This location error is typically calibrated out by the equation

$$\ddot{\bar{D}} = \ddot{\bar{R}}_m - \dot{\bar{\omega}} \times \bar{d} - \bar{\omega} \times (\bar{\omega} \times \bar{d}) \qquad (7)$$

TABLE 3.- ACCURACY CHARACTERISTICS OF TYPICAL COMMERCIAL LINEAR ACCELEROMETERS

TYPE	INPUT RANGE g	NONLINEARITY % FULL SCALE	ZERO OFFSET % FULL SCALE	RESOLUTION g	COMMENT
Timex AP-000	± 2.5	± 2	.05-.14	.0005	a.
Systron Donner 4310	±.5-±3.5	.05	.05	.001%	Noise = .05%
Lear Siegler		.2	.001g		b.
Sperry	± 1	.25	.0015g		c.
Lear Kistler 303T	± 3	±.05	±.02	.004	

a. Scale factor proportional to voltage and frequency

b. Noise = 33 μg, Cross-coupling = 10^{-5} g/g

c. Cross-coupling = .002 g/g, Cross alignment = ±.25°

Note that cross-coupling error is due to both misalignment of the instrument case and sensitivity of the instrument output to the perpendicular component of acceleration.

where

$\bar{\omega}^T = [p\ q\ r]$ - angular rate of aircraft

$\bar{d}^T = [x\ y\ z]$ - distance from c.g. to accelerometers

$\ddot{\bar{R}}_m$ = measured acceleration

$\ddot{\bar{D}}$ = acceleration of the c.g. which is the desired quantity to be determined

If, instead of the term $\bar{d}$, the term $(\bar{d} + \bar{d}_e)$ is used, where $\bar{d}_e$ is the error in the knowledge of $\bar{d}$, then errors in $\ddot{\bar{D}}$ are

$$\begin{aligned}
\ddot{D}_{ex} &= \dot{r}y_e - \dot{q}z_e + (q^2 + r^2)x_e - pqy_e - prz_e \\
\ddot{D}_{ey} &= \dot{p}z_e - \dot{r}x_e + (p^2 + r^2)y_e - pqx_e - qrz_e \\
\ddot{D}_{ez} &= \dot{q}x_e - \dot{p}y_e + (p^2 + q^2)z_e - prx_e - qry_e
\end{aligned} \tag{8}$$

These equations are decoupled and separated into lateral and longitudinal components for this study. Then, they reduce to

$$\begin{aligned}
\ddot{D}_{ex} &= -\dot{q}z_e + q^2x_e \\
\ddot{D}_{ey} &= \dot{p}z_e - \dot{r}x_e + y_e(p^2 + r^2) \\
\ddot{D}_{ez} &= \dot{q}x_e + z_e(q^2)
\end{aligned} \tag{9}$$

If the accelerometer location error components (x_e, y_e, z_e) are assumed to be one foot each for a typical aircraft response, then the linear terms in Eq. (9) are typically greater (for most aircraft maneuvers) in magnitude than the nonlinear terms by a factor of 30 or more. Thus, the nonlinear terms can be assumed to be negligible. The remaining terms are cross-coupling terms which relate the error in linear c.g. acceleration as a function of aircraft angular acceleration.

The angular accelerometer element operates on the force-balance principal with the seismic mass consisting of a nonmetallic liquid. In operation, this liquid mass tends to stay at rest when angularly disturbed. When coupled to an electromechanical device, it provides a measure of the force between the fluid at rest, and the changing attitude of the outside world. The method of detecting this relative motion consists of a paddle intersecting the toroid of fluid. The paddle is mechanically coupled to a torque motor, which is immersed in the fluid to eliminate mechanical seals. Standard servo force-balance techniques permit servo capture of the fluid mass to derive an angular acceleration signal.

Angular accelerometers are not as common as linear accelerometers, and their usage is more limited in flight test work. Because they are based on fluid

rotors, they are limited to low Mach number and medium to low altitude applications. One type, the Systron-Donner Model 4590 [10] has the characteristics presented in Table 4. Here, the temperature sensitivity, nonlinearity, hysteresis, and nonrepeatibility terms can be included as bias and scale factor errors. The resolution error can be included with the noise.

TABLE 4.- TYPICAL ANGULAR ACCELEROMETER CHARACTERISTICS
(FS: FULL SCALE)

Range: $\pm$ 1 rad/sec^2	Resolution: .001% FS
Bias: 0.05% FS	Noise: .07% FS RMS
Temp. Sensitivity: .03%/°F	Lin. Accel. Sensitivity: .2% FS/g
Non-linearity: 0.1% FS	Alignment: $\pm$ 1°
Hysteresis: 0.05% FS	Cross Axis Sensitivity:
Non-repeatability: 0.02% FS	0.01 rad/sec^2/rad/sec^2

As mentioned previously, some flight test centers use two parallel linear accelerometers mounted at the extremities of the aircraft to measure angular acceleration. In this case, the angular acceleration errors are a result of those basic to the linear accelerometers, the mounting uncertainty between the pair, and errors caused by flexure of the aircraft body. One test engineer reported that this procedure is not nearly as accurate as using the angular accelerometer. It was found that most test centers did not attempt to measure angular acceleration at all.

Air data errors.- An air data system typically consists of aerodynamic and thermodynamic sensors and a computer. The sensors measure the characteristics of the air surrounding the aircraft and convert them into electrical signals in specialized transducers. The computer calculates flight parameters such as true airspeed, free-stream static pressure, free-stream outside-air temperature and Mach number. The inputs required are static pressure (p_s), stagnation pressure (p_t), air temperature (T_s), and angle-of-attack (for supersonic aircraft.

Static pressure is measured through ports in the side of the fuselage or on a pitot-static tube. Because the air is moving past the aircraft, the pressure at various places on the aircraft's skin is different from the free-stream pressure by an amount called the static defect. The static defect depends on location, speed, altitude, and angle-of-attack. The measured reading also lags the actual value due to the time constant of the tubing leading to the transducer. A typical time constant is 0.25 sec. [11]

Stagnation pressure is measured with a tube that is open at the front and closed at the rear (pitot tube). In flight testing, the pitot tube is sometimes positioned or is servo driven to point into the relative wind.

To get an accurate air temperature measurement, a probe similar to a pitot tube is used. Impacting air is compressed to zero speed, causing total temperature to exist at the thermometer.

Mach number (M) is calculated, at subsonic speeds, from stagnation pressure and static pressure by using

$$M = \left(5 \left(\left(\frac{P_t}{P_s} \right)^{2/7} - 1 \right) \right)^{0.5} \tag{10}$$

The accuracy of the Mach number calculation thus depends on the accuracy of (p_t/p_s). In turn, the true airspeed (TAS or V) comes from combining Mach number and free-stream static air temperature, by the equation

$$V = M \sqrt{\gamma R T_s} = 38.967 \sqrt{T_s M} \tag{11}$$

Here, V is in knots, and T_s is in degrees Kelvin.

The transducers [11] which convert pressures and temperatures to voltages are the limiting factors in true airspeed accuracy. All air data systems measure static pressure and temperature. The third measurement may be either stagnation pressure (p_t) or dynamic pressure $(p_t - p_s)$. The transducers used are:

1. Displacement pressure - uses the expansion of an elastic diaphragm to produce a direct analog output.

2. Force-balance pressure - balances the diaphragm force against a calibrated standard.

3. Solid-state pressure - pressure difference deforms a crystal or semiconductor whose capacitance, output voltage, or change in resistance varies with pressure.

4. Temperature - variable resistance wire whose resistance increases approximately linearly with temperature.

On the STOLAND system [13], the air data system produced airspeed accuracies of $\pm$ 0.375 kts due to hysteresis, $\pm$ 0.25 kts due to resolution, and $\pm$ 0.05 kts due to repeatability errors at 60 kts airspeed. Wolowicz [14] reported large static pressure errors for angle-of-sideslip greater than 3°. Also, there is a Mach number calibration which is a function of Mach number and the ratio of the boom length to the fuselage diameter. For subsonic flow, this error varies from 3% to 5%, and it acts as a bias. However, this can be mostly calibrated. Also, there is up to $\pm$ 2% scatter in calibration data. As can be seen in Eq. (11), this Mach number scatter directly affects the accuracy of the calibrated airspeed.

From the above material, the scale factor error of typical low speed airspeed measurements is seen to be about 2%. Bias and noise have standard devia-

tions of about 0.5 kt (0.85 ft/sec). This accuracy deteriorates near the ground as is discussed later.

Angle-of-attack and sideslip measurement errors.- There are two methods commonly used to measure angle-of-attack and angle-of-sideslip. These are with vanes [14] and with differential pressure heads [15]. Both sensors are normally mounted on nose booms, although wing booms and fuselage mounting are sometimes used.

The wind vane typically has a natural frequency of 10 Hz with a damping ratio of 0.7. Vanes are subject to the following set of static errors.

1. Boom bending - components of this are proportional to normal acceleration (Δa_z), pitch acceleration ($\Delta \dot{q}$), and aerodynamic load ($\Delta\alpha$). The first two are cross coupling errors and the latter acts like a scale factor error.

2. Upwash - components are due to the geometry of the vane location with respect to the wing, fuselage, and boom. These terms are proportional to $\Delta\alpha$ and thus act as scale factor errors.

3. Pitching velocity - proportional to Δq so this acts as a cross coupling error to angle-of-attack. The error is

$$\Delta\alpha_e = \frac{x_v \Delta q}{V} \tag{12}$$

where x_v is the distance from the c.g. to the boom and V is the airspeed. Reference 8 gives this term as

$$\Delta\alpha_e = \frac{x_v g \Delta n_z}{V^2} + \frac{x_v \Delta\dot{\alpha}}{V} \tag{13}$$

which is equivalent.

4. Vane asymmetry - acts like a bias term.

5. Vane misalignment - acts like a bias term.

Most of these terms can be effectively calibrated out of the data. The largest correction is usually the total upwash correction which may be as large as 20% of the total reading for an aircraft traveling at high subsonic speeds. The smallest the upwash correction can practically be is about 4% [16]. Upwash effects are often removed by use of calibration curves, which are functions of vane position geometry; examples appear in Ref. 17.

The sideslip angle will have errors due to rolling and yawing velocities (Δp, Δr). Other error sources of the vanes are: (1) the phase lag between when a gust hits a vane and when it affects the aircraft [18], (2) phase lag of the recorder [14], (3) wing and fin twist and deflection [15], and ineffectiveness at low speed [2].

Differential pressure devices used to measure angle-of-attack and sideslip have additional error sources [15]. The angle-of-attack reading is affected by rolling velocity if the pressure head is mounted off the longitudinal axis of the aircraft. In addition, erroneous readings are caused by deviations from constant altitude and unaccelerated flight. These terms can be calibrated by putting the aircraft in steady climb and constant longitudinal acceleration conditions. Also, Gilyard [19] has found large discrepancies between the analytically determined dynamic lag of α and β sensors and lags experienced in flight test. This difference has been greatest for high Mach numbers.

Reference 2 states that for the XC-142A flight test program, there was a $\pm 0.7°$ scatter in the differential pressure data and a $\pm 1.25°$ scatter for vane data at cruise airspeed. At lower airspeeds, the data had worse scatter, and below 50 kts, the data were considered unreliable. The scatter is modeled as a combination of scale factor error, bias error, and noise.

There are two types of cross-coupling errors that can arise due to the above mentioned known error sources--to ignore the error sources or to account for them incorrectly. For example, from Eq. (12), if both vane location and c.g. location are precisely known and accounted for, there is no error. However, if the actual value of x_v is different from that used in the correction, or if no correction is made, an error in the measurement results. The error in x_v is thus divided into two parts, the error in knowledge of the vane location (ε_{vx}) and the error in knowledge of the c.g. location (ε_{cgx}). The separation of the contributions is made because vane location uncertainty only affects the $\Delta\alpha$ correction, while c.g. location uncertainties affect accelerometer corrections as well.

Control input measurement error.- The common way used to measure control inputs is by use of control position transducers (CPT). These consist of potentiometers with their setting spring loaded and attached to cables. The other end of the cables are attached to the control surface, linkage, or input device (stick, pedal) whose movement is to be measured. The linear or angular movement of the mechanical device translates into linear movement of the cable. This, in turn, translates into angular setting on the potentiometer.

The accuracy of the CPT reading is dependent on several factors. Actual control surface deflection may not be easy to measure; this is based on the construction of the aircraft and having a suitable place to mount the potentiometer. If the movement of a mechanical linkage leading to the surface is measured, error will be introduced by the reactions at the joints. Thus, the further the measurement is made from the actual control surface, the greater the error will be due to stiction, hysteresis, and threshold effects. A chief problem of these effects is the time lag between when a linkage movement is measured and when the control surface actually moves. This produces an effect where the control input measurement leads the actual control surface deflection. In terms of the block diagram of Figure 1, this lead effect would be represented by each of the other sensor output measurements having a greater phase lag than those of the control measurements. For analysis of high-frequency dynamics, this can produce significant error.

On the helicopter, the control input is measured in terms of the deflections of the swash plate. Because the control input is the integral of aerodynamic forces on the rotor blades during each cycle, the swash plate movement occurs before the net control effect is realized. To deduce what the control input precisely is (in terms of aerodynamic control forces and moments applied to the helicopter), the CPT reading must be processed with blade position information and the dynamic equations which represent the relationship of swash plate deflection and rotor movement. This must be carefully done, or the control input measurement will tend to be out of phase with the actual resultant dynamic output measurements.

If a stability augmentation system is operating in the aircraft, the actual control input will be the sum of automatic and manual inputs. Thus, the CPT must be mounted to measure total control input rather than just those inputs due to manual control (stick position).

The CPT is statically calibrated before flight by mounting a jig to the control surface and measuring its movement, as related to the CPT reading. The results are usually very repeatable. Calibration is normally repeated after flight. However, the control-surface can deflect somewhat differently in flight than on the ground due to aerodynamic loads. There will be linkage vibration and surface flutter that also will be measured. The CPT cable will have some flexing. One CPT build by Space Age Control has a range of $\pm$ 1.5 in. and an accuracy of $\pm$ 2% (scale factor).

Effects of Sampling, Digitizing, Recording, and Processing Flight Data

There are several ways in which the sensor data just described are processed before being used for identification of stability and control derivatives. Each method has its unique set of additional error sources and inherent accuracy of the data. In flight test investigations of small aircraft where the instrumentation volume is a problem or a situation where the number of parameters recorded may constitute a serious time lag in the recovery of the data, sophisticated data acquisition systems are used. Data acquisition systems are capable of handling the data to reasonable accuracy (0.1% to 1%) [14]. The pulse code modulation (PCM) procedure converts the analog signal from the sensor to digital format and records the digitized data on tape on a time-sharing basis. The errors in the digital data are modeled by the noise term n_2 in Figure 1.

Figure 2(a) shows a schematic drawing of a typical airborne PCM system. The analog signals from the sensors go to a PCM encoder to convert the signal to an identification coded, digitized format. The coded, digitized signals are then recorded in parallel on an onboard tape recorder on a time-sharing basis. To recover the data, the taped signals are processed through PCM decommutation, which unscrambles the individual sensor signals, to a format computer to provide real time data outputs in the form of strip charts or oscillograph readouts for an immediate look at the data. The real time data are also transmitted to a general-purpose computer which tabulates, plots, or performs analyses of the data.

Figure 2(b) shows a schematic drawing of the PCM system using telemetry. The main differences between the telemetered and airborne PCM systems involves the transmission of the coded, digitized signals in series to the decommutator

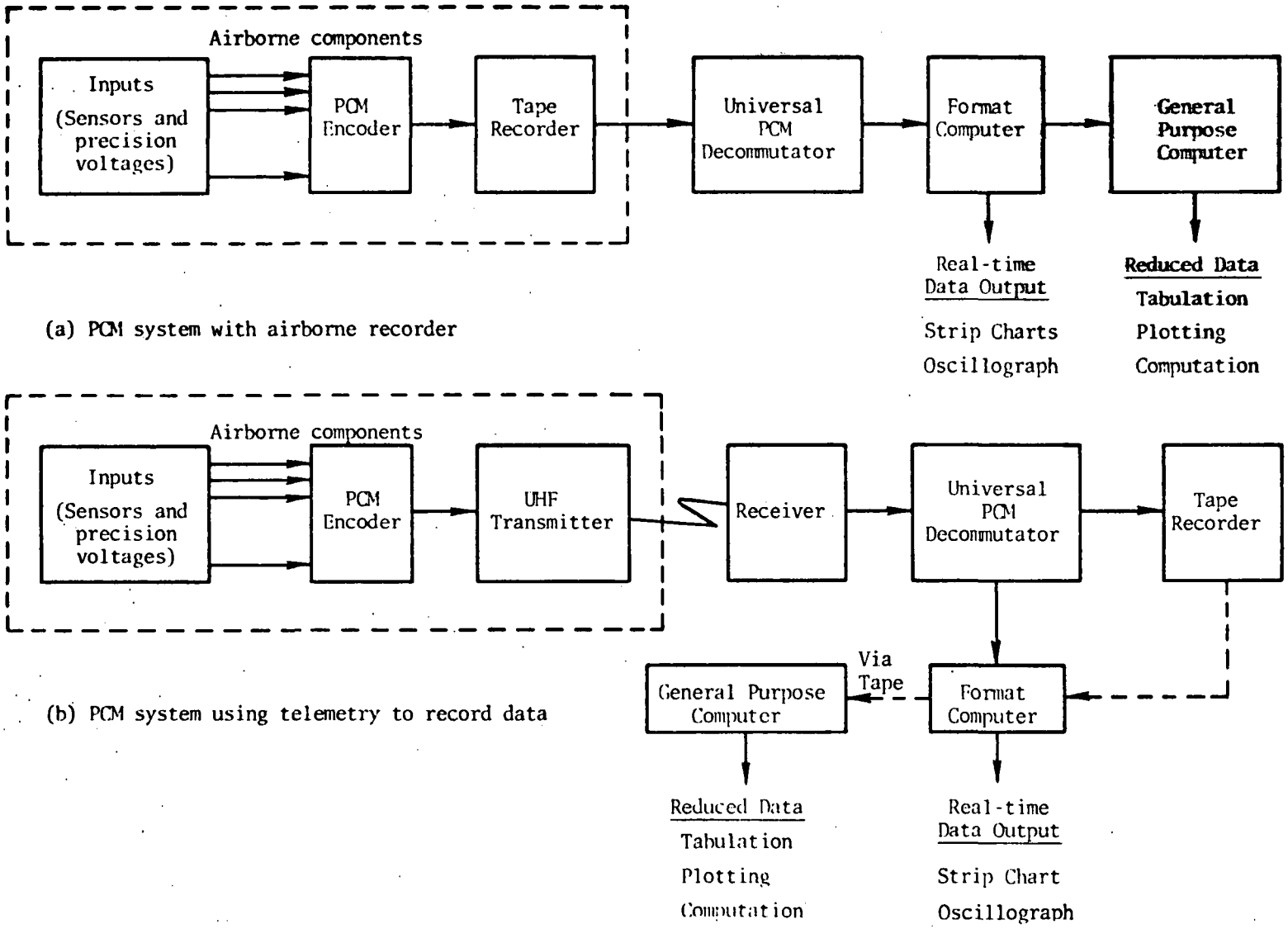

FIGURE 2.- FUNCTIONAL SCHEMATICS OF PULSE CODE MODULATION (PCM) DATA ACQUISITION SYSTEMS [6]

(instead of parallel to the recorder); this requires time synchronization of the signals before the signals are taped. Errors in the time synchronization are modeled as different time delays τ_1 in each data channel as depicted in Figure 1. In processing the data, the format computer identifies the individual data channels for real time data output.

In response to the increasing complexity and faster turnaround required, several real time test support systems have been built [20-22]. Each of these systems could be described as telemetry ground stations used in conjunction with a small computer preprocessor feeding a larger digital computer. A typical system is the Naval Air Test Center (NATC) Real Time Telemetry Processing System (RTPS), which was developed to allow data analysis to take place between maneuvers during a single flight [23].

The RTPS provides data flow as indicated by Figure 3. All of the indicated functions are integrated into a single facility except for position measurement (range) radar and remote telemetry antennas; these are connected to the RTPS by microwave link.

Test data enters the system by way of telemetry antennas or onboard instrumentation tape and proceeds in serial digital and/or analog form to the Telemetry Decoding Subsystem. In the case of telemetry (in-flight) data collection, all of the received data is recorded on wideband analog tape for backup in case of system malfunction and for further potential analysis. Having been demodulated from frequency or pulse-code modulation (FM or PCM), the data are transferred with time and quality information to the Data Channel Subsystem. In the Data Channel, all measurements are reduced to digital form, linearized, scaled to engineering units, limit checked, time-tagged, merged on a block basis, and recorded. A selected portion of the total Data Channel output is routed to the Real Time Computation Subsystem. Following correlation with range data (if required) and selection for display formatting, the processed results are displayed in the Project Engineer Station for evaluation.

At most flight test centers, the data collected is batch processed rather than in real time. At all centers, problems arise due to sampling, digitizing, commutating, and filtering the data. Problems of spikes or dropped points in the data due to sampling and commutation are common. Thus, procedures are required to insert valid data points by interpolation.

A special problem of sampling continuous data is that of aliasing. The data spectrum is considered to be virtually bandlimited if the frequency content above a certain frequency ω_o is small and presumably unimportant for conveying the information. For aircraft data, there will always be some higher frequency content due to vibrations, flutter, and power supply frequency. When such data are sampled, there will be unavoidable overlapping of spectral components. In reconstruction, frequencies originally outside the nominal band will appear at the filter output in the form of much lower frequencies. Thus, for example, the frequency $\omega_1 > \omega_0$ is measured as $\omega_s - \omega_1 < \omega_0$, where ω_s is the sampling frequency. This phenomena of downward frequency transition occurs whenever a frequency component is undersampled.

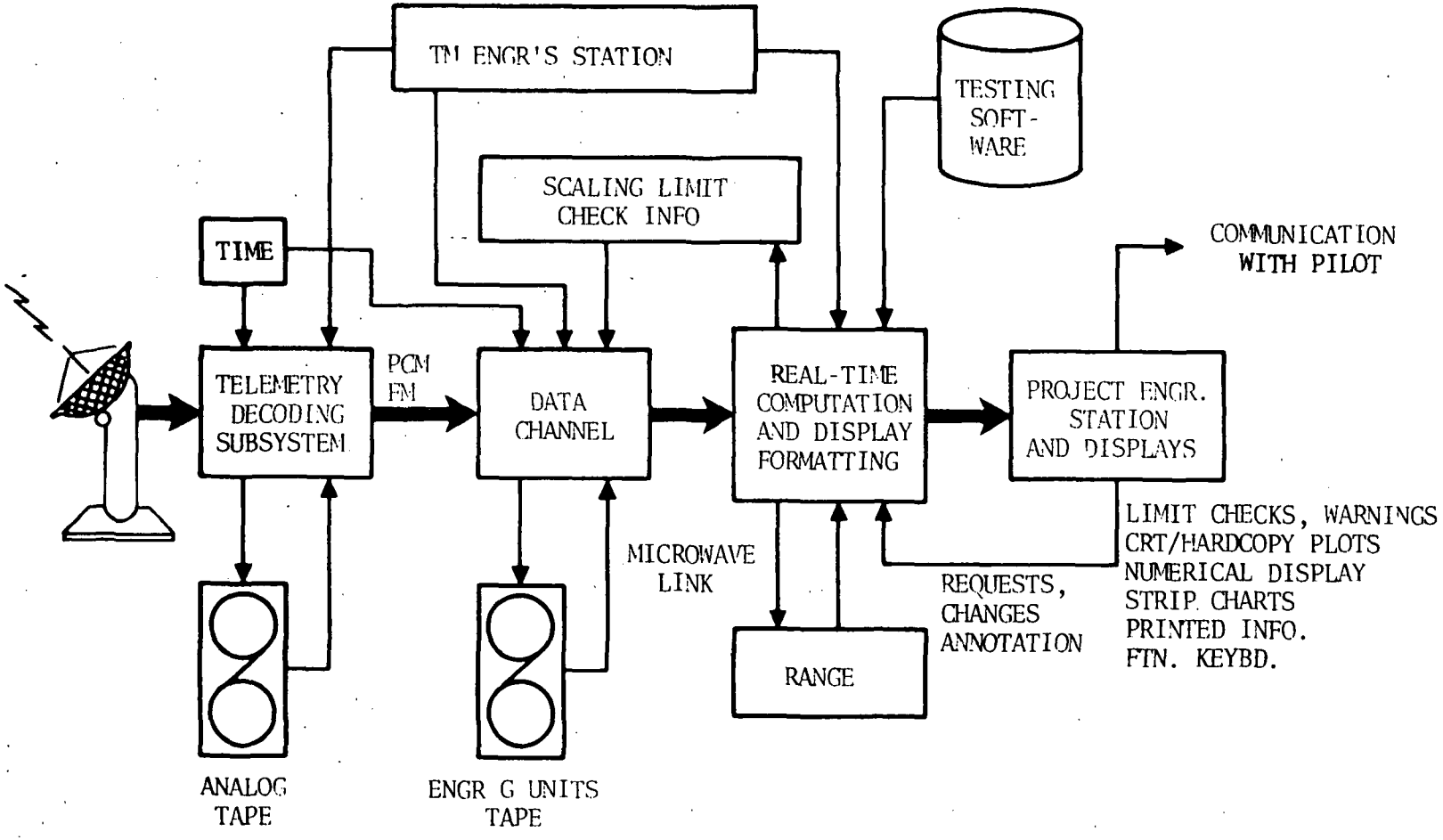

FIGURE 3.- DATA FLOW OF A TYPICAL REAL TIME FLIGHT TEST SUPPORT SYSTEM

The effect of aliasing is diminished by filtering the data as much as possible before sampling and sampling at much greater than the nominal Nyquist rate. Reference 2 presented detailed design specifications for prefilters which could be in a typical V/STOL flight test program. In order to preclude the injection of sensor response to spurious frequencies into the multiplexer/encoder, with a possible consequence of aliased data, a group of presample low-pass filters were included as part of the analog signal-processing chain.

The introduction of prefilters into the data processing sequence introduces another possible error source--unequal phase lags for each variable measured. The phase lag is represented by the constant f, in Figure 1. These lags are in addition to those caused by the normal response of the sensors and tape recorders. Attempts are usually made to adjust the filter parameters so the response is equal for all variables. Phase compensation is also done using software when calibrating the data before use in the parameter identification procedure. The phase lag due to data filtering must be combined with the inherent lags of the sensors and recording equipment to obtain the overall effect. Preflight calibration is usually required to determine what the overall lag is.

Another error source already mentioned is introduced because of the sequential sampling of the data variables. That is, each variable is sampled in turn for multiplexing, and then interpolation must be used later to determine the variables' magnitudes at the same time points. This is especially critical for studies of vehicles at high Mach numbers where buffeting, flutter, and other nonrigid behavior are being analyzed. It also becomes important when any of the sensor readings have information content concerning the vibrational environment that they are in.

Two other error sources which are convenient to consider together are the effects of white noise and data quantization on the error in the data finally used for parameter identification. The white noise comes from many sources in the data measurement and handling process. To some extent, it is limited by data filtering, but filtering also can remove useful information. The noise is typically modeled as having a Gaussian distribution with zero mean and standard deviation of σ.

The quantization error comes from digitizing the data for telemetry and numerical evaluation on the digital computer. This type of error affects the output of the multiplexer/encoder [2]. Quantization noise is uniformly distributed with bounds of $\pm 0.5Q$, where Q is b^{-m}; here, b is the radix of the encoding number system and m is the number of code elements used to express a measurement digitally. The RMS value of such quantization noise is $b^{-m}/2\sqrt{3}$. In a multichannel system having a large number of components, such errors can be treated as random. Other multiplexer/encoder errors having Gaussian distribution include effects of source impedance, back current, offsets, gain stability, sample and hold, drifts, and linearity.

The probability distribution of the error e in a signal, first contaminated by noise y of distribution $p_y(y)$ and then quantized, is [24],

$$p(e) = \int_{e-0.5}^{e+0.5} p_y(y)\, dy \tag{14}$$

After normalization in units of σ, this becomes

$$p(e/\sigma) \triangleq p(e') = \frac{1}{Q/\sigma} \int_{e'-0.5\,Q/\sigma}^{e'+0.5\,Q/\sigma} p_{y'}(y')\, dy' \tag{15}$$

For $p_y(y)$ being Gaussian, Eq. (11) can be integrated to produce the family of curves shown in normalized form in Figure 4. It is clear from these curves that

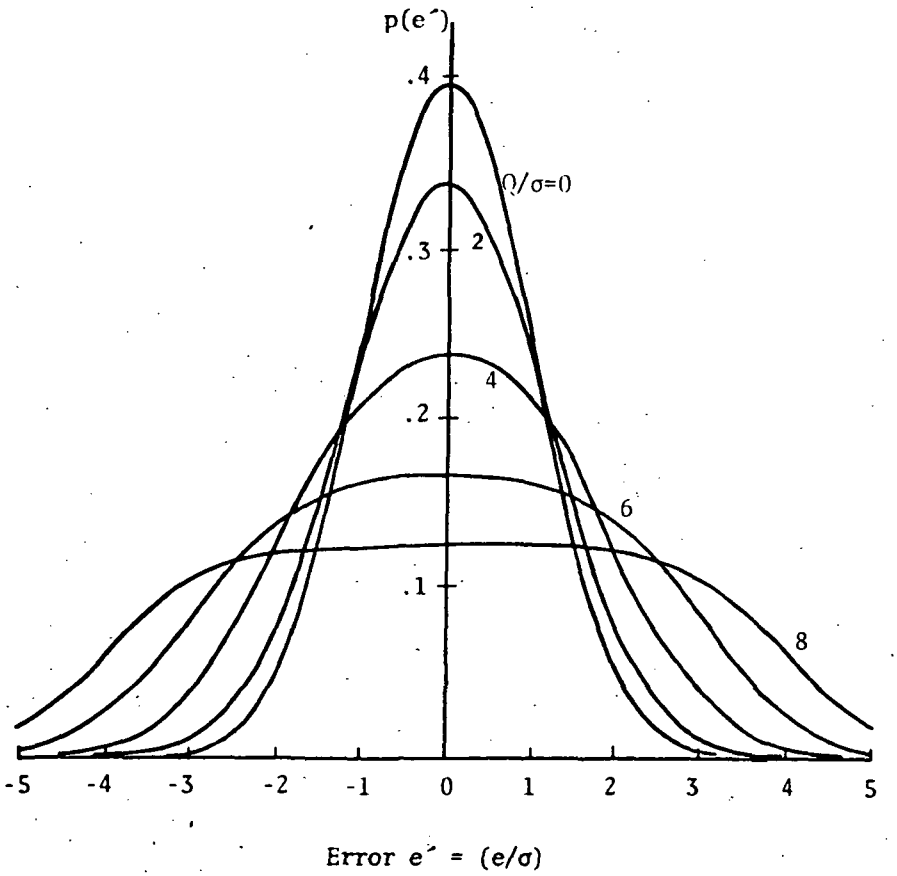

FIGURE 4.- DISTRIBUTION OF SIGNAL ERROR $e' = (e/\sigma)$ DUE TO COMBINED QUANTIZATION AND CONTAMINATION BY WHITE NOISE

the distribution becomes uniform as Q/σ increases, and for $Q/\sigma = 0$, the distribution is Gaussian. These curves are useful in determining the nature of the error characteristics due to the combined presence of noise and quantization. They also can be used to determine the level of confidence in which the error of a signal is bounded between certain values. Finally, they can be used to determine the minimum number of quantization steps required to produce a given signal quality.

The quantization level is set by the bit length of each recorded data point. This length is usually equal to or greater than eight bits. For a noise level of 1% full scale, this produces the Q/σ ratio to be on the order of 0.5 or less. Thus, as can be seen from Fig. 4, the distribution remains nearly Gaussian, and the quantization effects can be ignored.

General Observations of Instrumentation Procedures

Some general observations are now made concerning the instrumentation procedures followed at various flight test facilities. The intent here is to point out further the variations in test conditions, calibration procedures, and instrumentation accuracy found at different centers. The significance is that there is no uniformity to flight test instrumentation used. It is thus important that the engineer interested in identification of stability and control derivatives become familiar with the specific procedures of the test facility used so that the identified parameter accuracy may be ascertained. Procedures used include the following:

1. Instrumentation systems are generally designed so that frequency response is flat from zero up to 6-60 Hz. Prefiltering tends to eliminate frequency content of analog signals above these values. However, aliasing problems do exist. Lags are compensated for during data processing. However, an attempt is made to match the phase lag in all prefilters.

2. Great care is normally taken to mount the inertial instruments with their input axes perpendicular on pallets. However, the pallets are aligned in the aircraft with instruments ranging from a steel rule to a laser beam.

3. Attempts are made to design problems such as ground loops, power supply fluctuation, and time delay out of the system. Instrumentation voltage is typically monitored, and the associated scale factor error can be compensated for during data processing. Other data error sources include temperature variation, pressure variation, and RFI effects on telemetry. The chief installation problem is the presence of ground loops; however, they are usually easy to detect.

4. Test engineers may or may not specify instrumentation accuracy. When the instrumentation is specified, it consists of variables to be measured and their range, resolution, and frequency response. However, the actual system accuracy is usually based on what instrumentation is available, with appropriate compromises being made. If the data accuracies aren't specified, the test engineer chooses the

weighting matrix of his identification algorithm to correspond to the noisiness of the measured data.

5. All instruments are lab tested prior to their use to verify that they meet specification. Deviation plots are made for use in calibration after flight. Calibration of the PCM system is done prior to and after each flight for all movable sensors (surface deflections, pressure, temperature). Readings are taken and used for calibration and correction of data. The static errors (sensor calibration curves, digitization error, sampling delay, recorder error) are generally known at each stage of the data processing. However, it is difficult to remove the net effect of all these errors.

6. The PCM systems sample at rates from 0.4 to 200 sps. Words are 9 or more bits long. Up to 120 sec lengths of data are used for identification purposes.

7. Various techniques are used to compute the aircraft inertias and center of gravity position. The c.g. can move up to 30 inches during flight. The values of c.g. position used for identification vary from a single estimated point to continuously varying values which account for fuel burnoff.

8. Angular accelerometers are seldom used because of expense and failure at high Mach number. When they have been used, the results have been good. Sometimes parallel linear accelerometers are used to obtain angular acceleration. Otherwise, angular acceleration measures come from differentiating the measured angular rates.

9. The largest instrument lag is in the response of static and total pressure measurements. This is sometimes calibrated by measuring aircraft position with radar. In the B-70 program [25], lags of up to one minute were noted, in the response of the angle-of-attack sensors. Modification of pressure measurements are made for errors due to geometry, Mach number, flow angularity, and Reynolds number effects using flight, wind tunnel, and theoretical calibration values.

10. Flow angularity (α,β) corrections are made for geometry, boom bending, upwash, dynamic lags, vane floating, aerodynamic loads, and effects of pitch velocity and acceleration. A typical boom oscillation of $\pm$ 0.6 in. converts to $\pm$ 1.7° in angle-of-attack reading.

11. Pilots typically cycle the control inputs through maximum deflection at the beginning and end of each flight test. The data is used for CPT calibration. For helicopter flight test, the CPTs have been used to measure stick and swash plate movement.

This list of comments regarding flight test instrumentation could be extended. Many more details could be obtained from each of the flight test centers for each aircraft tested. In summary, many sources of error exist, many individuals are involved in the calibration and testing process (each having a different point of view), and few specific conclusions can be made concerning instrumentation prac-

tices followed at each flight test facility. The recommendation to the engineer using the data is to be aware of the error sources, their characteristics, and their magnitudes. Then models such as the one shown in Figure 1 can be used to determine the effect on the accuracy of the derived parameters. How this is done is the subject of the next chapter. But first it is necessary to summarize the range of parameter magnitudes which make up these error models.

Range of Error Magnitudes

In order to study the quantitative effects of instrument errors, numerical values of the parameters in the error models must be known. Ranges of values of typical instrumentation errors are presented in Table 5. These numbers represent statistical variations; they are based on summarizing absolute values given in Tables 1-3, other results of this chapter, and conversations with several individuals. Manufacturers' absolute accuracy ranges were assumed to be $\pm 2\sigma$ values which provides a conservative estimate of the instrument quality available. The random numbers are assumed to have Gaussian distribution, unless otherwise stated.

The values for the range of errors given in Table 5 represent the author's best judgments of the state of typical flight test instrumentation accuracy based on available information. There exist considerable manufacturers' data on available accuracies of rate gyros, rate integrating gyros, and linear accelerometers. Thus, the numerical values for the first three rows of Table 5 have the most supporting verification. Generally, test center laboratory calibration of gyros and accelerometers confirm manufacturers' claims; thus, manufacturers' specifications have a high probability of being correct.

The accuracy of wind angularity and airspeed measurements is less well known because of the uncertainty of environmental effects (mostly aerodynamic). A great deal of time is spent at test centers determining empirical models of the output of these instruments, and the accuracy is highly dependent on the aircraft, mounting position, and flight regime. The range of values presented in rows 5 and 6 in Table 5 was deduced based on review of calibration documentation and conversations held with several test engineers.

The instruments whose accuracies are least known are the angular accelerometer and the control position transducer (CPT). Angular accelerometers are seldom used and only limited manufacturers data exists on them. The results in row 4 of Table 5 are based on conservative generalization of the values presented in Table 4. The CPT's accuracy is highly dependent on where it is mounted on the control linkage, so it is very aircraft-dependent. There was a general reluctance on the test engineer's part to quote any specific accuracy values for the CPT output. Thus, the numbers presented in row 7 of Table 5 are based largely on what seems reasonable based on the CPT discussion presented earlier.

The numbers presented in Table 5 are the range of the instruments' outputs, noise, bias, scale factor, and typical cross coupling terms. From these values, a set of numbers can be selected to model a typical instrument set. Table 5 was used to select typical error magnitudes for the error analysis which was conducted in this study. The results are presented in the fourth chapter along with a discussion of the relative importance of each of the error sources.

TABLE 5.- FLIGHT TEST INSTRUMENTS AND THEIR RANGE OF ERROR MAGNITUDES

	Instrument/Device	Units	Full Scale Deflection	Random Noise (1σ)	Random Bias (1σ)	Random Scale Factor (1σ)	Cross Coupling Errors Other Errors (1σ)
1	Rate Gyros - p,q,r	°/sec	30-60	0.001-0.3	0.001-0.3	0.01-2.0	Mass Unbalance (°/sec-g): 0.01-0.1 Misalignment (°): 0.1-1.0
2	Rate Integrating Gryos - ϕ,θ,ψ	°	30-360	0.01-0.2	0.01-0.2	0.01-1.5	Misalignment (°): 0.1-1.0
3	Linear Accelerometer - $n_{x,y,z}$	g	0.5-3	0.001-0.7	0.001-0.003	0.025-1.0	Misalignment (°): 0.1-1.0 c.g. Uncertainty (ft): 0.25-1.0 Cross Axis Sensitivity (g/g): 0.001-0.005
4	Angular Accelerometer - $\dot{p},\dot{q},\dot{r}$	°/sec^2	60	0.05-0.1	0.05-0.1	0.1-0.2	Misalignment (°): 1.0 g. Sensitivity (%/g): 0.2-1.0 Cross Axis Sensitivity (-): 0.01
5	Wind Angularity (Vane) - α,β	°	$\pm$ 20	0.01-0.4	0.01-0.4	0.05-0.5	Angular Rate Sensitivity (°/°/sec): $\sim q$ Inertial Loads (°/g)
6	Airdata System u	ft/sec	1000	0.5-0.5	0.5-0.5	0.025V	Computed from Pressure and Temperature Time Constant: 0.25-10 sec
7	Control Inputs (CPT) - $\delta_e,\delta_c,\delta_r,\delta_a$	°, in	$\pm$ 30° $\pm$ 10 in	0.1-0.3° 0.05-0.15in	0.1-0.3° 0.05-0.15 in	2 0.5-2	Measure of Surface Deflection or Linkage

In addition to Table 5, the following three important sources of error are present:

Data channel dynamics bandwidth: 6-60 sec^{-1} ($\pm$ 5% 1σ)

Sample rate: 0.4-200 sps

Analog/digital handling noise: 0.2-1.0% Full Scale

Again, the values used in the study and the associated results are presented in the fourth chapter.

ERROR ANALYSIS TECHNIQUES

Two techniques are presented in this section to determine quantitatively the parameter variations which would result from using an output error identification algorithm in the presence of unmodeled instrument errors. These techniques were previously presented in Reference 5 and are extended here. The entire set of equations are presented for completeness. It is assumed that the identification algorithm is convergent and that it tends to minimize a quadratic function of the difference between actual and estimated aircraft trajectory measurements. The modified Newton-Raphson identification algorithm is specifically used.

Modified Newton-Raphson Parameter Identification Process

The modified Newton-Raphson algorithm [24] is essentially one of several output error identification methods which are used. This basic identification process is illustrated in Figure 5. The algorithm's objective is to choose parameters $\hat{p}$ of a mathematical model of the aircraft so that the difference between the output measurements of the model and the actual aircraft are minimized. With no measurement errors, external disturbances, or model structure inaccuracies, the output errors are minimized when the model parameters equal those of the aircraft. Output error identification methods have the following characteristics:

1. they require good initial estimates of the aircraft states and the parameters;
2. they give unbiased estimates in the presence of zero mean white measurement noise;
3. they can be used for identifying the parameters of aircraft with both linear and nonlinear equations of motion; and
4. they do not work well in the presence of random disturbances to the dynamics (process noise).

In this study, the aircraft equations of motion (used for simulation and estimation purposes), as perturbed from the nominal flight path, are assumed to be linear with constant coefficients. These equations are of the form

$$\dot{x} = F(p)x + G(p)u \quad ; \quad x(0) = x_o \tag{16}$$

where

$x \triangleq$ aircraft state vector

$u \triangleq$ control input vector

$F(p) \triangleq$ system dynamics matrix containing some of the unknown parameters p

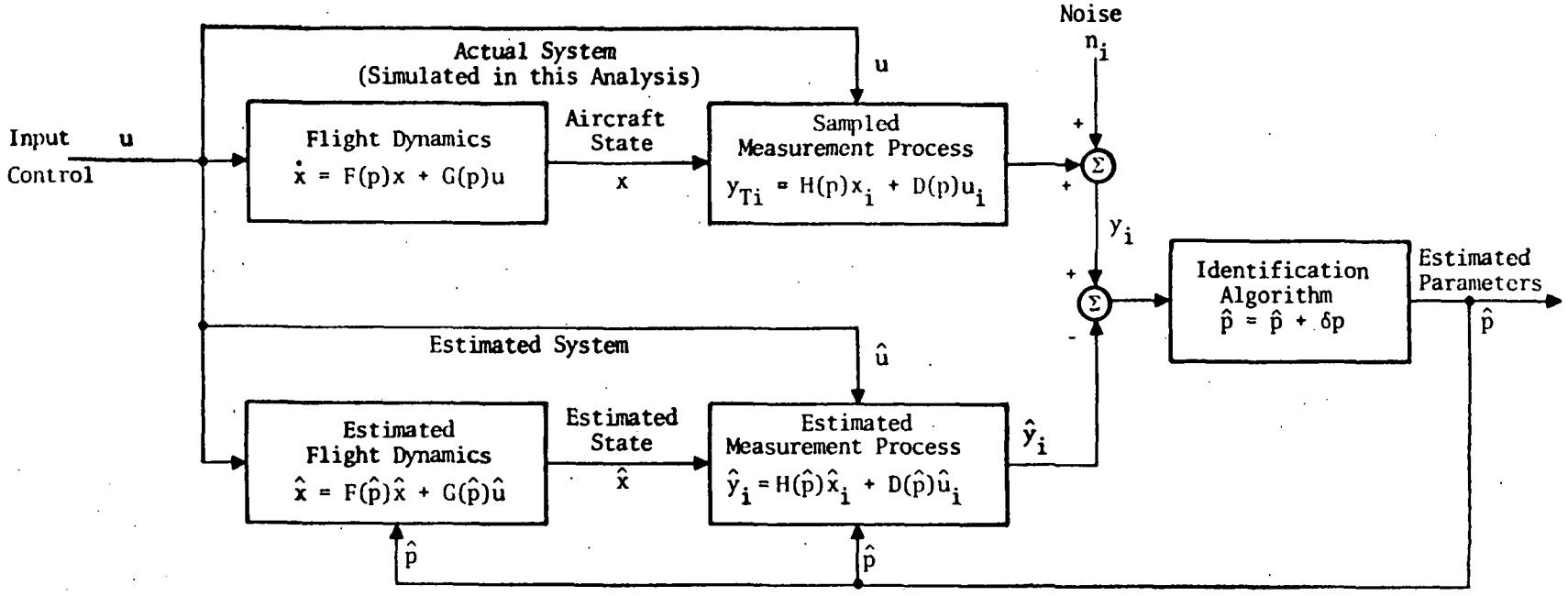

FIGURE 5.- THE OUTPUT ERROR IDENTIFICATION PROCESS

$G(p) \triangleq$ control distribution matrix containing the other unknown parameters

For simulating linear feedback control, the matrix F in Eq. (16) is replaced by $F-GC$, where C is a matrix of constant gains. This variation will be discussed further, later. The identification process identifies the parameters of F and G. If some of the parameters are well known, they can be treated as constants in F and G and removed from the vector p.

The output y of this system consists of measurements of the elements of x and $\dot{x}$. It is modeled as a sampled process by the equation

$$y_i = H(p)x_i + D(p)\ u_i + n_i \tag{17}$$

where H and D are other constant-coefficient matrices also containing elements of p. Again, with feedback control, H in Eq. (17) is replaced by $H-DC$. The vector n_i is contaminating noise. The subscript i indicates that the output is sampled at time i and processed by a digital computer.

The estimated equations of aircraft motion are of the same order and form as Eqs. (16) and (17), and they are represented by

$$\dot{\hat{x}} = F(\hat{p})\ \hat{x} + G(\hat{p})\ \hat{u} \quad ; \quad \hat{x}(0) = \hat{x}_o \tag{18}$$

Here, $F(\hat{p})$ and $G(\hat{p})$ are formed by using the estimated parameters $\hat{p}$. The state $\hat{x}$ comes from integrating Eq. (18) and using the measurements of u denoted by $\hat{u}$. The estimated output equation is

$$\hat{y}_i = H(\hat{p})\ \hat{x}_i + D(\hat{p})\ \hat{u}_i \tag{19}$$

If $\hat{p}$ equals p, $\hat{u} = u$, and $\hat{x}_o = x_o$, the only difference between y_i and $\hat{y}_i$ is due to the measurement noise n_i. In the Newton-Raphson identification scheme, it is assumed that n_i is a sequence of zero mean white noise vectors with the covariance matrix

$$E\{n_i\ n_j^T\} = R\delta_{ij} \tag{20}$$

Furthermore, it is assumed that the elements of n_i are independent so that R is a diagonal matrix.

The Newton-Raphson identification technique chooses parameters $\hat{p}$ which minimize the performance index or cost function

$$J = \sum_{i=1}^{N} (y_i - \hat{y}_i)^T\ R^{-1}\ (\hat{y}_i - \hat{y}_i) \tag{21}$$

where N is the number of points collected in the measurement sequence. This is done by iteratively applying the equation

$$p_{k+1} = p_k - \left[\frac{\partial^2 J}{\partial p^2}\right]^{-1} \frac{\partial J^T}{\partial p} \tag{22}$$

In some identification algorithms, the matrix R in Eq. (21) is fixed, based on the assumed value of the covariance matrix of the white noise. In other algorithms, R is iteratively computed from the recorded innovations sequence $(y_i - \hat{y})$. When the updated parameters estimates $\hat{p}_{k+1}$ are computed in Eq. (22), they are used again in Eqs. (18) and (19), to produce a new output estimate $\hat{y}_{k+1}$. The new R matrix is then computed, based on Eq. (20). This is done by first computing a mean value from $(y_i - \hat{y}_i)$, as follows:

$$\Delta y_m = \frac{1}{N} \sum_{i=1}^{N} (y_i - \hat{y}_i) \tag{23}$$

This is then used to compute the diagonal covariance estimate, as

$$R = \frac{1}{N} \sum_{i=1}^{N} (y_i - \hat{y}_i - \Delta y_m)^2 \tag{24}$$

In this study, it is assumed that the appropriate value of the covariance matrix R is known and correctly used in the cost function J. Thus, R is not updated, and Eqs. (23) and (24) are not used.

The first partial of J with respect to p is, from Eq. (21),

$$\frac{\partial J}{\partial p} = -2 \sum_{i=1}^{N} (y_i - \hat{y}_i)^T R^{-1} \frac{\partial \hat{y}_i}{\partial p} \tag{25}$$

The second partial is

$$\frac{\partial^2 J}{\partial p^2} = 2 \sum_{i=1}^{N} \left[\frac{\partial \hat{y}_i^T}{\partial p} R^{-1} \frac{\partial \hat{y}_i}{\partial p} - (y_i - \hat{y}_i)^T R^{-1} \frac{\partial^2 \hat{y}_i}{\partial p^2}\right] \tag{26}$$

This is often approximated by

$$\frac{\partial^2 J}{\partial p^2} = 2 \sum_{i=1}^{N} \left[\left(\frac{\partial \hat{y}_i}{\partial p}\right)^T R^{-1} \frac{\partial \hat{y}_i}{\partial p}\right] \tag{27}$$

Equations (25) and (27) are substituted into Eq. (22) to yield

$$\hat{p}_{k+1} = \hat{p}_k + \left[\sum_{i=1}^{N}\left(\frac{\partial \hat{y}_i}{\partial p}\right)^T R^{-1} \frac{\partial \hat{y}_i}{\partial p}\right]^{-1}\left[\sum_{i=1}^{N}\left(\frac{\partial \hat{y}_i}{\partial p}\right)^T R^{-1}\,(y_i - \hat{y}_i)\right] \tag{28}$$

Equation (28) is the "modified" Newton-Raphson optimization technique. During actual flight test data processing, Eq. (28) is applied repeatedly to update $\hat{p}$ until Eq. (25) approaches a zero value.

The variance of the estimated parameter vector due to noise is assumed to be

$$E\{\delta p\ \delta p^T\}_{Noise} = \left[\frac{\partial^2 J}{\partial p^2}\right]^{-1} \tag{29}$$

where

$$\delta p \triangleq p - \hat{p}$$

Equation (29) is obtained by assuming that the errors due to n_i are small so that J is a quadratic surface in the vicinity of $\hat{p}$ and p. Then, one can write

$$\delta p = -\left\{\left[\frac{\partial^2 J}{\partial p^2}\right]^{-1}\left(\frac{\partial J}{\partial p}\right)^T\right\} \tag{30}$$

where $y_i - \hat{y}_i$ is n_i, and y_i is generated using the correct parameter p. Thus, from Eqs. (29) and (30),

$$E\{\delta p\ \delta p^T\} = E\left\{\left[\frac{\partial^2 J}{\partial p^2}\right]^{-1}\left(\frac{\partial J}{\partial p}\right)^T \frac{\partial J}{\partial p}\left[\frac{\partial^2 J}{\partial p^2}\right]^{-1}\right\} \tag{31}$$

Because $\dfrac{\partial^2 J}{\partial p^2}$ has no noise dependence, this becomes

$$E\{\delta p\ \delta p^T\} = \left[\frac{\partial^2 J}{\partial p^2}\right]^{-1} E\left\{\left(\frac{\partial J}{\partial p}\right)^T \frac{\partial J}{\partial p}\right\}\left[\frac{\partial^2 J}{\partial p^2}\right]^{-1} \tag{32}$$

The inner term is expanded to yield

$$E\left\{\left(\frac{\partial J}{\partial p}\right)^T\left(\frac{\partial J}{\partial p}\right)\right\} = E\left\{\left[\sum_{i=1}^{N}\left(\frac{\partial y_i}{\partial p}\right)^T R^{-1}(y_i - \hat{y}_i)\right]\left[\sum_{j=1}^{N}(y_j - \hat{y}_j)^T R^{-1}\frac{\partial y_j}{\partial p}\right]\right\} \tag{33}$$

Suppose that because the measurement noise is assumed to be white,

$$E\{(y_i - \hat{y}_i)\ (y_j - \hat{y}_j)^T\} = S\delta_{ij}$$

The double summation reduces to a single summation, and the expectation is replaced by S yielding

$$E\left\{\left(\frac{\partial J}{\partial p}\right)^T\left(\frac{\partial J}{\partial p}\right)\right\} = \sum_{i=1}^{N}\left[\left(\frac{\partial y_i}{\partial p}\right)^T R^{-1}\ SR^{-1}\ \frac{\partial y_i}{\partial p}\right] \tag{34}$$

Now, if S equals R (that is, the weighting matrix R used in the cost function J is correct), then Eq. (34) is exactly equal to $\frac{\partial^2 J}{\partial p^2}$ from Eq. (27). By substituting this result in Eq. (32), the desired relation (Eq. (29)) is established.

Linearized Aircraft Equations of Motion and Output Measurements

The number of states required to model an aircraft vary depending upon the application [25-27]. Airplane and helicopter equations of motion are often decoupled into the longitudinal and lateral parts for ease of analysis. Furthermore, in flight testing, longitudinal and lateral inputs are usually separated so that only the longitudinal or lateral modes of the aircraft dynamics are excited. The equations are further simplified by assuming small perturbations from a steady flight condition; this allows the equations to be placed in linear form. Helicopter equations often include the rotor dynamics, and the exact form changes from design to design [28]. The need for rotor dynamics is often related to the development of a high performance control system [29]. However, for initial system analysis, the helicopter equations can be assumed to have the same form as that of the airplane [25].

One of the objectives of this study was to conduct a preliminary analysis of the effects of instrumentation errors on the accuracy of stability and control derivatives of the helicopter. These results were then to be related to control system efficiency resulting from the parameter uncertainty. For this preliminary study, a low order model of the helicopter which neglects rotor dynamics was considered sufficient.

Four linear equations can be used to represent either the longitudinal or lateral aircraft dynamics; these are placed in matrix form, as in Eq. (16). The control input u for the longitudinal dynamics of the airplane is the elevator deflection $\Delta\delta_e$. For the helicopter, the longitudinal controls are the collective $\Delta\delta_c$ and the differential collective $\Delta\delta_e$. The lateral controls for the airplane are the rudder deflection $\Delta\delta_r$ and the aileron deflection $\Delta\delta_a$. For the helicopter, the lateral controls are the roll cyclic $\Delta\delta_a$ and the yaw cyclic $\Delta\delta_r$.

In matrix form, the longitudinal equations are

$$\begin{bmatrix} \Delta\dot{\theta} \\ \Delta\dot{q} \\ \Delta\dot{w} \\ \Delta\dot{u} \end{bmatrix} = \begin{bmatrix} 0 & 1 & 0 & 0 \\ 0 & M_q & M_w & M_u \\ -g \sin\theta_o & Z_q + U_o & Z_w & Z_u \\ -g \cos\theta_o & X_q - W_o & X_w & X_u \end{bmatrix} \begin{bmatrix} \Delta\theta \\ \Delta q \\ \Delta w \\ \Delta u \end{bmatrix} + \begin{bmatrix} 0 & 0 \\ M_{\delta e} & M_{\delta c} \\ Z_{\delta e} & Z_{\delta c} \\ X_{\delta e} & X_{\delta c} \end{bmatrix} \begin{bmatrix} \Delta\delta_e \\ \Delta\delta_c \end{bmatrix} \tag{35}$$

Here,

$$x^T \triangleq [\Delta\theta \quad \Delta q \quad \Delta w \quad \Delta u] \tag{36}$$

and consists of perturbations in pitch, pitch rate, the normal component of relative velocity, and the longitudinal component of relative velocity. Also,

$$U_o = V_T \cos\alpha_o$$

$$W_o = V_T \cos\alpha_o$$

Often, the terms Z_q and X_q are negligible in Eq. (35). For the airplane, the terms $M_{\delta c}$, $Z_{\delta c}$, and $X_{\delta c}$ are also dropped.

In Eq. (35), the unknown parameters to be identified consist of

$$p^T \triangleq [M_q \quad M_w \quad M_u \quad M_{\delta e} \quad M_{\delta c} \quad Z_q \quad Z_w \quad Z_u \quad Z_{\delta e} \quad Z_{\delta c} \quad X_q \quad X_w \quad X_u \quad X_{\delta e} \quad X_{\delta c}] \tag{37}$$

The lateral equations are in the form

$$L\dot{x} = F'x + G'u \tag{38}$$

where L is a matrix which accounts for the cross-product of inertia term Ixz. The state

$$x \triangleq [\Delta\beta \quad \Delta p \quad \Delta r \quad \Delta\varphi] \tag{39}$$

consists of perturbations in the angle-of-sideslip, roll rate, yaw rate, and roll angle. Alternately, at low speeds, the angle-of-sideslip $\Delta\beta$ is replaced by the lateral velocity component Δv. The matrix L has the form

$$L \triangleq \begin{bmatrix} 1 & 0 & 0 & 0 \\ 0 & 1 & Ixz/Ixx & 0 \\ 0 & Ixz/Izz & 1 & 0 \\ 0 & 0 & 0 & 1 \end{bmatrix} \tag{40}$$

By letting $F = L^{-1}F'$ and $G = L^{-1}G'$, Eq. (38) can be modified to the more standard form

$$\dot{x} = L^{-1}F'x + L^{-1}G'u = Fx + Gu \tag{41}$$

In full form, the lateral equations are

$$\begin{bmatrix} \Delta\dot{v} \\ \Delta\dot{p} \\ \Delta\dot{r} \\ \Delta\dot{\varphi} \end{bmatrix} = \begin{bmatrix} Y_v & Y_p+W_o & Y_r-U_o & g\cos\theta_o \\ L_v^* & L_p^* & L_r^* & 0 \\ N_v^* & N_p^* & N_r^* & 0 \\ 0 & 1 & \tan\theta_o & 0 \end{bmatrix} \begin{bmatrix} \Delta v \\ \Delta p \\ \Delta r \\ \Delta\varphi \end{bmatrix} + \begin{bmatrix} Y_{\delta a} & Y_{\delta r} \\ L_{\delta a}^* & L_{\delta r}^* \\ N_{\delta a}^* & N_{\delta r}^* \\ 0 & 0 \end{bmatrix} \begin{bmatrix} \Delta\delta_a \\ \Delta\delta_r \end{bmatrix} \tag{42}$$

The starred (*) quantities are modified from their normal values due to L^{-1} in Eq. (41). In Eq. (42), the unknown parameters are

$$p^T \triangleq [Y_v\ Y_p\ Y_r\ Y_{\delta\alpha}\ Y_{\delta r}\ L_v^*\ L_p^*\ L_r^*\ L_{\delta\alpha}^*\ L_{\delta r}^*\ N_v^*\ N_p^*\ N_r^*\ N_{\delta\alpha}^*\ N_{\delta r}^*] \tag{43}$$

The instruments which are assumed to be available for longitudinal output measurements are:

1. pitch attitude gyro (θ)
2. pitch rate gyro (q)
3. angle-of-attack vane (α)
4. pitot tube or airspeed indicator (u)
5. longitudinal accelerometer (a_x)
6. normal accelerometer (a_z)
7. pitch angular accelerometer ($\dot{q}$)

The lateral output instruments are assumed to be

1. angle-of-sideslip vane (β)
2. roll rate gyro (p)
3. yaw rate gyro (r)
4. roll attitude gyro (φ)
5. lateral accelerometer (a_y)
6. roll angular accelerometer ($\dot{p}$)
7. yaw angular accelerometer ($\dot{r}$)

The relation between the instrument measurements and the equations of motion are obvious except for the accelerations, which are [14]:

$$\Delta a_x = \frac{1}{g}(\Delta\dot{u} + W_o\,\Delta q) + \cos\theta_o\,\Delta\theta$$

$$\Delta a_y = \frac{1}{g}(\Delta\dot{v} + U_o\,\Delta r - W_o\,\Delta p) - \cos\theta_o\,\Delta\varphi \qquad (44)$$

$$\Delta a_z = \frac{1}{g}(\Delta\dot{w} - U_o\,\Delta q) + \sin\theta_o\,\Delta\theta$$

Making the substitutions and fitting the longitudinal measurements into the form of Eq. (19) yields (for linear accelerations measured in g's)

$$\begin{bmatrix} \Delta\theta \\ \Delta q \\ \Delta\alpha \\ \Delta u \\ \Delta a_x \\ \Delta a_z \\ \Delta\dot{q} \end{bmatrix} = \begin{bmatrix} 1 & 0 & 0 & 0 \\ 0 & 1 & 0 & 0 \\ 0 & 0 & \cos\alpha_o/V_t & -\sin\alpha_o/V_t \\ 0 & 0 & 0 & 1 \\ 0 & X_q/g & X_w/g & X_u/g \\ 0 & Z_q/g & Z_w/g & Z_u/g \\ 0 & M_q & M_w & M_u \end{bmatrix} \begin{bmatrix} \Delta\theta \\ \Delta q \\ \Delta w \\ \Delta u \end{bmatrix} + \begin{bmatrix} 0 & 0 \\ 0 & 0 \\ 0 & 0 \\ 0 & 0 \\ X_{\delta e}/g & X_{\delta c}/g \\ Z_{\delta e}/g & Z_{\delta c}/g \\ M_{\delta e} & M_{\delta c} \end{bmatrix} \begin{bmatrix} \Delta\delta_e \\ \Delta\delta_c \end{bmatrix} \qquad (45)$$

The lateral measurements are

$$\begin{bmatrix} \Delta\beta \\ \Delta p \\ \Delta r \\ \Delta\varphi \\ \Delta a_y \\ \Delta\dot{p} \\ \Delta\dot{r} \end{bmatrix} = \begin{bmatrix} 1/V_T & 0 & 0 & 0 \\ 0 & 1 & 0 & 0 \\ 0 & 0 & 1 & 0 \\ 0 & 0 & 0 & 1 \\ Y_v/g & Y_p/g & Y_r/g & 0 \\ L_v^* & L_p^* & L_r^* & 0 \\ N_v^* & N_p^* & N_r^* & 0 \end{bmatrix} \begin{bmatrix} \Delta v \\ \Delta p \\ \Delta r \\ \Delta\varphi \end{bmatrix} + \begin{bmatrix} 0 & 0 \\ 0 & 0 \\ 0 & 0 \\ 0 & 0 \\ Y_{\delta a}/g & Y_{\delta r}/g \\ L_{\delta a}^* & L_{\delta r}^* \\ N_{\delta a}^* & N_{\delta r}^* \end{bmatrix} \begin{bmatrix} \Delta\delta_a \\ \Delta\delta_r \end{bmatrix} \qquad (46)$$

Equations (45) and (46) assume perfect measurements of the aircraft state x and the control input u.

Equations for Assessing the Effect of Measurement Errors on the Identification Process

Often, no other measurement errors except for the white noise indicated earlier are assumed to be present in the flight data used for identifying aircraft derivatives. Sometimes biases are assumed to affect the measurements and these terms are identified along with the equation parameters and state initial conditions. However, there are many other types of errors which do affect the estimation accuracy as discussed in the second chapter.

Instrument error model equations.- As discussed in the previous chapter, the measurements are affected by the dynamic characteristics of the instruments, filters, and recording equipment. The slowest instrument/smoothing filter combination found in the instrumentation survey had a cutoff frequency of 1 Hz; this is about a factor of two higher than that of the aircraft dynamics. The important aspects of the dynamic errors are the phase lag and amplitude attenuation of the instruments at frequencies below their natural frequencies. These characteristics can be approximately simulated by a first order lag, regardless of the order of the instrumentation dynamics. As stated in the previous chapter, the matrix equation representing this effect is

$$\dot{y}_L = -F_m y_L + F_m y_T \quad ; \quad y_L(0) = y_T(0) \tag{47}$$

where

y_L = "lagged" measurement

y_T = assumed true dynamic value of the quantity being measured

F_m = diagonal matrix of elements representing the inverse of the time constants of each data channel

Each of the diagonal elements of F_m has a mean value which is known, or deterministic. It also has a random component. The differences in the mean values of these elements are, therefore, deterministic errors, and they can be studied with the ensemble analysis technique discussed later. The effect of the random components of the lags must be studied with the Monte Carlo method.

Next, the effects of the static scale factor errors, biases, and cross-coupling on the measurements are included. For constant value of these outputs, the actual readings would be of the form

$$y_I = Ty_L + B \tag{48}$$

where

$$T = \begin{bmatrix} 1 + e_{11} & e_{12} & \cdots & \\ e_{21} & 1 + e_{22} & & \vdots \\ \vdots & & & \\ & \cdots & & 1 + e_{77} \end{bmatrix} \tag{49}$$

The diagonal terms in the T matrix represent scaling errors while off diagonal terms represent cross-coupling errors. The vector B represents the bias errors. The order in which the lags and the static errors of T and B affect the measurements can be interchanged. In the ensemble analysis that follows, there is a computational advantage to placing the lags first. For small effects assumed in the ensemble analysis, the results are identical.

The addition of the random noise for each instrument yields the final measurement equation

$$y_i = y_{Ii} + n_i \tag{50}$$

where y_i is the output measurement vector with all errors sampled at time i, and n_i is the random output noise vector with

$$E\{n_i\} = 0 \quad ; \quad E\{n_i \, n_j^T\} \triangleq R\delta_{ij}$$

The other source of measurement error is in the recording of the control input u by control position transducers or servo measurements. The measurement of u is subject to dynamic effects which are again approximated as first order lags by the equation

$$\dot{u}_L = -F_c u_L + F_c u \quad ; \quad u_L(0) = u(0) \tag{51}$$

Here,

u = assumed true value of the control input

u_L = "lagged" control

F_c = diagonal matrix of one over the time constants of the control measurements

These control measurements are also subject to scale factor errors and biases. As discussed in the second chapter, these errors can be represented by the equation

$$u_I = T_c u_L + B_c \tag{52}$$

The actual recorded control input is sampled and is also subject to noise. It is represented by the equation

$$\hat{u}_i = u_{Ii} + n_{ci} \tag{53}$$

where

$\hat{u}_i$ = control measurement vector with errors sampled at time i

n_{ci} = random control noise vector; $E\{n_{ci}\} = 0$; $E\{n_{ci}n_{cj}\} \triangleq R_c\delta_{ij}$

Equations (47)-(53) are Eqs. (1)-(4) of the second chapter.

The overall identification process flow diagram changes from that depicted in Figure 5 to that depicted in Figure 6. In the ensemble analysis which follows, the control measurement noise n_{ci} is ignored. This noise acts as a random disturbance to the system dynamics (process noise) and cannot be analyzed with ensemble methods. It is assumed that its effect can be included in the bias term B_c.

Particular errors studied.- Before proceeding to the analysis, a description is first presented of some of the error sources which are studied by the preceding equations. The diagonal elements of T, T_c, F_m, and F_c are the scale factor errors and inverse time constants. B and B_c are bias vectors.

Some of the specific errors which are included in the off-diagonal terms of the T matrix include:

1. α and β boom corrections
2. accelerometer and center-of-gravity (c.g.) location corrections
3. misalignments (accelerometers and gyros)
4. gyro and angular accelerometer effects due to linear acceleration

A simplified α boom correction equation is from Eq. (12)

$$\alpha_I = \alpha - \frac{x_{vcg}}{V} q \tag{54}$$

where V is aircraft total velocity and x_{vcg} is the angle-of-attack vane distance from the aircraft center-of-gravity (c.g.). The error in x_{vcg} is divided into two parts--the error in vane location (ε_{vx}) and the error in c.g. location (ε_{cgx}). If all seven longitudinal instruments are being used as in Eq. (45), introducing the error Eq. (54) into the T matrix Eq. (48) yields:

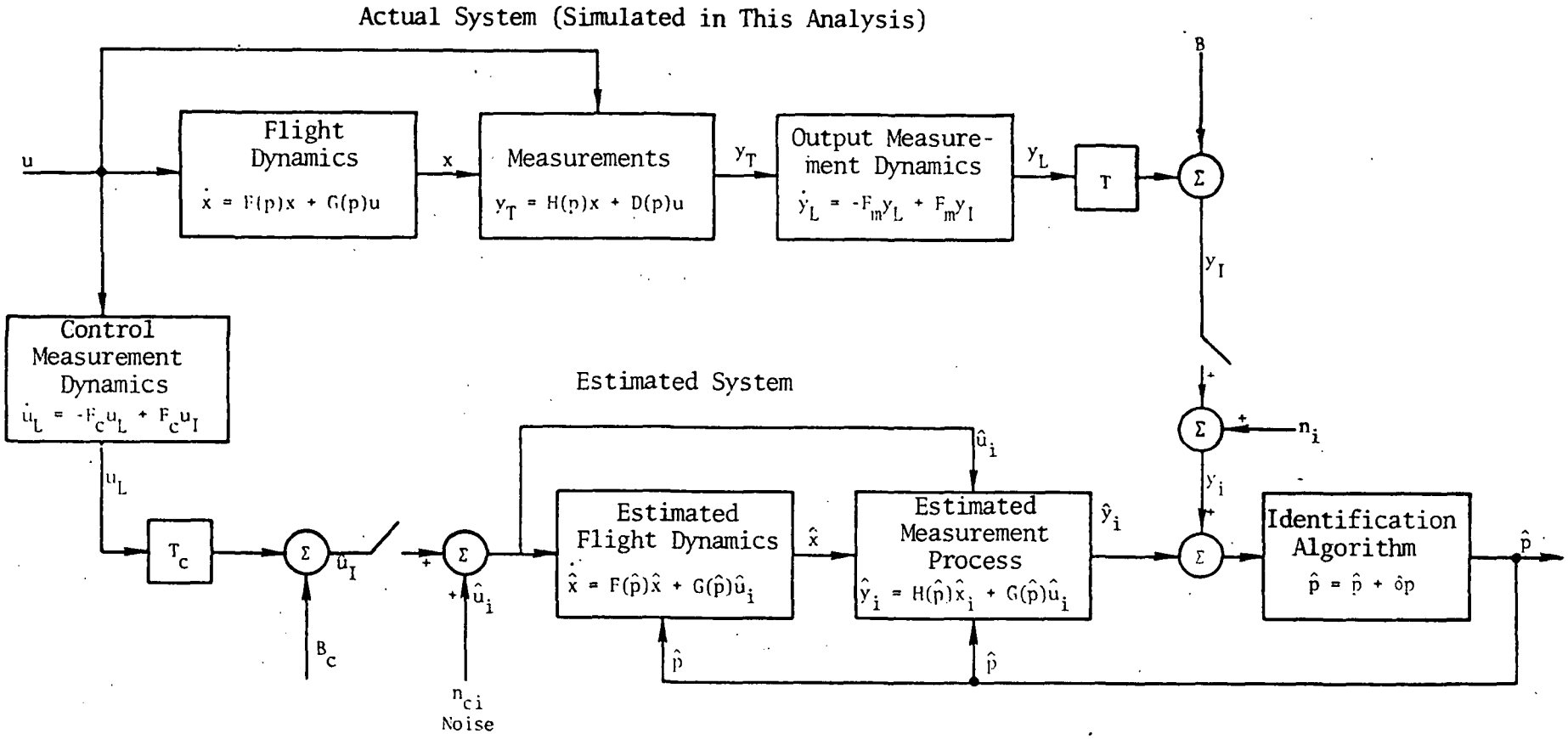

FIGURE 6.- EFFECT OF MEASUREMENT ERRORS ON THE IDENTIFICATION PROCESS

$$e_{32} = - \frac{\varepsilon_{vx} + \varepsilon_{cgx}}{V} \tag{55}$$

A similar error term affects the β vane.

Next consider the linear accelerometer errors of Eq. (9). If the value of x_{cg} and z_{cg} are in error because of the uncertainty in the c.g. position or the c.g. offset of the accelerometers is neglected, then the T matrix error terms for the longitudinal equations are

$$\begin{aligned} e_{57} &= -(\varepsilon_{al z} + \varepsilon_{cgz})/g \\ e_{67} &= (\varepsilon_{al x} + \varepsilon_{cgx})/g \end{aligned} \tag{56}$$

In Eq. (56), the terms

$\varepsilon_{alx', alz}$ = errors in the accelerometer location when a correction is made

= distance from c.g. to the accelerometer when a correction is not made

$\varepsilon_{cgx', cgz}$ = errors in the knowledge of the c.g. location

Similarly, the lateral accelerometer has the two errors

$$\begin{aligned} e_{56} &= (\varepsilon_{al z} + \varepsilon_{cgz})/g \\ e_{57} &= - (\varepsilon_{al x} + \varepsilon_{cgx})/g \end{aligned} \tag{57}$$

Other elements in the T matrix are due to mounting misalignments of the gyros and accelerometers. In the longitudinal equations, the terms

$$\begin{aligned} e_{56} &= - \gamma_{ax} \\ e_{65} &= \gamma_{az} \end{aligned} \tag{58}$$

appear, where γ_{ax} and γ_{az} are the small linear accelerometer misalignment angles. In the lateral equations, the T matrix contains the terms

$$\begin{aligned} e_{23} &= - \gamma_p \\ e_{32} &= \gamma_r \\ e_{67} &= - \gamma_p^{\bullet} \\ e_{76} &= \gamma_r^{\bullet} \end{aligned} \tag{59}$$

where γ_p, γ_r, $\gamma_p^{\bullet}$, and $\gamma_r^{\bullet}$ are misalignment angles of the rate gyros and angular accelerometers.

For the longitudinal measurements, the terms e_{25} and e_{26} in T are used to represent the rate gyro mass unbalance. Also, the terms e_{75} and e_{76} are used to model angular accelerometer sensitivity to linear acceleration.

For the lateral equations, the terms e_{25} and e_{35} model mass unbalance in the roll and yaw rate gyros. The terms e_{65} and e_{75} model the angular accelerometer errors due to linear acceleration.

From Eqs. (48), (50), (52) and (53)-(59), explicit static error model equations can be written for each of the instruments investigated in this study. These are presented in Tables 6 and 7. These tables define the notation used for each of the error sources.

TABLE 6.- EQUATIONS OF STATIC ERRORS FOR LONGITUDINAL INSTRUMENTS

Pitch Attitude Gyro	$\theta_i = (1 + \varepsilon_\theta)\Delta\theta + b_\theta + n_\theta$
Pitch Rate Gyro	$q_i = (1 + \varepsilon_q)\Delta q + b_q + n_q + \varepsilon_{25}\,\Delta a_x + \varepsilon_{26}\Delta a_x$
Angle-of-Attack Vane	$\alpha_i = (1 + \varepsilon_\alpha)\,(\Delta w \cos\alpha_o - \Delta u \sin\alpha_o)/V_T + b_\alpha + n_\alpha - (\varepsilon_{vx} + \varepsilon_{cgx})q/V_T$
Pitot-Static Tube	$u_i = (1 + \varepsilon_u)\Delta u + b_u + n_u$
Longitudinal Accelerometer	$a_{xi} = (1 + \varepsilon_{ax})\Delta a_x + b_{ax} + n_{ax} - \gamma_{ax}\,\Delta a_z/K + (\varepsilon_{a\ell z} + \varepsilon_{cgz})\Delta\dot{q}/(Kg)$
Vertical Accelerometer	$a_{zi} = (1 + \varepsilon_{az})\Delta a_z + b_{az} + n_{az} + \dot{\gamma}_{az}\,\Delta a_x/K - (\varepsilon_{a\ell x} + \varepsilon_{cgx})\Delta\dot{q}/(Kg)$
Pitch Angular Accelerometer	$\dot{q}_i = (1 + \varepsilon_{\dot{q}})\Delta\dot{q} + b_{\dot{q}} + n_{\dot{q}} + \varepsilon_{75}\Delta a_x + \varepsilon_{76}\Delta a_z$
Elevator or Differential Collective CPT	$\delta_{em} = (1 + \varepsilon_{\delta e})\Delta\delta_e + b_{\delta e}$
Collective CPT	$\delta_{cm} = (1 + \varepsilon_{\delta c})\Delta\delta_c + b_{\delta c}$

TABLE 7.- EQUATIONS OF STATIC ERRORS FOR LATERAL INSTRUMENTS

Angle-of-Sideslip Vane	$\beta_i = (1 + \varepsilon_\beta)\Delta\beta + b_\beta + n_\beta - (\varepsilon_{vx} + \varepsilon_{xcg})\Delta r/V_T$
Roll Rate Gyro	$P_i = (1 + \varepsilon_p)\Delta p + b_p + n_p - \gamma_p \Delta r/K + \varepsilon_{25} \Delta a_y$
Yaw Rate Gyro	$r_i = (1 + \varepsilon_r)\Delta r + b_r + n_r + \gamma_r \Delta p/K + \varepsilon_{35} \Delta a_y$
Roll Attitude Gyro	$\phi_i = (1 + \varepsilon_\phi)\Delta\phi + b_\phi + n_\phi$
Lateral Accelerometer	$a_{yi} = (1 + \varepsilon_{ay})\Delta a_y + b_{ay} + n_{ay} + (\varepsilon_{a\ell x} + \varepsilon_{xcg})\Delta\dot{r}/(Kg) - (\varepsilon_{a\ell z} + \varepsilon_{zcg})\Delta\dot{p}/(Kg)$
Roll Angular Accelerometer	$\dot{p}_i = (1 + \varepsilon_{\dot{p}})\Delta\dot{p} + b_{\dot{p}} + n_{\dot{p}} - \gamma_{\dot{p}} \Delta\dot{r}/K + \varepsilon_{65} \Delta a_y$
Yaw Angular Accelerometer	$\dot{r}_i = (1 + \varepsilon_{\dot{r}})\Delta\dot{r} + b_{\dot{r}} + n_{\dot{r}} + \gamma_{\dot{r}} \Delta\dot{p}/K + \varepsilon_{75} \Delta a_y$
Aileron or Roll Cyclic CPT	$\delta_{am} = (1 + \varepsilon_{\delta a})\Delta\delta_a + b_{\delta a}$
Rudder or Yaw Cyclic CPT	$\delta_{rm} = (1 + \varepsilon_{\delta r})\Delta\delta_r + b_{\delta r}$

Ensemble Analysis of Measurement Error Effects

As explained in the previous section, the modified Newton-Raphson identification scheme minimizes the cost function J of Eq. (21) by repeated application of Eq. (28). Convergence on the minimum is achieved when $\frac{\partial J}{\partial p} \cong 0$. In this study using the ensemble analysis, it is assumed that the true value of p is known. It is further assumed that the instrumentation errors cause the minimum point on the cost function surface J to shift a small amount from the true p. If the small error assumption is correct, only one application of Eq. (21) (with $\hat{p}$ set to p) can determine the shift due to the measurement error on the estimate of p. This

is the key assumption of the linear ensemble analysis which is used in this study. The resulting perturbation to the parameter vector is:

$$\delta p = \hat{p} - p = -\left[\frac{\partial^2 J}{\partial p^2}\right]^{-1} \frac{\partial J^T}{\partial p} \tag{60}$$

where

$\hat{p}$ = perturbed parameter estimate due to measurement errors

p = true value of the parameter

From Eq. (28), this can be written as

$$\delta p = + \left[\sum_{i=1}^{N} \left\{\frac{\partial y_i^T}{\partial p} R^{-1} \frac{\partial \hat{y}_i}{\partial p}\right\}\right]^{-1} \sum_{i=1}^{N} \frac{\partial \hat{y}_i^T}{\partial p} R^{-1} (y_i - \hat{y}_i) \tag{61}$$

The y_i represent the sampled output measurements taken from the aircraft (Eqs. (16), (17), (47)-(50)) and the $\hat{y}_i$ represent the estimated output values (Eqs. (18), (19)) obtained using the measured control input. The sensitivity term $\frac{\partial \hat{y}_i}{\partial p}$ in Eq. (61) is computed by the identification algorithm about the latest estimates of p. Again, for the ensemble analysis, this is taken as the correct value of p.

To compute $\frac{\partial \hat{y}_i}{\partial p}$ in Eq. (61) requires integration of

$$\dot{\hat{x}} = (F-GC)\hat{x} + Gu \quad ; \quad \hat{x}(0) = \hat{x}_o \tag{62}$$

where C is the feedback gain matrix whose elements are assumed known for the purposes of the study. This also assumes perfect measurement of the control input u. Also, the sensitivities of the states to parameter changes are found by integrating

$$\frac{d}{dt}\left(\frac{\partial \hat{x}}{\partial p_p}\right) = (F-GC)\left(\frac{\partial \hat{x}}{\partial p_p}\right) + \left(\frac{\partial F}{\partial p_p} - \frac{\partial G}{\partial p_p} C\right) \hat{x} + \frac{\partial G}{\partial p_p} u \; ; \; \frac{\partial \hat{x}}{\partial p_p} = 0 \tag{63}$$

Here, p_p is the parameter vector containing the elements presented in Eqs. (37) or (43). If state initial conditions are also estimated, the identification process integrates

$$\frac{d}{dt}\left(\frac{\partial \hat{x}}{\partial p_{IC}}\right) = (F-GC)\left(\frac{\partial \hat{x}}{\partial p_{IC}}\right) \quad ; \quad \frac{\partial \hat{x}}{\partial p_{IC}}(0) = I \tag{64}$$

Then, from Eq. (19), the output sensitivity matrix for the parameters p_p is

$$\frac{\partial \hat{y}}{\partial p_p} = (H\text{-}DC)\ \frac{\partial \hat{x}}{\partial p_p} + \left(\frac{\partial H}{\partial p_p} - \frac{\partial D}{\partial p_p}\ C\right)\ \hat{x} + \frac{\partial D}{\partial p_p}\ u \tag{65}$$

For the initial conditions, this becomes

$$\frac{\partial \hat{y}}{\partial p_{IC}} = (H\text{-}DC)\ \frac{\partial \hat{x}}{\partial p_{IC}} \tag{66}$$

If output measurement biases are also estimated, the sensitivities

$$\frac{\partial \hat{y}}{\partial p_b} = I \tag{67}$$

must be included. The total sensitivity used in Eq. (61) is then

$$\frac{\partial \hat{y}_i}{\partial p} \triangleq \left[\frac{\partial \hat{y}_i}{\partial p_p}\ \ \frac{\partial \hat{y}_i}{\partial p_{IC}}\ \ \frac{\partial \hat{y}_i}{\partial p_b}\right] \tag{68}$$

Output measurement errors affect the value of y_i in Eq. (61). By neglecting the measurement noise temporarily, the output y_i is the sampled value of y_I. The sensitivity of the error p in Eq. (61) to an error source e is

$$\frac{\partial}{\partial e}(\delta p) = \left[\frac{\partial^2 J}{\partial p^2}\right]^{-1} \sum_{i=1}^{N} \frac{\partial \hat{y}_i^T}{\partial p} R^{-1} \frac{\partial y_i}{\partial e} \tag{69}$$

This requires computation of the sensitivity matrix $\frac{\partial y_i}{\partial e}$.

The sensitivity of y_i to a bias element of B is approximately

$$\frac{\partial y_i}{\partial e} = \frac{\partial B}{\partial e} \tag{70}$$

For an element in T, this is

$$\frac{\partial y_i}{\partial e} = \frac{\partial T}{\partial e}\ ((H\text{-}DC)x + Du) \tag{71}$$

For an unestimated initial condition treated as an error source, the sensitivity of y_i is

$$\frac{\partial y_i}{\partial e} = (H\text{-}DC)\ \frac{\partial x_i}{\partial e} \tag{72}$$

where $\frac{\partial x}{\partial e}$ comes from integrating

$$\frac{d}{dt}\left(\frac{\partial x}{\partial e}\right) = (F-GC)\frac{\partial x}{\partial e} \quad ; \quad \frac{\partial x}{\partial e}(0) = I \tag{73}$$

For an unknown time constant in the matrix F_m, the sensitivity must be determined by integrating

$$\frac{d}{dt}\left(\frac{\partial y_L}{\partial e}\right) = \frac{\partial F_m}{\partial e}\left[-y_L + (H-DC)x + Du\right] - F_m\frac{\partial y_L}{\partial e} \quad ; \quad \frac{\partial y_L}{\partial e}(0) = 0 \tag{74}$$

The results of Eqs. (70)-(74) are combined into a general vector $\frac{\partial y_i}{\partial e}$ for each error e which affects the output measurements.

The sensitivity of parameter estimates due to control input measurement errors is of the form

$$\frac{\partial}{\partial e}(\delta p) \approx -\left[\frac{\partial^2 J}{\partial p^2}\right]^{-1} \sum_{i=1}^{N} \frac{\partial \hat{y}_i^T}{\partial p} R^{-1} \frac{\partial \hat{y}_i}{\partial e} \tag{75}$$

This requires knowing the sensitivity of the estimated output $\hat{y}_i$ to control measurement errors e.

For control measurement biases, the sensitivity of the control input is

$$\frac{\partial \hat{u}_i}{\partial e} = \frac{\partial B_c}{\partial e} \tag{76}$$

For scale factor errors, this is

$$\frac{\partial \hat{u}_i}{\partial e} = \frac{\partial T_c}{\partial e} u_i \tag{77}$$

The effect on the states is found by integrating

$$\frac{d}{dt}\left(\frac{\partial \hat{x}}{\partial e}\right) = (F-GC)\frac{\partial \hat{x}}{\partial e} + G\frac{\partial \hat{u}_i}{\partial e} \tag{78}$$

from Eq. (18). The resulting effect on the estimated output $\hat{y}_i$ is

$$\frac{\partial \hat{y}_i}{\partial e} = (H-DC)\frac{\partial \hat{x}_i}{\partial e} + D\frac{\partial \hat{u}_i}{\partial e} \tag{79}$$

Evaluation of the sensitivity to control measurement lags requires integrating

$$\frac{d}{dt}\left(\frac{\partial \hat{x}}{\partial e}\right) = F\frac{\partial \hat{x}}{\partial e} + G\frac{\partial u_L}{\partial e} \quad ; \quad \frac{\partial \hat{x}}{\partial e}(0) = 0 \tag{80}$$

$$\frac{d}{dt}\left(\frac{\partial u_L}{\partial e}\right) = -F_c \frac{\partial u_L}{\partial e} + \frac{\partial F_c}{\partial e}\left[-u_L + u\right] \; ; \; \frac{\partial u_L}{\partial e}(0) = 0 \qquad (81)$$

The resulting output sensitivity is again found from Eq. (79).

For random (stochastic) measurement errors, e_R, the total covariance of the individual parameters being identified is

$$E\{\delta p \delta p^T\}_{total} = E\{\delta p \delta p^T\}_{noise} + \frac{\partial(\delta p)}{\partial e_R} E\{e_R e_R^T\} \frac{\partial(\delta p)^T}{\partial e_r} \qquad (82)$$

where $E\{e_R e_R^T\}$ is the covariance matrix of the random measurement errors not including the measurement noise. The sensitivities $\frac{\partial(\delta p)}{\partial e_R}$ come from Eqs. (69) and (75). The covariance due to noise comes from Eq. (29). For mean (deterministic) errors, e_m, the expected error in the parameter is

$$E\{\delta p\} = \frac{\partial(\delta p)}{\partial e_M} E\{e_M\} \qquad (83)$$

The above error analysis is referred to here as the ensemble error analysis. It is valid for small errors which affect the measurements linearly. For large error magnitudes, a Monte Carlo error analysis must be made which is discussed next.

Monte Carlo Analysis of Measurement Error Effects

Sometimes it is useful to determine the effects of instrument errors by actually simulating the identification process and the measurement data contaminated by errors. If the errors are large, nonlinear errors are to be studied, or process noise exists, the one step assumptions and linearization which are used in the ensemble analysis method are not valid. Therefore, the simulated data analysis method complements the ensemble analysis. In this method, which uses Monte Carlo techniques, several different data sequences are simulated and used sequentially in the identification process.

The Monte Carlo analysis method is related to the ensemble analysis in that the basic equation utilized is Eq. (61). However, rather than computing the sensitivities $\frac{\partial y_i}{\partial e}$ or $\frac{\partial \hat{y}_i}{\partial e}$, the analysis computes the residual $(y_i - \hat{y}_i)$ in $\frac{\partial J}{\partial p}$.

The random error terms contained in B, T, B_c, T_c, F_m, F_c, and x_o are generated at the beginning of each simulation using the errors' standard deviations and a random number generator. These errors are held constant during each single Monte Carlo run, but are changed from run to run. The random noises n_i and n_{ci} are regenerated at each sample point during each run. Each of the deterministic error terms in T, F_m, and F_c are set equal to the constant mean values and are not changed during any of the runs.

For static output measurement errors occurring in T, B, and n_i only, the residual $(y_i - \hat{y}_i)$ in Eq. (61) is computed by

$$y_i = \hat{y}_i = T(Hx_i + Du_i) + B + n_i - (Hx_i + Du_i) \tag{84}$$

For random initial conditions, Eq. (16) must be integrated each time, and Eq. (84) gets changed to

$$y_i - \hat{y}_i = T(Hx_i + Du_i) + B + n_i - (H\hat{x}_i + Du_i) \tag{85}$$

For static control measurement errors, Eqs. (52) and (53) get combined so that at each sample point

$$\hat{u}_i = T_c u + B_c + n_{ci} \tag{86}$$

where n_{ci} is randomly generated each time point. Because of this change, Eqs. (62) - (64) require integration each pass through, and Eqs. (65) - (68) require reevaluation each pass through. With these changes, Eq. (86) becomes

$$y_i = \hat{y}_i = T(Hx_i + Du_i) + B + n_i - (H\hat{x}_i + D\hat{u}_i) \tag{87}$$

The error Δp_j in the parameter vector obtained from each run is saved. For m Monte Carlo runs, the mean error in p is

$$\overline{\Delta p} \triangleq E\{\Delta p\} = \frac{1}{m} \sum_{j=1}^{m} \Delta p_j \tag{88}$$

The sample covariance about this mean is

$$E\{\delta p \delta p^T\} = \frac{1}{m-1} \sum_{j=1}^{m} (\Delta p_j - \overline{\Delta p})(\Delta p_j - \overline{\Delta p})^T \tag{89}$$

Implementation of the Analysis Techniques

The ensemble analysis and Monte Carlo analysis techniques just described were coded into four digital computer programs for airplanes and helicopters. The longitudinal and lateral equations are both contained in the programs. These programs enable the assessment of uncertainty (due to instrumentation errors) in the accuracy of the aircraft parameters identified from flight test data. The User's Guide to the programs is presented in a separate document [30]. This document is a revision of Ref. 31 to include helicopter equations, feedback control, and other convenient program options.

The uses which can be made of these programs include the following:

(1) The determination of the effect of instrumentation errors on the statistical accuracy of the stability and control derivatives and other parameters identified from flight test data can be made. This includes the mean error and standard deviation of each of the parameters identified. The contribution of each error source on each parameter is determined.

(2) The effects of such variables as aircraft type and flight condition, control input sequence, and data sampling rate on the accuracy of the identified parameters can be determined.

(3) Trade off studies can be made between instrument quality and identification accuracy.

(4) Different combinations of instruments can be studied for use in collecting the flight data.

(5) Trade off studies between fewer instruments with greater quality and more instruments with larger errors can be made.

(6) The necessary instrument accuracy required in a flight test program to allow identifying aircraft parameters to a desired level of certainty can be specified.

(7) Different combinations of parameters can be assumed to be identified depending on whether certain parameters are well known or judged to be insignificant. Changing the specific parameters being identified changes the effect of instrumentation errors on these parameters.

STUDY OF THE EFFECTS OF INSTRUMENTATION ERRORS ON THE ACCURACY OF PARAMETER ESTIMATES

One of the main reasons numerical values of the stability and control derivatives (parameters) are desired is that they are used to design the control system gains for the aircraft. It is important to know how the performance of the control system depends on the accuracy of the parameter values. This knowledge dictates to what accuracy the parameters must be identified. In turn, the parameter accuracy requirement determines: (1) the necessary characteristics of the flight data to be processed, and (2) the accuracy requirements of the instrumentation system used to collect the data. The techniques presented in the previous chapter allow these assessments to be made.

A study of the effects of instrumentation errors on the accuracy of parameter estimates was conducted for a CH-46 helicopter at the three representative flight conditions discussed in the first section below. This study was performed using computer programs which apply the error analysis techniques presented in the previous chapter. This study is representative of the uses to which these error analysis techniques can be put. Moreover, this study serves as a guideline for more exhaustive and detailed studies which will benefit actual VTOL flight test programs.

In this chapter, flight control laws are first developed for steady flight conditions taken at cruise, transition, and hover points along a typical approach trajectory. A set of typical instrument accuracies are selected to study the error effects at the different flight conditions. Aircraft controls are chosen as inputs for simulated flight tests at these flight conditions. Then, the instrumentation parameters and control inputs are used to investigate the accuracy of stability and control derivatives which would be obtained from flight tests conducted at these different flight conditions.

Approach Flight Control Law Development

In this section, the open-loop dynamics of the helicopter following a curved decelerating approach trajectory are first presented. Methods of choosing feedback control gains for the helicopter are then discussed. Finally, control laws which minimize a quadratic cost function are developed.

Figures 7-9 present a typical curved terminal approach trajectory which might be followed in a future commercial application of VTOL aircraft. The airspeed is decreasing and the trajectory profile is curved in the vertical plane. The trajectory also curves in the horizontal plane, as will become feasible with the microwave landing system (MLS) or other volumetric coverage landing guidance systems of the future. Because of the deceleration, the stability and control derivatives are time-varying along this path. Numerical values of the CH-46 have been tabulated for various steady flight conditions in Reference 27. These tables can be used to determine by interpolation the time-varying parameter values along any flight path.

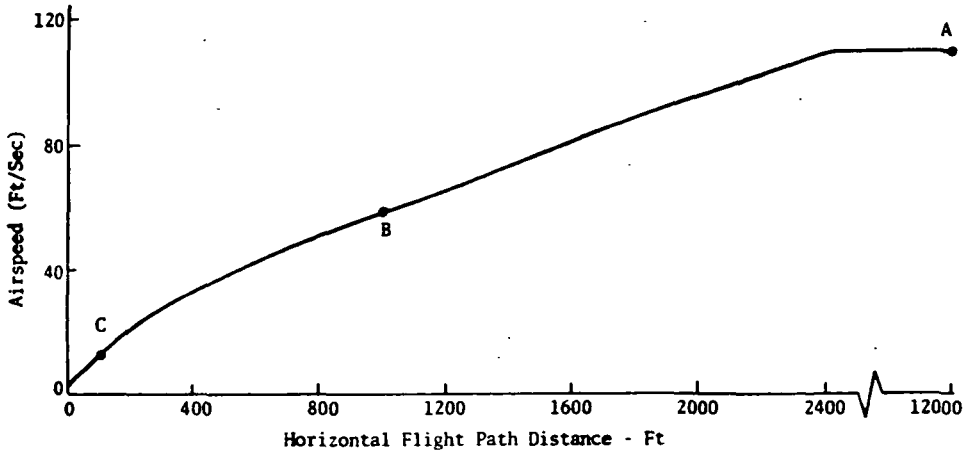

FIGURE 7.- TERMINAL APPROACH TRAJECTORY AIRSPEED

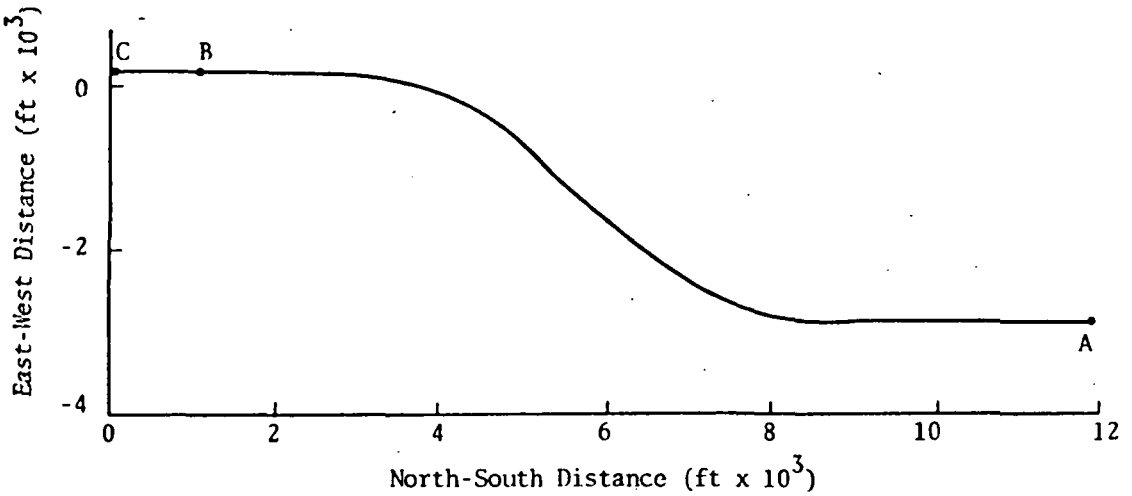

FIGURE 8.- TERMINAL APPROACH TRAJECTORY GROUND TRACK

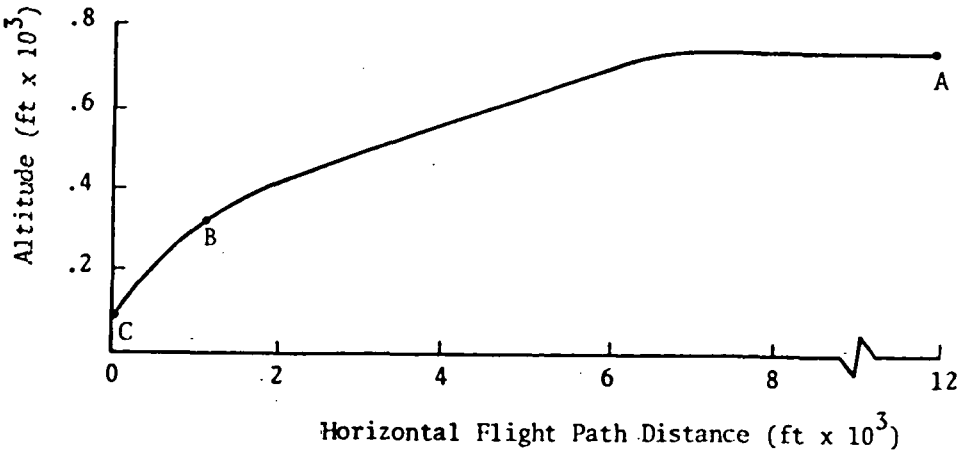

FIGURE 9.- TERMINAL APPROACH TRAJECTORY ALTITUDE PROFILE

For this study, three points have been selected on the approach trajectory for further investigation. These points represent cruise, transition from horizontal to vertical flight, and hover. These points are indicated by A, B, and C in Figures 7-9. From Reference 27, the stability and control derivatives at these three points have been determined, and they are presented in Table 8. As can be seen, the parameters vary somewhat along the flight path. It is assumed that these values and the linear models of Eqs. (35) and (42) represent correctly the dynamics of the uncontrolled vehicle which is the subject of the following investigation.

To illustrate how the stability and control derivatives can vary with flight condition, consider the plot of M_u vs. airspeed depicted in Figure 10. At airspeeds near cruise, M_u exhibits low sensitivity to changes in airspeed. Flight conditions in this region can be reasonably represented by a constant M_u over a fairly wide range of V. By contrast, at low airspeeds M_u increases rapidly to a maximum as V decreases and then diminishes as the hover condition is approached. Other stability and control derivatives exhibit a similar sensitivity to changes in airspeed near the hover condition.

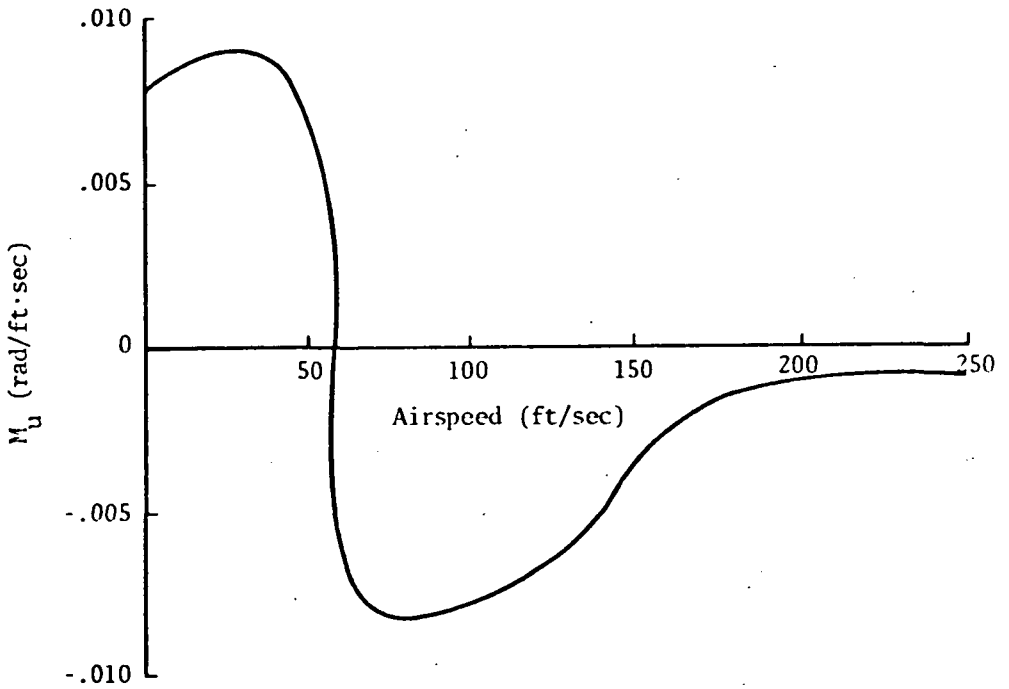

FIGURE 10.- M_u VS. AIRSPEED FOR 500 FT/MIN DESCENT RATE

TABLE 8.- STABILITY AND CONTROL DERIVATIVES FOR THE CH-46 HELICOPTER AT THREE POINTS ALONG THE APPROACH PATH

PARAMETER	UNITS	CRUISE	TRANSITION	HOVER	PARAMETER	UNITS	CRUISE	TRANSITION	HOVER
X_u	1/sec	- .0387	- .0123	- .0181	Y_v	1/sec	- .1268	- .0747	.1538
X_w	1/sec	.0884	.0776	.0501	Y_p	ft/sec	-1.2444	-1.2769	- .9370
X_q	ft/sec	.8188	1.0275	.7555	Y_r	ft/sec.	- .1100	- .1870	- .1088
$X_{\delta e}$	$ft/sec^2 in$	.1480	.1206	.1696	$Y_{\delta a}$	$ft/sec^2 in$	.9656	.9611	.9928
$X_{\delta c}$	$ft/sec^2 in$	.7717	.8889	1.1683	$Y_{\delta r}$	$ft/sec^2 in$	.1039	.1102	.1550
Z_u	1/sec	- .0126	- .1286	.0186	L_v^*	1/ft sec	- .0180	- .0097	- .0091
Z_w	1/sec	- .8323	- .5688	- .3426	L_p^*	1/sec	- .6632	- .7209	- .5936
Z_q	ft/sec	-1.8155	-1.6631	- .6497	L_r^*	1/sec	.0280	- .0262	.0176
$Z_{\delta e}$	$ft/sec^2 in$	.5571	.5198	.0227	$L_{\delta a}^*$	$1/sec^2 in$	.4719	.4707	.4763
$Z_{\delta c}$	$ft/sec^2 in$	-8.7743	-7.3132	-7.4086	$L_{\delta r}^*$	$1/sec^2 in$	- .2905	- .2892	- .2790
M_u	1/ft sec	- .0065	- .0042	.0081	N_v^*	1/sec ft	- .0014	- .0006	.0009
M_w	1/ft sec	.0131	.0189	- .0003	N_p^*	1/sec	.0226	.0473	.0344
M_q	1/sec	-1.4761	-1.2510	- .7079	N_r^*	1/sec	- .0541	- .0374	- .0509
$M_{\delta e}$	$1/in\ sec^2$	.4583	.3918	.3488	$N_{\delta a}^*$	$1/sec^2 in$	- .0201	- .0192	- .0173
$M_{\delta c}$	$1/in\ sec^2$	.0676	.0360	- .0492	$N_{\delta r}^*$	$1/sec^2 in$	.1994	.1996	.2025
θ_o	deg	4.1238	7.0459	9.1651					
α_o	deg	4.1238	14.9530	68.2010					
V_o	ft/sec	110.00	60.5760	9.7180					

It is useful to examine the characteristic equations representing the uncontrolled vehicle dynamics. These are formed by determining the eigenvalues of Eqs. (35) and (42) with parameter values taken from Table 8. The resulting characteristic equations are of the form

$$(s - \alpha_1 + j\beta_1)(s - \alpha_1 - j\beta_1)(s - \alpha_2)(s - \alpha_3) = 0 \tag{90}$$

The quantities $\alpha_1 \pm j\beta_1$, α_2, and α_3 are the roots of the characteristic equations. They are presented in Table 9 for each of the three points on the approach trajectory.

As can be seen, the dynamic response of the helicopter is unstable in both the lateral and longitudinal modes. For the longitudinal mode at cruise and transition conditions, one real pole is positive; at hover, the real part of the complex pair is positive. In the lateral mode, positive real and complex poles exist at cruise, and positive complex poles exist at transition and hover.

The degree of instability implied by Table 9 is rather severe. This points out the need for an automatic control system which augments the dynamics to provide stability. This stability augmentation is necessary for good ride quality in addition to easing the pilot workload in responding to flight path disturbances and changes in the nominal flight path. Such a system is commonly called a stability augmentation system (SAS).

TABLE 9.- UNCONTROLLED (OPEN-LOOP) POLES OF THE CH-46 EQUATIONS OF MOTION AT THREE POINTS ALONG THE APPROACH FLIGHT PATH

LONGITUDINAL				LATERAL			
POLE	CRUISE	TRANSITION	HOVER	POLE	CRUISE	TRANSITION	HOVER
α_1	-0.21105	-0.16415	+0.10729	α_1	+0.15069	+0.07440	+0.20414
β_1	0.34042	0.34943	0.51375	β_1	0.60138	0.52290	0.54232
α_2	+0.46527	+0.51315	-0.35391	α_2	-1.10046	-0.92482	-0.85321
α_3	-2.39026	-2.01695	-0.92928	α_3	+0.06319	-0.05697	-0.04590

The question arises as to how to choose the control law (gains) to account for the time-varying parameters and unstable response along the approach trajectory. To achieve a controlled (closed-loop) response with constant dynamics would require that the gains be continuously time-varying also. At the other extreme, it is possible that one set of fixed gains in the SAS is adequate to provide adequate response at any point in the expected flight regime. That is, the

fixed set of gains would allow some response variation, but this variation may be acceptable. Between these extremes, the possibility of using time-scheduled gains exists; this concept assumes that that uncontrolled response of the aircraft is piecewise constant.

It is beyond the scope of this study to determine what type of control gain schedule is required for the example approach trajectory. Instead, the trajectory is broken into several segments, and different piecewise constant gains are used along each segment. Specifically, three sets of control gains are determined for the cruise, transition, and hover conditions spoken of previously. Relative to this study, it is unnecessary to know how many other sets of gains would be required, or how the helicopter responds with these control gains when at some other point on the nominal approach. Instead, the main objective is to find out how the helicopter does respond with these control gains if the actual values of the parameters vary about the assumed values.

In mechanizing the SAS, it is assumed that perfect state measurements are available. The roll and pitch angles (φ, θ) and roll, pitch, and yaw rates (p, q, r) are assumed to come from gyros which are part of the flight control system. In addition, the airspeed variations (u, v, w) from the nominal values are assumed to come as commands from the flight guidance system.

Two methods of choosing the gains for the SAS were considered. In both cases, the control law is of the form

$$u = - Cx \tag{91}$$

where C is a gain matrix and x is the measured state. With the dynamics equation of the form

$$\dot{x} = Fx + Gu \tag{92}$$

the resultant closed-loop dynamics equation is

$$\dot{x} = (F-GC)x \; ; \quad x(t_o) = x_o \tag{93}$$

The first method is to choose the values of the gains in C such that the roots of the characteristic equation computed from (F-GC) are those selected as being desirable. This is known as pole placement, and a standard procedure exists for choosing the numerical values of the gains [32]. It requires transforming Eqs. (92) to controllable canonical form and using the controllability matrix along with the desired closed-loop roots. The advantage of this method is that the response desired is obtained exactly, and this response can be held constant for each segment of the approach path. The disadvantage is that the gains required to achieve this response may be so large that they cause the control system to saturate in attempting to mechanize the control.

The second method is to use the quadratic synthesis approach [33] for designing an optimal regulator. It has the advantage that the control feedback is naturally limited in magnitude so that it is more implementable. For this reason, it was the method chosen here. As long as the matrix pair (F,G) is controllable, a state compensated system can be generated with this method. A brief description of the details of the quadratic synthesis design procedure follows.

The control problem for this application is viewed as one of determining the optimal steady-state regulator. A cost function is defined as

$$J_Q = \lim_{t_f \to \infty} \frac{1}{2} \int_{t_o}^{t_f} x^T(t)\, Ax(t) + u^T(t)\, B_Q u(t)\, dt \tag{94}$$

where A is a positive semi-definite matrix and B_Q is a positive definite matrix. A and B_Q reflect the judgment of the importance of achieving precise state regulation at the cost of expended control energy. The transient response of the compensated system can be controlled by the proper choice of the ratio of elements in matrices A and B_Q.

The problem then is to determine the control input $u(t)$ so that the cost function J is minimized subject to the dynamic constraint described by Eq. (92). From Reference 33, the required solution is of the form of Eq. (91), where

$$C = B_Q^{-1} G^T K \tag{95}$$

The matrix K is the solution of the algebraic matrix equation

$$-KF - F^T K + KGB_Q^{-1} G^T K = A \tag{96}$$

An efficient computer program [28] which utilizes eigenvalue decomposition techniques to solve Eq. (96) has been used in the examples below for computing the feedback gain matrix C of Eq. (95).

The compensated or closed-loop system which results from the above choice of control is described by Eq. (93). The object of the ensuing investigation is to determine the sensitivity of the response described by Eq. (93) when the values of the parameters in F and G vary, with C fixed at its design value.

To solve Eq. (96) for K first requires specification of the weighting matrices A and B_Q. For the nominal condition, pitch angle and rate limits at 10° and 25°/sec are assumed for the longitudinal mode as suggested in Reference 27. The state cost weighting matrix in Eq. (94) for the CH-46 longitudinal dynamics is chosen to be inversely proportional to the square of these values. The nominal matrix A is thus given by

$$A = \text{diag}\{32{,}827,\ 5.252,\ 0,\ 0\}$$

for the longitudinal mode. Here, the units of the state variables $\Delta\theta$, Δq, Δw and Δu are radians, radians/sec, feet/sec, and feet/sec, respectively. The B_Q matrix is chosen as the identity matrix. For the lateral mode, the roll and yaw rates are also limited to 25°/sec. The roll angle is limited to 30°. Thus, the nominal A matrix for the lateral equations is given as

$$A = \text{diag}\{0,\ 5.2523,\ 5.2523,\ 3.6474\}$$

and the B_Q matrix is again taken as identity. The resulting control gains designed for the indicated flight conditions are given in Table 10.

With the gains listed in Tables 10 used with the parameters of Table 8, a new set of roots of the closed-loop characteristic equation result. These closed-loop roots are presented in Table 11.

TABLE 10.- FEEDBACK CONTROL GAINS FOR THREE POINTS ALONG THE APPROACH TRAJECTORY

	LONGITUDINAL			LATERAL		
GAIN	CRUISE	TRANSITION	HOVER	CRUISE	TRANSITION	HOVER
C_{11}	6.0281	5.9291	5.9819	-0.0204	-0.0097	0.0160
C_{12}	4.0830	4.5688	4.5444	2.0513	2.0678	2.9758
C_{13}	0.0228	0.0437	-0.0026	1.2671	0.6416	1.0246
C_{14}	-0.0229	-0.0260	0.0036	1.4345	1.6259	2.9211
C_{21}	0.4267	-0.0543	-0.8117	-0.0458	-0.0218	-0.0145
C_{22}	0.1274	-0.4438	-0.5750	-0.2569	-0.7725	-1.2023
C_{23}	-0.0007	-0.0097	0.0004	8.9461	4.4925	1.9184
C_{24}	0.0010	0.0066	0.0012	-1.3509	1.2117	-1.3688

TABLE 11.- CONTROLLED (CLOSED-LOOP) POLES OF THE CH-46 EQUATIONS OF MOTION AT THREE POINTS ALONG THE APPROACH FLIGHT PATH

LONGITUDINAL				LATERAL			
POLE	CRUISE	TRANSITION	HOVER	POLE	CRUISE	TRANSITION	HOVER
α_1	-0.89449	-0.86081	-1.10086	α_1	-0.78452	-0.59405	-0.53601
β_1	0.38152	0.12486	0.84334	β_1	0.66590	0.32533	0.12429
α_2	-0.08796	-0.11248	-0.33860	α_2	-1.22553	-1.15167	-1.15758
α_3	-2.36586	-1.86835	-1.14062	α_3	-0.71767	-0.56238	-0.39842

It is interesting to note the variation in the resulting closed-loop dynamics resulting from the control laws as implied by the pole values of Table 11. This is one of the shortcomings of quadratic synthesis. In a practical sense, there is probabily a need for adjusting the elements of the weighting matrices A and B_Q so that the response is more constant along the approach. This can be done by trial-and-error, which points out the art to control system design. For the purpose of this study, however, the closed-loop gains of Table 11 are adequate for preliminary investigation of the effects of parameter uncertainty on control performance and the effect of instrument errors on parameter uncertainty.

Instrument Error Sets

For the purposes of this study, sets of instrument error values were selected from Table 5; the standard deviations of the errors are shown in Table 12. The "base" error sets are meant to represent values typical of a reasonably accurate instrument package which one may expect to find in a carefully conducted flight test program. The "large" error sets represent a case of considerably less overall accuracy. For the large set and the longitudinal mode, the angle-of-attack vane and the airspeed indicator were deleted. For large errors in the lateral mode, the angle-of-sideslip vane was deleted. Instrument lags were also studied, but because their values vary somewhat, they are not listed in Table 12; they are presented later.

Selection of Aircraft Maneuvers

The importance of selecting suitable aircraft maneuvers (input design) in parameter identification cannot be overly stressed. If a flight test maneuver barely excites a mode governed by certain parameters and the data is corrupted by noise and other instrument errors, then those parameters will not be accurately identified.

The choice of control inputs which are optimal from a parameter identification viewpoint is a complex subject which is not addressed here. However, an interesting question with respect to input design was raised in the course of this study. The helicopter's parameters were such that the uncontrolled equations of motion were unstable, and stability was achieved by introducing linear state-variable feedback (see the previous section). What, then, is the best maneuver which excites the controlled system but allows accurate identification of the original aircraft parameters? It was regarded sufficient for purposes here to find suboptimal maneuvers which produced good information in the recorded data. That is, control sequences were chosen which excited the natural frequencies of the closed-loop helicopter system and produced outputs within the range of the instrumentation. The input was modified somewhat in an attempt to keep correlation between identified parameters, as revealed by the off-diagonal terms of the information matrix, small. Also, the control inputs were constrained to be of a form easily applied manually by experienced flight personnel.

TABLE 12(a).- LONGITUDINAL INSTRUMENT ERRORS - STANDARD DEVIATIONS

Instrument	Units	Random Noise		Random Bias		Scale Factor		Alignment (deg)		Initial Condition	
		Base	Large	Base	Large	Base	Large	Base	Large	Base	Large
Pitch Attitude Gyro (θ)	deg	0.02	0.2	0.02	0.2	0.2%	1.5%	---	---	0.02	---
Pitch Rate Gyro (q)	deg/sec	0.05	0.1	0.05	0.1	0.2%	1.0%	---	---	0.05	---
Angle-of-Attack Vane (α)	deg	0.1	---	0.1	---	0.1%	---	---	---	0.005	---
Pitot Tube (u)	ft/sec	1.0	---	1.0	---	2.5%	---	---	---	0.2	---
Forward Accelerometer (a_x)	g's	0.01	0.01	0.01	0.01	0.1%	1.0%	0.1	0.5	---	---
Vertical Accelerometer (a_z)	g's	0.01	0.01	0.01	0.01	0.1%	1.0%	0.1	0.5	---	---
Pitch Accelerometer ($\dot{q}$)	deg/sec^2	0.1	0.2	0.1	0.2	0.2%	2.0%	---	---	---	---
Differential Collective Pitch (δ_c)	in	---	---	0.05	0.1	0.5%	2.0%	---	---	---	---
Gang Collective Pitch (δ_c)	in	---	---	0.05	0.1	0.5%	2.0%	---	---	---	---

Other Errors:

Type	Units	Base	Large
c.g. Uncertainty e_{cgx}, e_{cgz}	ft	0.25	1.0
Mass Unbalance e_{25}, e_{26}	deg/sec · g	0.1	0.1
$\dot{q}$ Sensitivity to a_x, a_z e_{75}, e_{76}	deg/sec^2 · g	0.006	0.006

TABLE 12(b).- LATERAL INSTRUMENT ERRORS - STANDARD DEVIATIONS

Instrument	Units	Random Noise		Random Bias		Scale Factor		Alignment (deg)	
		Base	Large	Base	Large	Base	Large	Base	Large
Angle-of-Sideslip Vane (β)	deg	0.1	---	0.1	---	0.1%	---		
Roll Rate Gyro (p)	deg/sec	0.03	0.1	0.03	0.1	0.2%	1.0%	0.1	0.5
Yaw Rate Gyro (r)	deg/sec	0.03	0.1	0.03	0.1	0.2%	1.0%	0.1	0.5
Roll Attitude Gyro (ϕ)	deg	0.02	0.2	0.02	0.2	0.2%	1.5%		
Lateral Accelerometer (a_y)	g's	0.01	0.01	0.01	0.01	0.1%	1.0%		
Roll Accelerometer ($\dot{p}$)	deg/sec^2	0.1	0.2	0.1	0.2	0.2%	2.0%	0.1	0.5
Yaw Accelerometer ($\dot{r}$)	deg/sec^2	0.1	0.2	0.1	0.2	0.2%	2.0%	0.1	0.5

c.g. uncertainty (e_{cgx}, e_{cgz}): Base: 0.25 ft., Large: 1.0 ft.

Inputs were first developed for the longitudinal equations at the cruise flight condition. Time histories of the nominal control input and the aircraft response are shown in Figure 11. The nominal measurement data sequence contained 300 time points taken every 0.05 sec over a 15 sec interval. The differential pitch control (δ_c) consists of: (1) a sine wave whose frequency is that of the closed-loop complex poles (see Table 11), and (2) a superimposed sine wave with a 5 in. amplitude and timed to occur during the first two seconds. The collective pitch control (δ_c) is similar except that the short sine wave has a 2.5 in. amplitude and begins at 7.5 sec. The slower sine waves are intended to excite the two real modes. The control time histories for the longitudinal equations at the transition and near-hover flight conditions are not shown, but differ from Figure 11 by the frequency of the slower sine waves, which were set equal to the frequencies of the corresponding complex poles. Also, at the near-hover condition, the amplitudes of both "doublet" sine waves were adjusted to 2.0 in. and the amplitudes of both slow sine waves to 0.5 in. so that the aircraft did not exceed the linear range of the equations.

A similar philosophy was attempted for control time histories in the lateral cases. However, the resulting trajectories were found to contain insufficient information. That is, the standard deviations of the identified parameters, with this 15 sec span of data, were considered larger than they had to be. This was corrected by increasing the record length to 30 sec and adding two "pulses" to the yaw cyclic control. The number of recorded time points was retained at 300 by decreasing the sampling rate to once every 0.1 sec. The time histories of this lateral control and the resulting aircraft responses are shown in Figure 12 for the near-hover flight condition. Again, the control time histories for the lateral cases at cruise and transition differ by the frequency of the slower sine waves. These were set equal to the frequencies of the corresponding complex poles.

The Effects of Instrument Errors on Longitudinal Parameters

The study of the effects of longitudinal instrument errors was conducted primarily at the cruise flight condition. Certain cases were repeated at the transition and near-hover flight conditions for comparison. This section discusses the effects of both the baseline and large error sets, adding or omitting instruments, and changes in the control sequence and data length on the standard deviations of the parameter estimates. Also, the effects of variations in input and output measurement lags on the estimates are investigated. Results obtained from both ensemble analysis and Monte Carlo analysis are discussed. Table 13 is a summary of the ensemble analysis computer runs which provided the results presented in this section.

Basic set.- Four computer runs of the VTOL Ensemble Error Analysis Program were made to assess the effects of the longitudinal baseline instrument errors of Table 12. Case 1 contained only the output measurement errors: white noise, biases (which were not estimated by the identification algorithm), scale factor errors, accelerometer misalignments, c.g. location errors, pitch-rate gyro mass unbalance ($e_{2,5}$ and $e_{2,6}$), and pitch angular accelerometer sensitivity to linear acceleration ($e_{7,5}$ and $e_{7,6}$). Case 2 added the control measurement biases and

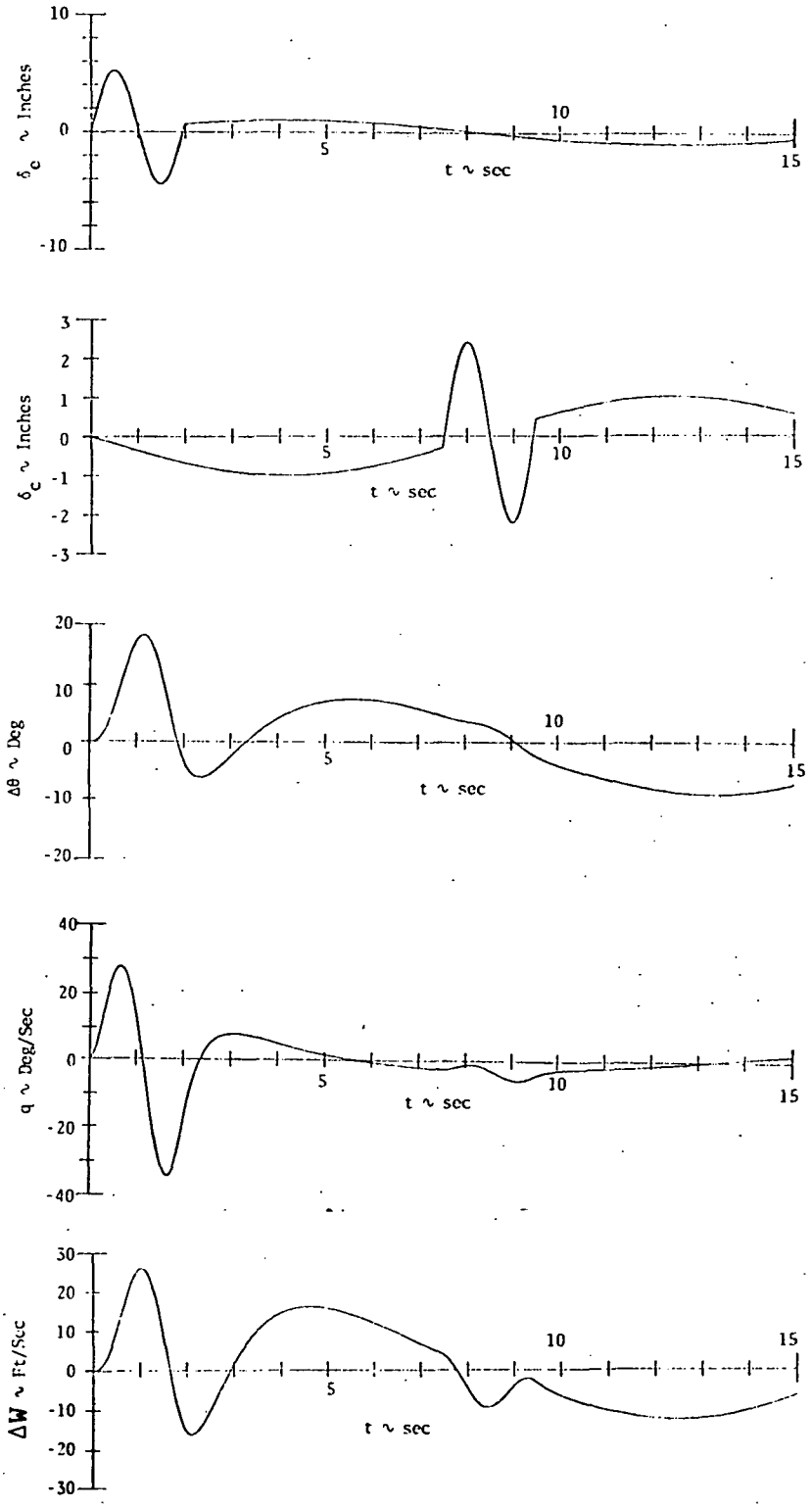

FIGURE 11.- NOMINAL TRAJECTORY FOR LONGITUDINAL MOTION AT CRUISE

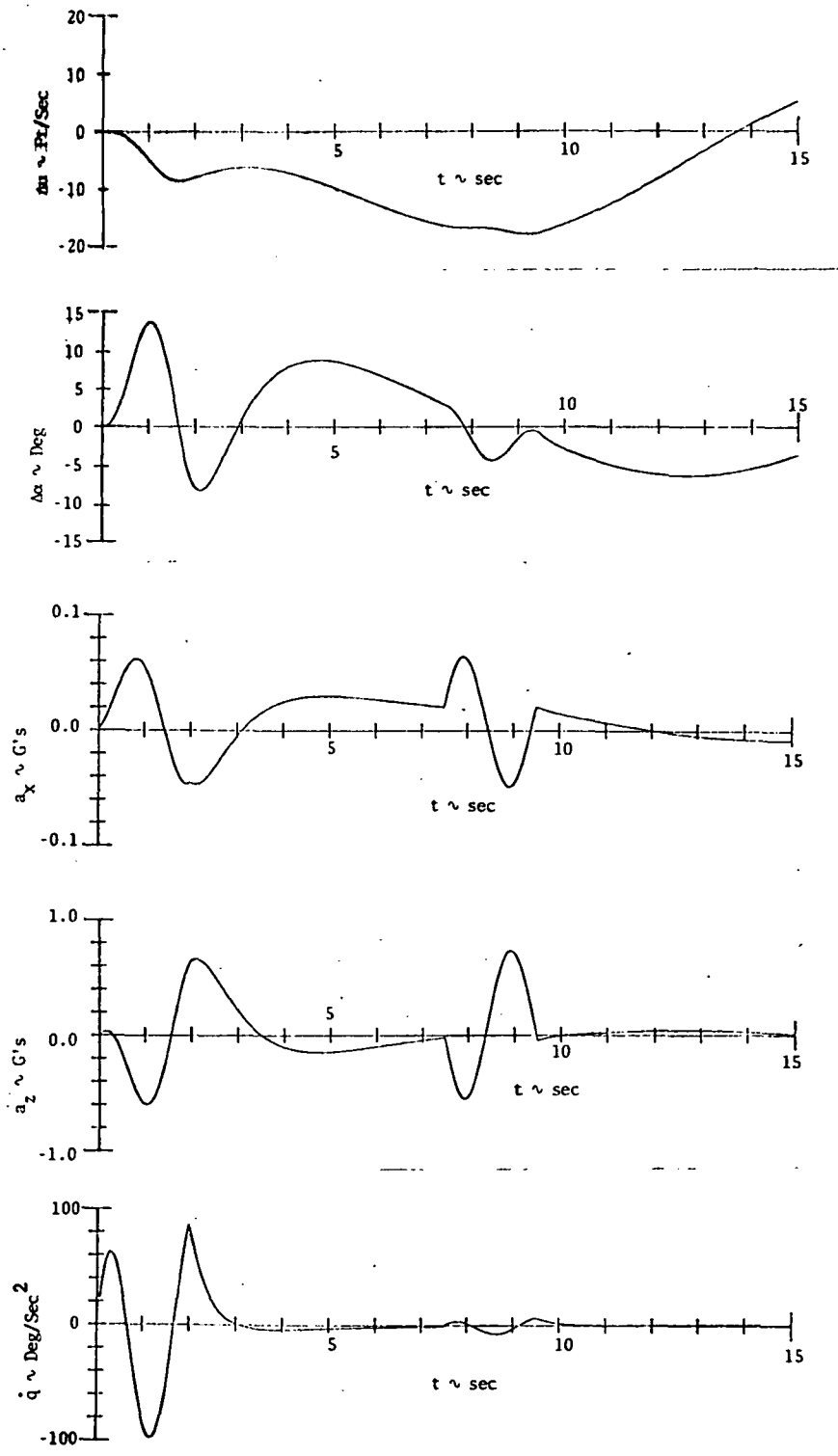

FIGURE 11.- (CONCLUDED)

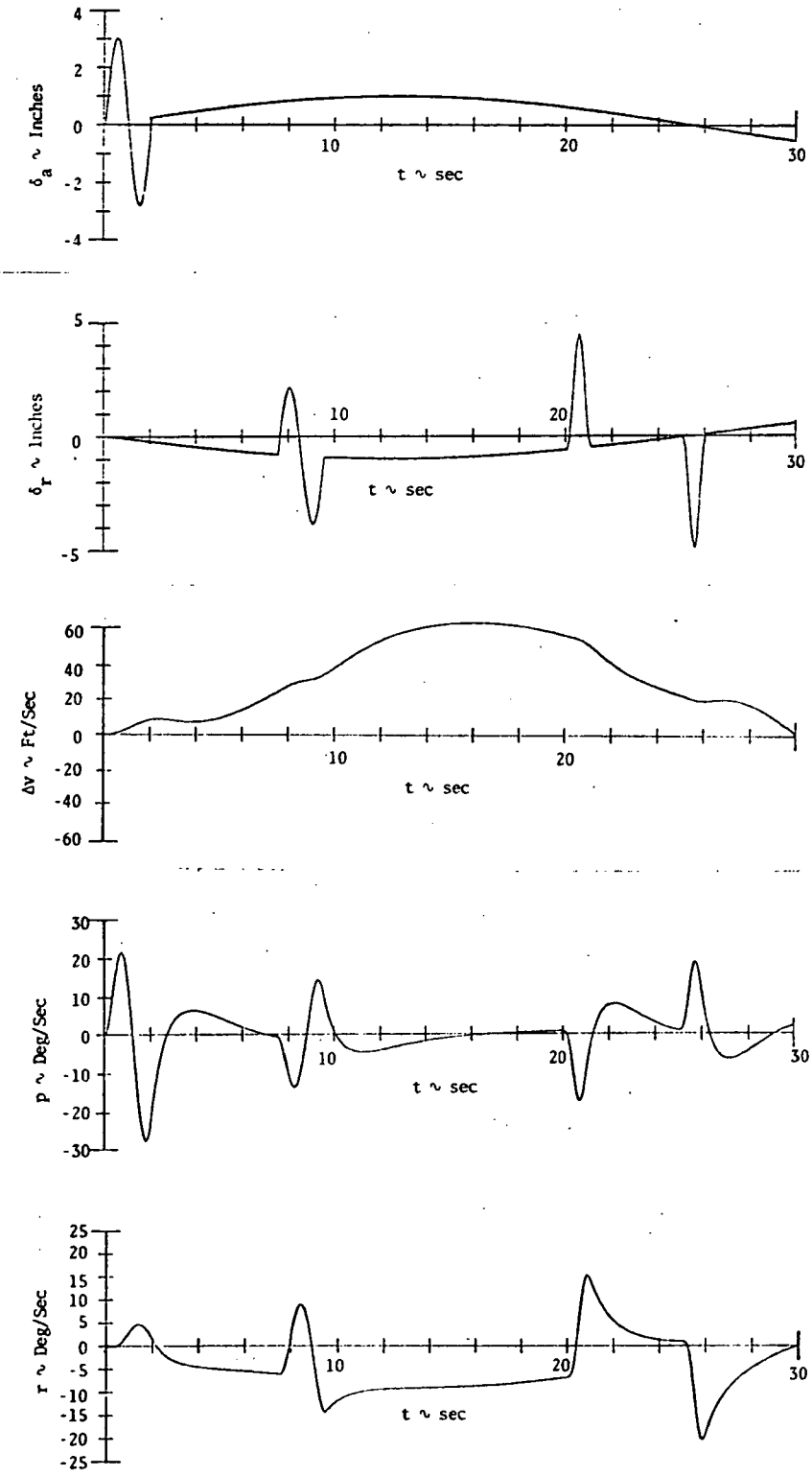

FIGURE 12.- NOMINAL TRAJECTORY FOR LATERAL MOTION NEAR-HOVER

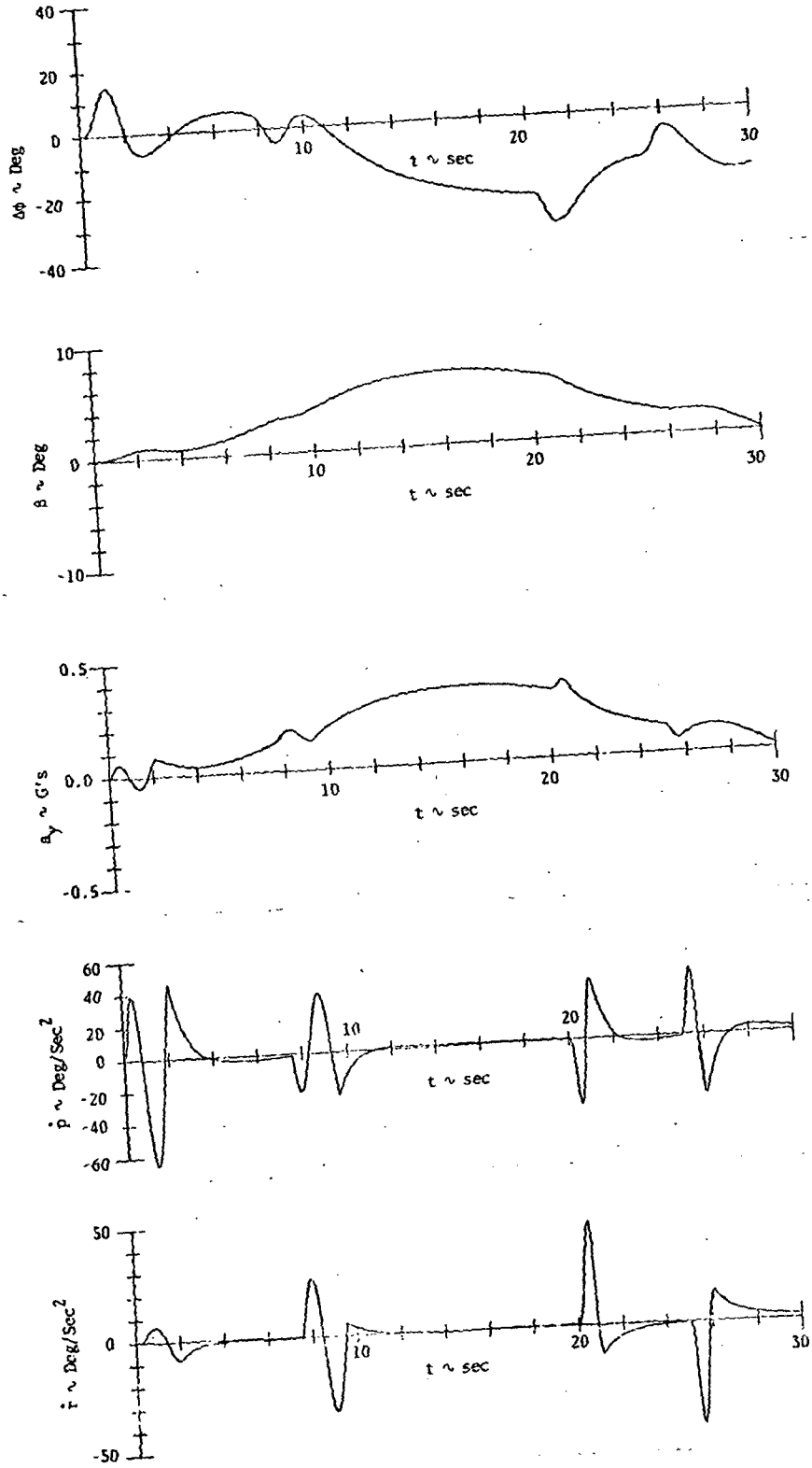

FIGURE 12.- (CONCLUDED)

TABLE 13.- SUMMARY OF ENSEMBLE ANALYSIS COMPUTER RUNS FOR THE LONGITUDINAL MODE

Case No.	Description of Instruments, Error Sources and Flight Regime			Bias & I.C. Estimated?	Compared with Cases __
	Regime	θ q α u a_x a_z $\dot{q}$	Comments		
1	Cruise	✓ ✓ ✓ ✓ ✓	No control or i.c. errors	No	
2	Cruise	✓ ✓ ✓ ✓ ✓	No i.c. errors	No	1
3	Cruise	✓ ✓ ✓ ✓ ✓	Nominal instruments & errors	No	1,2
4	Cruise	✓ ✓ ✓ ✓ ✓	Nominal instruments & errors	Yes	3
5	Transition	✓ ✓ ✓ ✓ ✓	Nominal instruments, no i.c.	No	2
6	Hover	✓ ✓ ✓ ✓ ✓	Nominal instruments, no i.c.	No	2
7	Cruise	✓ ✓ ✓ ✓ ✓ ✓ ✓	Nominal errors	No	3
8	Cruise	✓ ✓ ✓ ✓ ✓ ✓ ✓	Nominal errors	Yes	4,7
9	Cruise	✓ ✓ ✓ ✓ ✓ ✓	Nominal errors	No	7
10	Cruise	✓ ✓ ✓ ✓ ✓ ✓	Nominal errors	Yes	8
11	Cruise	✓ ✓ ✓ ✓	Nominal errors	Yes	4
12	Cruise	✓ ✓ ✓ ✓	"Doublet" sine wave input	Yes	11
13	Cruise	✓ ✓ ✓ ✓	30 sec. extra data (45 s. total)	Yes	11
14	Cruise	✓ ✓ ✓ ✓ ✓ ✓	30 sec. extra data	Yes	10,13
15	Cruise	✓ ✓ ✓ ✓ ✓ ✓	Identical time lags of .1667 sec. No i.c. errors.	No	2
16	Cruise	✓ ✓ ✓ ✓ ✓ ✓	Output measurement lags of .1667 sec. No i.c. errors.	No	2
17	Cruise	✓ ✓ ✓ ✓ ✓ ✓	Output measurement lags of .0333 sec. No i.c. errors	No	2,16
18	Cruise	✓ ✓ ✓ ✓ ✓ ✓	Large instrument errors	Yes	4

Nominal output instruments are θ-gyro, q-gyro, a_x and a_z accelerometers, and $\dot{q}$ accelerometer.

Nominal errors are the baseline values of all the longitudinal instrument errors of Table 12(a).

scale factor errors; Case 3 added initial condition errors (i.e., it contained all the basic errors); Case 4 contained all these errors but estimated the biases and initial condition errors, which effectively eliminated them. The instrument package in each case consisted of a pitch-attitude gyro, a pitch-rate gyro, longitudinal and normal accelerometers, and a pitch angular accelerometer.

The standard deviations of the parameter estimates due to noise only and due to all other instrument errors as computed by these four cases are listed in Table 14. The standard deviations of the parameters due to noise alone are the same in Cases 1, 2, and 3. Thus, they are only listed once. The instrument error sets studied do not contain deterministic errors (see the third chapter) so the expected value of the parameter errors are zero in each case.

TABLE 14.- ENSEMBLE ANALYSIS ERROR STANDARD DEVIATIONS OF PARAMETER ESTIMATES, CASES 1 TO 4

Parameter	Value*	Standard Deviations Due to Noise		Standard Deviations Due To All Errors			
		Cases 1, 2 & 3	Case 4	Case 1	Case 2	Case 3	Case 4
M_q	-1.47606	0.00086	0.00088	0.00354	0.01705	0.01706	0.01003
Z_q	-0.03169	0.00328	0.00332	0.00730	0.00772	0.00786	0.00499
X_q	0.01429	0.00283	0.00288	0.00740	0.05038	0.05045	0.00719
M_w	0.74996	0.00092	0.00104	0.00476	0.04729	0.04742	0.00813
Z_w	-0.83231	0.00415	0.00449	0.01158	0.01400	0.01736	0.00927
X_w	0.08842	0.00281	0.00287	0.00522	0.03966	0.03969	0.00791
M_u	-0.37084	0.00155	0.00177	0.00511	0.09034	0.09064	0.00606
Z_u	-0.01264	0.00624	0.00669	0.01057	0.03813	0.04327	0.00706
X_u	-0.03872	0.00109	0.00246	0.00564	0.06688	0.06700	0.00519
$M_{\delta e}$	26.25713	0.00660	0.00714	0.03407	0.29271	0.29341	0.10425
$Z_{\delta e}$	0.55709	0.02589	0.02733	0.12484	0.13208	0.14419	0.12167
$X_{\delta e}$	0.14798	0.02224	0.02243	0.11724	0.20926	0.20938	0.11987
$M_{\delta c}$	3.87480	0.00682	0.00715	0.03810	0.18731	0.18741	0.04205
$Z_{\delta c}$	-8.77426	0.02932	0.02948	0.04401	0.13670	0.13830	0.06423
$X_{\delta c}$	0.77170	0.02420	0.02525	0.05502	0.58318	0.58674	0.06562

*Units are consistent with Tables 8 and 12.

Each parameter's standard deviation due to all instrument errors was divided by the absolute value of the corresponding parameter and expressed in per cent. The results are shown graphically in Figure 13. From this figure, the following comments can be made:

(1) With only white noise in the measurements, four parameter estimates have error standard deviations exceeding 10% of the parameter value. These are Z_u at 49%, $X_{\delta e}$ at 15%, X_q at 20%, and Z_q at 10%. The first three are all associated with the longitudinal velocity perturbation, Δu. This suggests that the information content of the data sequence with respect to these parameters and Δu could be improved. Also, relative to the magnitude of perturbations in the other state variables shown in Figure 11, Δu's direct measurement accuracy is relatively poor. The eigenvectors associated with the closed-loop poles of Table 11 show that Δu motion is principally governed by the real pole at $-0.088\ \text{sec}^{-1}$. Thus, the 15 sec length of the data sequence provides only 1.3 time constants of this mode. Increasing data length can possibly decrease these error standard deviations; this point is examined by Case 13 discussed later.

(2) The addition of error sources other than white noise has a substantial effect on the parameter error standard deviations. In Case 1, which has all the output measurement static errors but no control errors, the standard deviations for six parameters (M_w, $M_{\delta e}$, $M_{\delta c}$, $Z_{\delta e}$, X_u, and $X_{\delta e}$) increased by a multiple of five or more over errors due to noise only.

(3) In Case 2, which adds the static control measurement errors, all parameter standard deviations except those of Z_q and Z_w increased by at least a factor of five over the deviations due to white noise only.

(4) The control measurement errors--biases and scale factor errors--are the dominant errors for twelve parameters. The exceptions are Z_q, Z_w, and $Z_{\delta e}$. This is reflected in Figure 13 by the large increases of the standard deviations of Case 2 over Case 1.

(5) The initial condition errors which are added in Case 3 produce little or no change.

(6) Estimating the output measurement biases and initial conditions (Case 4) resulted in lower error standard deviations for every parameter. Reviewing the sensitivity data of estimated stability and control derivatives to control biases ($\partial \delta p_p / \partial B_c$) showed that these error terms decreased when the output measurement biases were estimated. This appears to be because the effects of control bias are picked up as output measurement biases. Thus, the accuracy of the aircraft parameters is improved even though the true error source (input

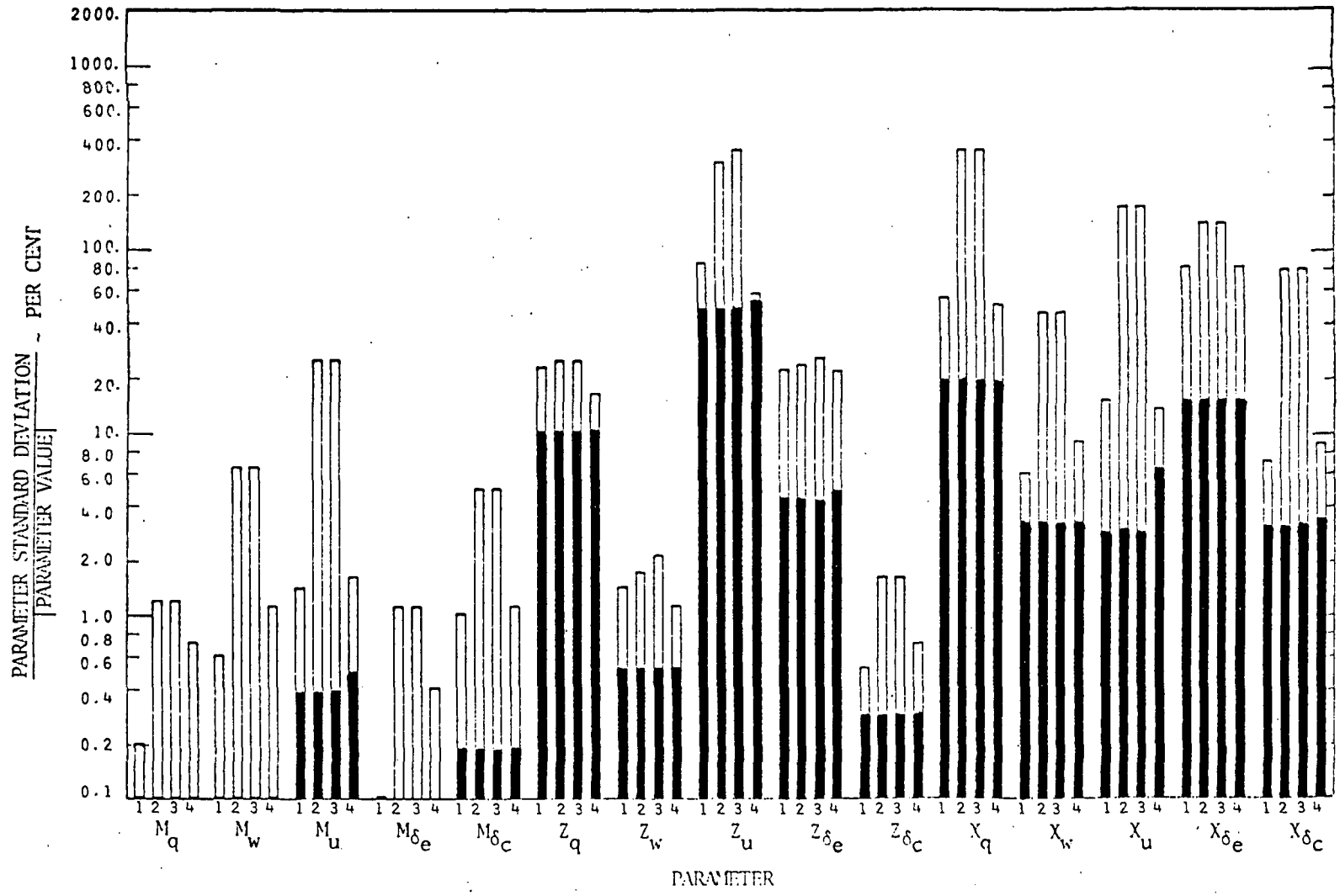

Shaded Portion of Each Bar Shows Standard Deviation Due to Noise Alone.

FIGURE 13.- COMPARISON OF ENSEMBLE ANALYSIS PARAMETER ERROR STANDARD DEVIATIONS FROM CASES 1 THROUGH 4: NOMINAL ERROR SET; CRUISE FLIGHT

bias) is incorrectly identified as an output bias. This simply underscores the relative importance of control biases just mentioned. Furthermore, it demonstrates for this instance, at least, the desirability of including output bias and initial condition estimation in the identification algorithm. Improvement was most pronounced for seven parameters (M_u, Z_u, X_q, X_w, X_u, $X_{\delta e}$, and $X_{\delta c}$). Each of these parameter estimates is associated with the longitudinal velocity perturbation. Finally, the indication is that it is probably desirable to estimate control measurement biases also.

An important result of the Ensemble Error Analysis procedure is the matrix of parameters sensitivities to the instrument errors, $\partial\delta p/\partial e$. Tables 15 and 16 present these sensitivities, respectively, for Case 3 (which contained all baseline errors and did not estimate output biases and initial conditions) and Case 4 (which did estimate them). A principal use of these sensitivities is to determine the effect a change in an error magnitude e_j has on a parameter estimate error Δp_i. This may be accomplished by means of the relationship

$$E\{\delta p_i^2\}_{new} = E\{\delta p_i^2\}_{old} + \left(\frac{\partial \delta p_i}{\partial e_j}\right)^2 \left(e^2_{j_{new}} - e^2_{j_{old}}\right) \qquad (104)$$

For example, the effect on the standard deviation of M_w due to changes in the bias in differential collective pitch stick position, $b_{\delta e}$, was computed using Eq. (104) and the appropriate sensitivity value from Table 15. The result is shown in Figure 14(a). Because $b_{\delta e}$ is the dominant error for this parameter, the standard deviation of M_w is highly dependent on $b_{\delta e}$. Similarly, Figure 14(b) shows how the accuracy of the M_w estimate varies with the pitch gyro scale factor, e_θ. Obviously, the dependence here is considerably less, even though e_θ produces the largest static error effect of the output measurement instruments. (The dominant error source e_i for a particular parameter p_j is the one which produces the largest absolute product when its standard deviation is multiplied by the sensitivity to that error; i.e., $\left|\frac{\partial p_j}{\partial e_i}\right| \sigma_{e_i}$ is the largest such product.)

Assume that it is necessary to identify M_w with an accuracy of one standard deviation equal to 20% of its expected value. Then Figure 14(a) shows that $b_{\delta e}$ must be less than 0.16 in. Figure 14(b) shows that even a 2% value for e_θ will not affect the M_w estimate appreciably. This demonstrates how one can determine the accuracy requirements of instruments to meet specified parameter estimation accuracies.

A second use of the sensitivities ($\partial\delta p/\partial e$) is to determine the major sources of error in each parameter estimate. This is done in conjunction with values of instrument errors from Table 5. For example, with the baseline error values of Table 12, the dominant error sources are those presented in Table 17.

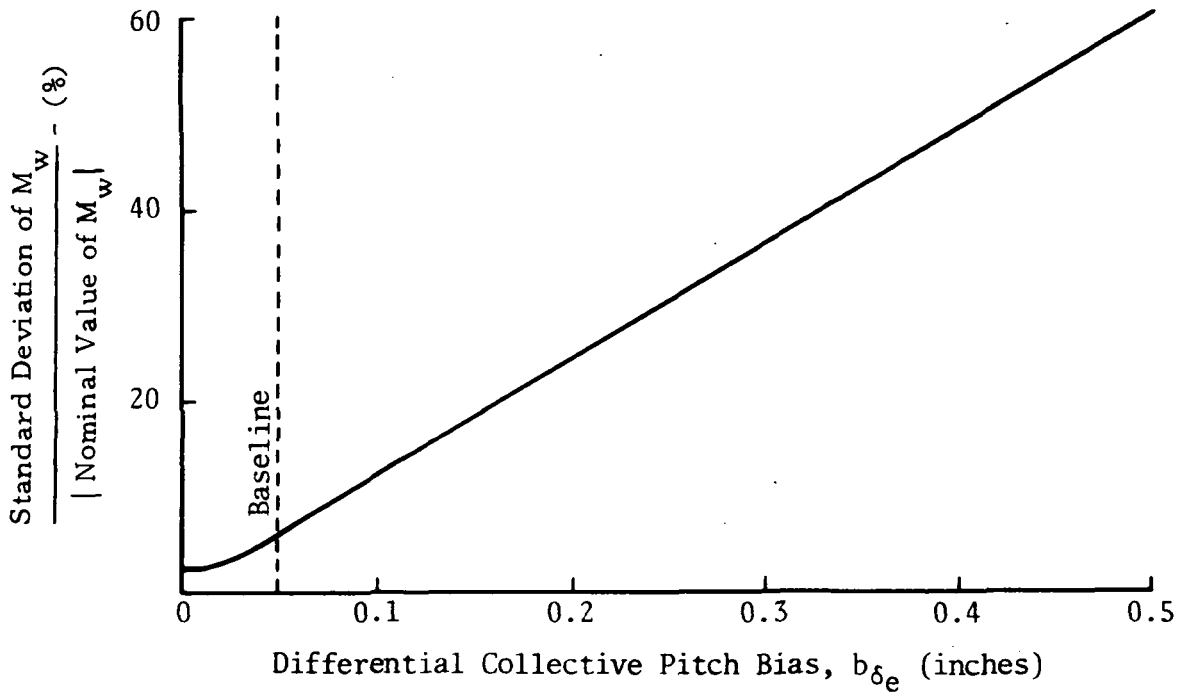

FIGURE 14(a).- VARIATION OF M_w ERROR WITH BIAS $b_{\delta e}$ COMPUTED FROM ENSEMBLE ANALYSIS SENSITIVITY

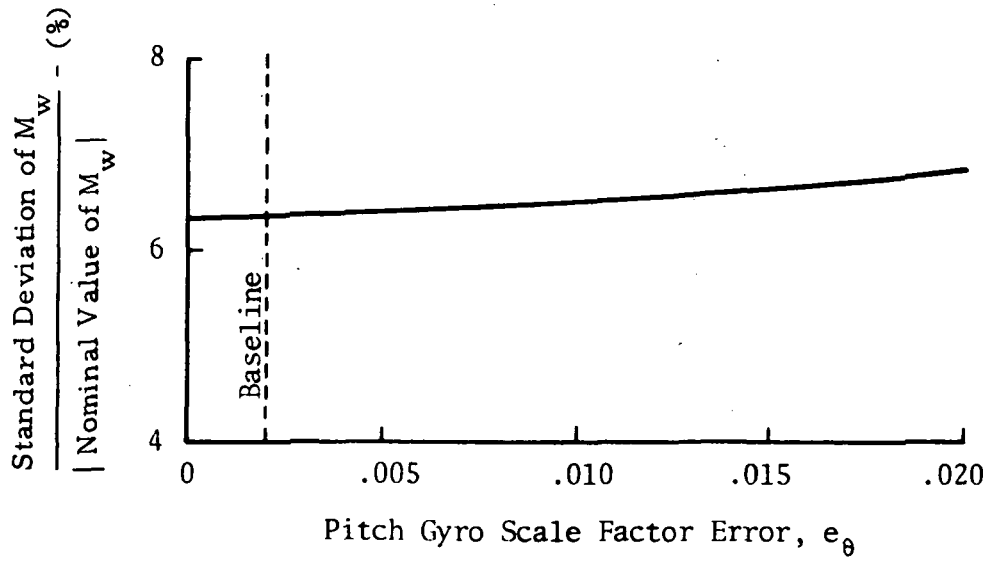

FIGURE 14(b).- VARIATION OF M_w ERROR WITH SCALE FACTOR ERROR e_θ COMPUTED FROM ENSEMBLE ANALYSIS SENSITIVITY

TABLE 15.- SENSITIVITIES OF ENSEMBLE ANALYSIS PARAMETER ERROR STANDARD DEVIATIONS TO INSTRUMENT ERROR SOURCES FROM CASE 3

	Biases on Output Measurements				
	b_θ	b_q	b_{a_x}	b_{a_z}	$b_{\dot{q}}$
Error Value:	0.200-01	0.300-01	0.100-01	0.100-01	0.100+00
M_q	-0.299-01	-0.105-01	-0.829-01	-0.509-01	-0.508-03
Z_q	0.593-02	-0.194-01	-0.391+00	0.428+00	-0.159-02
X_q	0.116+00	0.682-02	0.842-01	-0.783-01	0.115-04
M_w	0.113+00	0.118-01	0.133+00	0.866-01	0.642-03
Z_w	-0.582-02	0.297-01	0.502+00	-0.854+00	0.207-02
X_w	-0.687-01	0.202-01	-0.133+00	0.115+00	0.153-02
M_u	-0.190+00	0.426-01	-0.373-01	-0.839-01	0.175-02
Z_u	0.310-01	0.406-01	0.794+00	0.594-01	0.321-02
X_u	-0.186+00	-0.470-01	-0.332+00	0.442-01	-0.181-02
M_{δ_e}	0.691+00	0.597-01	0.648+00	0.402+00	0.279-02
Z_{δ_e}	-0.933-01	0.112+00	0.199+01	-0.360+01	0.820-02
X_{δ_e}	-0.286+00	0.105+00	-0.482+00	0.477+00	0.731-02
M_{δ_c}	-0.341+00	-0.929-01	-0.400+00	0.142+00	-0.535-02
Z_{δ_c}	0.306+00	0.549-01	-0.541+00	0.228+01	-0.162-02
X_{δ_c}	0.138+01	0.210+00	0.265+01	-0.139+00	0.118-01

NOTE: Units are consistent with Tables 8 and 12.
The notation 0.200-01 means 0.2×10^{-1}.

With regard to the data in Table 17, the following observations are made:

(1) In Case 1 (which contained only output measurement errors), an output bias appears as the largest source of error for seven parameters and as the second largest source of error for nine parameters. Thus, the output biases were the most important error sources, and they are followed in importance by the c.g. location errors, the rate-gyro mass unbalance in the x-direction ($e_{2,6}$), and the measurement scale-factor errors, in that order.

TABLE 15.- (CONTINUED)

	Scale Factor Errors on Output Measurements				
	e_θ	e_q	e_{a_x}	e_{a_z}	$e_{\dot{q}}$
Error Value:	0.200-02	0.200-02	0.100-02	0.100-02	0.200-02
M_q	0.228+00	0.121+01	0.100-02	-0.329-01	0.289+00
Z_q	-0.485+00	-0.769-01	-0.687-03	0.660-01	0.169+00
X_q	-0.177+00	-0.774-01	0.112-01	-0.329-01	0.607-01
M_w	0.123+01	0.150+00	0.125-02	0.134-01	0.439+00
Z_w	0.102+01	0.479+00	-0.838-02	-0.642+00	0.149+00
X_w	0.314+00	0.459+00	0.667-01	0.113+00	0.430+00
M_u	-0.527+00	-0.350+00	0.184-01	-0.366-01	-0.602+00
Z_u	-0.174+00	0.317+00	0.303-02	0.367+00	0.458+00
X_u	0.459+00	-0.465-01	-0.115-01	-0.532-01	-0.103+00
M_{δ_e}	0.733+01	0.625+01	0.285-01	-0.398-01	0.108+02
Z_{δ_e}	0.317+01	-0.858-01	-0.234-01	0.188+01	-0.116+01
X_{δ_e}	0.129+01	0.211+01	0.389-01	0.427+00	0.180+01
M_{δ_c}	0.388+00	0.204+01	-0.514-01	0.398+00	0.308+01
Z_{δ_c}	0.216+01	0.286+01	-0.150+00	-0.863+01	0.379+01
X_{δ_c}	0.177+01	0.455+01	0.585+00	0.117+01	0.857+01

NOTE: Units are consistent with Tables 8 and 12.

(2) In Case 3 (which differs from Case 1 by the addition of control biases, control scale factor errors, and state initial condition errors), the overwhelming source of error is the control bias $b_{\delta e}$. It is the dominant error source for 12 parameters. By comparing the total error standard deviations of these 12 parameters to the standard deviations due to $b_{\delta e}$ alone, it can be seen that the error introduced by $b_{\delta e}$ often exceeds the error due to all other sources put together. Moreover, other control errors appear as the second largest source of error for eight parameters. Besides the control errors, other important error sources are the c.g. location errors and the initial condition error for the vertical velocity component Δw. Other initial

TABLE 15.- (CONTINUED)

	Gyro Mass Unbalance		Angular Accelerometer Sensitivity to Linear Acceleration		Accelerometer Misalignment	
	$e_{2,5}$	$e_{2,6}$	$e_{7,5}$	$e_{7,6}$	γ_{a_x}	γ_{a_z}
Error Value:	0.100+00	0.100+00	0.600-02	0.600-02	0.100+00	0.100+00
M_q	0.149-02	-0.159-01	0.121-03	0.216-02	0.536-03	0.895-05
Z_q	0.559-03	0.175-03	-0.260-03	0.212-02	0.100-02	0.364-03
X_q	0.249-03	-0.510-02	0.113-03	-0.911-03	0.102-02	-0.520-05
M_w	0.253-02	-0.267-01	-0.393-04	-0.820-04	0.498-03	-0.943-05
Z_w	-0.153-02	0.118-01	0.231-03	-0.137-02	-0.272-02	0.956-03
X_w	-0.102-03	0.408-02	-0.151-03	0.220-02	0.108-01	-0.126-03
M_u	-0.192-02	0.188-01	-0.364-03	0.266-02	0.198-02	0.183-03
Z_u	0.931-03	-0.178-01	0.243-03	-0.645-03	-0.254-02	-0.180-02
X_u	0.293-03	-0.155-02	0.181-03	-0.218-02	-0.478-03	0.250-03
M_{δ_e}	0.443-02	0.532-01	-0.514-02	0.503-01	0.487-02	0.225-03
Z_{δ_e}	-0.923-02	0.705-01	0.126-02	-0.126-01	-0.891-02	-0.143-02
X_{δ_e}	-0.826-03	0.235-01	-0.900-03	0.120-01	-0.255-01	-0.436-03
M_{δ_c}	0.343-01	-0.356+00	0.425-02	-0.452-01	-0.581-02	-0.712-03
Z_{δ_c}	-0.125-02	0.335-01	0.307-03	0.133-02	-0.240-01	0.149-01
X_{δ_c}	0.894-02	-0.114+00	0.237-02	-0.795-02	0.111+00	-0.180-02

NOTE: Units are consistent with Tables 8 and 12.

condition errors do not appear. Other output measurement errors appear only four times in the table for this case. Thus, the importance of control errors far exceeds other sources of error when output biases and initial conditions are not estimated.

(3) In Case 4, the output biases and initial conditions are estimated, which effectively removes them as sources of error in the parameter estimates. It was explained previously that this also removes the control biases from importance as sources of error. However, the control scale-factor errors were not diminished. In fact, they remain as the first and/or second most important sources of error for every parameter except X_u. Other important error sources are the

TABLE 15.- (CONTINUED)

	State Initial Condition Error				C.G. Location Error	
	$\Delta\theta$	Δq	Δw	Δu	$e_{x_{cg}}$	$e_{z_{cg}}$
Error Value:	0.200-01	0.300-01	0.100+01	0.200+00	0.250+00	0.250+00
M_q	0.297-02	0.183-02	-0.477-03	-0.202-02	0.267-02	-0.393-02
Z_q	0.624-02	0.240-02	0.145-02	0.190-03	0.109-01	-0.160-03
X_q	-0.174-02	0.217-02	0.215-02	0.763-02	0.149-02	-0.251-01
M_w	0.722-02	0.557-02	0.316-02	0.725-02	-0.175-05	-0.659-06
Z_w	-0.630-02	-0.636-02	-0.103-01	-0.496-03	-0.131-01	0.500-05
X_w	0.168-01	0.712-02	0.962-03	-0.630-02	-0.450-05	0.131-01
M_u	0.268-02	-0.641-02	-0.681-02	-0.150-01	0.259-05	-0.438-05
Z_u	-0.228-01	0.949-02	0.204-01	0.599-02	0.646-02	0.307-05
X_u	0.403-02	-0.205-02	-0.363-02	-0.775-02	0.937-07	-0.647-02
M_{δ_e}	0.755-01	0.442-01	0.182-01	0.427-01	-0.968-05	-0.245-05
Z_{δ_e}	-0.592-01	-0.364-01	-0.578-01	-0.531-02	-0.458+00	0.194-04
X_{δ_e}	0.688-01	0.264-01	0.359-02	-0.295-01	-0.196-04	0.458+00
M_{δ_c}	0.785-01	0.296-01	0.112-02	00.286-01	-0.950-05	0.897-05
Z_{δ_c}	0.494-01	0.564-01	0.205-01	0.194-01	-0.675-01	0.185-04
X_{δ_c}	0.227+00	0.168+00	0.611-01	0.985-01	-0.170-04	0.675-01

NOTE: Units are consistent with Tables 8 and 12.

c.g. location errors and the scale-factor error on the pitch angular accelerometer.

(4) The gyro mass unbalance in the z-direction, the angular accelerometer sensitivities to linear acceleration, and the linear accelerometer misalignments were relatively minor error sources for all parameters in each case.

Comparison of instrument error effects at cruise, transition, and near hover.- Considered next were the effects of the baseline instrument errors at the transition and near-hover flight conditions. Two computer runs (Cases 5 and 6) similar to Case 3, which was for cruise, were made at the transition and near-hover points (see Figures 7, 8 and 9 and Table 8). The control input sequences of these cases were similar but not identical, as discussed in this chapter under "Selection of Aircraft Maneuvers." Output biases and initial condition errors were not estimated.

TABLE 15.- (CONCLUDED)

	Control Bias		Control Scale Factor	
	b_{δ_e}	b_{δ_c}	e_{δ_e}	e_{δ_c}
Error Value:	0.500-01	0.500-01	0.500-02	0.500-02
M_q	0.275+00	0.277-01	-0.187+01	-0.143-01
Z_q	0.152-01	-0.148-01	0.455+00	0.539-01
X_q	-0.991+00	-0.106+00	0.230+00	0.130-02
M_w	-0.921+00	-0.111+00	-0.160+00	0.282-02
Z_w	-0.510-03	0.108+00	-0.114+01	-0.624-01
X_w	0.774+00	0.462-01	-0.128+01	-0.226-01
M_u	0.178+01	0.225+00	0.140+01	-0.128-01
Z_u	-0.674+00	-0.272+00	-0.963+00	0.198-01
X_u	0.133+01	0.141+00	-0.290+00	0.247-02
M_{δ_e}	-0.539+01	-0.646+00	-0.209+02	0.872-01
Z_{δ_e}	0.369+00	0.640+00	-0.444+01	-0.426+00
X_{δ_e}	0.342+01	0.261+00	-0.522+01	-0.858-01
M_{δ_c}	0.364+01	0.296+00	-0.100+01	-0.367+01
Z_{δ_c}	-0.230+01	-0.413+00	-0.771+01	0.797+01
X_{δ_c}	-0.114+02	-0.163+01	-0.139+02	-0.902+00

NOTE: Units are consistent with Tables 8 and 12.

True parameter values, the error standard deviations of the parameter estimates due to white noise alone and those due to all errors are listed in Table 18. Similar information is shown graphically in Figure 15, where the error standard deviations are expressed as percentages of the associated parameter values. The following observations are made from Figure 15:

(1) The addition of error sources other than white noise has a substantial effect on parameter error standard deviations in transition and near-hover, as was previously noted at the cruise condition. Again, the principal sources of these errors are the control biases and control scale factors.

TABLE 16.- SENSITIVITIES OF ENSEMBLE ANALYSIS PARAMETER ERROR STANDARD DEVIATIONS TO INSTRUMENT ERROR SOURCES FROM CASE 4

	Scale Factor Errors				
	e_θ	e_q	e_{a_x}	e_{a_z}	$e_{\dot{q}}$
Error Value:	0.200-02	0.200-02	0.100-02	0.100-02	0.200-02
M_q	0.304+00	0.118+01	0.380-03	-0.297-01	0.259+00
Z_q	-0.373+00	-0.162+00	0.322-02	0.374-01	0.114+00
X_q	-0.430+00	-0.140-01	0.138-01	-0.348-01	0.206+00
M_w	0.965+00	0.187+00	0.352-02	-0.195-02	0.560+00
Z_w	0.784+00	0.823+00	-0.194-01	-0.517+00	0.299+00
X_w	0.332+00	0.405+00	0.691-01	0.801-01	0.489+00
M_u	-0.390+00	-0.236+00	0.167-01	-0.194-01	-0.531+00
Z_u	-0.863-01	-0.237+00	0.749-02	0.206+00	0.212+00
X_u	0.127+01	-0.308+00	-0.257-01	0.648-03	-0.896+00
$M_{\delta e}$	0.557+01	0.654+01	0.419-01	-0.121+00	0.116+02
$Z_{\delta e}$	0.238+01	0.150+01	-0.781-01	0.253+01	-0.446+00
$X_{\delta e}$	0.110+01	0.203+01	0.561-01	0.262+00	0.242+01
$M_{\delta c}$	0.766+00	0.170+01	-0.501-01	0.312+00	0.309+01
$Z_{\delta c}$	0.166+01	0.226+01	-0.130+00	-0.886+01	0.418+01
$X_{\delta c}$	-0.131+01	0.401+01	0.576+00	0.983+00	0.888+01

(2) At all three flight conditions, the parameters M_q, $M_{\delta e}$, $M_{\delta c}$, Z_w and $Z_{\delta c}$ may be accurately determined. That is, their error standard deviations are always less than 10% of their true value. M_w also may be accurately determined in cruise and transition. The deceptively large percentage value in its error standard deviation in Case 6 occurs because the true parameter value becomes nearly zero in the near-hover condition (see Table 18). A similar situation exists for $Z_{\delta e}$, whose true value becomes much smaller near hover. Otherwise, at cruise and transition, the error standard deviation of $Z_{\delta e}$ is less than 25%.

TABLE 16.- (CONTINUED)

	Gyro Mass Unbalance		Angular Accelerometer Sensitivity to Linear Acceleration		Accelerometer Misalignment	
	$e_{2,5}$	$e_{2,6}$	$e_{7,5}$	$e_{7,6}$	γa_x	γa_x
Error Value:	0.100+00	0.100+00	0.600-02	0.600-02	0.100+00	0.100+00
M_q	0.125-02	-0.150-02	0.227-03	0.950-03	0.501-03	0.167-04
Z_q	0.366-03	0.219-02	-0.116-03	0.624-03	0.112-02	0.314-03
X_q	0.999-03	-0.655-02	-0.170-03	0.259-02	0.113-02	0.474-05
M_w	0.291-02	-0.269-01	-0.262-03	0.261-02	0.820-03	-0.201-04
Z_w	-0.720-03	0.576-02	-0.170-03	0.283-02	-0.368-02	0.102-02
X_w	-0.444-03	0.716-03	0.137-03	-0.785-03	0.108-01	-0.119-03
M_u	-0.173-02	0.809-02	-0.484-04	-0.594-03	0.116-02	0.205-03
Z_u	-0.155-02	-0.285-02	0.458-03	-0.366-02	-0.257-03	-0.175-02
X_u	-0.381-02	0.224-01	0.721-03	-0.108-01	-0.961-04	0.198-03
$M_{\delta e}$	0.677-02	0.501-01	-0.639-02	0.648-01	0.673-02	0.177-03
$Z_{\delta e}$	-0.507-02	0.418-01	-0.637-03	0.725-02	-0.144-01	-0.121-02
$X_{\delta e}$	-0.896-04	-0.602-02	0.224-03	0.178-02	-0.258-01	-0.371-03
$M_{\delta c}$	0.331-01	-0.360+00	0.563-02	-0.594-01	-0.568-02	-0.661-03
$Z_{\delta c}$	-0.285-02	0.430-01	0.535-03	0.362-03	-0.217-01	0.146-01
$X_{\delta c}$	-0.209-03	-0.441-01	0.745-03	0.707-02	0.119+00	-0.183-02

(3) The observation was made at the cruise condition that parameters M_u, Z_u, X_q, X_w, X_u, $X_{\delta e}$, and $X_{\delta c}$, associated with the longitudinal velocity perturbation, have relatively large error standard deviations. Similar situations occur in transition and near-hover. As before, this suggests that the information content of the data sequence with respect to these parameters and Δu could be improved.

The specific results of these observations differ, but the general trends appear to be the same at all three flight conditions. The cruise condition is chosen as the basis for the remainder of the study of the longitudinal mode. Much more in-depth study is required of different phases of flight to allow making general conclusions regarding instrumentation error effects as a function of flight conditions.

TABLE 16.- (CONCLUDED)

	Location Error		Control Bias		Control Scale Factor	
	$e_{x_{cg}}$	$e_{z_{cg}}$	b_{δ_e}	b_{δ_c}	e_{δ_e}	e_{δ_c}
Error Value:	0.250+00	0.250+00	0.500-01	0.500-01	0.500-02	0.500-02
M_q	0.267-02	-0.393-02	0.677-05	-0.310-06	-0.190+01	-0.134-01
Z_q	0.109-01	-0.161-03	0.128-04	0.177-05	0.474+00	0.602-01
X_q	0.150-02	-0.251-01	-0.110-04	0.121-05	0.319+00	-0.246-02
M_w	-0.223-05	-0.825-06	-0.467-06	0.135-05	-0.145+01	0.233-02
Z_w	-0.130-01	0.680-05	-0.276-04	-0.485-05	-0.140+01	-0.889-01
X_w	-0.613-05	0.131-01	-0.276-04	-0.269-05	-0.127+01	-0.136-01
M_u	0.349-05	-0.453-05	-0.677-04	-0.504-05	0.111+01	-0.122-01
Z_u	0.645-02	0.790-06	0.323-04	0.202-05	-0.267+00	0.530-01
X_u	0.107-05	-0.647-02	0.121-03	0.124-06	-0.346+00	0.387-02
M_{δ_e}	-0.121-04	-0.329-05	-0.638-05	0.697-05	-0.200+02	0.834-01
Z_{δ_e}	-0.458+00	0.288-04	-0.116-03	-0.223-04	-0.595+01	-0.563+00
X_{δ_e}	-0.271-04	0.458+00	-0.213-03	-0.138-04	-0.530+01	-0.451-01
M_{δ_c}	-0.145-04	0.723-05	0.364-04	0.715-05	-0.104+01	-0.364+01
Z_{δ_c}	-0.675-01	0.157-04	0.780-04	0.129-04	-0.682+01	0.800+01
X_{δ_c}	-0.267-04	0.675-01	0.425-03	0.165-04	-0.106+02	-0.883+00

Effects of adding or omitting instruments.- Obtaining accurate air data in helicopter flight testing is complicated by the rotor downwash and the difficulties inherent at low airspeeds or high angles-of-attack. For these reasons, little confidence is placed in the air directional or pitot tube data when velocity is less than about 60 knots, and this is the justification for omitting these instruments at the transition and near-hover flight conditions. However, in cruise one may expect that including air data in the identification algorithm would enhance the accuracy of the parameter estimates. But this is not necessarily the case.

Adding (or omitting) instruments will restructure the matrix of parameter sensitivities to instrument errors and may result in increased sensitivities of some parameters to unmodeled instrument errors. This effect was observed for cruise flight conditions when an angle-of-attack vane and pitot tube were added to the longitudinal instrument set. Two computer runs were performed: Case 7 did not estimate output biases and initial conditions, and Case 8 did. Their results are compared to Cases 3 and 4 in Figure 16, and the following observations are made:

TABLE 17.- ENSEMBLE ANALYSIS ERROR STANDARD DEVIATIONS AND DOMINANT ERROR SOURCES FOR LONGITUDINAL PARAMETERS AT CRUISE

Parameter Value	Case 1 (See Notes A and C)					Case 3 (See Notes A, B, and C)					Case 4 (See Notes A, B, and D)				
	Total S.D.	Largest Error		Second Error		Total S.D.	Largest Error		Second Error		Total S.D.	Largest Error		Second Error	
		Source	S.D.	Source	S.D.		Source	S.D.	Source	S.D.		Source	S.D.	Source	S.D.
M_q -1.47606	0.00354	e_q	0.00242	$e_{2,6}$	0.00159	0.01706	b_{δ_e}	0.01373	e_{δ_c}	0.00937	0.01003	e_{δ_e}	0.00948	e_q	0.00235
Z_q -0.03169	0.00730	b_{az}	0.00428	b_{ax}	0.00391	0.00786	b_{az}	0.00428	b_{ax}	0.00391	0.00499	e_{xcg}	0.00272	e_{δ_e}	0.00237
X_q 0.01429	0.00740	e_{zcg}	0.00628	b_θ	0.00231	0.05045	b_{δ_e}	0.04954	e_{zcg}	0.00628	0.00719	e_{zcg}	0.00628	e_{δ_e}	0.00160
M_w 0.74996	0.00476	$e_{2,6}$	0.00267	e_θ	0.00247	0.04742	b_{δ_e}	0.04603	e_{δ_e}	0.00801	0.00813	e_{δ_e}	0.00725	$e_{2,6}$	0.00269
Z_w -0.83231	0.01158	b_{az}	0.00854	b_{ax}	0.00502	0.01736	Δw_{IC}	0.01026	b_{az}	0.00854	0.00927	e_{δ_e}	0.00698	e_{xcg}	0.00326
X_w 0.08842	0.00522	e_{zcg}	0.00327	b_θ	0.00137	0.03969	b_{δ_e}	0.03869	e_{δ_e}	0.00639	0.00791	e_{δ_e}	0.00636	e_{zcg}	0.00327
M_u -0.37084	0.00511	b_θ	0.00381	$e_{2,6}$	0.00188	0.09064	b_{δ_e}	0.08921	b_{δ_c}	0.01126	0.00606	e_{δ_e}	0.00556	e_q	0.00106
Z_u -0.01264	0.01057	b_{ax}	0.00794	$e_{2,6}$	0.00178	0.04327	b_{δ_e}	0.03369	Δw_{IC}	0.02042	0.00706	e_{xcg}	0.00161	e_{δ_e}	0.00133
X_u -0.03872	0.00564	b_θ	0.00375	b_{ax}	0.00332	0.06700	b_{δ_e}	0.06626	b_{δ_c}	0.00703	0.00619	e_θ	0.00255	$e_{2,6}$	0.00224
M_{δ_e} 26.25713	0.03407	$e_{\dot{q}}$	0.02154	e_θ	0.01467	0.29341	b_{δ_e}	0.26942	e_{δ_e}	0.10434	0.10425	e_{δ_e}	0.09979	e_q	0.02318
Z_{δ_e} 0.55709	0.12484	e_{xcg}	0.11449	b_{az}	0.03596	0.14419	e_{xcg}	0.11449	Δw_{IC}	0.05779	0.12167	e_{xcg}	0.11448	e_{δ_e}	0.02975
X_{δ_e} 0.14798	0.11724	e_{zcg}	0.11451	b_θ	0.00571	0.20938	b_{δ_e}	0.17086	e_{zcg}	0.11451	0.11987	e_{zcg}	0.11451	e_{δ_e}	0.02649
M_{δ_c} 3.87480	0.03810	$e_{2,6}$	0.03557	b_θ	0.00682	0.18741	b_{δ_e}	0.18181	$e_{2,6}$	0.03557	0.04205	$e_{2,6}$	0.03598	e_{δ_c}	0.01821
Z_{δ_c} -8.77426	0.04401	b_{az}	0.02281	e_{xcg}	0.01687	0.13830	b_{δ_e}	0.11511	e_{δ_c}	0.03983	0.06423	e_{δ_c}	0.04002	e_{δ_e}	0.03412
X_{δ_c} 0.77170	0.06602	b_θ	0.02769	b_{ax}	0.02654	0.58674	b_{δ_e}	0.57059	b_{δ_c}	0.08156	0.06562	e_{δ_e}	0.05305	$e_{\dot{q}}$	0.01776

Units are consistent with Tables 8 and 12.

Notes: A. Baseline errors for output measurements from Table 5.1, control and state time histories as shown in Fig. 15, five instruments (pitot tube and angle-of-attack vane omitted).
B. Baseline values of control biases, control scale factor errors, and state initial conditions added.
C. Output biases and state initial conditions are not estimated.
D. Output biases and state initial conditions are estimated.

TABLE 18.- ENSEMBLE ANALYSIS COMPARISON OF STANDARD DEVIATIONS OF LONGITUDINAL PARAMETER ESTIMATES AT CRUISE, TRANSITION, AND NEAR-HOVER

Parameter	Cruise (Case 2)			Transition (Case 5)			Near-Hover (Case 6)		
	Value	Standard Deviation due to Noise	Standard Deviation due to All Errors	Value	Standard Deviation due to Noise	Standard Deviation due to All Errors	Value	Standard Deviation due to Noise	Standard Deviation due to All Errors
M_q	-1.47606	0.00086	0.01705	-1.25100	0.00086	0.01636	-0.70791	0.00135	0.06132
Z_q	-0.03169	0.00328	0.00772	-0.02903	0.00335	0.01536	-0.01134	0.00633	0.01614
X_q	0.01429	0.00283	0.05038	0.01793	0.00285	0.10145	0.01319	0.00352	0.13530
M_w	0.74996	0.00092	0.04729	1.08289	0.00157	0.07648	-0.01914	0.00217	0.09310
Z_w	-0.83231	0.00415	0.01400	-0.56880	0.00709	0.03996	-0.34255	0.00955	0.02637
X_w	0.08842	0.00281	0.03966	0.07760	0.00364	0.29808	0.05007	0.00540	0.19148
M_u	-0.37084	0.00155	0.09034	-0.24064	0.00155	0.18176	0.46685	0.00227	0.19960
Z_u	-0.01264	0.00624	0.03813	-0.12860	0.00590	0.09444	0.01860	0.01197	0.04864
X_u	-0.03872	0.00109	0.06688	-0.01230	0.00180	0.08740	-0.01815	0.00238	0.15684
M_{δ_e}	26.25713	0.00660	0.29271	22.44849	0.00581	0.30420	19.98563	0.00951	0.18323
Z_{δ_e}	0.55709	0.02589	0.13208	0.51980	0.02263	0.09583	0.02265	0.04017	0.07913
X_{δ_e}	0.14798	0.02224	0.20926	0.12060	0.01917	0.56097	0.16963	0.03943	0.13304
M_{δ_c}	3.87480	0.00682	0.18731	2.06265	0.00674	0.08179	-2.82021	0.00790	0.03248
Z_{δ_c}	-8.77426	0.02932	0.13670	-7.31320	0.02958	0.04748	-7.40857	0.03393	0.05838
X_{δ_c}	0.77170	0.02420	0.58318	0.88890	0.02520	0.23609	1.16835	0.03163	0.06882

NOTE: Units are consistent with Table 8.

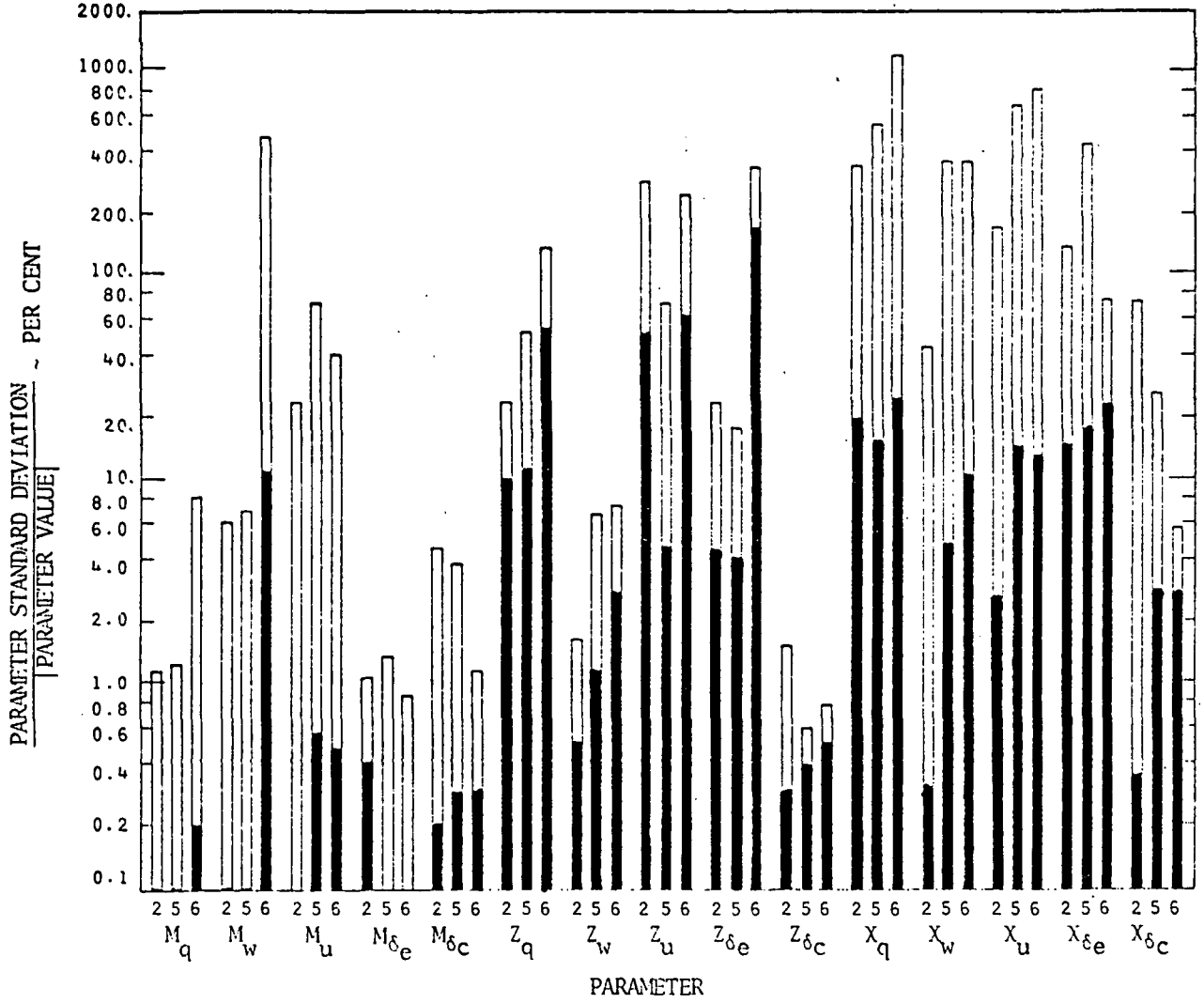

Shaded Portion of Each Bar Shows Standard Deviation Due to Noise Alone.

FIGURE 15.- ENSEMBLE ANALYSIS COMPARISON OF PARAMETER ERROR STANDARD DEVIATIONS FROM CASES 2, 5, AND 6: EFFECTS AT CRUISE, TRANSITION, AND NEAR-HOVER

(1) Parameter estimates whose standard deviations are less than 30% of the true parameter value were neither improved nor degraded appreciably. This is not surprising since these parameters are fairly well identified from information supplied by the original five instruments. That is, when a parameter's standard deviation is small, good information is present from the instrument combination which produces data to identify that parameter.

(2) From Case 3 to Case 7, the estimates of Z_u, X_u, and $X_{\delta c}$ were improved by adding the two instruments, but the standard deviations are still quite large compared to their corresponding parameter values. Also, the estimates of Z_q, X_q, X_w, and $X_{\delta e}$ were degraded by factors of 2.8, 1.3, 1.2, and 1.3, respectively. This was caused by an increased sensitivity to the control biases and the introduction of the additional bias in measuring Δu.

(3) From Case 4 to Case 8, both of which estimated initial conditions and measurement biases except b_u,* the estimate of Z_u improved substantially, the estimate of X_u degraded substantially due to increased sensitivity to $b_{\delta e}$; all other estimates were left relatively unchanged.

Hence, the addition of an angle-of-attack vane and a pitot tube has a mixed effect on the parameter estimates. The engineer must determine with regard to the test goals which parameters must be known to good accuracy. Then he must decide which instruments to use to produce the desired results. Another possibility would be to restructure the cost function weighting matrix and thereby reduce the sensitivities of the parameter errors to control biases.

The effect of deleting the pitch angular accelerometer but retaining the angle-of-attack vane and pitot tube measurements was investigated by performing two more computer runs at the cruise flight condition. Case 9 did not estimate measurement biases and initial conditions, and Case 10 did. Neither case showed any appreciable change in the accuracy of any parameter estimate. For these cases, this implies that the pitch angular accelerometer does not add much information to what the identification algorithm extracts from the other instruments. This is fortunate because angular accelerometers are not commonly used in flight testing.

*For the longitudinal mode, the system equations are so structured that the longitudinal speed perturbation's initial value appears to have almost the same effect on the output equations as does a bias in the pitot tube or air speed indicator. In other words, both of these parameters are not simultaneously observable from a data sequence over a short time span. Thus, the pitot tube bias is not identified, and it enters as an error source. Most of this error is identified as a forward speed initial condition.

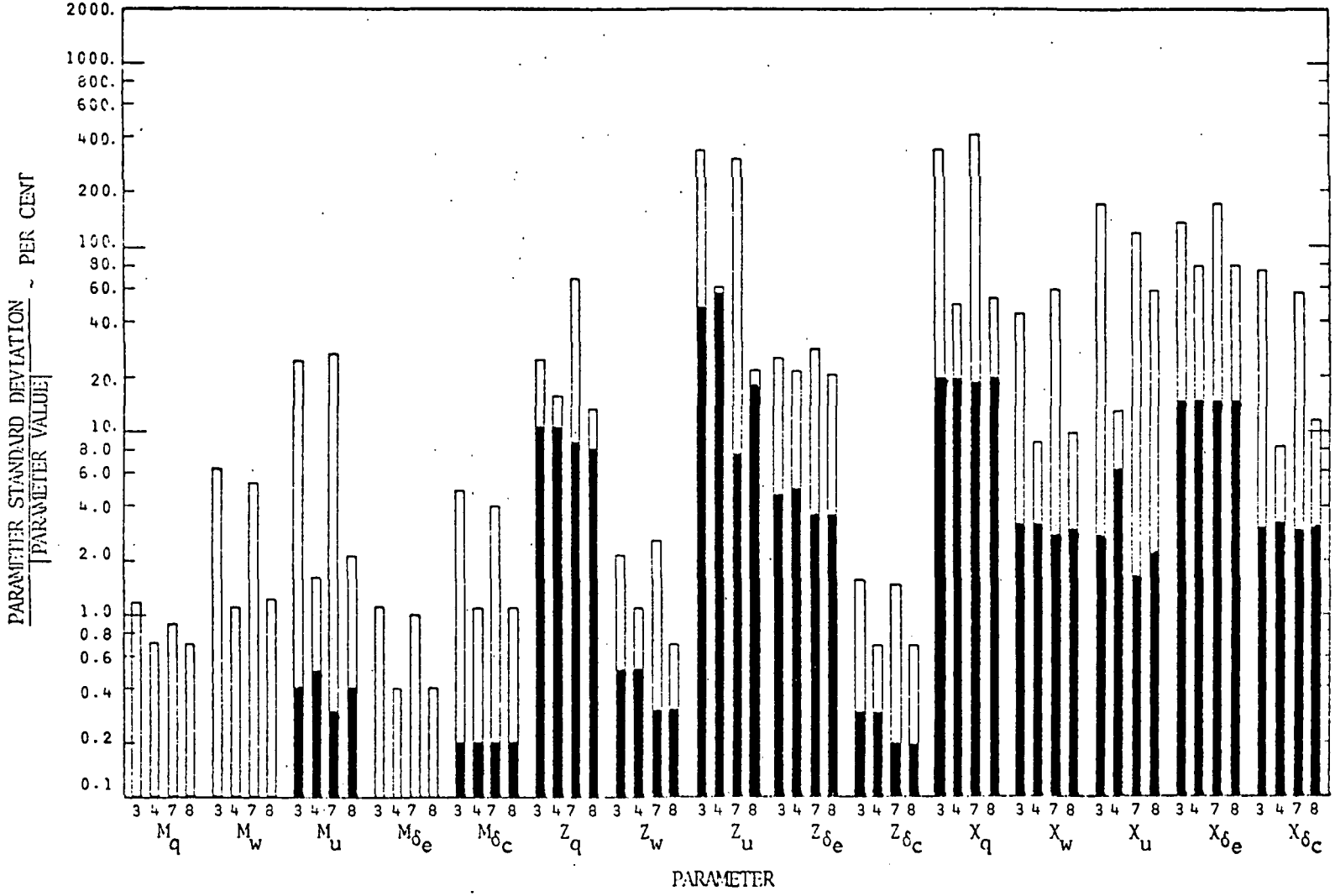

Shaded Portion of Each Bar Shows Standard Deviation Due to Noise Alone.

FIGURE 16.- ENSEMBLE ANALYSIS COMPARISON OF PARAMETER ERROR STANDARD DEVIATIONS FROM CASES 3, 4, 7, AND 8: EFFECTS OF ADDING PITOT TUBE AND ANGLE-OF-ATTACK VANE

The next run in this series was Case 11, which had only four instruments--the pitch-attitude and pitch-rate gyros and the longitudinal and normal accelerometers. The results were compared with Case 4. Again, it was found that omitting the angular accelerometer made no appreciable change in the accuracy of the parameter estimates. Again, it appears that the angular accelerometer adds little information to that available from the four instruments just mentioned.

Effects of control sequence and data length.- The important role which the control input sequence has in parameter identification has been discussed previously. It is a simple matter to demonstrate that if a mode is not excited, then estimates of associated parameters will be inaccurate. As an example, Case 12 was generated as being similar to Case 11 except that the slow sine waves in the δ_e and δ_c control sequences were omitted (see Figure 11). This left only the "doublet" sine wave in δ_e beginning at $t = 0$ and another in δ_c beginning at $t = 7.5$ sec. Recall that the slow sine waves had the same frequency as the complex conjugate poles of the closed-loop system. Thus, removing the slow sine waves means that the slow mode is not excited as strongly.

The error standard deviations of the parameter estimates expressed as percentages of the associated parameter values are shown in Figure 17 for both Cases 11 and 12. A comparison shows that estimates of Z_u and X_u become much less accurate (56% to 330% and 12% to 57%, respectively), and no estimates improve appreciably due to this change in the control input sequence.

After that predictable result was obtained, an attempt was made to devise a control sequence which would improve the accuracy of the parameter estimates. It was noted previously that the input sequence and data length of the maneuver shown in Figure 11 may be responsible for the relatively large error standard deviations of the parameters associated with the longitudinal velocity perturbations, Δu. The mode principally governing Δu has a time constant of 11.4 sec. Therefore, it was decided that a new input sequence should be devised which would be identical to the baseline maneuver shown in Figure 11 for the first 15 sec and which would thereafter excite the Δu mode and contain at least two time constants of its motion. The intent was to retain all the information of the baseline maneuver and to add information on the Δu mode. This was done, and the resulting input and outputs of this run are shown in Figure 18. After the control inputs cease at $t = 20$ sec, Δu is 22 ft/sec, and it slowly decays to 2 ft/sec at $t = 45$ sec.

Case 13 used this maneuver and took measurements with four instruments--the pitch-attitude and pitch-rate gyros and the linear accelerometers. The results are compared in Figure 17 with Case 11, which used the same instruments but utilized only the 15 sec baseline maneuver. As can be seen, the error standard deviation of Z_u was substantially increased from 56% to 128% of the true parameter value. X_u improved from 12% to 5%; X_w and $X_{\delta c}$ degraded from 9% to 14% and from 8% to 14%, respectively. The other parameter estimates were essentially unaffected.

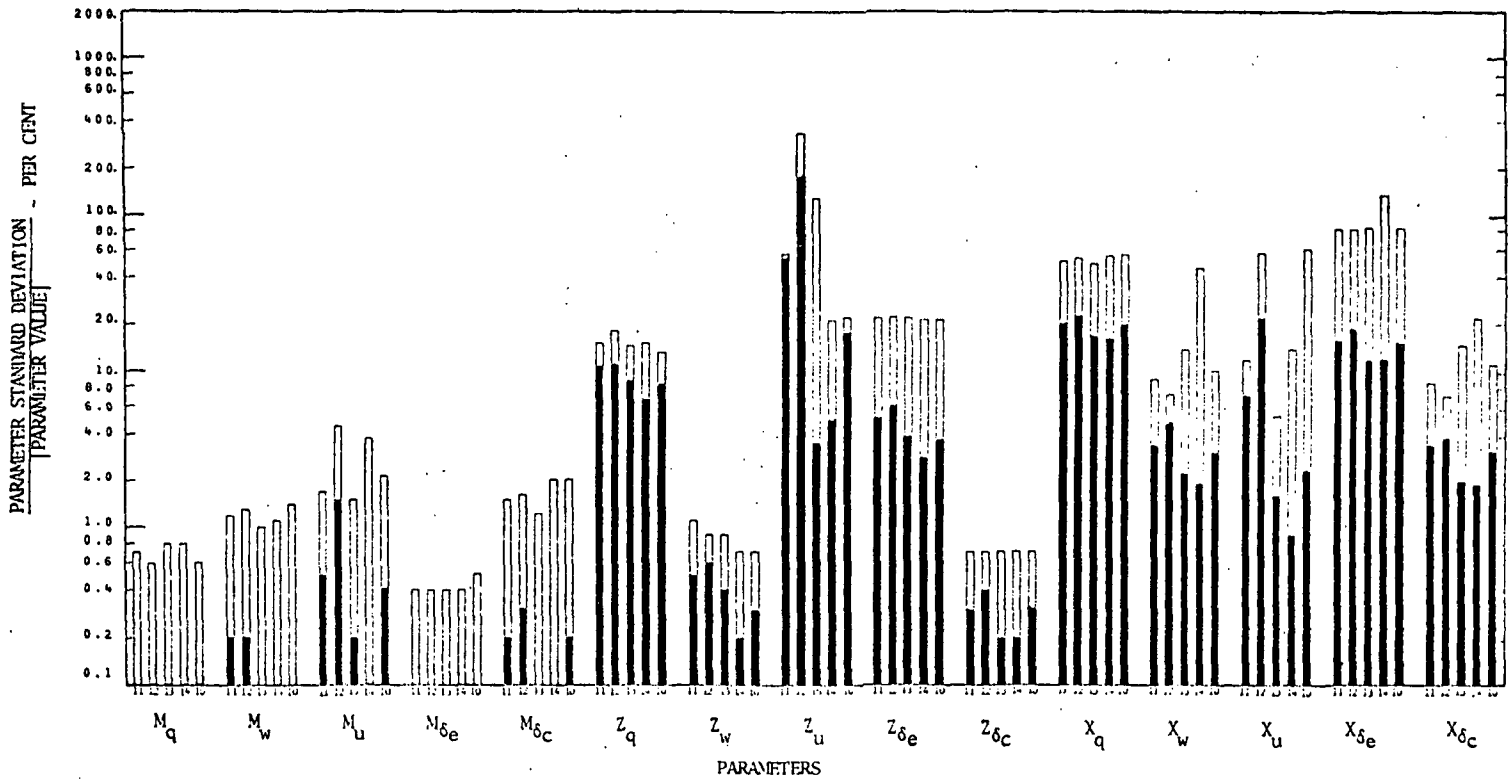

Shaded Portion of Each Bar Shows Standard Deviation Due to Noise Alone.

FIGURE 17.- ENSEMBLE ANALYSIS COMPARISON OF PARAMETER ERROR STANDARD DEVIATIONS FROM CASES 10 THROUGH 14: EFFECTS OF CHANGES IN CONTROL INPUT AND DATA LENGTH

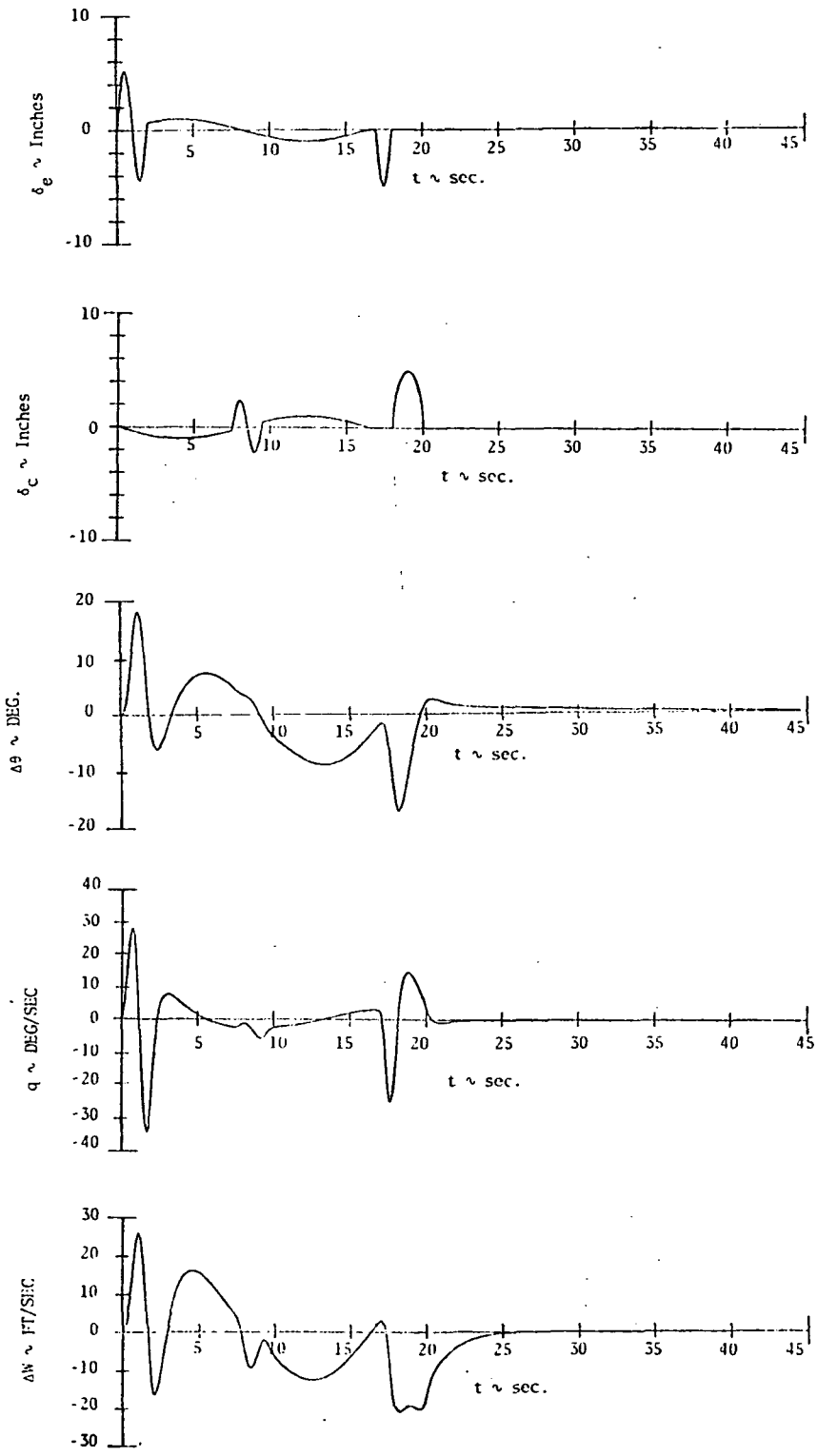

FIGURE 18.- LONGITUDINAL MEASUREMENT AND CONTROL TIME HISTORIES FOR 45 SEC DATA LENGTH

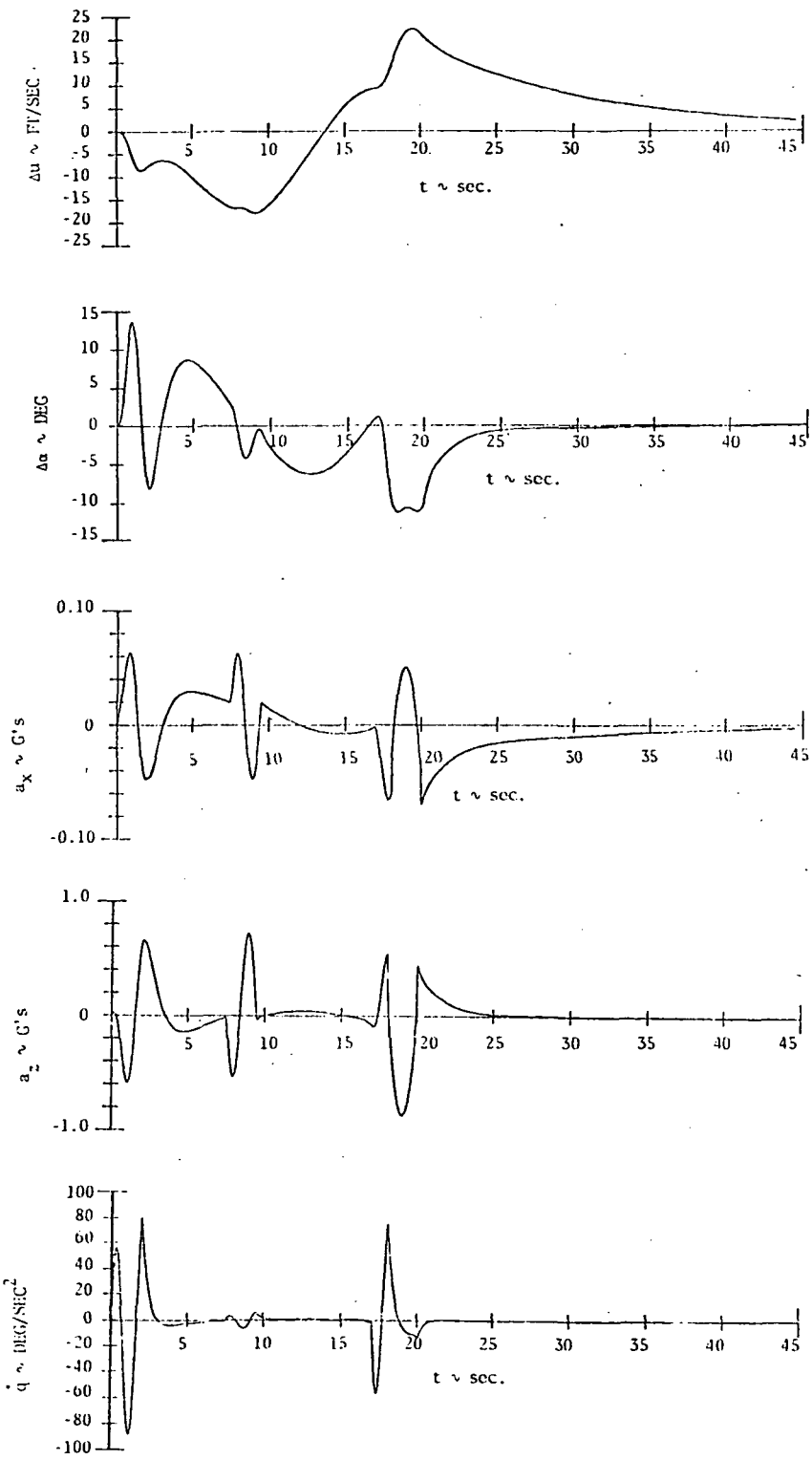

FIGURE 18.- (CONCLUDED)

At first, this degradation of the Z_u estimate accuracy seemed surprising. The new maneuver should have provided more information on Z_u because the Δu mode was more strongly excited, and the excitation of the baseline maneuver was retained. However, the implication is that the four inertial instruments are not extracting this inherent information. This is seen in Figure 18 where θ, q, a_x, and a_z are all nearly zero after t = 25 sec (i.e., during the slow decay in Δu). In fact, what information is extracted by these instruments after t = 15 sec (the end of the baseline maneuver) causes a 16-fold increase in sensitivity of the error in the Z_u estimate with respect to the scale factor error on δ_e (determined by examining the error sensitivity matrix). What was apparently needed was a direct measurement of Δu to better extract the information inherent in the maneuver. Then, the identification scheme could rely on this new measurement for its information on Z_u and rely much less on the original four instruments.

However, the previous results showed that while adding a pitot tube and angle-of-attack vane substantially improved the estimate of Z_u, other parameter estimates could be degraded. This was true here, as well. Case 14 repeated Case 13 with the addition of these two instruments. Its results are also shown in Figure 17. The error standard deviation of Z_u dropped to 21% of the parameter value, which is a very good improvement over previous cases. However, the estimates of X_w, X_u, $X_{\delta e}$, and $X_{\delta c}$ were all degraded. Again, this was due to the substantially increased sensitivity of the estimates to control errors. The sensitivity of $X_{\delta e}$ to $b_{\delta e}$ increased from -0.931×10^{-4} in Case 13 to -2.95 in Case 14.

It is of further interest to compare Cases 14 and 10. Both have six instruments and the same control input up to 15 sec. However, Case 14 has the additional 30 sec of data. The results are also shown in Figure 17. It is noted from this figure that the error contribution due to noise is always decreased in the longer run. This follows the theory that if more information is added, the effect of noise diminishes. But continuing to use data from a run in which there is poor excitation of all states but Δu actually can increase the effect of the other instrument errors, as can be seen in Figure 17. Although the total deviation of X_u decreased from 60% to 14%, the X_w, $X_{\delta e}$, and $X_{\delta c}$ deviations increased from 10% to 45%, 72% to 130%, and 11% to 22%, respectively, by adding 30 sec more data.

Based on the above examples, it can be seen that different combinations of instruments, control inputs, and lengths of data give varying results. Specifically, the following were observed:

(1) Adding instruments does not always improve parameter accuracy.

(2) Adding more data does not always improve parameter accuracy.

Thus, the engineer who is conducting identification flight tests should very carefully consider what data and instrument combinations are used. It is important to know the error magnitudes of the instrumentation.

Deterministic errors due to input and output measurement lags.- The Ensemble Error Analysis Program treats input and output measurement lags deterministically. When lags are assumed to be deterministic sources of error, they have no effect on the random distribution of the parameter estimate errors. However, the lags do produce mean errors in the estimates. Lags do have some random variation, and the resulting effects can be studied with the Simulated Data Analysis Program. Nonetheless, certain basic effects on the mean estimate errors were established by use of the ensemble technique, and they are now discussed.

When making computer runs which involved lags in either input or output measurements, the integration step-size was chosen to be less than or equal to three-tenths of the shortest time constant. In other words, three time constants contained at least ten integration steps. This was to ensure accurate simulation of the system. However, the sampling rate was not changed.

The effect of all output and input measurement lags having identical time constants was studied in Case 15. This case is similar to Case 2 (see Table 13) except output and input measurement lags were added and the time constants set to 0.1667 sec. The resulting mean errors of the parameter estimates were very nearly zero. All were less than 0.1% of the corresponding parameter values. This result is independent of the time constant value, as can be shown mathematically. What this result means physically is that input and output measurements which are lagged equally produce a system which is equivalent to the system without any lags. The parameter estimates made from this equivalent system are not biased from the true parameter values. Thus, the instrumentation design goal should be to set the dynamic characteristics of all data measurement channels to be equivalent.

Next, the effects of lags in the output measurements when no lags exist in the input measurements were studied. This situation results when control measurements are measured in terms of stick deflection; the stick deflection leads the actual control input.

Table 19 presents the deterministic (mean) parameter errors resulting from lags of 0.1667 sec (Case 16) and 0.0333 sec (Case 17). These mean errors are divided by the true parameter values to obtain the percentage error. As can be seen, going from 0.1667 sec to 0.0333 sec decreases the mean error in 11 of the 15 parameters. This indicates that the smaller the lag differences, the smaller the mean error. However, this isn't uniformly true, and Case 17 points out that even small differences in the lags can have a substantial effect on the parameter errors. The mean errors of Z_q, Z_u, and $Z_{\delta e}$ are quite large.

Further study is required of the lag effect. The random portion of the lags are addressed using Monte Carlo analysis later in this chapter.

Comparison of results obtained using the large and nominal error sets. The large set of instrument errors in Table 12 was used in Case 18, which otherwise duplicated Case 4. That is, these cases contained random output and input

TABLE 19.- COMPARISON OF ENSEMBLE ANALYSIS PARAMETER MEAN ERRORS DUE TO NO CONTROL LAGS

Parameter	Value	Case 16: Output Lag Time Constant=.1667		Case 17: Output Lag Time Constant=.0333	
		Mean Error	%	Mean Error	%
M_q	-1.47606	-0.24306	16.5	-0.35003	23.7
Z_q	-0.03169	-0.021557	68.0	0.10087	318.3
X_q	0.01429	-0.017833	124.8	0.00295	20.6
M_w	0.74996	0.32681	43.6	0.19802	26.4
Z_w	-0.83231	0.0061787	0.7	-0.18913	22.7
X_w	0.08842	0.095193	107.7	-0.02875	32.5
M_u	-0.37084	-0.18373	49.5	0.01658	4.5
Z_u	0.01264	0.15755	1246.4	-0.07480	591.8
X_u	-0.03872	-0.020695	53.4	-0.01853	47.9
M_{δ_e}	26.25713	12.194	46.4	3.5270	13.4
Z_{δ_e}	0.55709	0.20505	36.8	-0.74124	133.1
X_{δ_e}	0.14798	0.46624	315.1	-0.09466	64.0
M_{δ_c}	3.87480	1.7652	45.6	0.71735	18.5
Z_{δ_c}	-8.77426	-2.1854	24.9	-0.35730	4.1
X_{δ_c}	0.77170	0.99354	128.7	-0.39643	51.4

measurement errors, used all instruments but the angle-of-attack vane and pitot tube, and estimated output biases and initial conditions. The results of these cases appear in Table 20.

The standard deviations due to white noise alone increased only slightly from Case 4 to Case 18. The total error standard deviations increased for every parameter. Although this is certainly not surprising, neither is it a foregone

TABLE 20.- COMPARISON OF ENSEMBLE ANALYSIS PARAMETER ESTIMATE ERRORS DUE TO NOMINAL AND LARGE ERROR SETS

		Case 4 (Nominal Error Set)						Case 18 (Large Error Set)					
		Total s.d.		s.d. due to Noise		Largest Error		Total s.d.		s.d. due to Noise		Largest Error	
Parameter	Value	Value	%	Value	%	Source	s.d.	Value	%	Value	%	Source	s.d.
M_q	-1.47606	.01003	.7	.00088	0.1	$e_{\delta e}$	.00948	.04492	3.0	.00233	0.2	$e_{\delta e}$	.03896
Z_q	-0.03169	.00499	15.8	.00332	10.5	$e_{x_{cg}}$	.00272	.01176	37.1	.00343	10.8	$e_{x_{cg}}$	.01088
X_q	0.01429	.00719	50.3	.00288	20.1	$e_{z_{cg}}$	.00628	.02538	177.6	.00295	20.7	$e_{z_{cg}}$	.02511
M_w	0.74996	.00813	1.1	.00104	0.1	$e_{\delta e}$	.00725	.03265	4.4	.00310	0.5	$e_{\delta e}$	.02744
Z_w	-0.83231	.00927	1.1	.00449	0.5	$e_{\delta e}$	.00698	.01842	2.2	.00478	0.6	$e_{x_{cg}}$	.01304
X_w	0.08842	.00791	9.0	.00287	3.2	$e_{\delta e}$	.00636	.01574	17.8	.00312	3.5	$e_{z_{cg}}$	.01306
M_u	-0.37084	.00606	1.6	.00177	0.5	$e_{\delta e}$	.00556	.03117	8.4	.00470	1.3	$e_{\delta e}$	.02469
Z_u	-0.01264	.00706	55.9	.00669	52.9	$e_{x_{cg}}$	.00161	.01033	81.7	.00712	56.4	$e_{x_{cg}}$	.00645
X_u	-0.03872	.00519	13.4	.00246	6.4	e_{θ}	.00255	.00777	20.1	.00324	8.4	$e_{z_{cg}}$	.00647
$M_{\delta e}$	26.25713	.10425	0.5	.00714	0.0	$e_{\delta e}$	.09979	.50616	1.9	.01829	0.1	$e_{\delta e}$	.37550
$Z_{\delta e}$	0.55709	.12167	21.8	.02733	4.9	$e_{x_{cg}}$	.11448	.46090	82.7	.02817	5.1	$e_{x_{cg}}$	.45790
$X_{\delta e}$	0.14790	.11987	81.0	.02243	15.2	$e_{z_{cg}}$	.11451	.45906	310.2	.02299	15.5	$e_{z_{cg}}$	.45802
$M_{\delta c}$	3.87480	.04205	1.1	.00715	0.2	$e_{2,6}$	.03598	.10854	2.8	.01940	0.5	e_q	.07394
$Z_{\delta c}$	-8.77426	.06423	0.7	.02948	0.3	$e_{\delta c}$	.04002	.20385	2.3	.03036	0.3	$e_{\delta c}$	.16224
$X_{\delta c}$	0.77170	.06562	8.5	0.02525	3.3	$e_{\delta e}$	.05305	.10979	14.2	.02742	3.6	γ_{n_x}	.07551

conclusion since the weighting matrix, R^{-1}, in Case 18 is different from the one in Case 4; the standard deviations of the white noise have different values. These parameter deviation increases ranged from a 46% increase in the standard deviation for Z_u to a 425% increase for M_u. (However, the error standard deviation of M_u with the large errors is still only 8% of the parameter value.)

For ten parameters, the source of the largest error was unchanged. For Z_w, X_w, and X_u, the c.g. location errors became the dominant error source. For $M_{\delta c}$, the angular accelerometer scale factor error became the largest error source, and for $X_{\delta c}$, the misalignment of the longitudinal accelerometer dominated. The result of these changes is that c.g. location errors replaced the differential collective scale factor error ($e_{\delta e}$) as the largest error source for the majority of parameters.

Monte Carlo results from the simulated data analysis program.- The effects of large instrumentation errors and random components of the measurement lags are best studied by using the Monte Carlo technique. A "large" instrument error means that the error mangitude is large enough such that the one-step convergence criterion used to derive the ensemble analysis technique does not hold very well. Thus, the effect of the large error determined by using the two techniques would produce totally different answers. To ascertain what constitutes "large" errors involves comparing the results of the two techniques as applied to the same flight test condition. It is advantageous to use the ensemble analysis technique if the errors are "small" and random components of lag are considered negligible.

Before discussing the results of using the Monte Carlo technique on the previously considered flight test condition examples so that some comparisons can be made, it is of interest to examine the number of samples required to make a suitably accurate Monte Carlo run. A tradeoff exists between computer run time and statistical accuracy of the results.

The Monte Carlo technique can be a very expensive procedure in terms of hours of computer time. It was found in this study that 40 to 50 Monte Carlo samples using a trajectory with 300 time points took about one hour. Each sample was iterated using the identification algorithm until all parameters converged to within 1% of their magnitude. Analyzing the same trajectory with the ensemble program took about one minute of computer time. Obviously, considerable savings can be realized by using the ensemble method.

Another consideration is that increasing the number of Monte Carlo samples gives diminishing returns. Consider the following example. Suppose n Monte Carlo Samples are taken, and from these samples an estimate of the variance, s^2, is made for the error, δp, of a parameter estimate. Let σ^2 be the true variance of the parameter estimate error, which is unknown. By methods of elementary statistics [34], one can determine an interval about s^2 which contains σ^2 with a specified level of confidence. The 90% and 95% confidence intervals of

the normalized variance, σ^2/s^2, is presented in Figure 19 as a function of the number of Monte Carlo samples upon which s^2 is based. This figure shows that the 95% confidence interval for the variance of the error, σ^2, based on 50 samples is $0.69\ s^2$ to $1.51\ s^2$. Similarly, the interval based on 200 samples is $0.83\ s^2$ to $1.22\ s^2$, which has about half the width of the interval at 50 samples ($0.39\ s^2$ compared to $0.82\ s^2$).

It is also possible to compute an interval about the sample mean which contains the true (population) mean with a specified level of confidence. Let μ be the true mean of the parameter estimate errors and $\overline{\Delta p}$ be the mean based on n Monte Carlo samples. Figure 20 shows, as a function of n, the 90% and 95% confidence intervals about the normalized sample mean, $\overline{\Delta p}/s$, in which falls the normalized true mean, μ/s. It is again the case that in order to halve the width of the confidence interval, it is necessary to multiply the number of Monte Carlo samples by approximately four.

Seven computer runs of the Simulated Data Analysis Program were performed to study the longitudinal parameter errors. The differences among these seven cases are summarized in Table 21. In each case, the instrument set consisted of the pitch rate and attitude gyros, pitch angular accelerometer, and normal and longitudinal accelerometers; the angle-of-attack vane and pitot tube were omitted. Measurement biases and initial conditions were not estimated. The control input sequence was the same 15 sec sequence used in the Ensemble Analysis Program (see Figure 11). At transition conditions, this sequence was modified as described previously.

TABLE 21.- SUMMARY OF SIMULATED DATA COMPUTER RUNS FOR LONGITUDINAL EQUATIONS

Case	Flight Regime	Error Set	Lag Inverse Time Constants	
			Mean, $\bar{f}$	Standard Deviation, σ_f
1M	Cruise	Baseline	0.0 sec^{-1}	0.0 sec^{-1}
2M	Cruise	Baseline	6.0 sec^{-1}	0.3 sec^{-1}
3M	Cruise	Baseline	30.0 sec^{-1}	0.3 sec^{-1}
4M	Cruise	Baseline	30.0 sec^{-1}	1.5 sec^{-1}
5M	Cruise	Baseline	12.0 sec^{-1}	0.6 sec^{-1}
6M	Cruise	Large	12.0 sec^{-1}	0.6 sec^{-1}
7M	Transition	Baseline	12.0 sec^{-1}	0.6 sec^{-1}

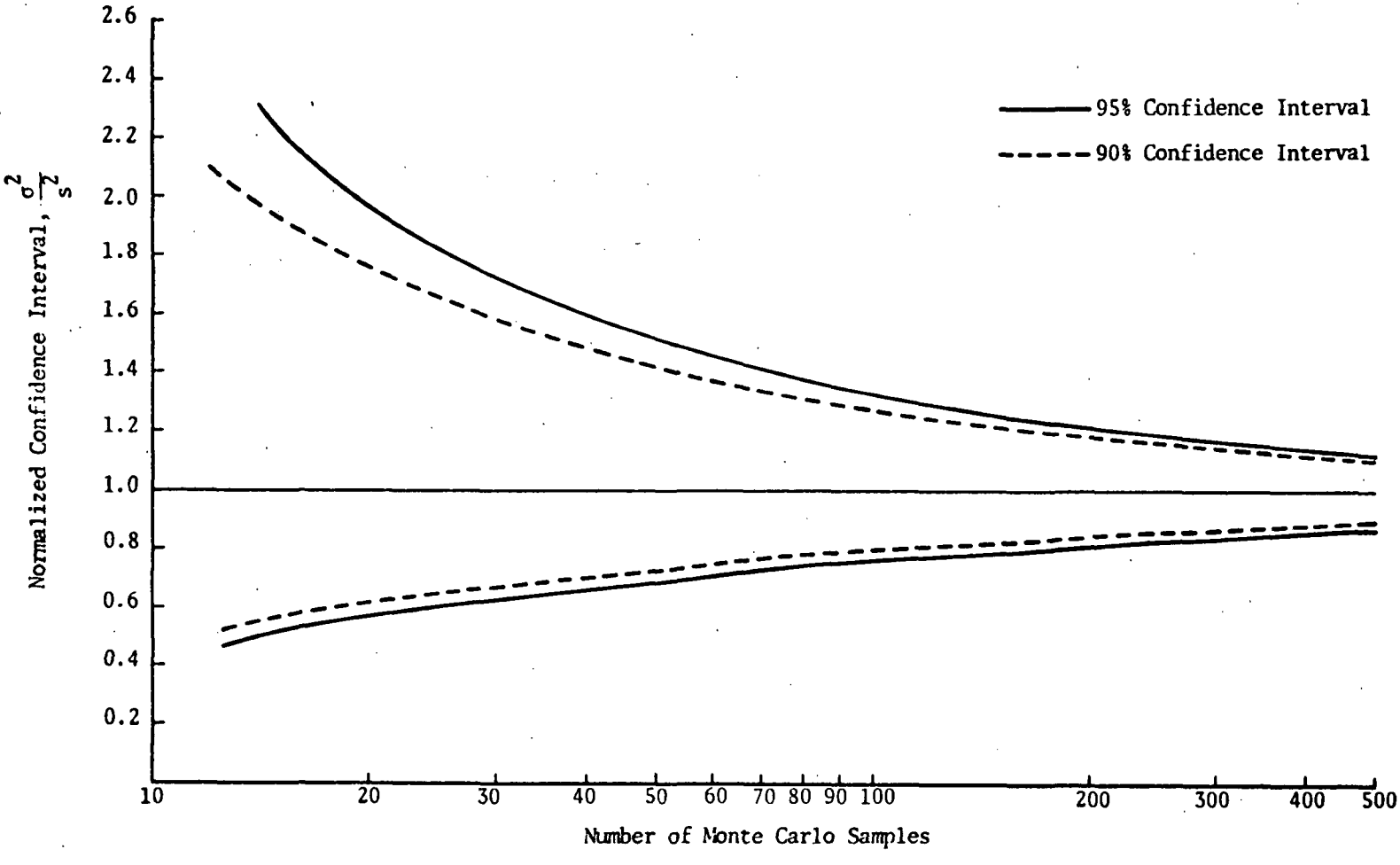

FIGURE 19.- CONFIDENCE AS A FUNCTION OF THE NUMBER OF MONTE CARLO SAMPLES

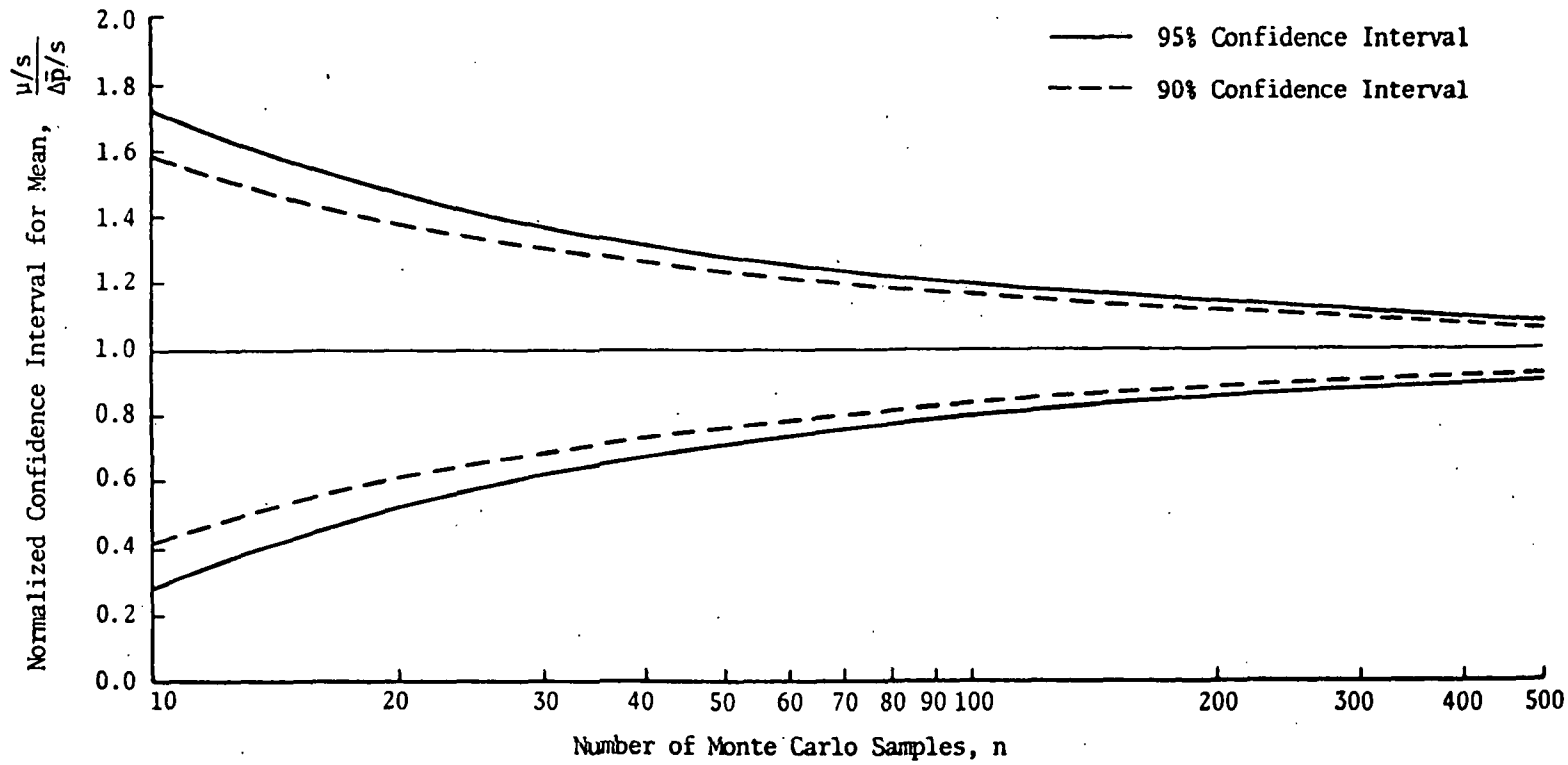

FIGURE 20.- CONFIDENCE INTERVALS FOR μ/s ABOUT $\Delta p/s$

Case 1M is similar to Case 2 described previously, and can be used to compare the results of the Ensemble and Simulated Data Analysis Programs. Case 1M contained 44 Monte Carlo samples. The standard deviations of the parameter errors from Cases 2 and 1M are compared in Table 22.

The following comments are offered:

(1) It is interesting to note how many error standard deviations, σ_E, from the Ensemble Program fall within the 95% intervals about the Monte Carlo error standard deviations, σ_{MC}. Strictly speaking, this has limited significance because these standard deviations may differ by 30%, but each may be 15% from the true standard deviation if it should be midway between them. On the other hand, if most of the Ensemble standard deviations fell outside the interval, their accuracy would be questionable. Fortunately, this is not the case. The

TABLE 22.- COMPARISON OF PARAMETER ESTIMATE ERRORS FROM ENSEMBLE AND MONTE CARLO ANALYSES

Parameter	Value ~p	Ensemble s.d. $\sim\sigma_E$	$\left\|\frac{\sigma_E}{p}\right\|$ %	Monte-Carlo s.d. $\sim\sigma_{MC}$	$\left\|\frac{\sigma_{MC}}{p}\right\|$ %	$\frac{\sigma_E}{\sigma_{MC}}$	$\frac{\sigma_E-\sigma_{MC}}{\|p\|}$ %
M_q	-1.47606	.01705	1.2	.01404	1.0	1.21	0.2
Z_q	-0.03169	.00772	24.4	.01075	33.9	0.72	- 9.5
X_q	0.01429	.05038	325.5	.04704	329.2	1.07	23.3
M_w	0.74996	.04729	6.3	.03951	5.3	1.20	1.0
Z_w	-0.83231	.01400	1.7	.01623	1.9	0.86	- 0.2
X_w	0.08842	.03966	44.9	.04730	53.5	0.85	- 8.6
M_u	-0.37084	.09034	24.4	.09259	25.0	0.98	- 0.6
Z_u	-0.01264	.03813	301.7	.03417	270.3	1.12	31.4
X_u	-0.03872	.06688	172.7	.07790	201.2	0.86	-28.5
M_{δ_e}	26.25713	.29271	1.1	.24412	0.9	1.20	0.2
Z_{δ_e}	0.55709	.13208	23.7	.15710	28.2	0.84	- 4.5
X_{δ_e}	0.14798	.20926	141.4	.24420	165.0	0.86	-23.6
M_{δ_c}	3.87480	.18731	4.8	.11914	3.1	1.57	1.7
Z_{δ_c}	-8.77426	.13670	1.6	.10963	1.2	1.25	0.4
X_{δ_c}	0.77170	.58318	75.6	.38080	49.3	1.53	26.3

95% confidence interval about σ_E/σ_{MC} is 0.82 to 1.25, and 12 of the 15 parameters fall in this interval.

(2) Another point of interest is seen in the ratio of the difference of σ_E and σ_{MC} to the true parameter value. This ratio is less than 10% for ten parameters. The remaining five parameters are X_q, Z_u, X_u, $X_{\delta e}$, and $X_{\delta c}$, and they all have large standard deviations relative to their value in the first place. To get better values of the deviations of these parameters would require many more Monte Carlo runs. And significantly, the ensemble analysis results predict the general magnitude of these quite well.

As a means of determining what effect the variation in identified parameters has on vehicle performance, two measures of this performance must be considered; these are basic stability and handling quality. They are reflected by the closed-loop poles of the aircraft. The Monte Carlo analysis program is ideal to examine the scatter of these poles due to parameter uncertainty. Thus, for each of the Monte Carlo runs, the values of the parameters identified in each pass were printed out. These values were then used to compute the open-loop and closed-loop poles.

For Case 1M, the open-loop and closed-loop poles were computed from the converged parameter estimates for each of the 44 Monte Carlo samples. They are shown in the root plots of Figure 21. As can be seen, the real parts of each of the open-loop poles vary in intervals of about 0.2 sec^{-1} in length, and the frequency of the complex pair varies about 0.1 sec^{-1}.

The closed-loop poles are more scattered than the open-loop poles. Thus, the feedback control tends to scatter the response characteristics. Fortunately for this set of instrument errors, the closed-loop poles all remain in the stable half of the complex plane; but the closed-loop dynamics do vary over a wide range. The real poles fall within intervals from -0.06 to -0.31 and from -1.98 to -2.51. The complex poles vary along an arc centered at the origin. The extremes of the arc are at about $-0.85 \pm j\,0.46$. In three cases, the poles split along the real axis, which means the oscillatory mode disappears altogether. The variation along the arc implies that the natural frequency of these poles varies very little while the damped frequency varies substantially. From Figure 21 it can be seen that even the baseline values of instrument errors may cause marked variations in the flying qualities of the controlled helicopter. This result may be sensitive to the feedback control law which is used.

Table 23 presents the mean and standard deviations of the parameter errors for Cases 1M through 4M. These four cases were all at the cruise flight condition and contained the baseline set of instrumentation errors. They differ by their values for the mean, $\bar{f}$, and standard deviation, σ_f, of the inverse time constants of the input and output measurement lags.

A comparison of Cases 1M and 2M indicates what may be expected when a relatively substantial random lag ($\bar{f}$ = 6 sec^{-1}, σ_f = 0.3 sec^{-1}) is present in the input and

output measurement systems (Case 2M) as opposed to no lags at all (Case 1M). The mean parameter error for two parameters in Case 2M are very large. The mean error in X_q is 424%, and in Z_u 937% of their respective parameter values. Significant mean errors also exist in $X_{\delta e}$ (108% of true parameter value), $X_{\delta c}$

TABLE 23.- ERRORS IN PARAMETER ESTIMATES FOR SIMULATED DATA ANALYSIS - CASES 1M THROUGH 4M

Parameter		CASE 1M (n=44, $\bar{f}$=0, σ_f=0)		CASE 2M (n=21, $\bar{f}$ = 6 sec^{-1}, σ_f = 0.3 sec^{-1})		CASE 3M (n=36, $\bar{f}$ = 30 sec^{-1}, σ_f = 0.3 sec^{-1})		CASE 4M (n=37, $\bar{f}$ = 30 sec^{-1}, σ_f = 1.5 sec^{-1})	
Name	Value	$\Delta\bar{p}$	s	$\Delta\bar{p}$	s	$\Delta\bar{p}$	s	$\Delta\bar{p}$	s
M_q	-1.4761	-0.0032	0.0140	0.2323	0.0809	0.1929	0.0234	0.1946	0.0331
Z_q	-0.0317	-0.0024	0.0108	-0.0042	0.0530	0.0125	0.0103	0.0111	0.0128
X_q	0.0143	0.0054	0.0470	0.0606	0.0769	0.0079	0.0429	0.0079	0.0424
M_w	0.7500	0.0112	0.0395	-0.0232	0.0322	0.0125	0.0620	0.0122	0.0603
Z_w	-0.8323	0.0020	0.0162	0.0412	0.0621	0.0393	0.0143	0.0404	0.0196
X_w	0.0884	-0.0082	0.0473	0.0471	0.0983	0.0697	0.0371	0.0704	0.0366
M_u	-0.3708	-0.0415	0.0926	-0.2288	0.3736	-0.2302	0.1269	-0.2296	0.1262
Z_u	-0.0126	0.0138	0.0342	0.1180	0.1562	0.0428	0.0543	0.0430	0.0538
X_u	-0.0387	0.0140	0.0779	-0.0301	0.0583	0.0075	0.0867	0.0067	0.0859
$M_{\delta e}$	26.2571	0.0630	0.2441	-0.7850	0.9078	-0.4510	0.3662	-0.4577	0.3708
$Z_{\delta e}$	0.5571	-0.0069	0.1571	-0.0523	0.2761	0.0129	0.1469	0.0213	0.1564
$X_{\delta e}$	0.1480	-0.0531	0.2442	0.1599	0.5621	0.2471	0.1940	0.2501	0.1930
$M_{\delta c}$	3.8748	0.0269	0.1191	-0.0045	0.1718	0.2731	0.1381	0.2677	0.1559
$Z_{\delta c}$	-8.7743	-0.0113	0.1096	-0.0425	0.2693	0.1979	0.1843	0.1953	0.1790
$X_{\delta c}$	0.7717	0.1557	0.3808	0.7192	0.3669	2.0038	0.4944	2.0108	0.5016

NOTE: "n" is the number of Monte Carlo samples run for each case.

(93%), X_u (78%), M_u (62%), and X_w (53%). For all other parameters, the mean error is less than 16% of the corresponding true parameter values.

Thirteen of the parameter standard deviations from Case 2M are larger than those from Case 1M. The greatest increases were for Z_q (which in Case 2M is larger than the value in Case 1M by a factor of 5.0), Z_u (4.6), M_u (4.0), $X_{\delta e}$ (2.3), and X_w (2.1). The deviations for X_u and $X_{\delta e}$ show a moderate decrease. For both of these parameters, the 95% confidence has some overlap with the 95% confidence interval about the Case 2M value. It is even possible, therefore, that the actual values of these deviations increased slightly.

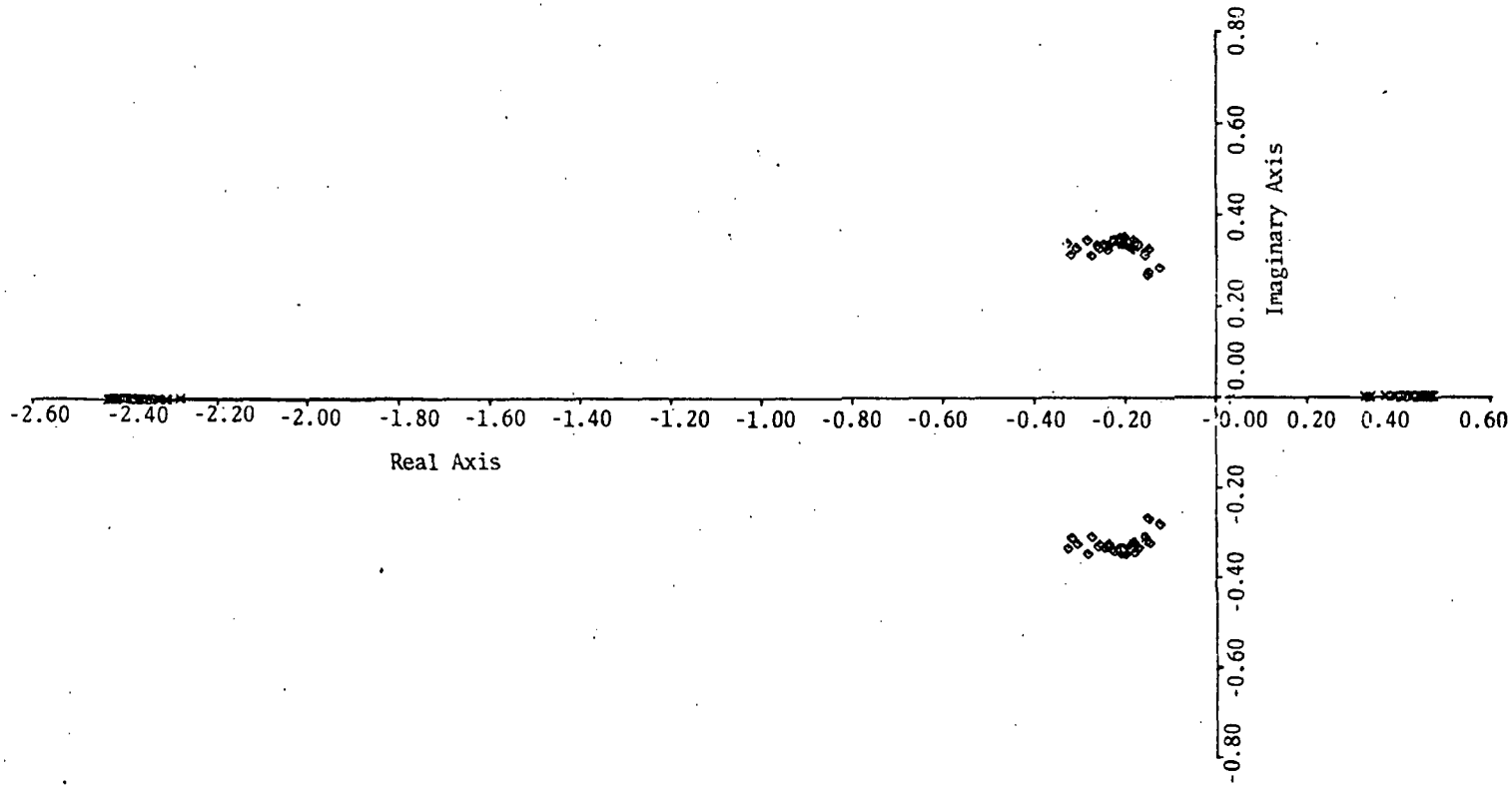

FIGURE 21(a).- ROOT PLOT SHOWING SCATTER OF OPEN-LOOP POLES FOR CASE 1M OF THE MONTE CARLO ANALYSIS

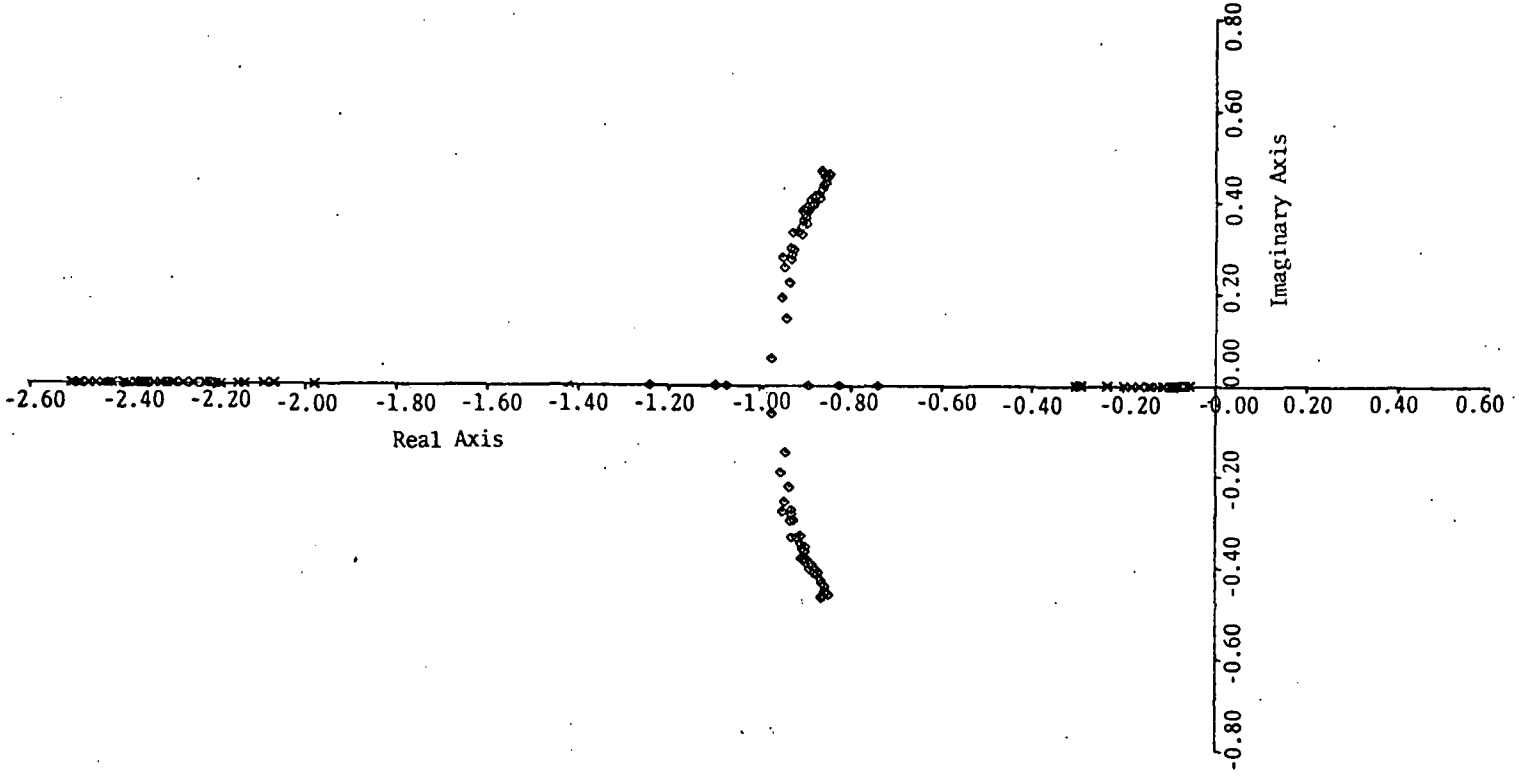

FIGURE 21(b)- ROOT PLOT SHOWING SCATTER OF CLOSED-LOOP POLES FOR CASE 1M OF THE MONTE CARLO ANALYSIS

The significant increases in both the mean and standard deviation for many parameter errors make it clear that the relatively substantial random components of lags in Case 2M are primary sources of error. The next step was to shorten the lag time constant to a relatively smaller value and compare the result to the case with no lags.

This was done in Case 3M for which $\bar{f} = 30\ \text{sec}^{-1}$ and $\sigma_f = 0.3\ \text{sec}^{-1}$. (Recall that $\bar{f}$ and σ_f describe the inverse of the lag time constants. Also, note that the value of σ_f, the variation in the lags, was the same in Cases 2M and 3M.) As in Case 2M, the mean errors for many parameters in Case 2M are relatively large compared to the corresponding parameter value. The mean error in Z_u is 340% of its value, $X_{\delta c}$ 260%, $X_{\delta e}$ 167%, X_w 79%, M_u 62%, X_q 55%, Z_q 39%, and all remaining mean errors are less than 20%. The largest mean errors in Cases 2M and 3M occur for the same parameters. These parameters are associated with the forward speed (Δu) mode, and the ensemble analysis showed that they possessed the larger deviations, as discussed previously. These same error effects carried over into Monte Carlo analysis results when random lags are present.

The effect on the sample deviations of the parameter errors of the lags in Case 3M compared to no lags in Case 1M is not so dramatic. In fact, decreases occur in the sample deviations for Z_q, X_q, Z_w, $Z_{\delta e}$, and $X_{\delta e}$. For each of these parameter deviations, the 95% confidence intervals overlap, which means that the true deviations may actually increase or that any decrease is moderate. The largest apparent increases in error deviations occur for M_q, M_w, Z_u, and $M_{\delta e}$, which are 50% to 70% greater than their values in Case 1M. The general conclusion, however, is that the lags in Case 3M have relatively little effect on the error deviations but do have relatively large effects on the error means.

There is a primary error source that causes these large mean errors. In the actual data collection, the continuous control input is sampled, and the resulting simulated state ($\hat{x}$) is computed from piecewise constant data. For these examples, the control input was held constant over the 0.05 sec sample length. This tends to cause the estimated state measurement $\hat{y}_i$ to lag behind the sampled actual measurement y_i. To compensate for this error, the sample rate of the control input can be increased, and interpolation schemes can be used to determine control magnitude between sample points.

This mean error was not specifically predicted by the Ensemble Analysis Program because it is based on continuous measurement of the control input. However, the mean can be approximated by putting in lags in the control measurement but not the output measurements.

One may intuitively expect the error deviations in Case 2M to be worse than those in Case 3M because the mean of the lag time constants is greater. For twelve parameters this is the case; their error deviations increase by factors of

1.2 for $M_{\delta c}$, up to 4.3 for Z_w, and 5.1 for Z_q. The sample standard deviations decrease for M_w, X_u, and $X_{\delta c}$.

Case 4M is similar to Case 3M except that the standard deviation of the lag inverse time constants is increased fivefold to $\sigma_f = 1.5\ \text{sec}^{-1}$. On the whole, there is very little difference between these cases in either the means or standard deviations of the parameter errors. Thus, the amount of scatter of actual time constants about the mean within reasonable limits does not have a significant effect for fast filters.

Cases 5M and 6M (see Table 24) both have lags such that $\bar{f} = 12\ \text{sec}^{-1}$ and $\sigma_f = 0.6\ \text{sec}^{-1}$. They differ in that Case 5M has the baseline error set, and Case 6M has the large error set from Table 12. Recall that the large errors include the larger noise covariance, R. As discussed previously, this means that the weighting matrix of the cost function is altered, and larger instrument errors do not necessarily imply larger parameter errors.

The mean error increased for M_w (by a factor of 2.7), Z_w (1.7), X_u (1.7), and M_q (1.07). The mean errors for X_q, $Z_{\delta e}$, and $Z_{\delta c}$ changed sign, but the 95% confidence intervals for X_q and $Z_{\delta e}$ contained zero in Case 6M. The mean errors for Z_q, $M_{\delta e}$, $X_{\delta e}$, and $M_{\delta c}$ decreased, but the 95% confidence intervals from the two cases have some overlap. The mean errors for X_w, M_u, Z_u, and $X_{\delta c}$ decrease, and there is no overlap in confidence intervals.

Table 24 also compares the effect of random lags at cruise and transition (Cases 5M and 7M). In general, the parameter standard deviations seem to be larger at transition, although this is not uniformly true.

Plots of the open- and closed-loop poles for Cases 1M through 7M appear in Figures 21 through 27. Significant variations in both the open- and closed-loop dynamics are evident in these figures. In particular, note that extreme closed-loop poles cross into the right-half plane for Case 2M (Figure 22(b)) and Case 6M (Figure 26(b)). Thus, the effect of random lags can affect the basic stability of the aircraft in addition to handling qualities.

Instrument accuracy needed to meet specified parameter accuracy.- As an example of how one would determine the accuracy required to meet a specified parameter accuracy, consider the following. Suppose it is decided that all longitudinal parameter estimates should have error standard deviations of not more than 30% of the corresponding parameters' absolute values. Suppose, also, it is decided that a situation similar to Case 14 holds the greatest promise of achieving that end. Specifically, the 45 sec data sequence is to be used; and six measurements, including the angle-of-attack vane and pitot tube, are to be used.

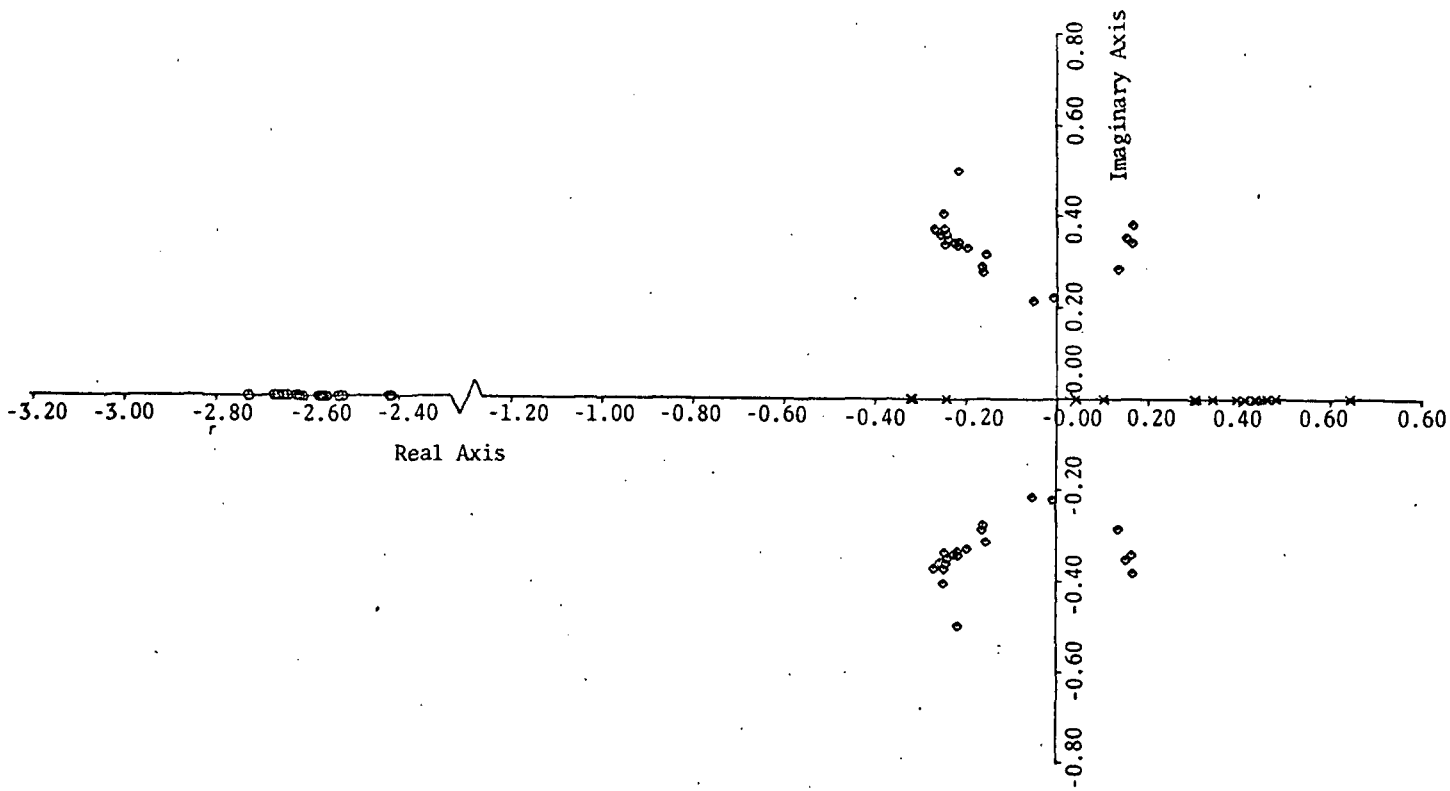

FIGURE 22(a).- ROOT PLOT SHOWING SCATTER OF OPEN-LOOP POLES FOR CASE 2M OF THE MONTE CARLO ANALYSIS

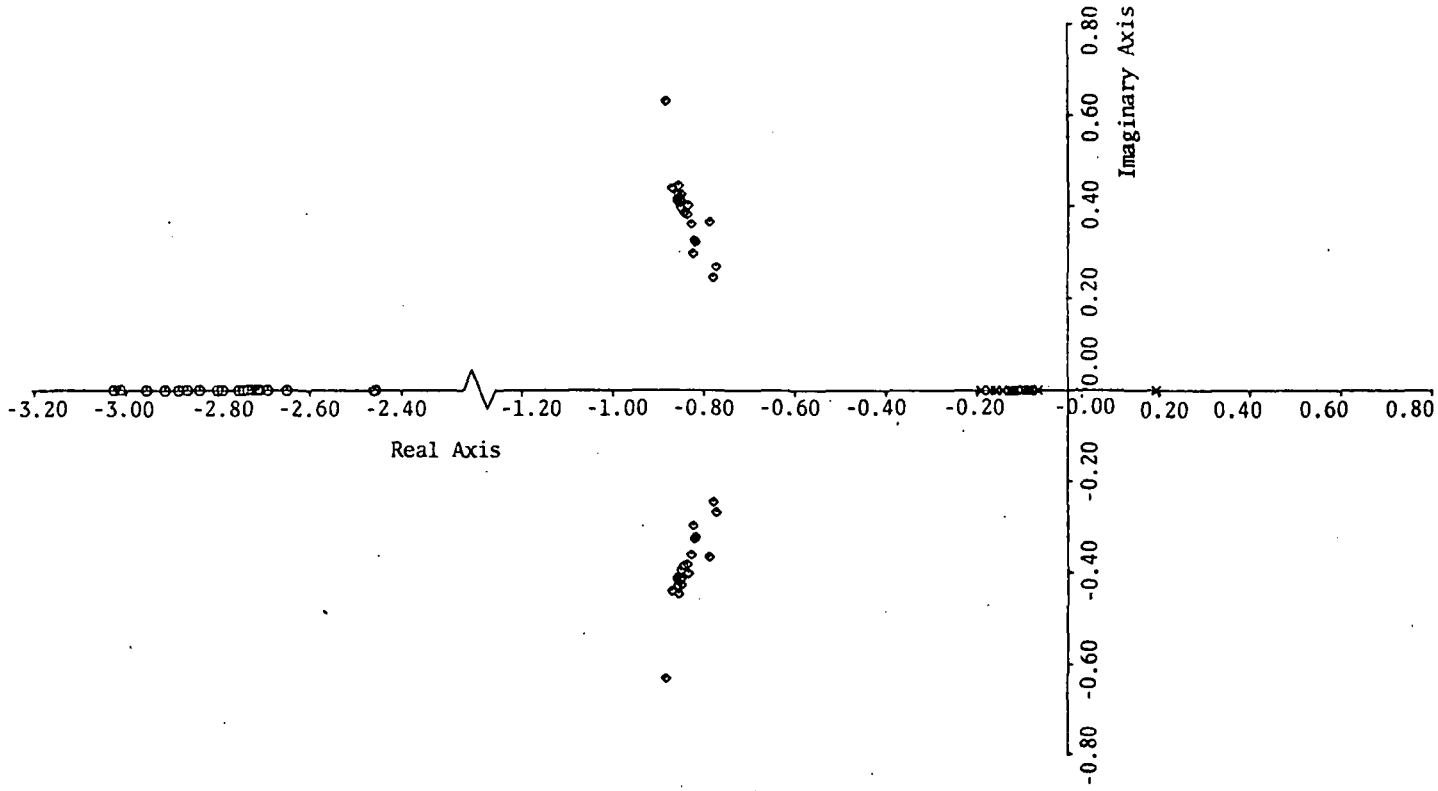

FIGURE 22(b).- ROOT PLOT SHOWING SCATTER OF CLOSED-LOOP POLES FOR CASE 2M OF THE MONTE CARLO ANALYSIS

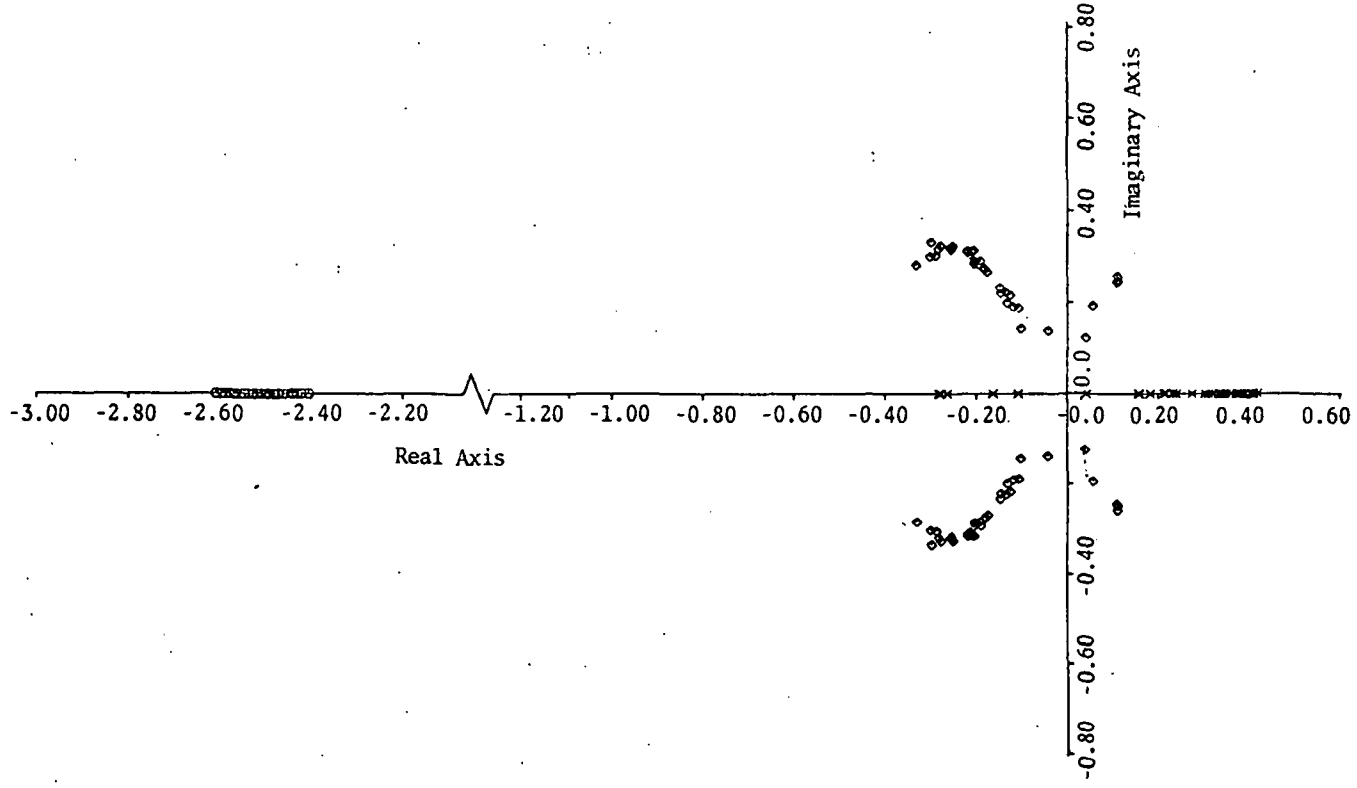

FIGURE 23(a).- ROOT PLOT SHOWING SCATTER OF OPEN-LOOP POLES FOR CASE 3M OF THE MONTE CARLO ANALYSIS

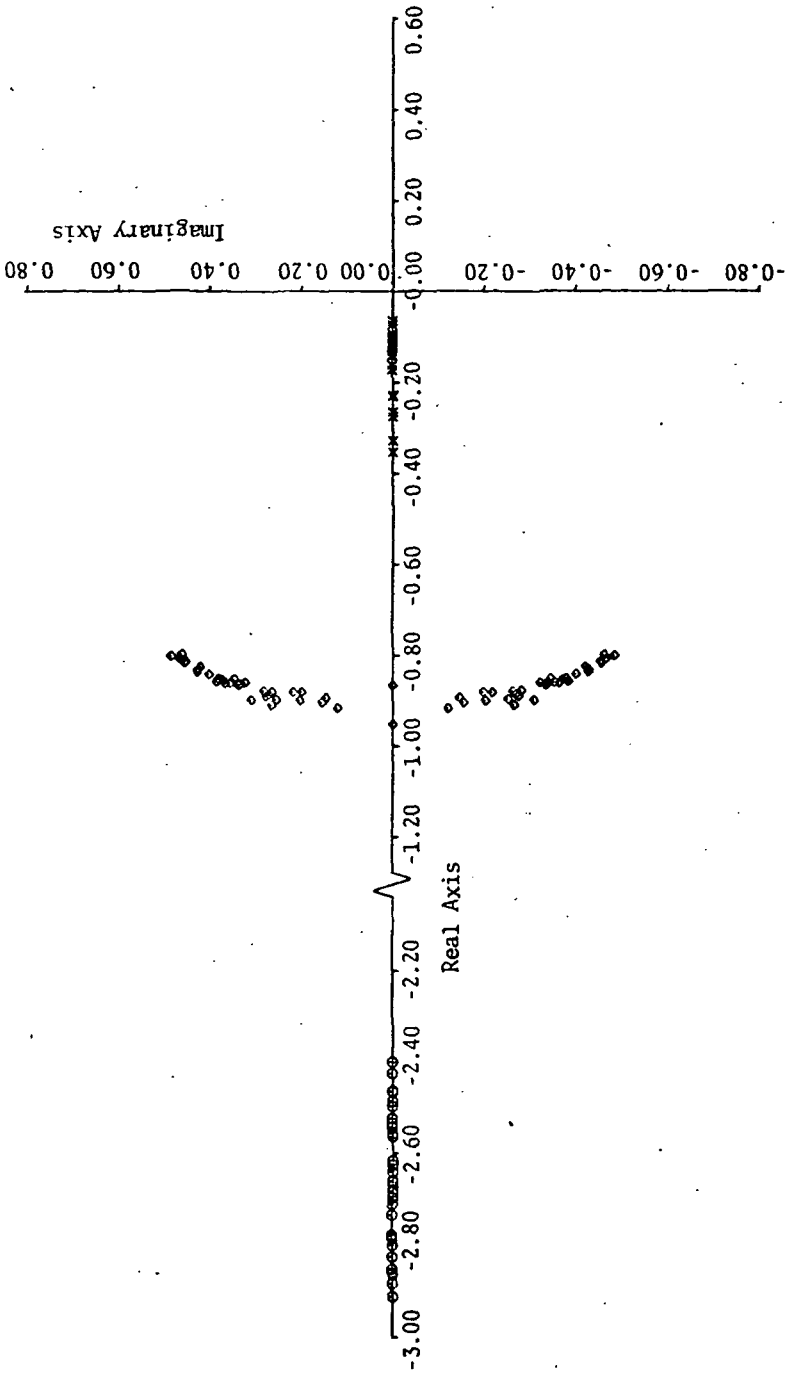

FIGURE 23(b).- ROOT PLOT SHOWING SCATTER OF CLOSED-LOOP POLES FOR CASE 3M OF THE MONTE CARLO ANALYSIS.

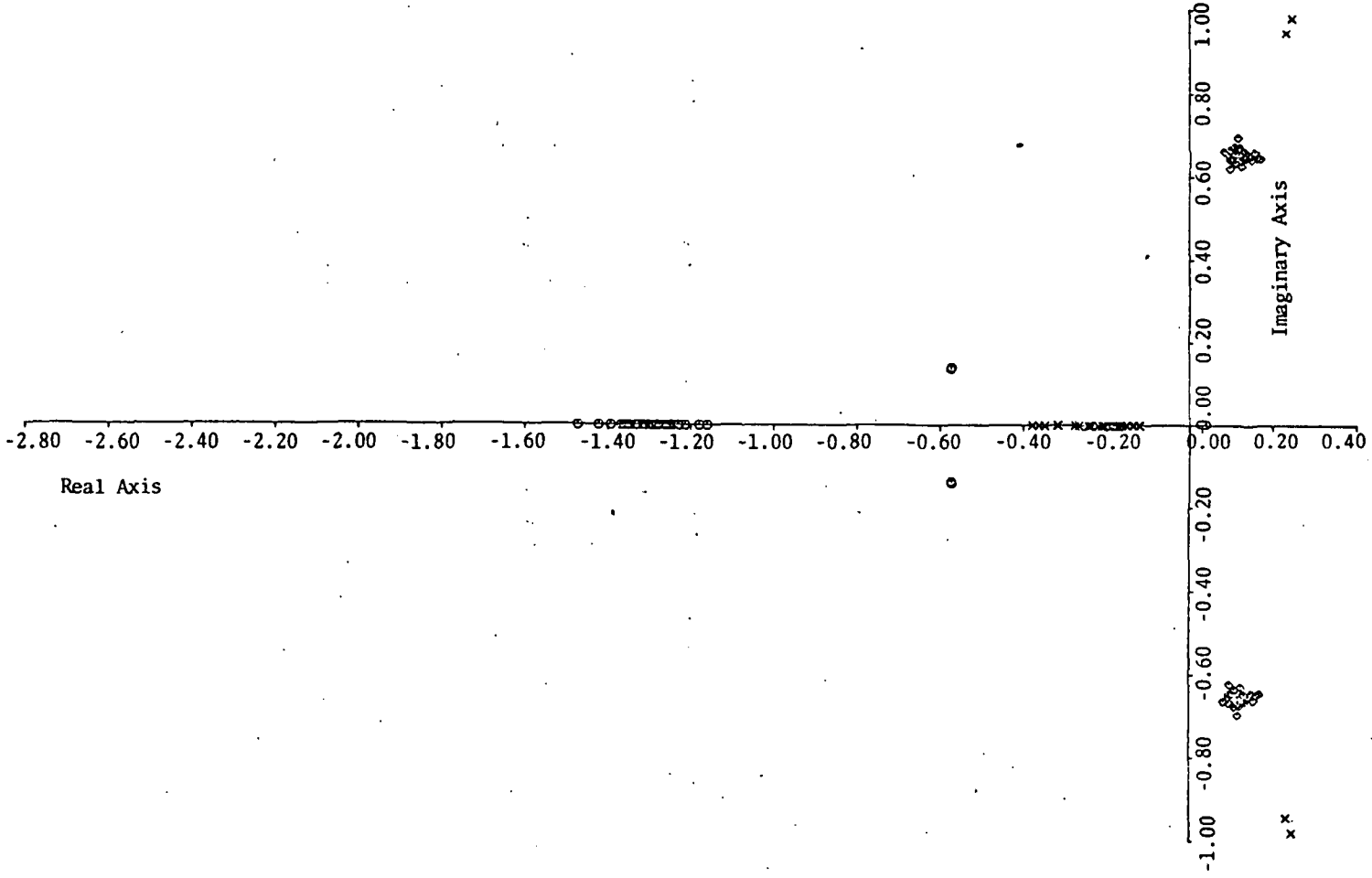

FIGURE 24(a).- ROOT PLOT SHOWING SCATTER OF OPEN-LOOP POLES FOR CASE 4M OF THE MONTE CARLO ANALYSIS

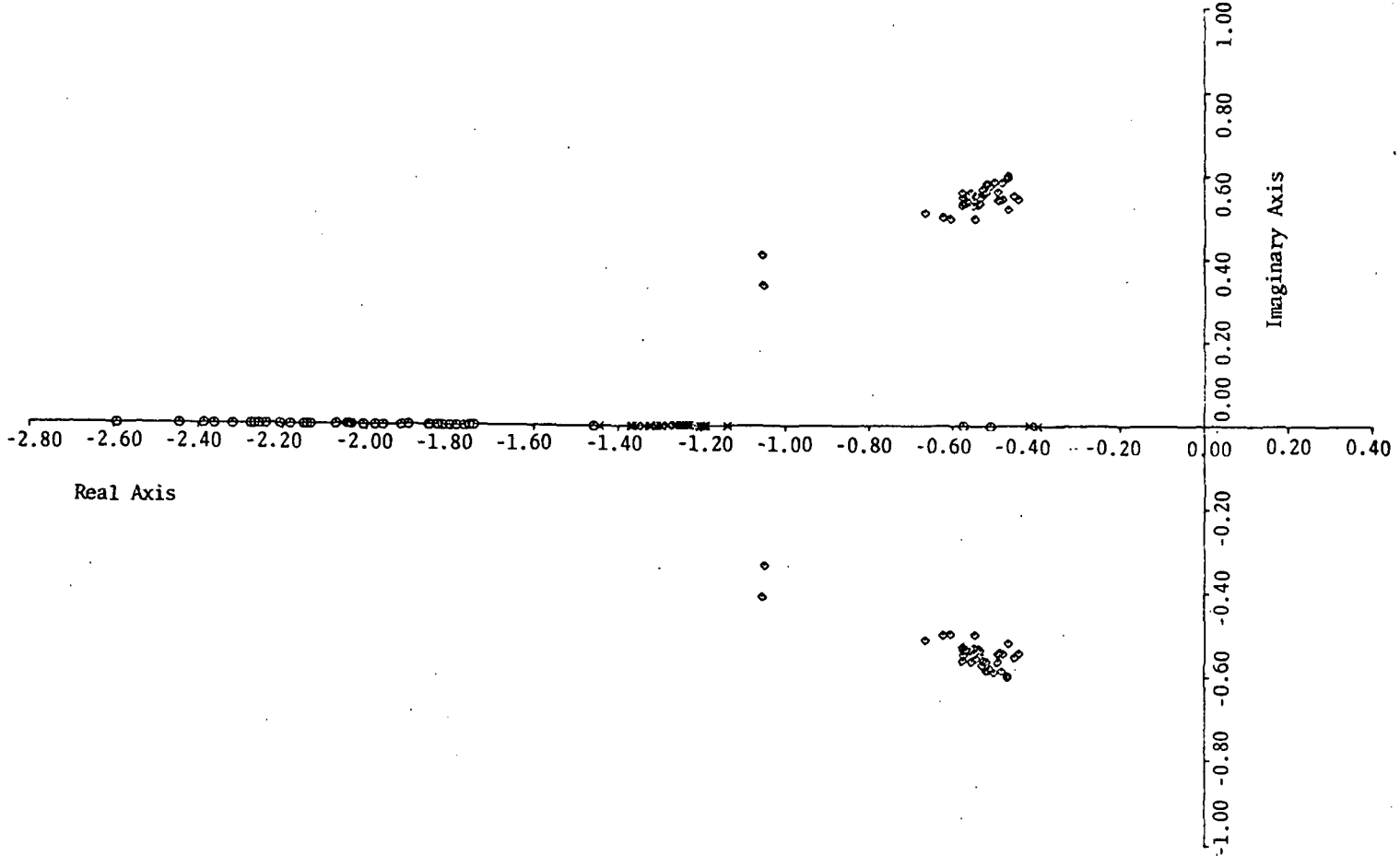

FIGURE 24(b).- ROOT PLOT SHOWING SCATTER OF CLOSED-LOOP POLES FOR CASE 4M OF THE MONTE CARLO ANALYSIS

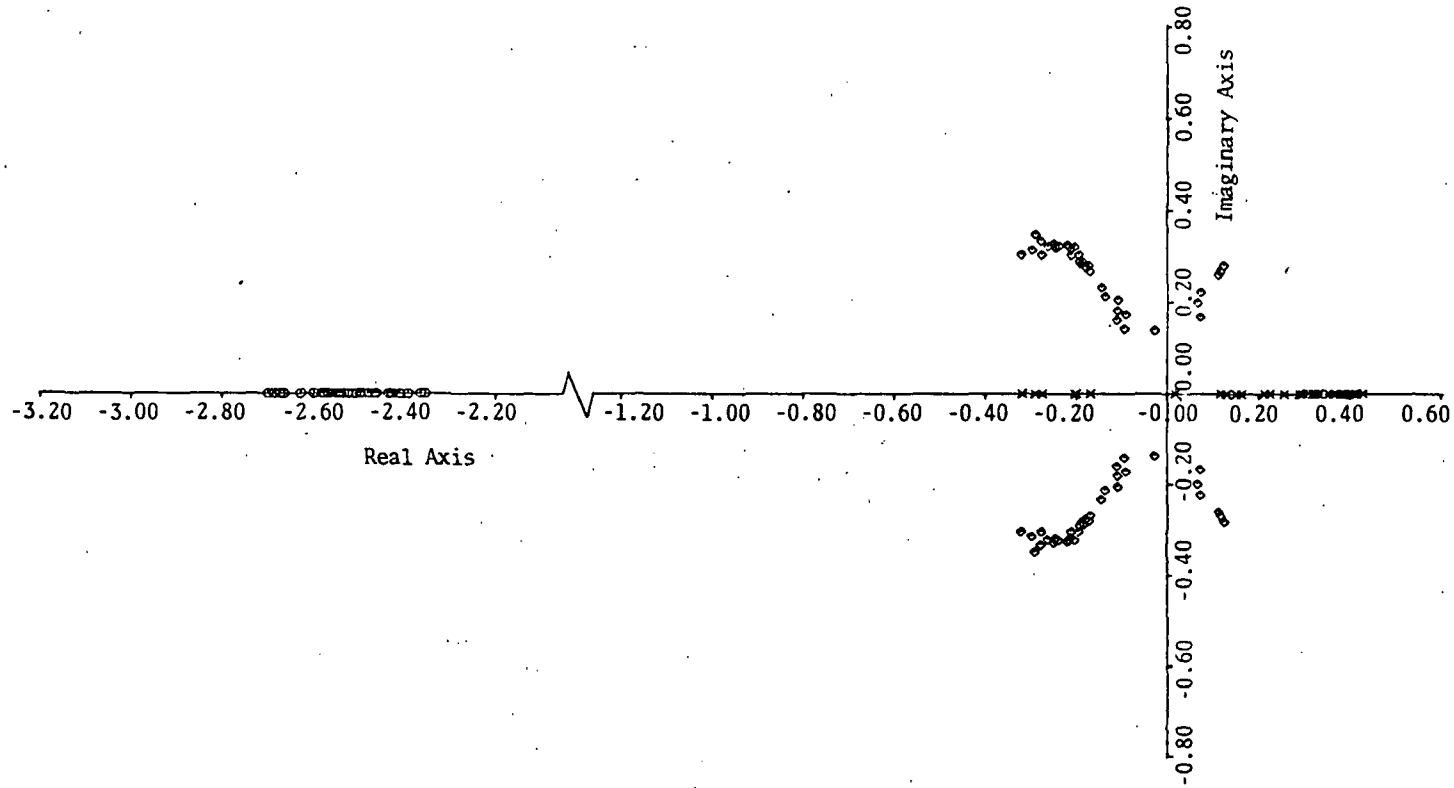

FIGURE 25(a).- ROOT PLOT SHOWING SCATTER OF OPEN-LOOP POLES FOR CASE 5M OF THE MONTE CARLO ANALYSIS

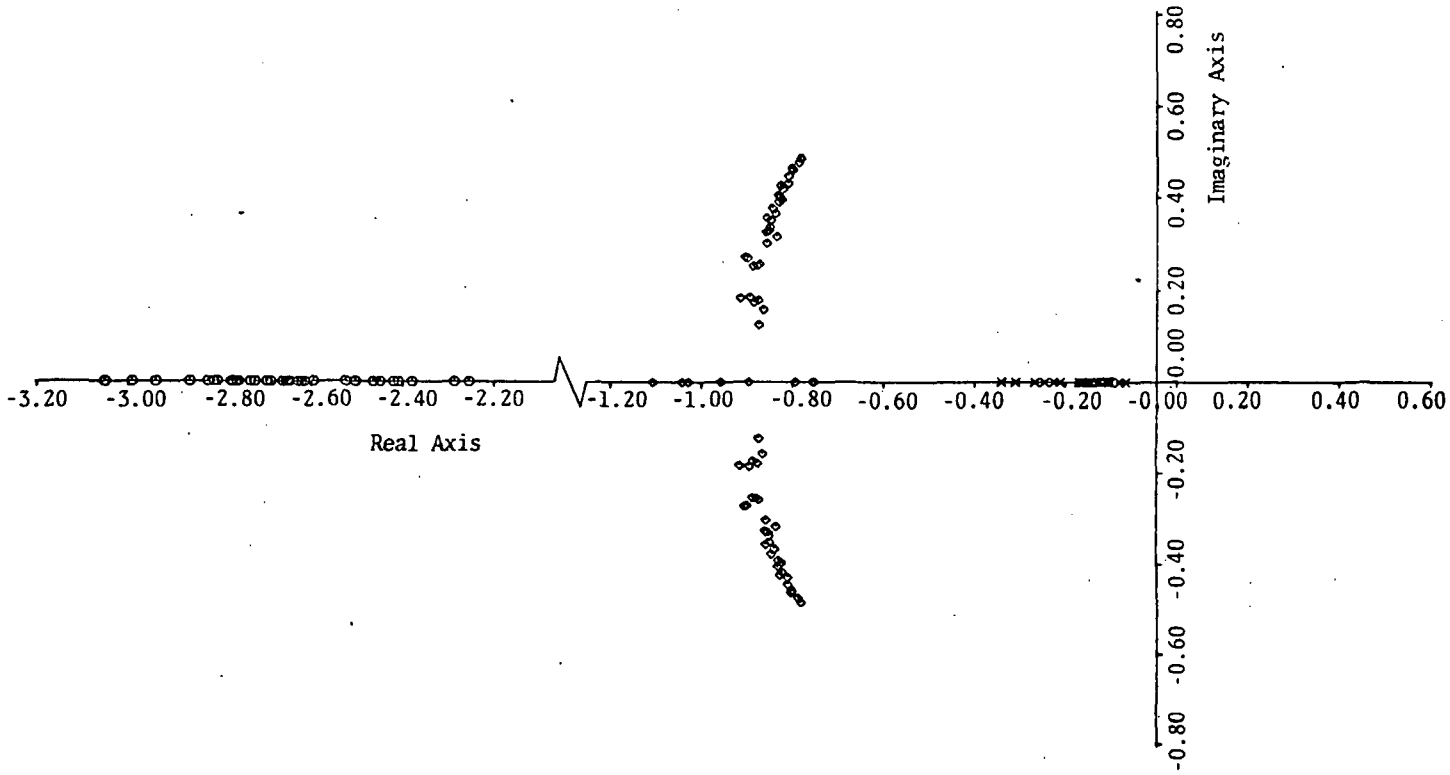

FIGURE 25(b).- ROOT PLOT SHOWING SCATTER OF CLOSED-LOOP POLES FOR CASE 5M OF THE MONTE CARLO ANALYSIS

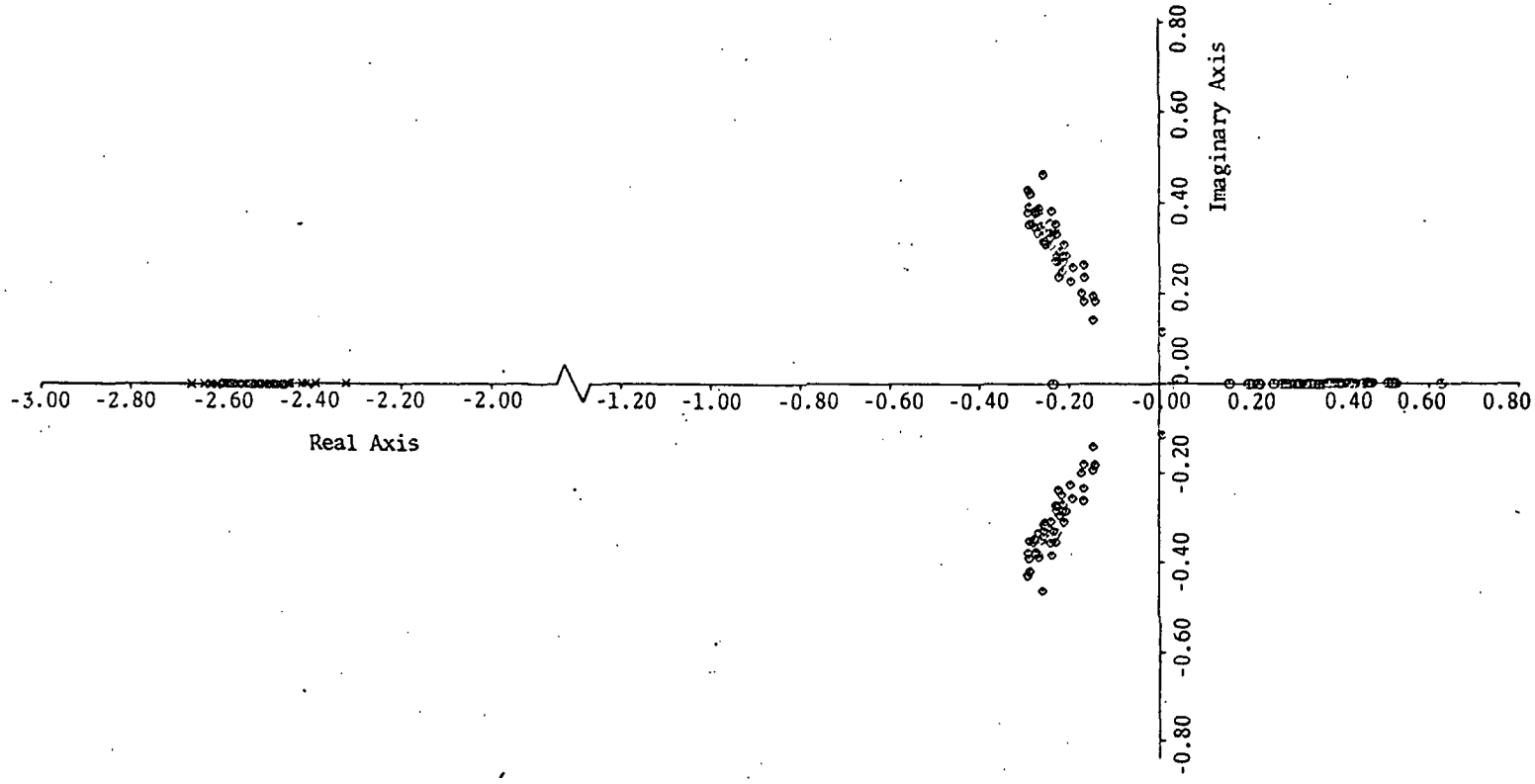

FIGURE 26(a).- ROOT PLOT SHOWING SCATTER OF OPEN-LOOP POLES FOR CASE 6M OF THE MONTE CARLO ANALYSIS

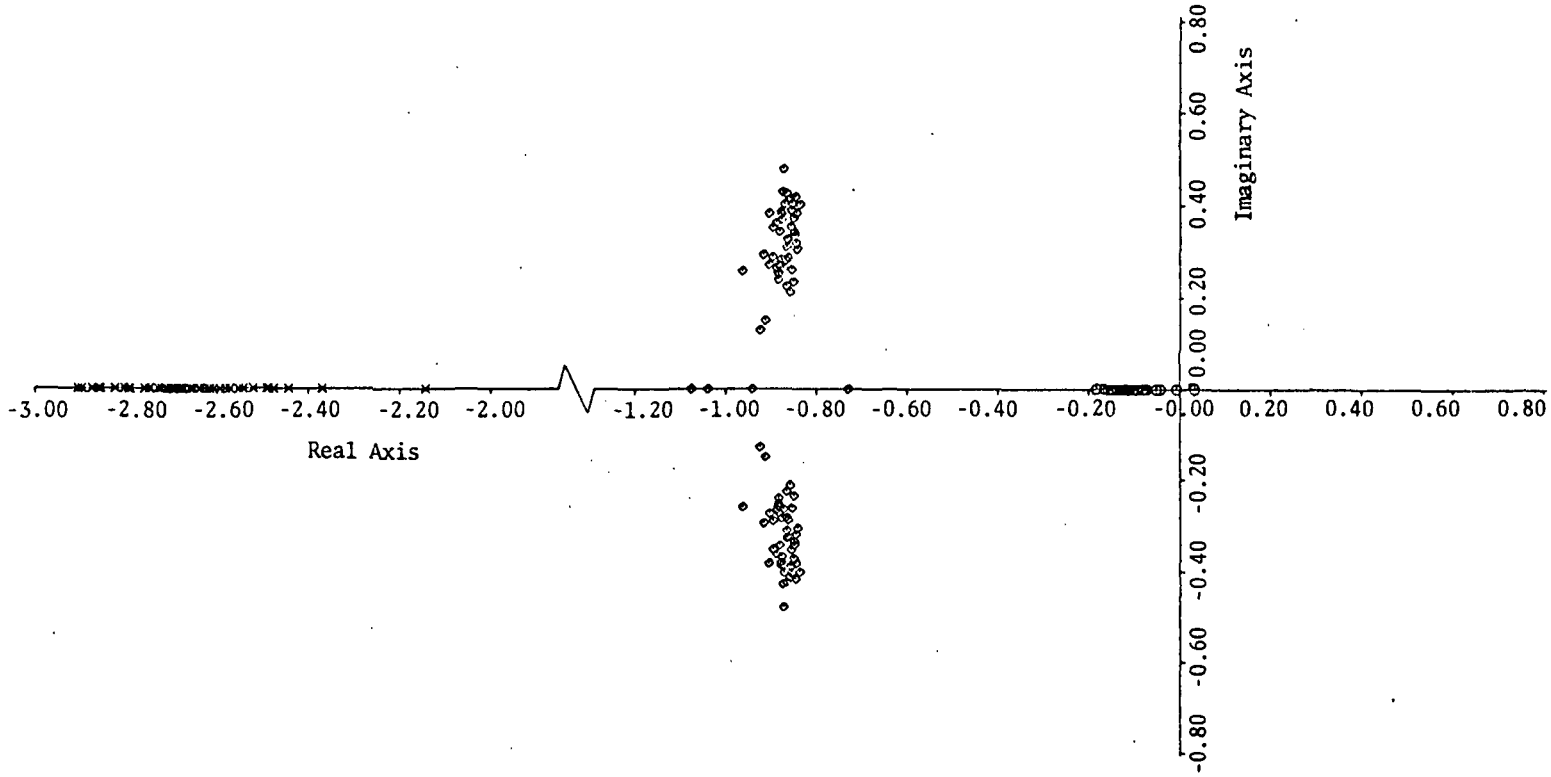

FIGURE 26(b).- ROOT PLOT SHOWING SCATTER OF CLOSED-LOOP POLES FOR CASE 6M OF THE MONTE CARLO ANALYSIS

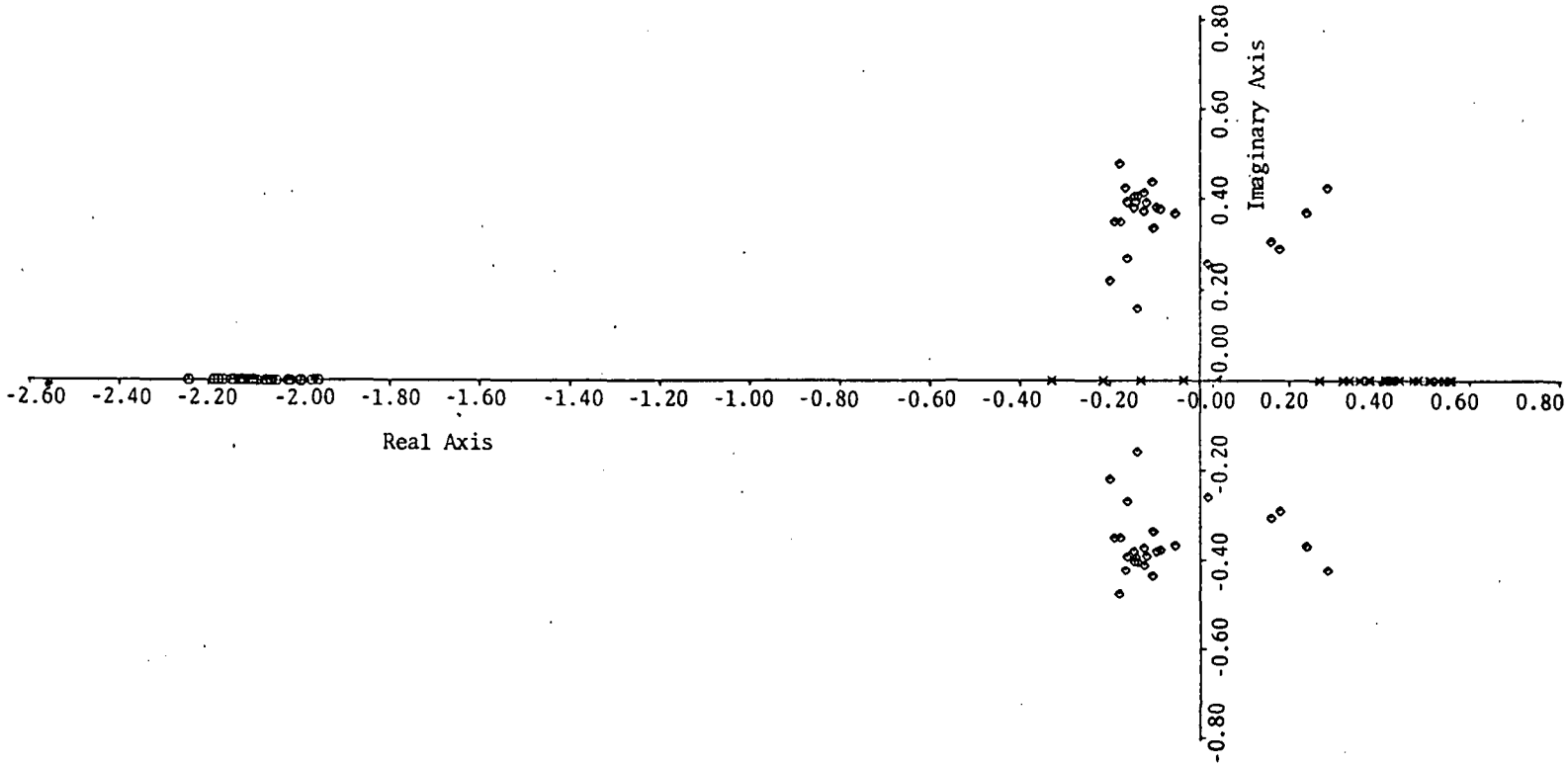

FIGURE 27(a).- ROOT PLOT SHOWING SCATTER OF OPEN-LOOP POLES FOR CASE 7M OF THE MONTE CARLO ANALYSIS

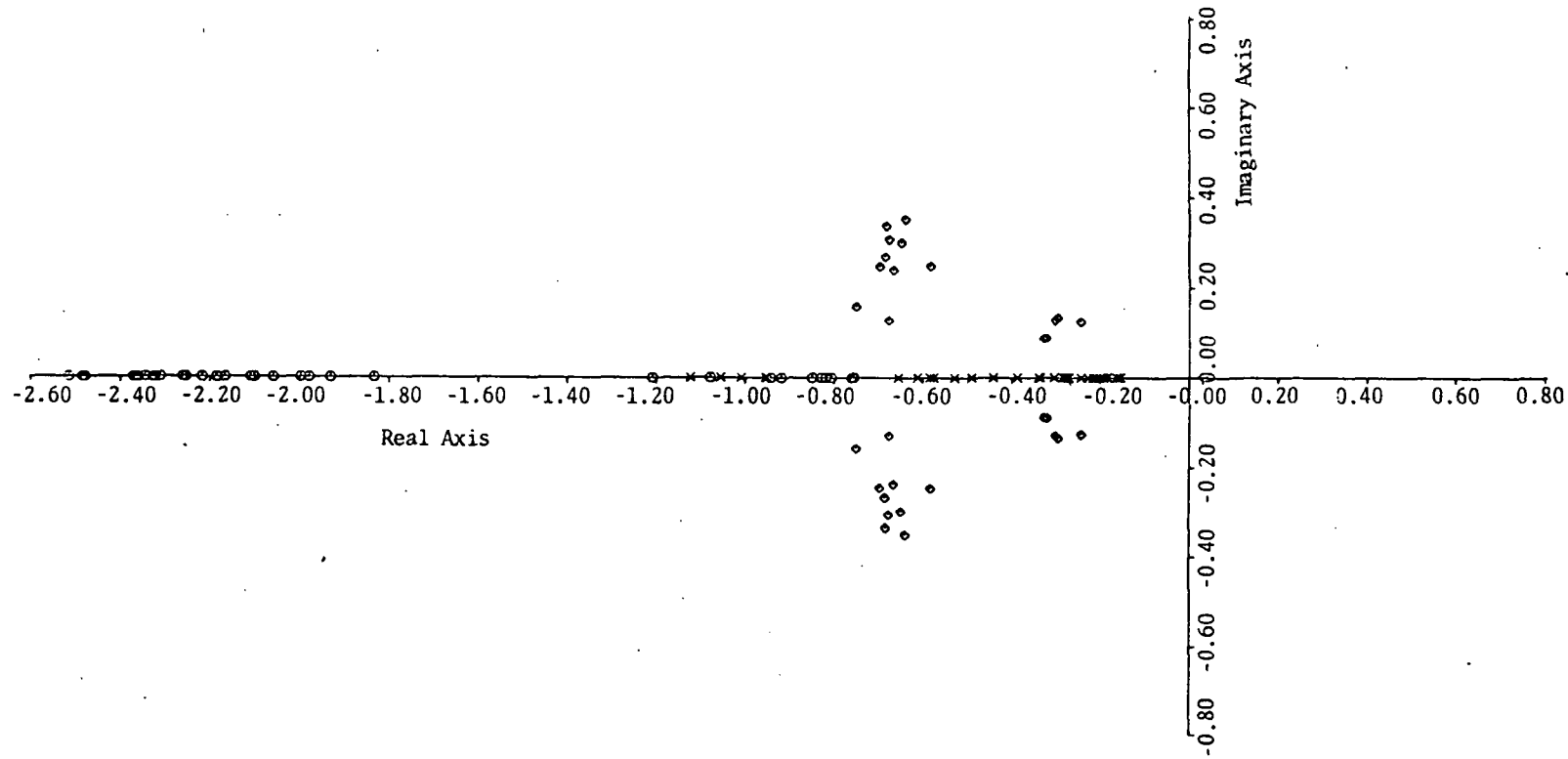

FIGURE 27(b).- ROOT PLOT SHOWING SCATTER OF CLOSED-LOOP POLES FOR CASE 7M OF THE MONTE CARLO ANALYSIS

TABLE 24.- ERRORS IN LONGITUDINAL PARAMETER ESTIMATES FOR MONTE CARLO ANALYSIS (Normal and Large Errors at Cruise and Normal Errors at Transition)

Cruise Parameters		CASE 5M (n=37, $\bar{f}$ = 12 sec^{-1}, σ_f = 0.6 sec^{-1}, Cruise)		CASE 6M (n=50, $\bar{f}$ = 12 sec^{-1}, σ_f = 0.6 sec^{-1}, Cruise, Large Errors)		Transition Parameters	CASE 7M (n=26, $\bar{f}$ = 12 sec^{-1}, σ_f = 0.6 sec^{-1}, Transition)	
Name	Value	$\Delta\bar{p}$	s	$\Delta\bar{p}$	s	Value	$\Delta\bar{p}$	s
M_q	-1.4761	0.2127	0.0569	0.2141	0.0686	-1.2510	0.1975	0.0468
Z_q	-0.0317	0.0215	0.0184	0.0175	0.0203	-0.0290	0.0622	0.0445
X_q	0.0143	0.0316	0.0457	-0.0046	0.0255	0.0179	0.0491	0.0508
M_w	0.7500	0.0072	0.0670	0.0191	0.0608	1.0829	-0.0405	0.0730
Z_w	-0.8323	0.0291	0.0289	0.0491	0.0237	-0.5688	-0.1348	0.1069
X_w	0.0884	0.0445	0.0388	0.0126	0.0148	0.0776	-0.0162	0.1351
M_u	-0.3708	-0.2444	0.1322	-0.0577	0.1444	-0.2406	-0.2689	0.1390
Z_u	-0.0126	0.0517	0.0618	0.0041	0.0584	-0.1286	0.0651	0.1410
X_u	-0.0387	0.0040	0.0797	0.0067	0.0314	-0.0123	0.0004	0.0719
$M_{\delta e}$	26.2571	-0.5262	0.5784	-0.1777	0.7749	22.4485	-0.4570	0.4513
$Z_{\delta e}$	0.5571	-0.0392	0.1716	0.0041	0.4520	0.5198	-0.3749	0.2022
$X_{\delta e}$	0.1480	0.1349	0.1981	0.0943	0.4030	0.1206	-0.0216	0.2451
$M_{\delta c}$	3.8748	0.2545	0.1443	0.2053	0.1672	2.0626	0.2479	0.1172
$Z_{\delta c}$	-8.7743	0.1124	0.1311	-0.1230	0.2137	-7.3132	-0.0926	0.0893
$X_{\delta c}$	0.7717	1.8170	0.4565	0.2396	0.1885	0.8889	0.8459	0.2231

From Figure 17, it can be seen that for Case 14, all parameters except X_q, X_w, and $X_{\delta e}$ have error standard deviations less than the prescribed 30% limit. Using the sensitivities of the parameter estimates to instrument errors, $\partial p/\partial e$, it was found that the dominant errors for these three parameters are the control biases and the z_{cg} location errors. Also, through use of these sensitivities, it was calculated that the error in X_q could be reduced to 30% and the error in X_w

reduced to 29%, if the standard deviation of the differential collective control bias is reduced to 0.025 inch and the Z_{cg} location error is reduced to 1.0 inch. Even then, the error in $X_{\delta e}$ would improve only from 134% to 73%, still above the 30% limit. These calculations were done according to the procedure discussed previously in this chapter.

To proceed further with this example, by reducing the error in $X_{\delta e}$ below 30% would require an even less realistic constraint on $b_{\delta e}$, the differential collective control bias. The engineer must decide whether: (1) to accept a 73% error in $X_{\delta e}$, which he is likely to do since $X_{\delta e}$ is one of the least important parameters, or (2) to construct the identification algorithm such that it is possible to estimate the control measurement biases and, thereby, eliminate their influence on the parameter errors. Because control biases are usually the dominant errors for most parameters, this latter course of action is very promising, but it did not fall within the scope of this study.

The Effects of Instrument Errors on Lateral Parameters

Ensemble analysis results.- To study instrument error effects on lateral parameter accuracy, a series of seven cases was made using the ensemble analysis program. These cases are listed in Table 25. Six instruments were assumed present in Cases 19 and 20--the roll and yaw rate gyros, the roll angle gyro, the

TABLE 25.- SUMMARY OF ENSEMBLE ANALYSIS COMPUTER RUNS IN LATERAL MODE

Case No.	Description of Instruments and Flight Regime			Biases Estimated?	Compared with Cases __
	p r ϕ a_y $\dot{p}$ $\dot{r}$	Regime	Errors		
19	✓ ✓ ✓ ✓ ✓ ✓	Near-hover	Nominal	No	
20	✓ ✓ ✓ ✓ ✓ ✓	Near-hover	Nominal	Yes	19
21	✓ ✓ ✓ ✓	Near-hover	Nominal	No	19
22	✓ ✓ ✓ ✓	Near-hover	Nominal	Yes	20,21
23	✓ ✓ ✓ ✓	Cruise	Nominal	No	21,22
24	✓ ✓ ✓ ✓	Transition	Nominal	No	21
25	✓ ✓ ✓ ✓	Near-hover	Large	Yes	22

lateral accelerometer, and the roll and yaw angular accelerometers. The input sequence and resulting trajectory were as illustrated in Figure 12. There were 300 sample points of data taken every 0.1 sec over a 30 sec time span. The nominal instrument error magnitudes of Table 12(b) were used. Case 19 did not estimate output biases, and Case 20 did. (All except b_{φ} which cannot be distinguished from the roll angle initial condition error.) The near-hover flight regime was selected for these runs. Initial condition errors were not present. Also, the angle-of-sideslip vane was not used based on the assumption that it would not normally function well in a near-hover flight condition. The results of Cases 19 and 20 are shown in Figure 28. Here again, the standard deviations of each parameter due to noise only and due to all error effects are shown, as normalized by actual parameter magnitudes. The values are depicted in percentage error.

As can be seen in Figure 28, estimating biases (Case 20) did not uniformly improve the estimates of the parameters. Although Y_r, N_v^*, N_p^*, N_r^*, and $N_{\delta a}^*$ improved from 640% to 85%, 21% to 6%, 64% to 9%, 28% to 9%, and 13% to 6%, respectively, L_p^* degraded from 145% to 260%. In general, estimating biases was a good procedure for this flight regime, but again the choice should be made depending on what accuracy is desired for specific parameters.

It was noted that in Case 19, the roll cyclic measurement bias $b_{\delta a}$ was the most dominant error for seven parameters, and second most dominant error for seven other parameters. Also, the yaw cyclic measurement bias $b_{\delta r}$ was the most prominent error for five parameters and the second most dominant error for five parameters. Thus, without estimating biases, the control biases are still the dominant error sources, as was true for the longitudinal mode.

When output measurement biases were estimated in Case 20, $b_{\delta a}$ becomes the dominant error for eleven parameters, and second in importance for one other parameter. The error $b_{\delta r}$ is the second most dominant error for nine parameters. Thus, unlike the longitudinal mode, estimating output measurement biases does not displace the control biases from their position as the dominant error source. This is because the parameter sensitivities to control biases are not reduced substantially in the lateral mode when output biases are estimated.

Next, two more runs, Cases 21 and 22, were made which delete the angular accelerometers from the instrument set. The results are also presented in Figure 32. These cases can then be compared with Cases 19 and 20. The results are mixed. Not estimating biases with six instruments (Case 19) gives the least errors for $Y_{\delta a}$, $Y_{\delta r}$, L_v^*, L_p^*, and $L_{\delta a}^*$. Estimating biases with six instruments (Case 20) gives the least errors for $L_{\delta r}^*$, $N_{\delta a}^*$, and $N_{\delta r}^*$. When biases are not estimated when four instruments are used (Case 21), the least errors for Y_v and Y_p are produced. Finally, estimating biases with four instruments (Case 22) produces the best estimates of L_r^*, N_v^*, N_p^*, and N_r^*. For the cases examined, the improvements produced by the angular accelerometers are not significant. This is in line with the results of the longitudinal study. However, the final decision on whether these

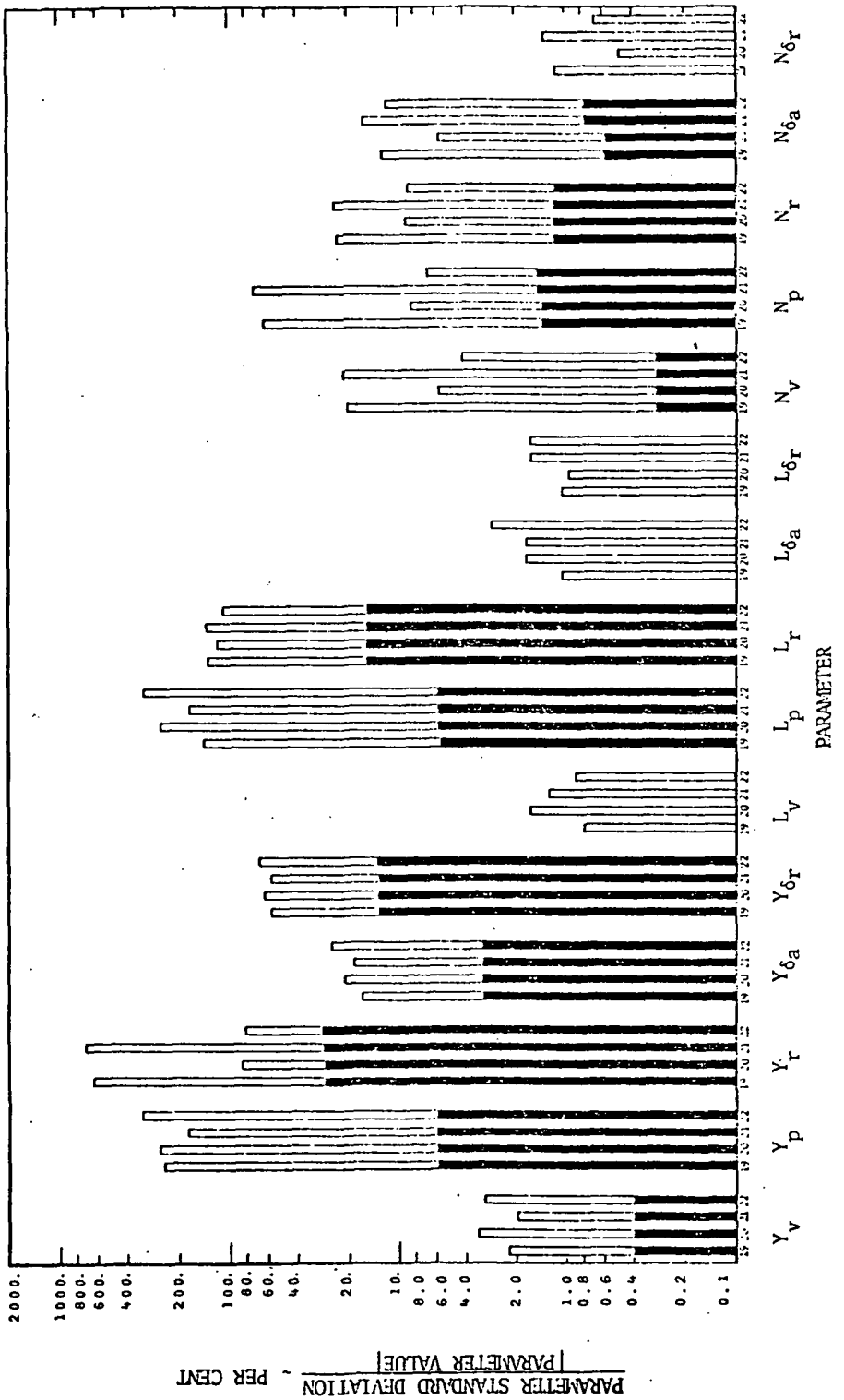

Shaded Portion of Each Bar Shows Standard Deviation Due to Noise Alone.

FIGURE 28.- ENSEMBLE ANALYSIS COMPARISON OF PARAMETER ERROR STANDARD DEVIATIONS FROM CASES 19 THROUGH 22: EFFECTS OF NOMINAL ERROR VALUES ON LATERAL PARAMETERS NEAR-HOVER

instruments should be used must be based on specific accuracy requirements placed on individual parameters.

The next set of runs, Cases 23 and 24, essentially duplicated Run 21 at cruise and transition conditions. Biases were not estimated. The inputs were slightly modified so that the slower frequency sine waves of the control input had the same frequency as the complex poles of the system at each flight condition. The results of these runs are presented in Table 26. In this table, the magnitude of the parameters at each flight condition are first listed. Then, the standard deviations due to noise only and due to all errors are given. These deviations are normalized by the parameter magnitude so that the numbers are percentage errors.

From Table 26, it can be seen that the trends in the error magnitudes are the same at all three flight conditions. The accuracies of Y_r, L_r^*, and N_p^* are poor at all conditions. Eight of the parameters have their largest errors at cruise, and the other seven have their largest errors during transition. The results obtained from the ensemble analysis appear to be quite accurate except for perhaps Y_r.

As a final example, the large errors of Table 12 were run in the near-hover conditions for Case 25. Biases were estimated, and the results are compared with Case 22 in Table 27. Again, standard deviations of the parameters are normalized by the parameter values, and the error deviations are presented in percentages.

From Table 27, it can be seen that the variation due to noise goes up using the larger errors for each parameter. The total variation of each parameter due to all instrument errors increases by over a factor of two for ten of the fifteen parameters, and, in fact, the deviations of Y_r, $Y_{\delta a}$, and L_r^* become quite large. Four parameters' deviations ($L_{\delta a}^*$, $L_{\delta r}^*$, N_v^*, and $N_{\delta a}^*$) remain about the same. But the surprising result is that the deviation on Y_p decreases from 330% to 177%. Although this is still poor, it points out a key factor in the effect of various instrument errors. This factor is the weighting matrix R^{-1} that it used in the identification algorithm. For the lateral equations studied here, the change in the weighting matrix due to the large noise errors actually decreased the variation in Y_p. A fruitful area of future development might be to devise an optimum weighting matrix R^{-1} that takes into account all instrument errors and produces the smallest variations in all parameters.

A further result observed in Table 27 is that the large error magnitudes are unacceptable in obtaining reasonable parameter deviations. In fact, if all parameters are to be estimated to within 50% (1σ) of their nominal value, even the baseline error set must be improved.

Simulated data analysis results.- The Simulated Data Analysis of the lateral parameter errors proceeded along lines similar to the longitudinal study. Six computer runs were performed, and the characteristics of these runs are summarized in Table 28. In each case, the instrument set consisted of the roll attitude

TABLE 26.- COMPARISON OF ENSEMBLE ANALYSIS LATERAL PARAMETER DEVIATIONS AT CRUISE, TRANSITION, AND NEAR-HOVER FLIGHT CONDITIONS

Parameter	Cruise (Case 23)			Transition (Case 24)			Near Hover (Case 21)		
	Value	Standard Deviation due to Noise %	Standard Deviation due to All Errors %	Value	Standard Deviation due to Noise %	Standard Deviation due to All Errors %	Value	Standard Deviation due to Noise %	Standard Deviation due to All Errors %
Y_v	-0.12676	1.2	7.1	-0.07470	1.0	19.6	0.15375	0.4	2.0
Y_p	-0.2172	4.8	146.1	-0.02229	5.2	206.4	-0.01635	5.9	177.6
Y_r	-0.00192	101.1	8558.6	-0.00326	34.2	3211.4	-0.00190	28.3	705.3
Y_{δ_a}	0.96563	3.3	27.6	0.96110	3.2	40.4	0.99282	3.2	18.3
Y_{δ_r}	0.10393	20.8	49.2	0.11020	19.3	62.8	0.15500	13.6	59.0
L_v^*	-1.02886	0.1	6.0	-0.55634	0.1	0.9	-0.52386	0.0	1.3
L_p^*	-0.66320	0.3	10.5	-0.72089	0.1	2.7	-0.59364	0.3	2.4
L_r^*	0.02800	14.3	93.4	-0.02619	6.2	157.9	0.01763	15.9	140.7
$L_{\delta_a}^*$	27.03903	0.0	2.3	26.96798	0.0	3.1	27.28769	0.0	1.8
$L_{\delta_r}^*$	-16.64557	0.0	4.3	-16.56765	0.0	0.7	-15.98667	0.0	1.7
N_r^*	-0.08251	0.5	28.0	-0.03667	0.5	18.6	0.05191	0.3	21.9
N_p^*	0.02264	3.0	99.3	0.04734	1.0	31.6	0.03442	1.5	74.1
N_r^*	-0.05406	2.9	71.4	-0.03741	1.5	37.2	-0.05093	1.2	24.8
$N_{\delta_a}^*$	-1.15377	0.8	5.2	-1.10237	0.7	34.0	-0.99385	0.8	17.1
$N_{\delta_r}^*$	11.42421	0.1	4.0	11.43395	0.1	0.6	11.60240	0.0	1.4

TABLE 27.- COMPARISON OF ENSEMBLE ANALYSIS LATERAL PARAMETER DEVIATIONS AT NEAR-HOVER FOR LARGE AND BASELINE INSTRUMENT ERROR MAGNITUDES

Parameter	Value	Baseline Errors (Case 22)		Large Errors (Case 25)	
		Standard Deviation due to Noise %	Standard Deviation due to All Errors %	Standard Deviation due to Noise %	Standard Deviation due to All Errors %
Y_v	0.15375	0.4	3.1	0.5	8.9
Y_p	-0.01635	6.0	330.3	13.1	176.9
Y_r	-0.00190	28.7	81.3	87.6	356.6
Y_{δ_a}	0.99282	3.2	25.4	3.3	49.1
Y_{δ_r}	0.15500	13.6	68.4	13.7	223.1
L_v^*	-0.52386	0.1	0.9	0.3	2.1
L_p^*	-0.59364	0.3	2.0	0.4	6.1
L_r^*	0.01763	15.9	112.5	20.3	242.4
$L_{\delta_a}^*$	27.28769	0.0	2.9	0.1	2.4
$L_{\delta_r}^*$	-15.98667	0.0	1.7	0.2	2.3
N_r^*	0.05191	0.3	4.3	1.3	5.9
N_p^*	0.03442	1.5	6.8	4.5	24.0
$N_{\delta_r}^*$	-0.05093	1.2	9.1	2.2	29.9
$N_{\delta_a}^*$	-0.99385	0.8	12.3	2.7	14.0
$N_{\delta_r}^*$	11.60240	0.0	0.7	0.2	2.4

gyro, roll and yaw rate gyros, and lateral accelerometer. The angle-of-sideslip vane and angular accelerometers were omitted. Measurement biases and initial conditions were not estimated. The control input sequence was the same 30 sec sequence used in the Ensemble Analysis Program (see Figure 12). At transition and cruise conditions, this sequence was modified as described previously.

Case 9M used the baseline error set at the near-hover flight condition and had no lags; thus, it may be compared to Case 21. The results of Case 9M are presented in Table 29. The estimated mean errors based on the 50 Monte Carlo

TABLE 28.- SUMMARY OF SIMULATED DATA COMPUTER RUNS FOR LATERAL EQUATIONS

Case	Flight Regime	Error Set	Lag Inverse Time Constants	
			Mean, $\bar{f}$	Standard Deviation, σ_f
9M	Near Hover	Baseline	0.0 sec^{-1}	0.0 sec^{-1}
10M	Near Hover	Baseline	6.0 sec^{-1}	0.3 sec^{-1}
11M	Transition	Baseline	6.0 sec^{-1}	0.3 sec^{-1}
12M	Cruise	Baseline	6.0 sec^{-1}	0.3 sec^{-1}
13M	Near Hover	Baseline	12.0 sec^{-1}	0.6 sec^{-1}
14M	Near Hover	Large	12.0 sec^{-1}	0.6 sec^{-1}

samples of Case 9M are small relative to the true parameter value for every parameter except Y_r. In Case 21, these values are practically zero. The 95% confidence intervals about the mean errors in Case 9M contain zero except for N_r^* and $N_{\delta a}^*$, where zero is very close to one boundary of the interval.

The error standard deviations also agree well between Case 21 and Case 9M. The values from the ensemble analysis fall within the 95% confidence intervals about the values from the Monte Carlo analysis for 14 parameters. The single exception is L_v^*, whose ensemble error deviation is 0.820 of the Monte Carlo value; the lower bound of the confidence interval is 0.826. Thus, for these cases the ensemble analysis results compare very closely to the Monte Carlo results for static errors.

Case 10M was similar to Case 9M except for the addition of input and output measurement lags, for which the mean, $\bar{f}$, and standard deviation, σ_f, of the time constants were 6.0 sec^{-1} and 0.3 sec^{-1}, respectively. This relatively slow filtering speed had major effects on both the means and standard deviations of the parameter errors. Large mean errors occurred for Y_p (108% of the true parameter value, L_r^* (165%), N_p^* (188%), and Y_r (1663%). Significant mean errors were seen for L_p^* (27%), N_r^* (76%), and $N_{\delta a}^*$ (63.5%). All other mean errors

TABLE 29.- ERRORS IN PARAMETER ESTIMATES FROM MONTE CARLO ANALYSIS CASES 9M THROUGH 12M

Near Hover Parameters		Case 9M (n=50, f=0, σ=0, Near Hover)		CASE 10M (n = 50, f=6 sec^{-1}, σ_f = 0.3 sec^{-1}, Near H.)		Transition Parameters	CASE 11M (n = 50, f=6 sec^{-1}, σ_f = 0.3 sec^{-1}, Trans.)		Cruise Parameters	CASE 12M (n = 39, f=6 sec^{-1}, σ_f = 0.3 sec^{-1}, Cruise)	
Name	Value	$\Delta\bar{p}$	s	$\Delta\bar{p}$	s	Value	$\Delta\bar{p}$	s	Value	$\Delta\bar{p}$	s
Y_v	0.1538	0.0006	0.0036	0.0047	0.0040	-0.0747	-0.0198	0.0269	-0.1268	-0.0101	0.0189
L_v^*	-0.5239	-0.0011	0.0085	0.0624	0.0167	-0.5563	0.1077	0.0288	-1.0289	0.3147	0.2091
N_v^*	0.0519	0.0020	0.0105	-0.0089	0.0117	-0.0367	-0.0220	0.0063	-0.0825	-0.1048	0.0379
Y_p	-0.0164	-0.0077	0.0324	-0.0177	0.0342	-0.0223	0.0778	0.0680	-0.0217	0.0607	0.2092
L_p^*	-0.5936	-0.0010	0.0117	0.1621	0.0263	-0.7209	0.2392	0.0576	-0.6632	0.2629	0.3047
N_p^*	0.0344	-0.0008	0.0214	-0.0648	0.0236	0.0473	-0.0576	0.0232	0.0226	-0.0582	0.0681
Y_r	-0.0019	0.0028	0.0145	0.0316	0.0138	-0.0033	-0.0383	0.1593	-0.0019	-0.1336	0.3220
L_r^*	0.0176	0.0008	0.0229	-0.0291	0.0311	-0.0262	0.0605	0.0700	0.0280	-0.0034	0.6849
N_r^*	-0.0509	0.0041	0.0117	0.0385	0.0124	-0.0374	0.0014	0.0148	-0.0541	0.1289	0.1775
Y_{δ_a}	0.9928	-0.0315	0.1803	-0.0831	0.1848	0.9611	0.7404	0.7400	0.9656	0.0384	0.2931
$L_{\delta_a}^*$	27.2877	0.0550	0.5265	-3.4312	1.0660	26.9680	-3.6360	1.6650	27.0390	-3.7689	1.9637
$N_{\delta_a}^*$	-0.9938	-0.0599	0.1658	0.6307	0.2658	-1.1024	0.8015	0.3995	-1.1538	1.1964	0.6592
Y_{δ_r}	0.1550	-0.0124	0.1012	-0.0194	0.1020	0.1102	0.3364	0.1704	0.1039	0.2063	0.1899
$L_{\delta_r}^*$	-15.9867	-0.0399	0.2722	2.0200	0.5656	-16.5677	3.0747	0.7086	-16.6456	3.3045	1.1908
$N_{\delta_r}^*$	11.6024	0.0094	0.1710	-0.8227	0.3003	11.4340	-0.9975	0.3045	11.4242	-1.1036	0.7011

were less than 17% of the corresponding parameter value. These mean errors are again due to holding the samples control input constant while integrating to compute the estimated state $\hat{x}$.

The error standard deviations increased significantly for L_v^* (the Case 10M value is two times the Case 9M value), L_p^* (2.2 times), L_r^* (1.4 times), $L_{\delta a}^*$ (2.0 times), $N_{\delta a}^*$ (1.6 times), $L_{\delta r}^*$ (2.1 times), and $N_{\delta r}^*$ (1.8 times). The estimate for the Y_r error deviation decreased somewhat, but the 95% confidence intervals based on these two cases have a large overlap.

Case 11M at the transition flight condition and Case 12M at the cruise condition are comparable to Case 10M (see Table 29). Parameters which have significant mean errors near-hover (Case 10M) also have significant mean errors at one or both of the other flight conditions. Specifically, Y_p, N_p^*, Y_r, and $N_{\delta a}^*$ had large mean errors in all three cases, and L_r^*, N_r^*, and $Y_{\delta r}$ had large mean errors in two of the cases. $Y_{\delta a}$ has a large mean error at transition but not at the others. Parameters with large error deviations at the near-hover condition invariably had large deviations in the other two cases. In addition, N_r^* and $Y_{\delta a}$ possess relatively large error deviations at transition and cruise.

The results of Cases 13M and 14M are presented in Table 30. These cases differ only in that the former used the baseline error set and the latter used the large set of instrumentation errors. The mean error of eleven parameters increased from Case 13M to 14M; all these increases were by a factor less than two. Mean errors for Y_v, Y_p, and Y_r decreased by 36%, 33%, and 7%, respectively. The mean error of $Y_{\delta r}$ changed sign, but the 95% confidence intervals about this mean error include zero in both cases.

The error standard deviations of fourteen parameters increased; only Y_p showed a decreased error deviation. The greatest increases occurred for Y_v (the Case 14M value is 3.4 times the Case 13M value), $Y_{\delta r}$ (3.3), $Y_{\delta a}$ (2.8), and N_r^* (2.7). Hence, the error deviations for the lateral parameters show a greater tendency to increase than do the longitudinal parameter deviations when large instrumentation errors are present. Thus, the lateral equation stability and control derivative accuracy appears to be more sensitive to increases in instrumentation errors than does the accuracy in the longitudinal mode.

Plots of the open- and closed-loop poles for the Monte Carlo samples of Cases 9M through 14M appear in Figures 29 through 34. As was true for the longitudinal dynamics, significant variations in the lateral dynamics (stability and handling quality) may occur, particularly for the closed-loop system.

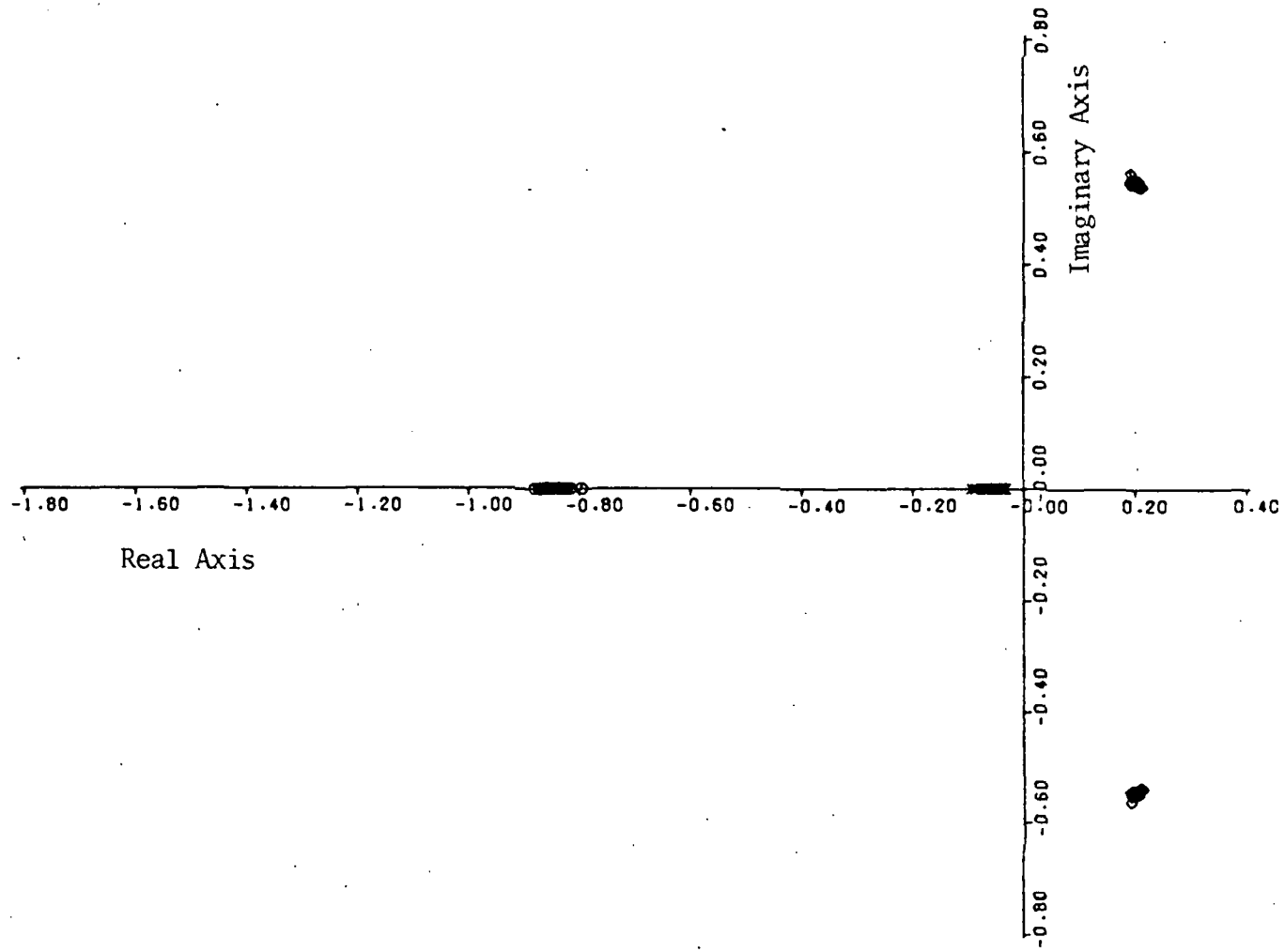

FIGURE 29(a).- ROOT PLOT SHOWING SCATTER OF OPEN-LOOP POLES FOR CASE 9M OF THE MONTE CARLO ANALYSIS

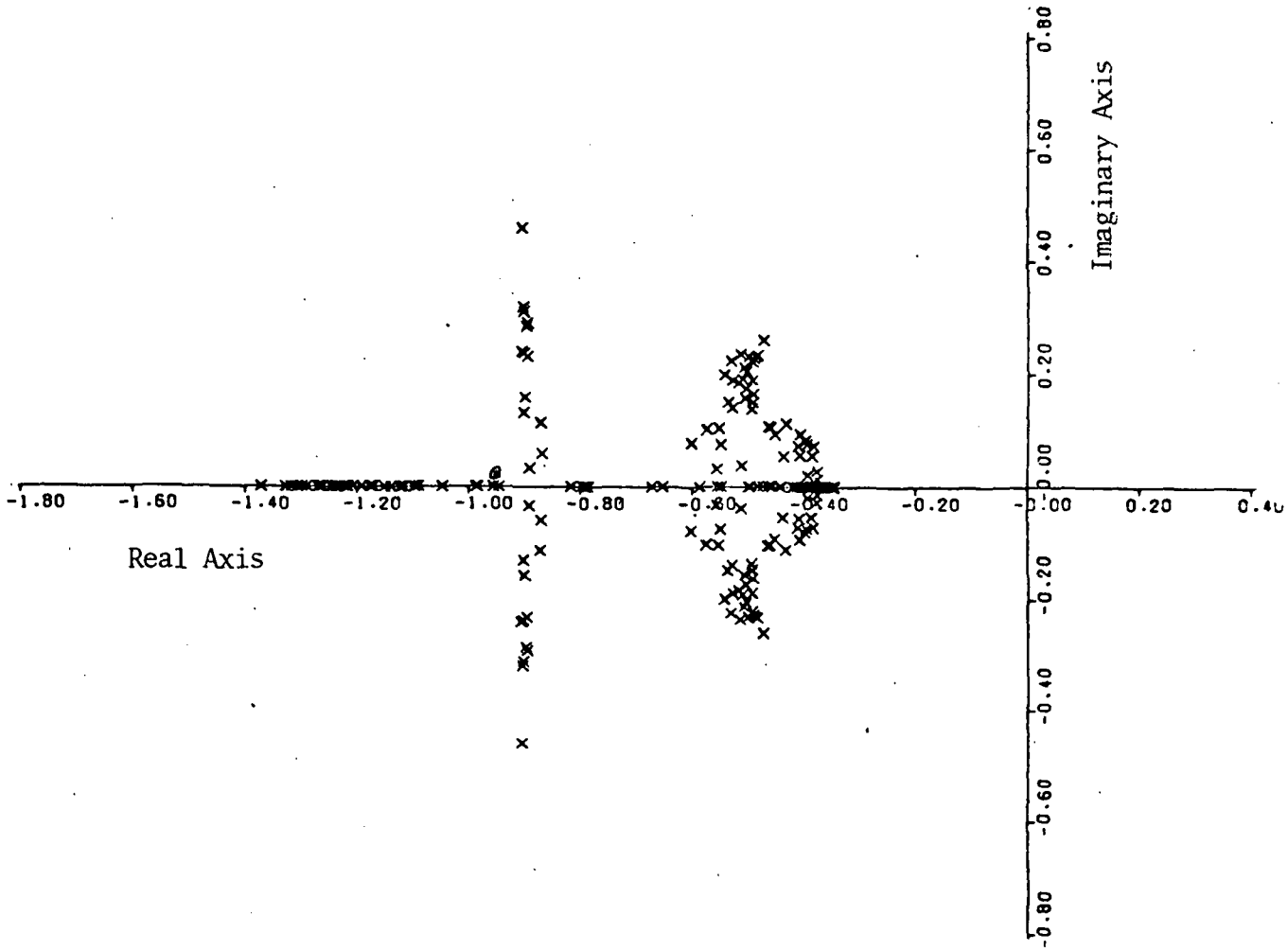

FIGURE 29(b).- ROOT PLOT SHOWING SCATTER OF CLOSED-LOOP POLES FOR CASE 9M OF THE MONTE CARLO ANALYSIS

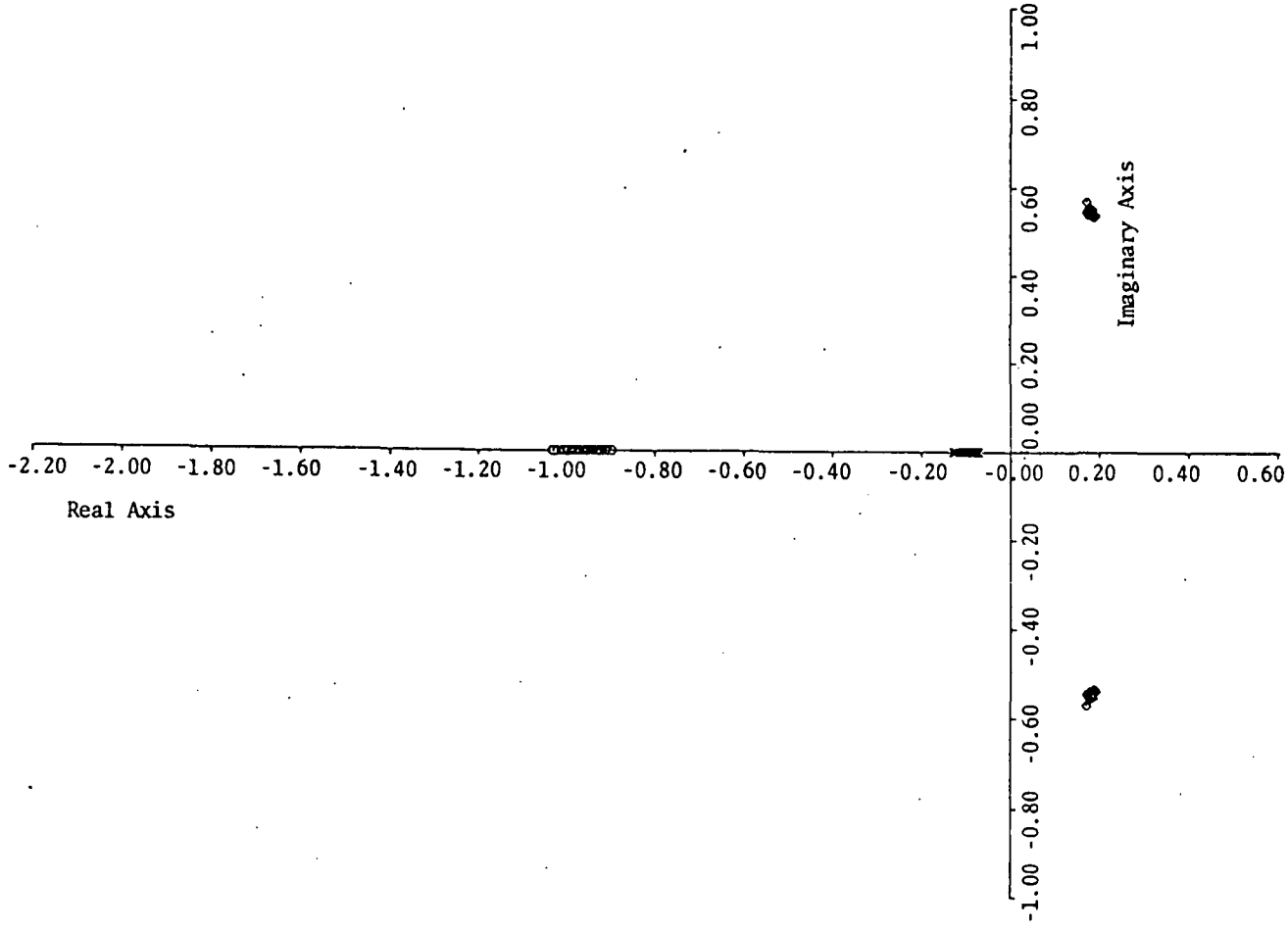

FIGURE 30(a).- ROOT PLOT SHOWING SCATTER OF OPEN-LOOP POLES FOR CASE 10M OF THE MONTE CARLO ANALYSIS

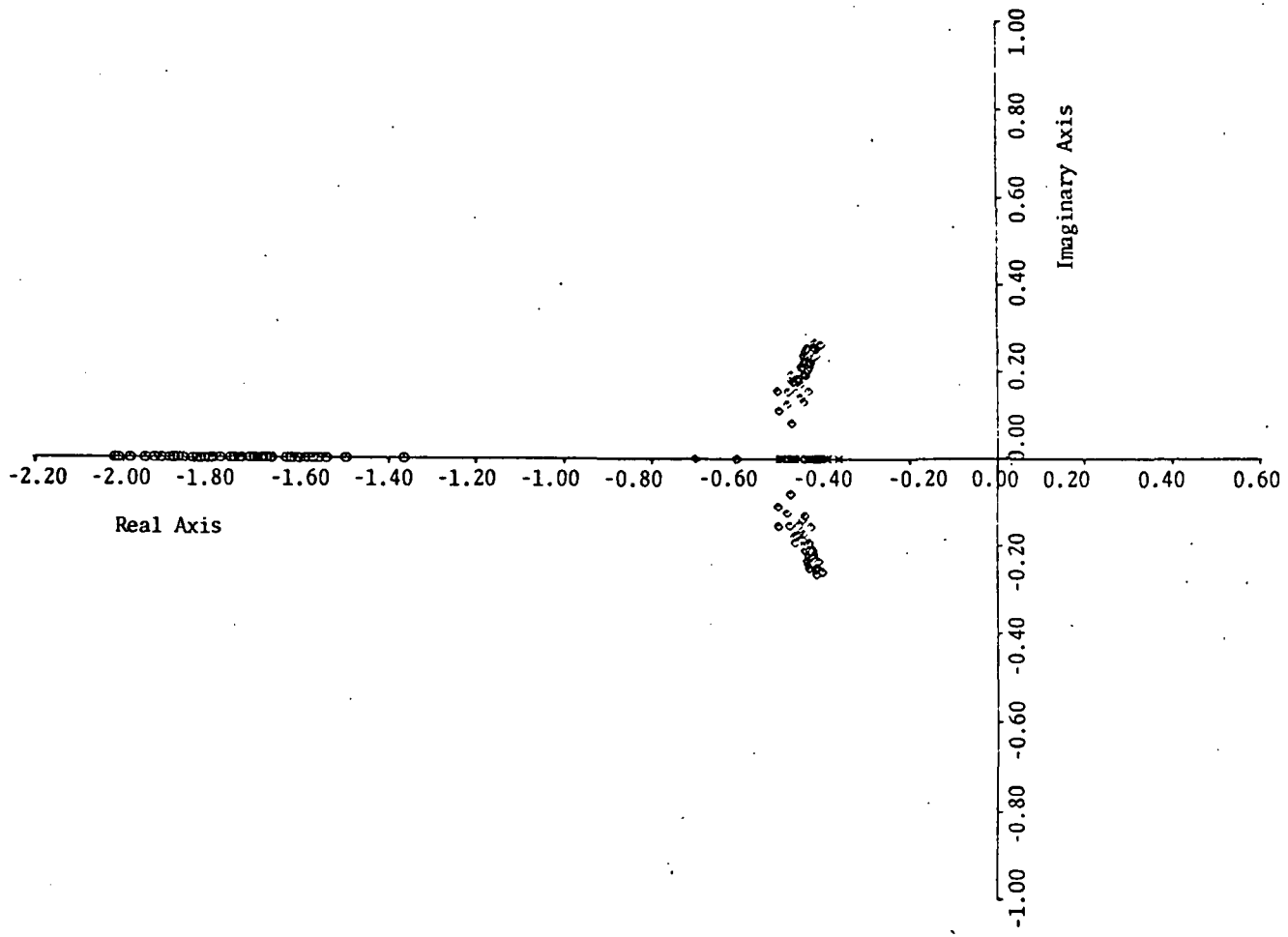

FIGURE 30(b).- ROOT PLOT SHOWING SCATTER OF CLOSED-LOOP POLES FOR CASE 10M OF THE MONTE CARLO ANALYSIS

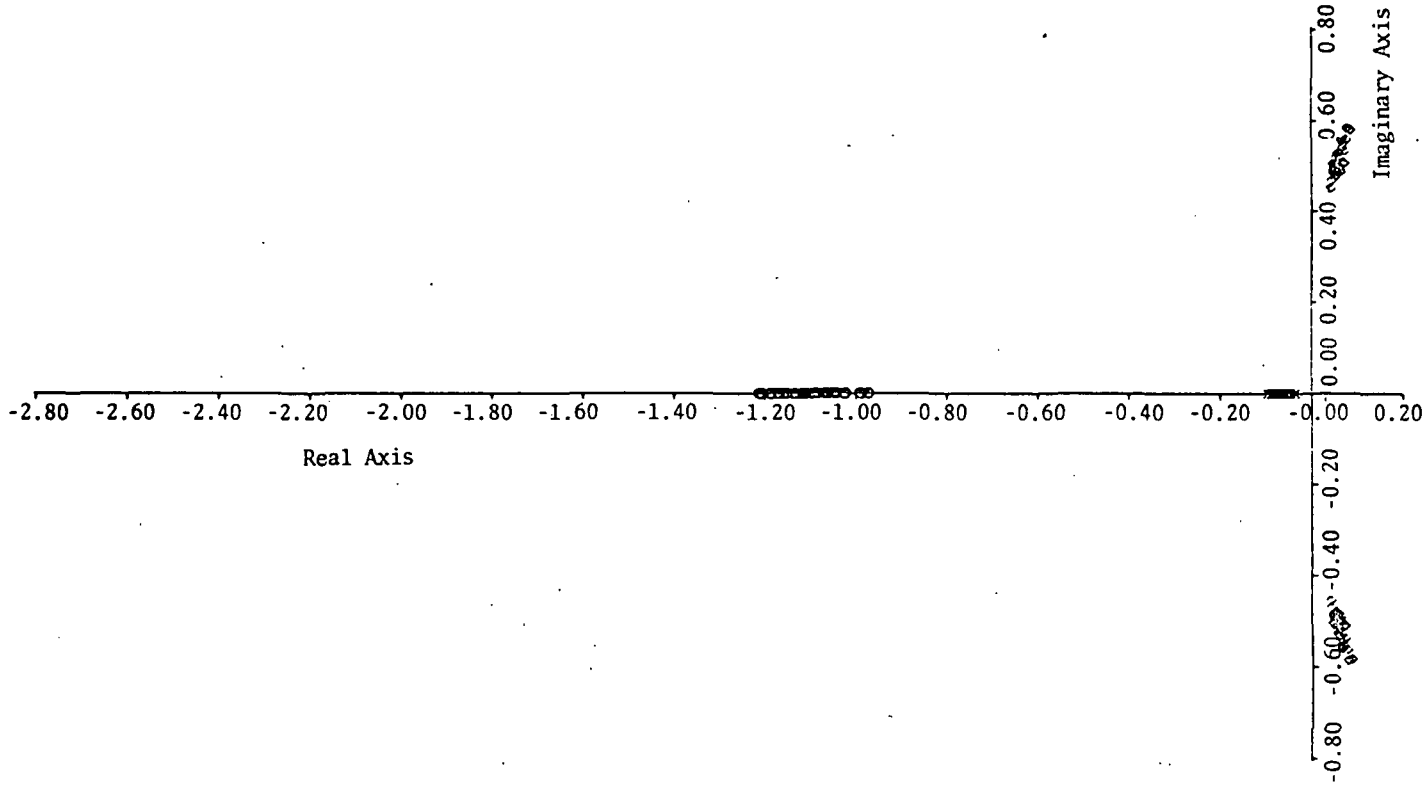

FIGURE 31(a).- ROOT PLOT SHOWING SCATTER OF OPEN-LOOP POLES FOR CASE 11M OF THE MONTE CARLO ANALYSIS

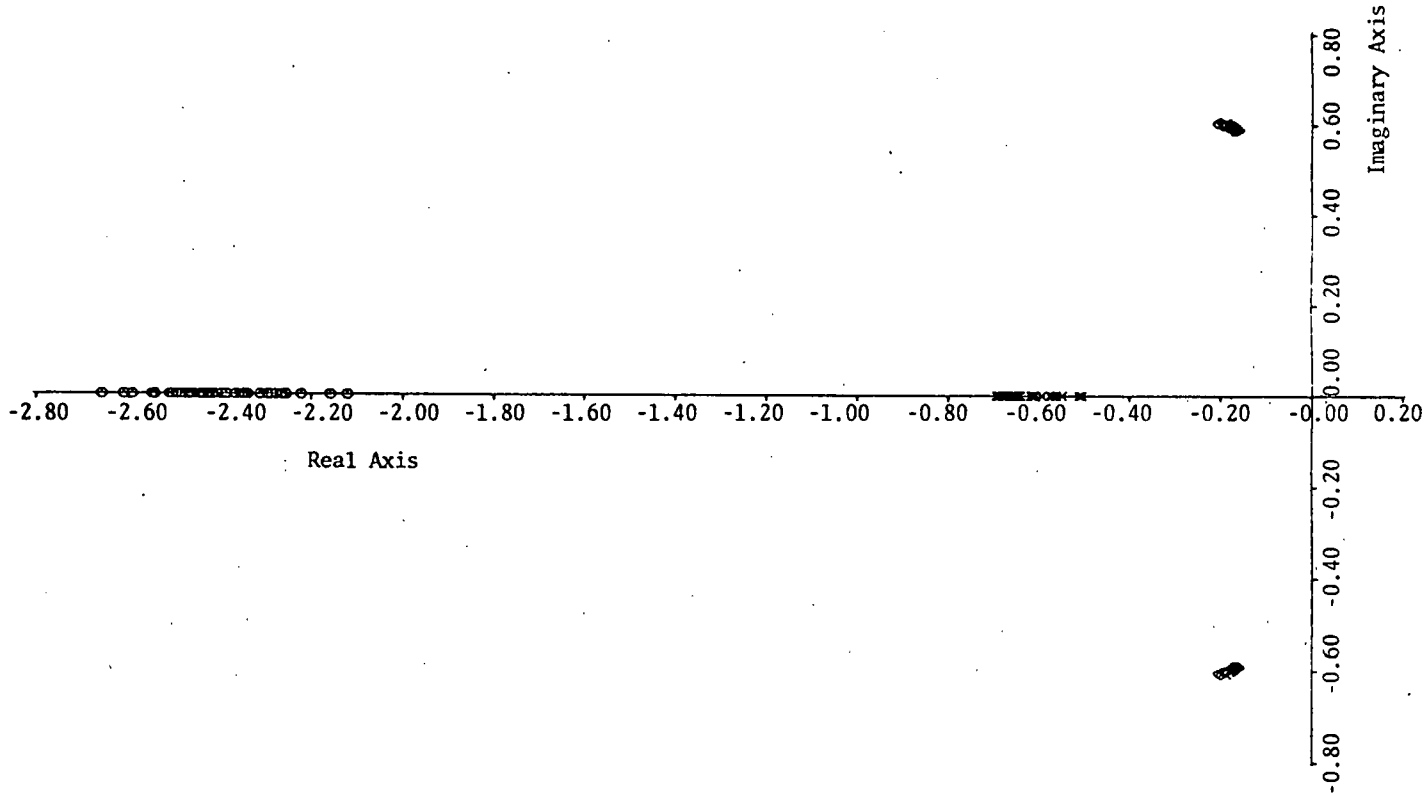

FIGURE 31(b).- ROOT PLOT SHOWING SCATTER OF CLOSED-LOOP POLES FOR CASE 11M OF THE MONTE CARLO ANALYSIS

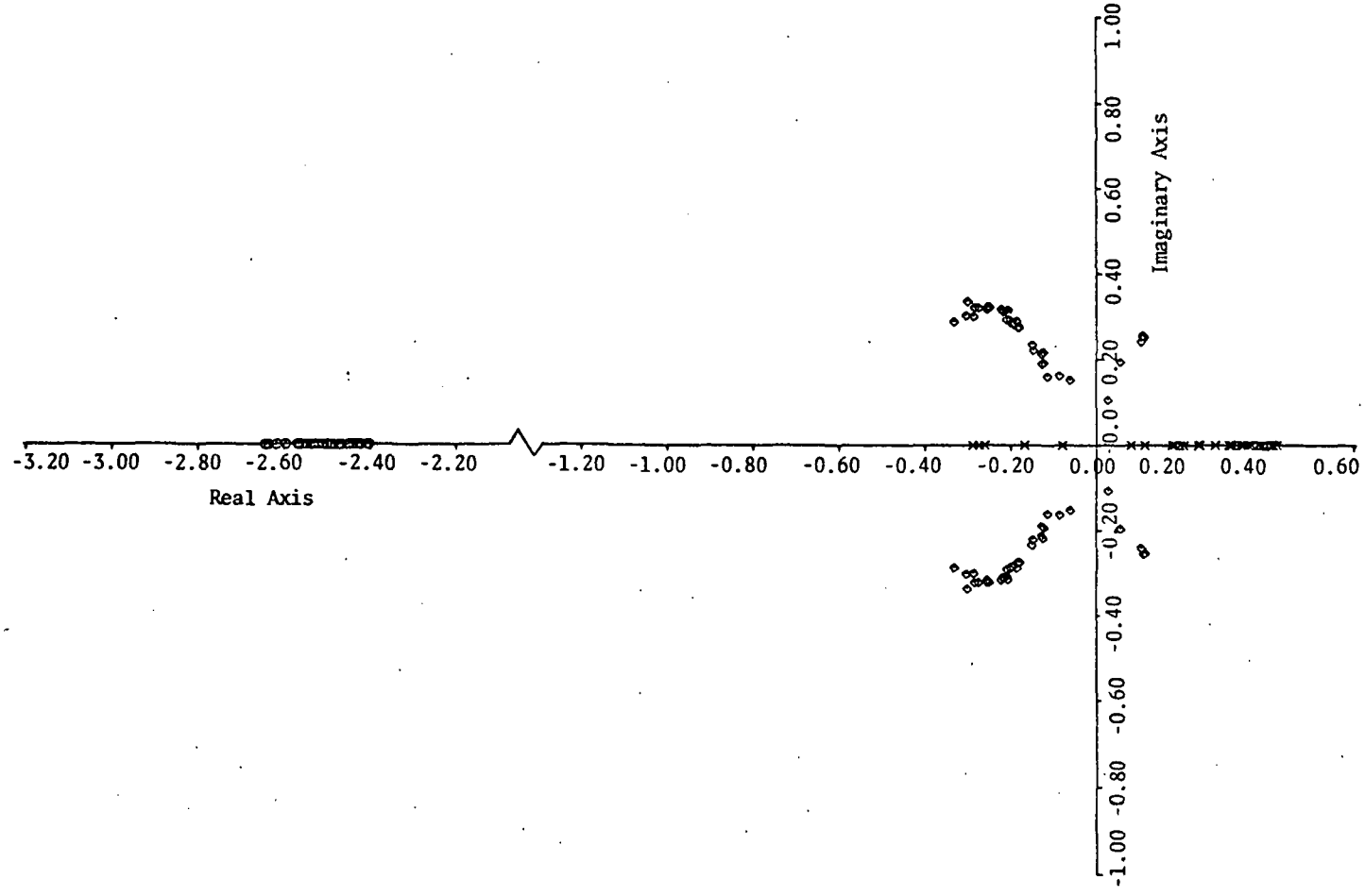

FIGURE 32(a).- ROOT PLOT SHOWING SCATTER OF OPEN-LOOP POLES FOR CASE 12M OF THE MONTE CARLO ANALYSIS

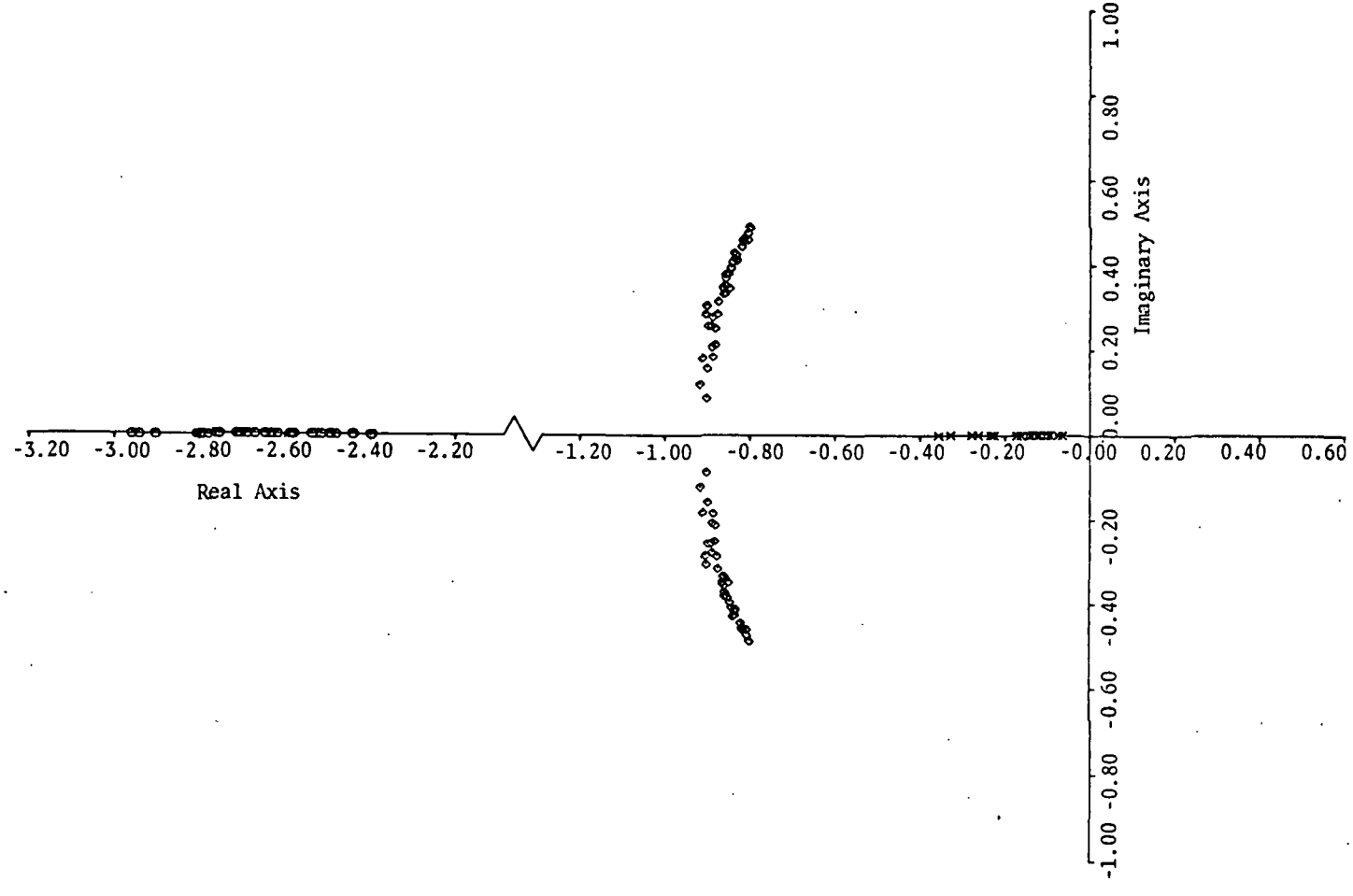

FIGURE 32(b).- ROOT PLOT SHOWING SCATTER OF CLOSED-LOOP POLES FOR CASE 12M OF THE MONTE CARLO ANALYSIS

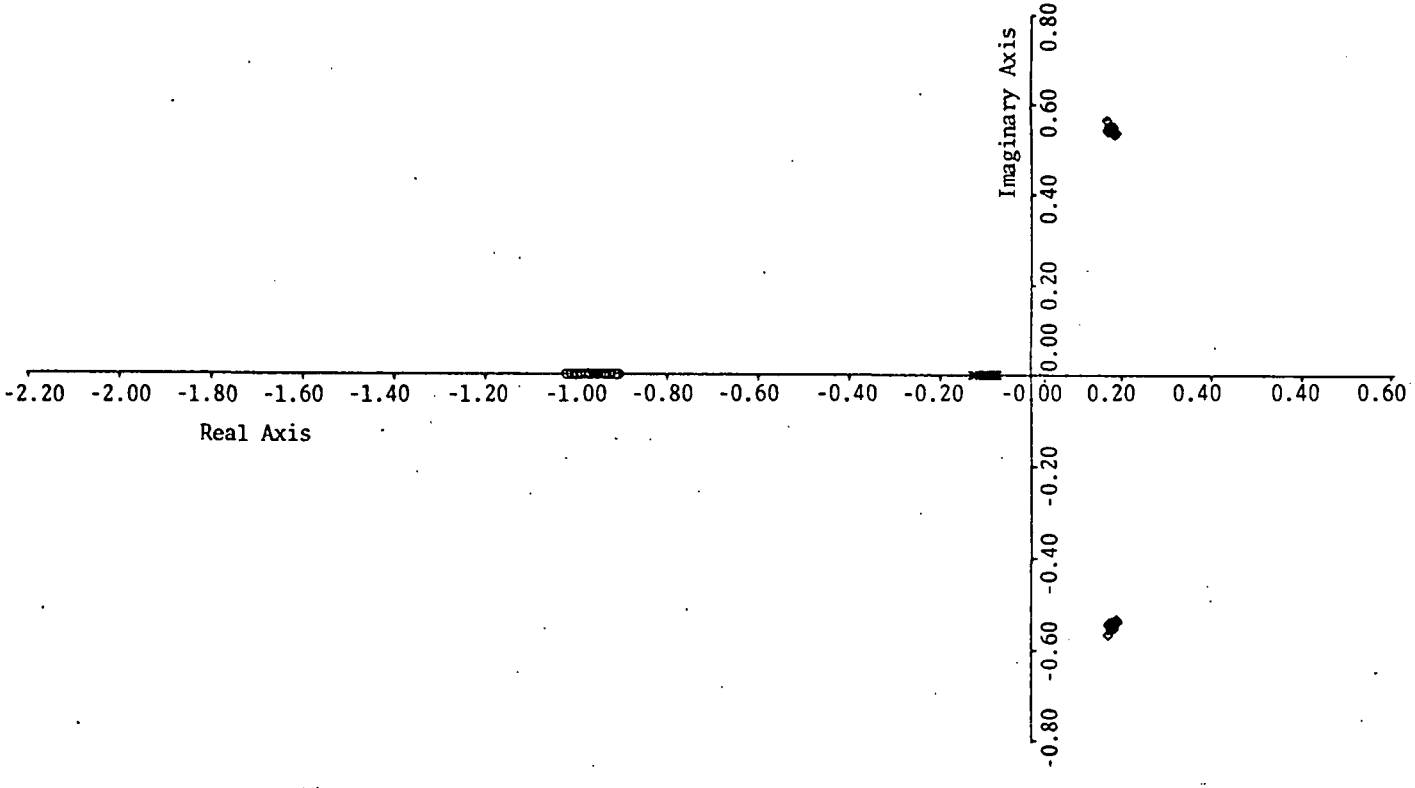

FIGURE 33(a).- ROOT PLOT SHOWING SCATTER OF OPEN-LOOP POLES FOR CASE 13M OF THE MONTE CARLO ANALYSIS

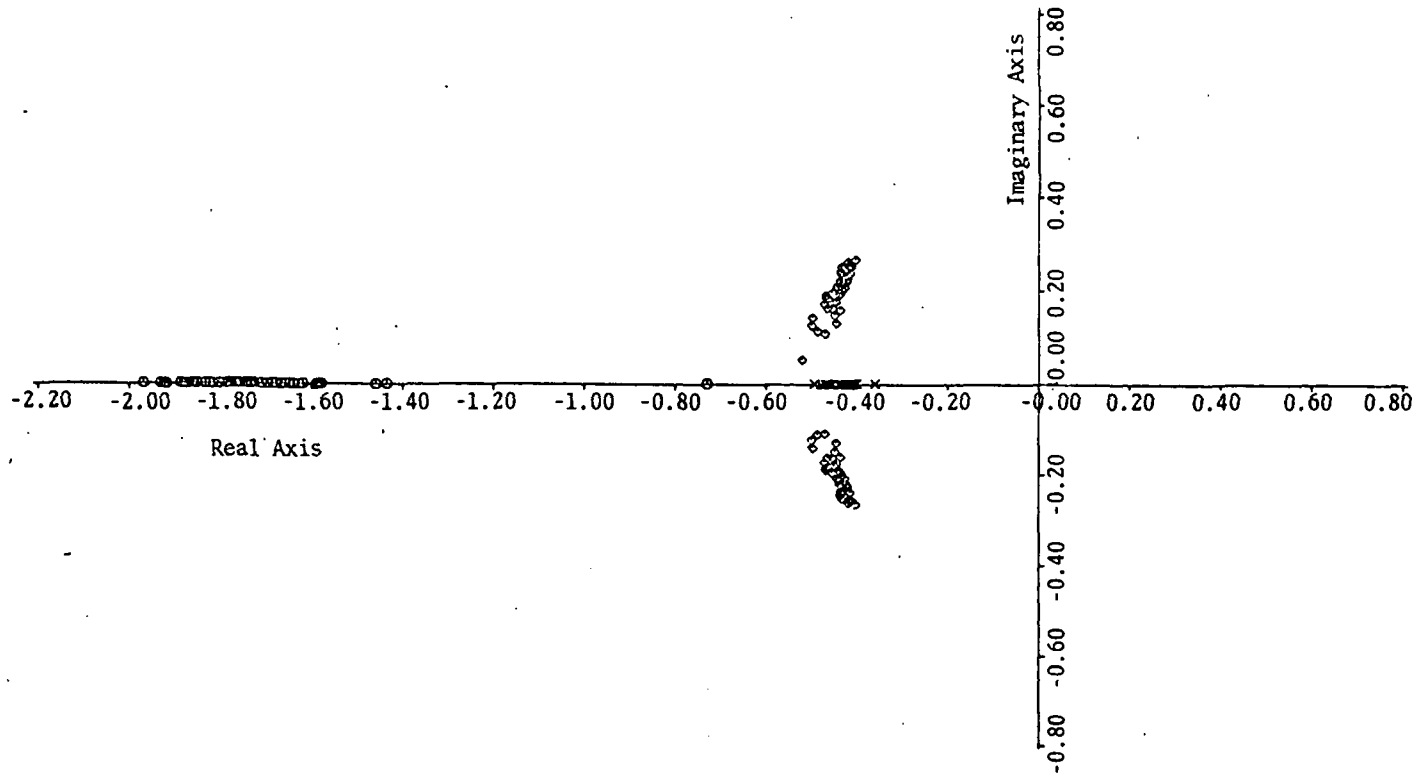

FIGURE 33(b).- ROOT PLOT SHOWING SCATTER OF CLOSED-LOOP POLES FOR CASE 13M OF THE MONTE CARLO ANALYSIS

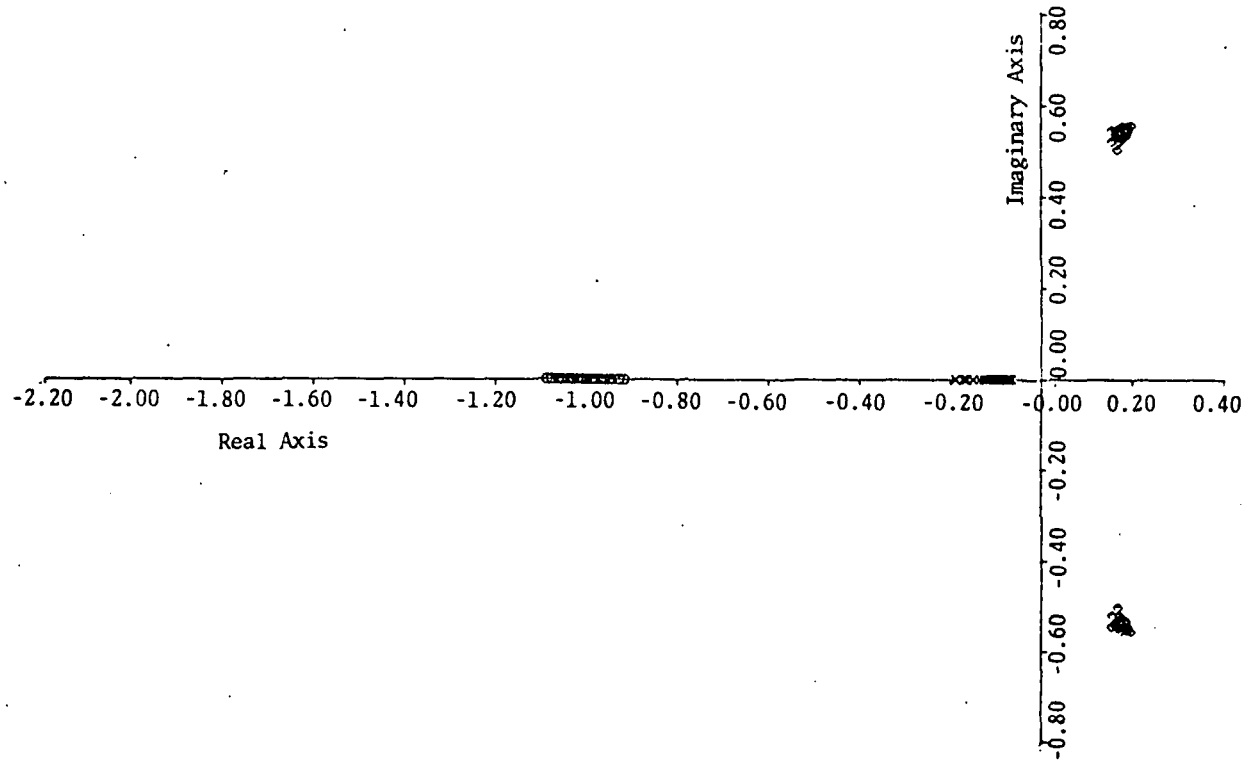

FIGURE 34(a).- ROOT PLOT SHOWING SCATTER OF OPEN-LOOP POLES FOR CASE 14M OF THE MONTE CARLO ANALYSIS

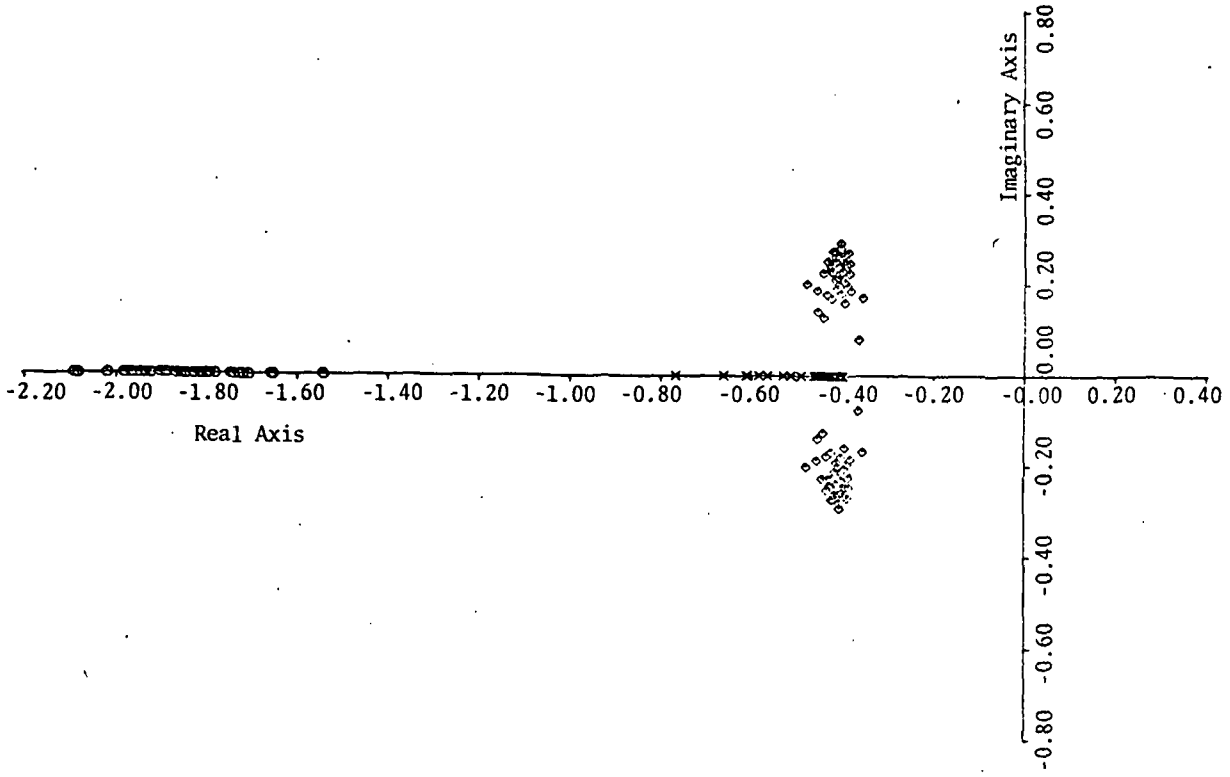

FIGURE 34(b).- ROOT PLOT SHOWING SCATTER OF CLOSED-LOOP POLES FOR CASE 14M OF THE MONTE CARLO ANALYSIS

TABLE 30.- ERRORS IN PARAMETER ESTIMATES FROM MONTE CARLO DATA ANALYSIS, CASES 13M AND 14M

Near Hover Parameters		CASE 13M (n = 50, f=12 sec^{-1}, σ_f = 0.6 sec^{-1}, Hover, Small Error Set)		CASE 14M (n = 50, f=12 sec^{-1}, σ_f = 0.6 sec^{-1}, Hover, Large Error Set)	
Name	Value	Δp	s	Δp	s
Y_v	0.1538	0.0047	0.0035	0.0030	0.0118
L_v^*	-0.5239	0.0607	0.0178	0.0681	0.0276
N_v^*	0.0519	-0.0088	0.0110	-0.0107	0.0285
Y_p	-0.0164	-0.0162	0.0334	-0.0108	0.0258
L_p^*	-0.5936	0.1625	0.0219	0.2119	0.0529
N_p^*	0.0344	-0.0642	0.0215	-0.0784	0.0429
Y_r	-0.0019	0.0315	0.0142	0.0274	0.0336
L_r^*	0.0176	-0.0276	0.0273	-0.0495	0.0628
N_r^*	-0.0509	0.0371	0.0110	0.0557	0.0300
Y_{δ_a}	0.9928	-0.0790	0.1800	-0.0908	0.5105
$L_{\delta_a}^*$	27.2877	-3.3793	0.7676	-3.5295	0.9079
$N_{\delta_a}^*$	-0.9938	0.6297	0.2126	0.7188	0.5222
Y_{δ_r}	0.1550	-0.0137	0.0992	0.0074	0.3288
$L_{\delta_r}^*$	-15.9867	1.9663	0.4002	2.1233	0.4889
$N_{\delta_r}^*$	11.6024	-0.7906	0.2042	-0.7986	0.3651

SUMMARY, CONCLUSIONS, AND RECOMMENDATIONS

Methodology

This study addressed the problem of determining the extent to which instrumentation errors cause degradation in the knowledge of stability and control derivatives identified from flight test data. The resultant degradation of the flight control system performance based on these derivatives was also addressed. The procedure followed in this study was as follows:

(1) The instrumentation systems used for typical flight tests were surveyed, and the main sources of data errors were noted. From the errors, a set of linear error models (equations for each measurement channel) previously developed [5] were verified. The ranges of magnitudes of the error coefficients were compiled in tabular form.

(2) Two analytical techniques--ensemble analysis and Monte Carlo analysis--previously developed [5] were modified to include helicopter equations of motion. These equations were coded into computer programs for determining the effects of instrumentation errors on the identified helicopter parameter accuracy. The first method determines the statistical variation in the parameters by computing their sensitivity to each type of error. The second method simulates the identification process with randomly generated error sources. The statistical variation is then computed from the results of several runs. The analysis techniques are based on the assumption that an output error identification technique such as the modified Newton-Raphson algorithm is used.

(3) The perturbation equations of motion of the CH-46 helicopter were studied at three points along a curved, decelerating landing approach. Flight conditions (stability and control derivatives) at cruise, transition, and near-hover for both longitudinal and lateral equations of motion were selected for analysis. Feedback control laws for a stability augmentation system were developed for each of these sets of equations because all sets were inherently unstable. The results based on three degree-of-freedom decoupled lateral and longitudinal equations may not be applicable to the curved, decelerating portions of the reference trajectory.

(4) The instrument error models and helicopter equations of motion were used in the analysis programs to determine what effects instrument errors have on stability and control derivative accuracy. The effects of different error magnitudes, control input sequence, sample rate, length of data, types of instruments used, and number of parameters identified on the stability and control derivative accuracy were investigated. These accuracy results were used in turn to determine the resultant variation in the open- and closed-loop poles of the helicopter system.

Instrumentation Errors

From the survey of instrumentation practices, the following comments can be made:

(1) The "best available" instrumentation is generally used in flight testing rather than a procedure of specifying and procuring instruments with known laboratory established error magnitudes.

(2) Little is known about the statistical distribution and variations of most instrument errors. Manufacturers typically specify performance within some absolute bounds.

(3) Of the error information available for instruments, the gyros and linear accelerometers are best understood and most easily tested. Air data systems and wind vanes are calibrated in flight, and their accuracy is dependent upon empirical adjustments. Angular accelerometers are not often used, so little general information is available on their accuracy. The accuracy of control position transducer readings is highly dependent upon where the instrument is mounted relative to the control surface. Thus, the control input measurement error is highly aircraft dependent.

(4) There are many time-varying, environment dependent, and nonlinear error sources in the instrumentation which are very difficult to model. However, all of these errors can be encompassed by linear models containing random white noise, scale factor, bias, cross-coupling terms, and first-order lags.

(5) The chief errors in data processing, recording, digitizing, and sampling come from differences in the filter time constants and various sources of noise.

Error Analysis Program Capability

The two statistical analysis techniques which have been coded into digital computer programs as part of this study allow rapid assessment of the instrumentation error effects. The uses which can be made of these programs include the following:

(1) The determination of the effect of instrumentation errors on the statistical accuracy of the stability and control derivatives and other parameters identified from flight test data can be made. This includes the mean error and standard deviation of each of the parameters identified. The contribution of each error source on each parameter is determined.

(2) The effects of such variables as aircraft type and flight condition, control input sequence, and data sampling rate on the accuracy of the identified parameters can be determined.

(3) Trade off studies can be made between instrument quality and identification accuracy.

(4) Different combinations of instruments can be studied for use in collecting the flight data.

(5) Trade off studies between fewer instruments with greater quality and more instruments with larger errors can be made.

(6) The necessary instrument accuracy required in a flight test program to allow identifying aircraft parameters to a desired level of certainty can be specified.

The two error analysis techniques compliment each other. The ensemble analysis is well suited to determine the effects of small static instrument errors (all errors studied but the random magnitude of the dynamic lags) on the identified parameter uncertainty. The Monte Carlo analysis allows the study of effects of random uncertainty in dynamic lags plus more accurate determination of the effects of large static errors.

Limitations of the analysis techniques are as follows:

(1) The recorded data may be optimally filtered as part of the identification process. This is not considered.

(2) The equations of motion of the helicopter may be more complex than the four-state models coded into the programs. The addition of rotor dynamics equations and coupled lateral-longitudinal modes may be more suitable for analysis of control requirements.

Instrumentation Error Effects for the CH-46 Helicopter

The error analysis programs were used to study instrumentation error effects on the accuracy of identified stability and control derivatives of the CH-46 helicopter. It was assumed that the CH-46 was flying at steady conditions at cruise, transition, and near-hover points along a typical approach profile. Typical data spans and sample rates were used. Simulated control inputs were designed to cause perturbations from these nominal conditions, and it was assumed that various combinations of instrumentation were used to obtain state variable and control input measurements. Two sets of instrument error magnitudes--a nominal set and a large error set--were studied. The ensemble analysis program was used extensively to study the effect of the static instrumentation errors for both longitudinal and lateral equations of motion. The Monte Carlo analysis program was then used to compare results with the ensemble program and to determine the effect of random dynamic lag magnitudes. This study of the CH-46 helicopter produced many results and a large quantity of data. The details are presented in the previous chapter, and the key points are summarized here.

Based on a series of ensemble analysis program runs which use the longitudinal equations, the following points can be made:

(1) When static measurement errors were added to those caused by white noise, all parameter standard deviations except for Z_q and Z_w increased by at least a factor of five over the deviations due to white noise only. The parameters Z_u, X_q, X_u, and $X_{\delta e}$ had standard deviations greater than 100% of the parameter magnitudes.

(2) The dominant error sources for twelve of fifteen parameters were the control measurement errors. However, estimating output measurement biases substantially reduced the effect of the control measurement biases. This was because the control biases propagated through the equations of motion and had the same effect on the output as would output measurement biases. Directly estimating control measurement biases could potentially reduce the control measurement error effect further.

(3) The instrumentation had the same relative effect at the cruise, transition, and near-hover flight conditions studied.

(4) Adding angle-of-attack and airspeed measurements decreased the uncertainty of three parameters (Z_u, X_u, and $X_{\delta c}$) at cruise, but the errors were still large. However, the estimate variations of four other parameters were increased due to increased control error sensitivity and added error sources. The conclusion is that these instruments' usage must be based on specific parameter accuracies desired. Also, these instruments do not operate at low speeds and low altitudes for helicopters.

(5) The angular accelerometer did not contribute additional useful information for the conditions examined in this study. It could be omitted from the instrument set for the error magnitudes used in this study.

(6) If all dynamic lags are identical and measurements are essentially continuous, there are no resultant error effects due to the lags' presence.

(7) Adding extra input data to process or extra instruments does not necessarily improve parameter estimates. For one case examined where the data span was increased from 15 sec to 45 sec, the standard deviation of Z_u increased from 56% to 128% of true value because of instrumentation errors.

(8) Changing error magnitudes and the associated weighting matrix used in the identification algorithm changes the relative importance of various error sources.

(9) An example case was studied where the objective was to identify the stability and control derivatives such that the standard deviation of each parameter's uncertainty was less than 30%. By revising the nominal set of instrument errors presented in Table 12 so that the standard deviations of the control biases and the $z_{c.g.}$ location errors are reduced, 14 out of 15 parameter error standard deviations became less than 30% of the respective parameter values. This example demonstrated the utility of the programs developed in this study for specifying instrumentation accuracy to achieve identified parameter accuracy of a certain level.

(10) For small instrumentation errors and without random variations in lags, the ensemble analysis provides accurate estimates of the effects of instrumentation error on parameter uncertainty for considerably less expense (1.5%) than the Monte Carlo analysis. The Monte Carlo analysis can provide more accurate estimates of the effect of instrumentation errors, but added improvement is at the expense of taking a large number of computed samples.

The Monte Carlo analysis program was used to make the following comments with respect to the longitudinal mode:

(1) The closed-loop poles of the helicopter equations of motion may vary significantly from the design point because of errors in the identified parameters due to unmodeled instrument errors. Typical complex poles had frequency varying from 0 to 0.46 sec^{-1}. This affects handling qualities.

(2) The random lags (mean of 6 sec^{-1}; standard deviation of 0.3 sec^{-1}) increased the uncertainty in five parameters (Z_q, Z_u, M_u, $X_{\delta e}$, X_w) by over a factor of two. Increasing the mean inverse time constant of each lag to 30 sec^{-1}, greatly reduced these errors.

(3) A large source of mean error uncovered by the Monte Carlo runs is due to sampling the control input and holding it constant between sample points while determining the state estimates $\hat{x}$ for the identification algorithm.

Based on a series of ensemble error analysis program runs which used the lateral equations, the following points can be made:

(1) The effects of static errors were the same for the lateral mode as for the longitudinal mode. These errors caused a substantial increase in the identified parameter uncertainty.

(2) Estimating output measurement biases did not uniformly improve the estimates of the lateral parameters. Whether biases should be estimated depends on what accuracy is desired for specific parameters.

(3) Control biases again were the dominant error sources for most parameters, whether or not output biases were estimated.

(4) In general, adding roll and yaw angular accelerometers did not significantly improve the parameter estimates.

(5) The results obtained from studying the near-hover flight condition generally held true for cruise and transition flight conditions.

The Monte Carlo analysis program was used to study the effect of random lags on the estimation of parameters of the lateral equations of motion. Comments which can be made from this study are:

(1) The ensemble analysis and Monte Carlo analysis results were very close for cases where no random lags were considered.

(2) As with the longitudinal mode, significant mean parameter errors were again caused by a combination of measurement lags and the fact that the sampled control was held constant while computing the estimated state $\hat{x}$ for the identification algorithm.

(3) Lags having mean inverse time constants of 6.0 sec^{-1} and having standard deviations of 0.3 sec^{-1} caused substantial increase in the deviations of L_v^* (2.0 times), L_p^* (2.2), L_r^* (1.4), $L_{\delta a}^*$ (2.0), $N_{\delta a}^*$ (1.6), $L_{\delta r}^*$ (2.1), and $N_{\delta r}^*$ (1.8) as compared to the accuracy obtained when no random components of the lags were present.

(4) There was a greater deviation in the identified lateral parameters due to large and baseline instrumentation errors than for the longitudinal parameters.

Recommendations

In the simulation of a typical flight test of the CH-46 helicopter, it was shown that typical unmodeled instrumentation errors caused wide scatter of the closed-loop poles of the aircraft. This scatter places a large uncertainty on the predicted handling qualities or gust response of the aircraft, and can even make the basic stability of the aircraft questionable in some flight regimes. Thus, this study has pointed out the important need for evaluating the effect of instrumentation errors on the accuracy of identified stability and control derivatives. It is strongly recommended that the program developed in this effort be used to specify instrumentation accuracy requirements before flight test begins.

This effort has not been exhaustive in terms of examining how the instrumentation errors can be compensated for by improved or modified software. It is recommended that the following additional studies be made:

(1) The effects of rotor dynamics and coupling between lateral and longitudinal equations on the control requirements of the helicopter should be ascertained. If these effects are important, the dynamic models used in the programs developed in this study should be expanded to include them.

(2) The programs should be modified to include the following options:

(a) Ability to identify control measurement biases.

(b) Computation of the R weighting matrix used in the identification algorithm based on the statistics of the innovations sequence $(y - \hat{y})$ for each iteration of the Monte Carlo program.

(c) Extra polation of the sampled control sequence in computing the estimated state $\hat{x}$ so that it more nearly matches the real state x determined from the real continuous control.

These options should then be exercised to determine the possible improvements to parameter uncertainty that these software changes can provide.

(3) The sensitivity of the parameter uncertainty to the specific feedback control law should be investigated whenever feedback is required to provide adequate stability to the aircraft. This was the case for the CH-46 helicopter models studied in this effort.

For a future flight test, a study should be made to determine how accurately the open-loop poles of the aircraft must be known to guarantee aircraft performance within certain acceptable limits. By performance is meant stability, ride quality, and gust response. The resulting allowable open-loop pole uncertainty should then be used to specify the allowable uncertainty that is acceptable for each of the stability and control derivatives. This uncertainty can then be used in turn to specify the required instrumentation accuracy and control input sequence to be used during flight tests to identify the stability and control derivatives.

Page Intentionally Left Blank

REFERENCES

1. "Ad hoc Team Report on F-111 Stall/Post Stall/Spin Presentation Program," Aeronautical Systems Division, Air Force Systems Command, U.S.A.F., August 1970.

2. Hill, R.W., Clinkenbeard, I.L., and Bolling, N.F., "V/STOL Flight Test Instrumentation Requirements for Extraction of Aerodynamic Coefficients," AFFDL-TR-68-154, Air Force Flight Dynamics Laboratory, WPAFB, Ohio, December 1968.

3. Burns, B.R.A., "The Effects of Instrumentation Errors on Stability Derivative Measurements," Proceedings of the 3rd International Symposium on In-Flight Test Instrumentation, Cranfield, England, April 1964.

4. Gerlach, O.H., "High Accuracy Instrumentation Techniques for Non-Steady Flight Measurements," Flight Test Instrumentation, Vol. III, (M.A. Perry, ed.), Pergamon Press, London, 1964.

5. Sorensen, J.A., "Analysis of Instrumentation Error Effects on the Identification Accuracy of Aircraft Parameters," NASA CR-112121, National Aeronautics and Space Administration, Washington, D.C., May 1972.

6. Sorensen, J.A., Tyler, J.S. and Powell, J.D., "Evaluation of Flight Instrumentation for the Identification of Stability and Control Derivatives," 2nd AIAA Atmospheric Flight Mechanics Conference, Moffett Field, Calif., September 1972.

7. Bryant, W.H., and Hodge, W.F., "Effects of Flight Instrumentation Errors on the Estimation of Aircraft Stability and Control Derivatives," Symposium on Parameter Estimation Techniques and Applications in Aircraft Flight Testing, NASA Flight Research Center, Edwards, Calif., April 1973.

8. Pitman, Jr., G.R., Inertial Guidance, John Wiley & Sons, N.Y., N.Y., 1962.

9. Coffman, V.D., "Gyro Modeling Test Results," SUDAAR No. 457, Guidance and Control Laboratory, Stanford University, May 1973.

10. "Rate Gyroscope Technical Handbook," U.S. Time Corporation, Irvington-on-Hudson, N.Y., 1971.

11. Kayton, M., and Fried, W.R., Avionics Navigation Systems, John Wiley & Sons, N.Y., N.Y., 1969.

12. Sage, B.B. and Morris, H., "Principles of Operation, Low Range Fluid Rotor Angular Accelerometers," Systron Donner Corp., Concord, Calif., 1966.

13. Bradburn, P., "Performance Specification," STOLAND data, Sperry Flight Systems Division, Phoenix, Arizona, December 15, 1971.

14. Wolowicz, C.H., "Considerations in the Determination of Stability and Control Derivatives and Dynamic Characteristics from Flight Data," AGARD Report 549 - Part I, 1966.

15. Allen, R.V. and Archambault, R.G., "Flight Test Calibration of the Douglas 5-Probe Differential Pressure Head for Measuring Angles-of-Attack and Sideslip," Report No. Dev-1864, Douglas Aircraft Co., September 1964.

16. Mayer, J.P., "Corrections to the Measurement of the Angle-of-Attacks in Flight," Flight Research Center, NACA, February 1963.

17. Beeler, D.E., "Flight Techniques for Determining Airplane Drag at High Mach Numbers," NACA TN 3821, 1956.

18. Wingrove, R.C., "Quasi-Linearization Technique for Estimating Aircraft States from Flight Data," Journal of Aircraft, Vol. 10, No. 5, May 1973.

19. Gilyard, G.B., and Belte, D., "Flight-Determined Lag of Angle-of-Attack and Sideslip Sensor in the YF-12A Airplane from Analysis of Dynamic Maneuvers," NASA TN, 1974.

20. Germond, P.J., "C-5 Flight Test Telemetry Data Processing System," Proceedings of the AIAA 3rd Aircraft Design and Operations Meeting, 1971.

21. Rymer, J.W., "What Should Real-Time Testing Offer?," Naval Air Test Center, Patuxent River, Md., 1972.

22. Vinokur, M., "Amplitude-Quantized Sample of Unknown Signal Plus Noise," Proceedings of IEE, Vol. 118, No. 3/4, March/April 1971.

23. Lamb, Jr., J.P., "The Influence of Geometry Parameters Upon Lag Error in Airborne Pressure Measuring Systems," WADC Tech. Report 57-351, July 1967.

24. Taylor, Jr., L.W., Iliff, K.W., and Powers, B.G., "A Comparison of Newton-Raphson and Other Methods for Determining Stability Derivatives from Flight Data," AIAA Third Flight Test, Simulation and Support Conference, Houston, Texas, March 1969.

25. Seckel, E., Stability and Control of Airplanes and Helicopters, Academic Press, New York, 1964.

26. Hall, Jr., W.E., Gupta, N.K., and Smith, R.G., "Identification of Aircraft Stability and Control Coefficients for the High Angle-of-Attack Regime," Final Report No. 2, Systems Control, Inc., Palo Alto, Calif., March 1974.

27. Anon., "Digital Flight Control and Landing System for the CH-46C Helicopter," Report No. 6200-933013, Bell Aerospace Co., Buffalo, N.Y., May 1970.

28. Bryson, Jr., A.E., and Hall, Jr., W.E., "Optimal Control Filter Synthesis by Eigenvector Decomposition," SUDAAR No. 436, Stanford University, Stanford, Calif., November 1971.

29. Bryson, Jr., A.E., and Hall, Jr., W.E., "Synthesis of Hover Autopilots for Rotary-Wing VTOL Aircraft," SUDAAR No. 446, Stanford University, Stanford, Calif., June 1972.

30. Mohr, R.L. and Taniguchi, N., "Flight Instrumentation Specification for Parameter Identification - User's Guide," NASA CR-132676, National Aeronautics and Space Administration, Washington, D.C., February 1975.

31. Taniguchi, N., Plevyak, G., and Sorensen, J.A., "Flight Instrumentation Specification for Parameter Identification - User's Guide," NASA CR-112122, National Aeronautics and Space Administration, Washington, D.C., May 1972.

32. Singer, R.A., "The Design and Synthesis of Linear Multivariable Systems with Application to State Estimation," SU-SEL-68-030, Stanford Electronic Labs, Stanford, Calif., June 1968.

33. Bryson, Jr., A.E. and Ho, Y.C., Applied Optimal Control, Blaisdale Publishing Co., Waltham, Mass., 1969.

34. Dunn, O.J., and Clark, V.A., Applied Statistics: Analysis of Variance and Regression, John Wiley & Sons, N.Y., 1974.

DISTRIBUTION LIST

NAS1-12876

	No. Copies
NASA Langley Research Center Hampton, VA 23665 Attn: Report & Manuscript Control Office, Mail Stop 180A Ward F. Hodge, Mail Stop 494	 1 25
NASA Ames Research Center Moffett Field, CA 94035 Attn: Library, Mail Stop 202-3	 1
NASA Flight Research Center P.O. Box 273 Edwards, CA 93523 Attn: Library	 1
NASA Goddard Space Flight Center Greenbelt, MD 20771 Attn: Library	 1
NASA Lyndon B. Johnson Space Center 2101 Webster Seabrook Road Houston, TX 77058 Attn: JM6/Library	 1
NASA Marshall Space Flight Center Huntsville, AL 35812 Attn: Library	 1
Jet Propulsion Laboratory 4800 Oak Grove Drive Pasadena, CA 91103 Attn: Library, Mail 111-113	 1
NASA Lewis Research Center 21000 Brookpark Road Cleveland, OH 44135 Attn: Library, Mail Stop 60-3	 1
NASA John F. Kennedy Space Center Kennedy Space Center, FL 32899 Attn: Library, IS-DOC-1L	 1
National Aeronautics & Space Administration Washington, D.C. 20546 Attn: KSS-10/Library RG/NASA Headquarters	 1 1
NASA Scientific & Technical Information Facility 6571 Elkridge Landing Road Linthicum Heights, MD 21090	 14 plus reproducible